



2809076557

**REFERENCE ONLY****UNIVERSITY OF LONDON THESIS**

Degree PhD Year 2006 Name of Author BENTLEY  
Kate Anne

**COPYRIGHT**

This is a thesis accepted for a Higher Degree of the University of London. It is an unpublished typescript and the copyright is held by the author. All persons consulting the thesis must read and abide by the Copyright Declaration below.

**COPYRIGHT DECLARATION**

I recognise that the copyright of the above-described thesis rests with the author and that no quotation from it or information derived from it may be published without the prior written consent of the author.

**LOAN**

Theses may not be lent to individuals, but the University Library may lend a copy to approved libraries within the United Kingdom, for consultation solely on the premises of those libraries. Application should be made to: The Theses Section, University of London Library, Senate House, Malet Street, London WC1E 7HU.

**REPRODUCTION**

University of London theses may not be reproduced without explicit written permission from the University of London Library. Enquiries should be addressed to the Theses Section of the Library. Regulations concerning reproduction vary according to the date of acceptance of the thesis and are listed below as guidelines.

- A. Before 1962. Permission granted only upon the prior written consent of the author. (The University Library will provide addresses where possible).
- B. 1962 - 1974. In many cases the author has agreed to permit copying upon completion of a Copyright Declaration.
- C. 1975 - 1988. Most theses may be copied upon completion of a Copyright Declaration.
- D. 1989 onwards. Most theses may be copied.

*This thesis comes within category D.*

- This copy has been deposited in the Library of WCL
- This copy has been deposited in the University of London Library, Senate House, Malet Street, London WC1E 7HU.



# **Adaptive Behaviour through Morphological Plasticity in Natural and Artificial Systems**

*Katie Bentley*

A dissertation submitted in partial fulfillment  
of the requirements for the degree of  
**Doctor of Philosophy**  
of the  
**University of London.**

Department of Computer Science  
University College London

2006

UMI Number: U591845

All rights reserved

INFORMATION TO ALL USERS

The quality of this reproduction is dependent upon the quality of the copy submitted.

In the unlikely event that the author did not send a complete manuscript and there are missing pages, these will be noted. Also, if material had to be removed, a note will indicate the deletion.



UMI U591845

Published by ProQuest LLC 2013. Copyright in the Dissertation held by the Author.  
Microform Edition © ProQuest LLC.

All rights reserved. This work is protected against  
unauthorized copying under Title 17, United States Code.



ProQuest LLC  
789 East Eisenhower Parkway  
P.O. Box 1346  
Ann Arbor, MI 48106-1346

# Abstract

Our concept of intelligence is changing. Embodiment has led to the rise of morphologies in Artificial Intelligence (AI) research. This thesis focuses on two research questions: 1) How can system morphologies, well-adapted to changing environments, be designed? 2) How can adaptive behaviour be generated through morphology? It is the fundamental argument of this thesis that *morphological plasticity* (MP), the environmentally induced variation in growth or development, can provide a solution to both questions.

Specifically, this thesis is based around a detailed study of diatom valve morphogenesis. Diatoms, a unicellular organism, construct intricate siliceous structures (valves) around themselves which exhibit high plasticity to the environment. Diatom valve morphogenesis is a good example of how morphologies can be well-adapted to *changing* environments, an open problem in AI, and how adaptive behaviour can be generated through morphological processes alone. Through a constructivist approach this thesis contributes to both understanding of MP in natural systems and the design of MP algorithms for artificial adaptive systems.

Several original models and frameworks are defined within this thesis: the Nature's Batik Model of basic diatom valve morphogenesis; the Cellanimat, a 'Dynamic Morphology' based on the unicell, capable of MP driven adaptive behaviour through its unique 'Artificial Cytoskeleton' model of cytoskeletal dynamics; the Environment-Phenotype Map framework; and the Cellanimat Colony Model, which combines all previous models for the investigation of MP mechanisms during diatom colony formation. Cellanimat dynamics and optimization are thoroughly investigated and the model is shown to be multi-functional, evolvable, scalable and reasonably robust.

# Acknowledgements

Firstly, I would of course like to thank my parents and family for their understanding, endless patience, encouragement and support. Huge thanks go to my dear Ben, without his constant support, and knowing encouragement through the daily troubles of PhD research, this thesis would not have been possible.

My most grateful thanks go to my supervisor Chris Clack for tireless effort, constant encouragement and superb management. I would like to thank my second supervisor Eileen Cox for her infectious enthusiasm for diatoms! Her encouragement, support and guidance throughout have been invaluable and the experience of working at the Natural History Museum was priceless. Many thanks to Peter Bentley for starting the whole thing off, initial supervision, guidance and inspiration, for reading the whole thesis and providing much needed feedback and all credit goes to him for steering me towards diatoms in the first place!

I would like to thank Tom Quick, Sanjeev Kumar and Tim Hutton for many enjoyable Artificial Life discussions and valuable advice. On the biology side I am indebted to Anna Koffer for patient explanation of the cytoskeleton and huge thanks go to Angus Cameron and the gang from Cancer Research UK for constant enthusiastic tutorials and discussions of cell biology, and for the suggestion to model phagocytosis.

This thesis was funded in part by SAIC and part funded by a departmental grant. I am most grateful to Angela Sasse for all her support and rapid life-saving financial help and guidance.

# Contents

<b>1</b>	<b>Introduction</b>	<b>14</b>
1.1	Thesis Overview . . . . .	16
1.2	Publications . . . . .	18
<b>2</b>	<b>Morphologies and AI: a review</b>	<b>19</b>
2.1	Intelligence, embodiment and philosophy: the rise of morphologies . . . . .	19
2.2	In the beginning: direct encoded morphologies . . . . .	22
2.3	Importance of development: indirect encodings . . . . .	23
2.3.1	Developmental Algorithms and Computational Embryology . . . . .	23
2.3.2	Virtual creatures . . . . .	24
2.3.3	The POE model . . . . .	26
2.3.4	Advances and Limitations . . . . .	26
2.4	Shift in control: cheap design . . . . .	27
2.4.1	Passive Dynamic Walker . . . . .	28
2.4.2	Morphological Computation and the XOR robot . . . . .	29
2.4.3	Limitations . . . . .	30
2.5	Morphological Plasticity: future direction for AI? . . . . .	31
2.5.1	Dynamic Morphologies: a definition . . . . .	32
2.5.2	Morpho-functional Machines and connectivity . . . . .	33
2.5.3	Self-assembly, Collective and Modular Robotics . . . . .	34
2.5.4	Dynamic Morphologies in AI . . . . .	35
2.6	A Taxonomy of Morphological Plasticity in AI . . . . .	36
2.7	Thesis Stance: A Summary . . . . .	38
<b>3</b>	<b>Nature's Batik</b>	<b>40</b>
3.1	Introduction to Diatoms . . . . .	40
3.1.1	Diatom Phenotypic Plasticity . . . . .	42
3.2	Diatom Valve Morphogenesis . . . . .	43
3.2.1	Valve morphogenesis in raphid diatoms . . . . .	43
3.3	The Nature's Batik Model . . . . .	46
3.3.1	Valve Growth . . . . .	46

3.3.2	Computer evolution of valve morphologies . . . . .	50
3.4	Results and discussion . . . . .	52
3.4.1	Evolved Valves . . . . .	52
3.4.2	Growth patterns . . . . .	52
3.4.3	Areas for improvement of the model . . . . .	55
3.5	Summary . . . . .	56
<b>4</b>	<b>Cell and Cellanimat</b>	<b>57</b>
4.1	The Cell Basics . . . . .	58
4.2	The Cytoskeleton . . . . .	60
4.2.1	Focus . . . . .	61
4.2.2	Dynamics . . . . .	62
4.2.3	Environment and the Transduction Pathway . . . . .	63
4.3	The Cellanimat: an overview . . . . .	65
4.3.1	Cellanimat subsystem overview . . . . .	68
4.3.2	Cellanimat macromolecule overview . . . . .	69
4.3.3	The Environment-Phenotype Map . . . . .	69
4.3.4	Example: The Protrusions E-P Map . . . . .	70
4.4	The Cellanimat: Rules of Play . . . . .	72
4.4.1	Creation . . . . .	73
4.4.2	Assessment: CA Rules . . . . .	76
4.4.3	Assessment: actin agent rules (asynchronous) . . . . .	78
4.4.4	Assessment: Nucleator Agent Rules . . . . .	86
4.5	Pseudo code overview . . . . .	87
4.6	Summary . . . . .	88
<b>5</b>	<b>Cellanimat multifunctionality: from chemotaxis to phagocytosis</b>	<b>90</b>
5.1	Experiment A: chemotaxis . . . . .	90
5.1.1	Experimental Set Up . . . . .	91
5.1.2	Motility results . . . . .	93
5.1.3	Chemoattractant exposure . . . . .	93
5.1.4	Morphological change . . . . .	93
5.1.5	System effects on the environment . . . . .	96
5.1.6	Conclusions . . . . .	96
5.2	Experiment B: phagocytosis vs chemotaxis . . . . .	96
5.2.1	The process of phagocytosis . . . . .	97
5.2.2	Experimental setup . . . . .	98
5.2.3	Default parameters . . . . .	99
5.2.4	Multifunctionality . . . . .	100



5.2.5	Improving the E-P Map . . . . .	103
5.2.6	Extreme ingestion . . . . .	104
5.2.7	Summary . . . . .	104
<b>6</b>	<b>Cellanimat dynamics and optimization</b>	<b>106</b>
6.1	Overview of studies . . . . .	107
6.2	<b>Study One.</b> Redundancy and compositional dynamics . . . . .	108
6.2.1	During chemotaxis . . . . .	108
6.2.2	During phagocytosis . . . . .	111
6.2.3	Subsystem redundancy . . . . .	112
6.2.4	Macromolecular redundancy . . . . .	112
6.2.5	Optimization of WN rule . . . . .	114
6.3	<b>Study Two.</b> Agent volume: optimization and robustness . . . . .	115
6.3.1	Optimization of PIP2-profilin functions . . . . .	117
6.3.2	Agent projection with optimized PIP2 function . . . . .	119
6.4	<b>Study Three.</b> The role of profilin: recycling or saturation? . . . . .	119
6.4.1	Dynamics of profilin recycling . . . . .	120
6.4.2	Finding the Critical Saturation Point and optimized profilin parameters . . . . .	124
6.5	<b>Study Four.</b> The role of cofilin: actin recycling in the Cellanimat . . . . .	128
6.5.1	Deterministic P(LOSS) . . . . .	129
6.5.2	Results . . . . .	129
6.6	<b>Study Five.</b> The extent of an optimal TP . . . . .	130
6.6.1	Receptor density optimization . . . . .	130
6.7	<b>Study Six.</b> Compositional dynamics with the optimized model . . . . .	131
6.7.1	Phagocytosis . . . . .	132
6.7.2	Chemotaxis . . . . .	132
6.8	<b>Study Seven.</b> Saturation GA, evolution of an optimal parameter set . . . . .	132
6.8.1	Crossover and mutation . . . . .	133
6.8.2	Fitness Function . . . . .	134
6.8.3	Results . . . . .	135
6.9	Summary . . . . .	137
<b>7</b>	<b>A case study in morphological plasticity: diatom colony formation</b>	<b>138</b>
7.1	Background . . . . .	138
7.2	Three example genera . . . . .	141
7.3	Possible reasons for colony formation . . . . .	144
7.3.1	Sexual reproduction . . . . .	145
7.3.2	Fluid flow . . . . .	145
7.3.3	Defence against grazers . . . . .	145

7.3.4	Sinking rate increase or decrease? . . . . .	145
7.3.5	The null environmental hypothesis . . . . .	147
7.3.6	Summary and environmental hypothesis . . . . .	147
7.4	Morphogenetic mechanisms . . . . .	148
7.4.1	Schmid's tricornate spine mechanism . . . . .	149
7.4.2	Pickett-Heaps' seta formation mechanisms . . . . .	149
7.5	Summary . . . . .	151
<b>8</b>	<b>The Cellanimat Colony Model</b>	<b>153</b>
8.1	Overview of the Cellanimat Colony Model mechanism . . . . .	154
8.1.1	The Colony Environment-Phenotype Map . . . . .	155
8.1.2	Hypotheses . . . . .	155
8.2	Initialization . . . . .	155
8.3	Cellanimat . . . . .	159
8.4	Silica deposition: re-implementing the Nature's Batik Model . . . . .	160
8.4.1	Blocks . . . . .	161
8.4.2	Silica . . . . .	164
8.5	The EP functions . . . . .	165
8.5.1	EPa: Activation (type 2-active) . . . . .	165
8.5.2	EPb: Obstacle (type 2-passive) . . . . .	166
8.5.3	EPc: Redistribution (type 3-active) . . . . .	166
8.5.4	Height and interlocking spines . . . . .	168
8.5.5	WASP activation investigation . . . . .	168
8.5.6	Clear ArtCyto . . . . .	170
8.5.7	Quantification of Connectedness . . . . .	172
8.5.8	Light, time and structure . . . . .	173
8.6	Results . . . . .	175
8.6.1	A larger version . . . . .	177
8.7	Discussion . . . . .	182
8.7.1	Future study: Dominant Spines . . . . .	185
8.7.2	Predictions and suggested experimentation . . . . .	186
<b>9</b>	<b>Summary and conclusions</b>	<b>188</b>
9.1	Summary . . . . .	188
9.1.1	Specific contributions . . . . .	191
9.2	Conclusions . . . . .	192
9.3	Future work . . . . .	193
9.3.1	Biological modelling . . . . .	193
9.3.2	Cellanimat properties as a developmental/adaptive system . . . . .	193

9.3.3 Applications in other domains . . . . .	194
<b>Appendices</b>	<b>196</b>
<b>A Basic shape and pattern generative algorithms</b>	<b>197</b>
A.1 Cellular Automata . . . . .	197
A.2 L-systems . . . . .	197
A.3 Reaction Diffusion . . . . .	198
A.4 Agent Swarms . . . . .	199
<b>B Glossary</b>	<b>200</b>
B.1 Cell Biology terms . . . . .	200
B.2 Diatom related terms . . . . .	202
<b>Bibliography</b>	<b>206</b>

# List of Figures

1.1	Thesis Scope . . . . .	15
2.1	Traditional animat . . . . .	21
2.2	Direct encoding . . . . .	22
2.3	Golem project . . . . .	23
2.4	Karl Sims creatures . . . . .	25
2.5	Sims brain/body division . . . . .	25
2.6	Braitenberg vehicles . . . . .	28
2.7	Passive Dynamic Walker . . . . .	29
2.8	Kawai's linear cluster robot . . . . .	33
2.9	Swarm bots . . . . .	35
3.1	SEM image of diatom <i>Mastogloia</i> . . . . .	41
3.2	(a) Centric diatom <i>Arachnoidiscus sp.</i> , (b) pennate diatom <i>Diploneis heemskeriana</i> . . . . .	41
3.3	<i>Craspedostauros australis</i> almost complete valve . . . . .	44
3.4	<i>Craspedostauros australis</i> morphological features labelled. . . . .	44
3.5	<i>Craspedostauros australis</i> early Raphe development . . . . .	45
3.6	<i>Craspedostauros australis</i> forming virgae and vimines . . . . .	45
3.7	Nature's Batik Model schematics . . . . .	47
3.8	(a) Radiating striae. (b) Pore centers placed within striae. . . . .	49
3.9	<i>Gomphonema truncatum</i> offset pores . . . . .	49
3.10	Evolved valves with Nature's Batik Model . . . . .	53
3.11	Frames showing the growth of valve <i>d.</i> . . . .	53
3.12	Frames showing organic material . . . . .	54
3.13	Three stages during growth of one evolved valve . . . . .	55
3.14	Valves grown with hand specified genotypes using larger resolution and offset pores . . . . .	56
4.1	The cell and cytoskeleton . . . . .	59
4.2	Actin monomer polar binding sites . . . . .	60
4.3	Actin filament branching in real cells . . . . .	61
4.4	Actin filaments in a human fetal lung fibroblast cell . . . . .	62
4.5	Cytoskeletal accessory proteins . . . . .	64

*List of Figures*

10

4.6	Actin recycling through filaments . . . . .	65
4.7	Flow diagram of cellular morphological plasticity . . . . .	66
4.8	comparison of traditional Animat and Cellanimat architecture . . . . .	67
4.9	Cellanimat schematic . . . . .	68
4.10	Protrusions E-P Map EP <sub>1</sub> function for filament formation . . . . .	71
4.11	Filament formation EP <sub>1</sub> function in practice. . . . .	71
4.12	Cellanimat pseudo code . . . . .	73
4.13	creation diagrams and key . . . . .	75
4.14	Voxel substates . . . . .	75
4.15	Transduction Pathway pseudo code . . . . .	78
4.16	Diagrams of Cellanimat in progress through the assessment rules . . . . .	79
4.17	Actin agent states . . . . .	80
4.18	Detailed diagram of agent state changes during binding events . . . . .	82
4.19	Actin agents bound in filaments further substates representing polarity . . . . .	83
4.20	Detailed diagram of agent state changes during disassociation . . . . .	83
4.21	Actin agent orientation calculation . . . . .	84
4.22	diagrams showing the membrane contraction and tidy functions in action . . . . .	85
4.23	Nucleator agent states . . . . .	86
5.1	Schematic of chemotaxis stages . . . . .	91
5.2	Initial view of Cellanimat in its environment . . . . .	92
5.3	Graph showing average Cellanimat chemotaxis performance . . . . .	94
5.4	Graph explaining the peak in chemoattractant exposure . . . . .	94
5.5	Cellanimat chemotactic morphologies compared to real fibroblast cell . . . . .	95
5.6	The four stages of phagocytosis . . . . .	98
5.7	Initial views of Cellanimat in environment A and B . . . . .	99
5.8	Graphs showing averaged performance . . . . .	101
5.9	Screenshots of chemotaxis in environment A . . . . .	101
5.10	Zoomed in screen shots showing filamentous structure . . . . .	102
5.11	Screen shots showing phagocytosis throughout the different experiments . . . . .	102
5.12	Morphometrics calculations . . . . .	103
5.13	Screen shots of one phagocytosis run . . . . .	104
5.14	Screen shots of one run of extreme ingestion . . . . .	105
6.1	Cellanimat compositional dynamics during chemotaxis . . . . .	109
6.2	Detailed screen shots of chemotaxis . . . . .	110
6.3	Cellanimat compositional dynamics during phagocytosis . . . . .	111
6.4	Protein redundancy results . . . . .	113
6.5	Pseudo code for the new WN rule . . . . .	115

6.6	Diagram of the new WN rule in practice . . . . .	115
6.7	2D projection results varying agent volumes during phagocytosis . . . . .	117
6.8	Frequency graph of instances of 'no behaviour' as agent volume varies . . . . .	118
6.9	Pseudo code of new PIP2 release function . . . . .	118
6.10	Average sum of profilin detected by activating actin agents . . . . .	121
6.11	Averaged amount of profilin removed in PrUptake function . . . . .	122
6.12	Frequency charts showing failure rate of the PrRelease function . . . . .	122
6.13	Pseudo code for the original and new versions of the PrUptake rules . . . . .	124
6.14	Validation of new PrUptake rule . . . . .	125
6.15	Effects of profilin recycling . . . . .	126
6.16	2D projection results varying profilin parameters . . . . .	127
6.17	1D cofilin projection . . . . .	129
6.18	Effects of WASP radius of activation . . . . .	131
6.19	1D projection varying P(REC) . . . . .	132
6.20	Compositional dynamics with the Updated Model during chemotaxis . . . . .	133
6.21	Compositional dynamics with the Updated Model during phagocytosis . . . . .	134
6.22	Crossover in the Saturation GA . . . . .	136
6.23	Evolutionary dynamics of the Saturation GA. . . . .	136
7.1	<i>Aulacoseira granulata</i> colony . . . . .	139
7.2	Schematic of the euphotic zone in the water column . . . . .	140
7.3	<i>A. granulata</i> SEM images . . . . .	142
7.4	<i>Chaetoceros decipiens</i> colony . . . . .	143
7.5	General morphology of the genus <i>Skeletonema</i> . . . . .	144
7.6	Schmids Tricornate spines mechanism . . . . .	150
7.7	Pickett-Heaps proposed models for setae formation by the cytoskeleton . . . . .	151
8.1	Initial model layout views . . . . .	156
8.2	3D model as a stack of 2D slices . . . . .	157
8.3	Simulation structure . . . . .	157
8.4	Types of agent movement compared . . . . .	160
8.5	Side views of agents in cells . . . . .	160
8.6	Silica deposition stages through the dimensions . . . . .	161
8.7	Dimensionality in growth process in SEM of <i>Diadesmis</i> . . . . .	161
8.8	Side views of silica deposition in model . . . . .	162
8.9	Side views of silica and blocking material in model . . . . .	163
8.10	Slice through view of block and rib centres . . . . .	163
8.11	The growing SDV in the Cellanimat Colony Model . . . . .	166
8.12	The four stages of the Mchange rule . . . . .	167

8.13	3D space required for filaments to push into sister cell . . . . .	168
8.14	WASP activation regimes . . . . .	169
8.15	WASP activation regimes effects on morphology . . . . .	171
8.16	<i>Diademsis</i> SEM showing interlocking spines resistance to separation . . . . .	172
8.17	The Connectedness quantification . . . . .	173
8.18	Timing effects on morphology . . . . .	175
8.19	Screen shots of morphology through the 3D stack with low delay setting . . . . .	176
8.20	Screen shots of morphology through the 3D stack with high delay setting . . . . .	176
8.21	Frequency distribution of Connectedness values obtained . . . . .	177
8.22	(a) interlocking dovetail joints in Env A (b) separation spines in Env B . . . . .	177
8.23	slice through view of interlocking valves . . . . .	178
8.24	slice through view of separation valves . . . . .	178
8.25	Separation valves grown in larger version in Env B . . . . .	179
8.26	Silica deposition study of separation valves grown in larger version in Env B . . . . .	180
8.27	Linking valves grown in Env A with larger version . . . . .	181
8.28	Side views of larger version linking valves grown in Env A . . . . .	182
8.29	Silica structures of larger version linking valves grown in Env A . . . . .	183
8.30	Single Cellanimat views of larger version linking valves grown in Env A . . . . .	184
8.31	Dominant spine formation . . . . .	185
9.1	preliminary ‘ball catching’ Cellanimat experiment . . . . .	195
9.2	Schematic of collective robotics version of Cellanimat . . . . .	196
A.1	CA neighbourhood . . . . .	198
A.2	Example L-system . . . . .	198
A.3	Reaction diffusion diagram . . . . .	199

# List of Tables

2.1	Summary of activity in Paul (2004) XOR robot. . . . .	30
2.2	Taxonomy of morphological plasticity in AI compared with natural systems. . . . .	37
2.3	Brief overview of research progression . . . . .	39
3.1	Possible states for grid cells and their classes. . . . .	46
3.2	Static parameters and their usual setting in experiments . . . . .	51
3.3	The genes, their order in the genotype and the possible ranges for each. . . . .	51
3.4	The sample of evolved valve's fitnesses and genotypes . . . . .	54
4.1	The subsystems of the Cellanimat. . . . .	68
4.2	The protein selection used in the Protrusions E-P Map example. . . . .	72
4.3	Cellanimat threshold parameters. . . . .	74
4.4	2D Cellanimat creation parameters. . . . .	74
4.5	Cellanimat agent attributes . . . . .	77
4.6	Cellanimat acronym descriptions . . . . .	80
5.1	The parameters used in experiment A: chemotaxis . . . . .	92
5.2	The default Cellanimat parameter settings. . . . .	98
5.3	The default Cellanimat parameter settings. . . . .	101
5.4	Averaged behavioural results (distance or engulfment); Chemo t=100, Phago t=250 . . .	103
6.1	Protein redundancy results . . . . .	114
6.2	Redundancy results using new WN rule . . . . .	116
6.3	Genes and their viable parameter ranges . . . . .	135
6.4	Highest scoring genotype. . . . .	137
7.1	Table showing the adaptive strategies in the evolution of phytoplankton . . . . .	141
7.2	Table showing the logical possibilities for sinking rate dynamics and related triggers . . .	148
8.1	Model creation parameters . . . . .	158
8.2	Model assessment parameters . . . . .	164



## Chapter 1

# Introduction

Organisms in nature exhibit complex adaptive behaviours that far surpass the ability of current state-of-the-art autonomous software and robotics. To understand intelligence and inspire new technology it is therefore prudent to closely study and indeed imitate natural systems. This thesis is an interdisciplinary exploration of the interplay between design and adaptive behaviour in natural and artificial systems.

The idea that embodiment is fundamental to intelligence (Brooks, 1991a) has hailed a new era in AI, in which the body plays an increasingly important role. Morphogenesis, ‘the generation of morphological form’ (e.g. body shape, structure and colour) is fast becoming a key research theme in AI (Capcarrere, M. S., Freitas, A. A., Bentley, P. J., Johnson, C. G. and Timmis, J., 2005). Understanding morphogenesis could aid the design of efficient devices. Morphogenesis could provide a more scalable and robust methodology for the design of well-adapted AI systems and devices (Goodwin, B. C. et al., 1993; Bentley, 1999a) but research currently is far from delivering all the answers. The open challenge in AI is to design systems able to cope within increasingly complex and changeable environments (Wilson, 1990). System morphologies in AI tend to be grown or optimized for a single environment/task and cannot adapt to cope with changing environments (Eggenberger, 1997; Hornby, G. and Pollack, J., 2001a; Iida, 2005). Adaptive behaviour mechanisms have almost exclusively focused on brain-centric models, ignoring exploitation of morphological properties for improved performance (Floreano, D. and Urzelai, J., 1999; Harvey, I. et al., 1996). As such this thesis strives for a new direction: adaptive morphological designs for systems up to the challenge of changeable environments.

Intelligent systems research has a dual aim to both create artificial intelligent/adaptive systems and understand intelligence (Floridi, 1999). This thesis aims to investigate the role of morphologies in adaptive behaviour, as related to both these objectives through: 1) the creation of a novel bio-inspired computer model and 2) constructivist modelling of biological systems to gain a deeper understanding in natural systems.

It is the fundamental argument of this thesis that *morphological plasticity* (MP) is a key factor in 1) generating adaptive behaviour without a brain (‘no brainer’ adaptive behaviour) and 2) the development of morphologies well-adapted to changing environments. Morphological Plasticity is the environmentally induced variation in growth or development (Piersma, T. and Drent, J., 2003). Through adaptive growth in relation to the environment morphological designs can stay well-adapted, in spite of environ-

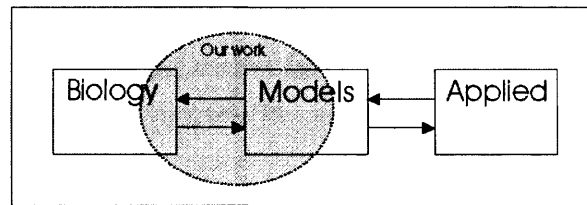


Figure 1.1: The three stages in bio-inspired design of artificial intelligent systems. This thesis fits in at the early stages of research development, at the interface of modelling with biology with contributions in both directions.

mental changes, and adaptive behaviour can be generated by the re-organisation in form. Understanding morphological plasticity could aid the production of systems that can autonomously adapt their design, during the system's 'lifetime', to changes in the problem space.

It was of course necessary to limit investigations and set achievable targets. To that end a single celled organism the diatom was used as a biological case study throughout. Two other animal cell types were also modelled. Single celled organisms were chosen as they exhibit morphological dynamics that surpass those of multicellular organisms. Due to its fluid nature, a unicell can rapidly reorganize its entire inner structure and outer body shape, transport organelles from one side to the other and even split itself in two; all in direct response to environmental changes (Alberts, B. et al., 1994).

Specifically this thesis is based on a detailed study of diatom valve morphogenesis. Diatoms construct beautiful, intricate siliceous structures around themselves improving survivability (Round, F.E. and Crawford, R. M. and Mann, D. G., 1990). To this date no consensus has been reached on how a single cell performs such a feat. This intriguing example of morphogenesis could illuminate useful mechanisms, not just for AI, but also for nanotechnology, due to the nano-level synthesis of silica structures involved (Gordon, R. and Parkinson, J., 2005). Diatom morphogenesis involves a high level of plasticity to the environment (Trobajo, R. et al., 2002). Diatom colonies are a fascinating example of morphological plasticity to cope in a fluctuating niche, they play a central role in this investigation.

The grand research scheme: 'designing bio-inspired artificial adaptive systems for complex environments' can be divided into three stages: 1) biological research; 2) modelling of biology, qualitative or quantitative; 3) bio-inspired models applied to non-biological problems. Each stage can produce results that feedback into the previous stage, thus enlarging understanding of intelligence in natural systems as well as informing artificial intelligent system design. It was not within the scope of this thesis to attempt to work at every stage of this process. Fig. 1.1 shows where the work in this thesis fits in, contributing to both computing and biology.

Without matching living systems in detail cellular automata and agent based models (see Appendix A), favoured models in this thesis, can still show that some set of mechanisms or rules is sufficient to generate the phenomenon of interest (Holland, 2003; Hogeweg, 2000). They are more computationally efficient than mathematical models and relate more closely to biologists' conceptualization, breaking down the language barrier in interdisciplinary collaboration. Holland (2003) noted that it is not easy

to build analytic equation based models to describe embryogenesis (developmental process of egg to embryo), and even if this were managed, the usual tools for analyzing such systems, such as determination of fixed points or statistical analysis, offer few insights. This thesis has the following overarching hypotheses and objectives:

### **Primary Hypothesis**

A Biologically-based morphological plasticity algorithm, in the absence of a centralized controller, can generate adaptive behaviour and a well-adapted morphology in an animat in a changing environment.

### **Secondary Hypothesis**

Morphological plasticity simulation can be used to formulate a biological hypothesis to identify key issues for further biological experimentation.

### **Objectives:**

- 1 Investigate diatom morphogenesis to provide biological inspiration for new artificial systems.
- 2 Create a novel algorithmic model based on MP.
- 3 Show the model can generate adaptive behaviour/design in changing environments.
- 4 Investigate the properties of the model.
- 5 Use the model as a test bed to formulate a new hypothesis of MP in diatom colony formation.

## **1.1 Thesis Overview**

Chapter 2 contains a review of morphologies in AI, emphasizing the increasing role that the body plays in AI research and our concept of ‘intelligence’. It will be argued that morphological plasticity is at the cutting edge of AI research. A review of the state of the art in morphologically plastic systems is given as well as a history of non-plastic morphogenesis in AI. The term ‘Dynamic Morphology’ will be introduced, for systems capable of MP, and a taxonomy of MP in AI presented.

Chapter 3 introduces diatoms, their morphogenesis and plasticity. Starting simply, first the non-plastic morphogenesis case is considered. The ‘Nature’s Batik Model’, a cellular automata model of diatom valve morphogenesis, is presented, so called because it works on the premise that silica is deposited around an organically produced template similar to the artistic method of Batik (Schmid, 1980). A genetic algorithm was used to evolve valves using a fitness function selecting for functionality rather than aesthetic value, showing that the simulated valves were functionally similar to real diatoms. This chapter addresses Objective One of the thesis.

The Nature’s Batik Model was however very abstracted and simple. It did not explain how the ‘organic template’ was formed or controlled. It was only a first step in the quest to understand and harness morphological plasticity mechanisms. Most cellular morphological behaviours are executed by

the *cytoskeleton* (Alberts, B. et al., 1994). The cytoskeleton is a complex distribution of proteins which acts as a transport network, contractile muscle and/or structural support. Due to its non-rigidity it can rapidly disassemble and reform in a more advantageous distribution. The organic template in diatom morphogenesis is believed to be no exception (Schmid, 1980). Thus in Chapter 4 focus moves to the cytoskeleton to understand MP mechanisms.

‘The Cellanimat’, powered by the ‘Artificial Cytoskeleton’ (ArtCyto) mechanism, utilizing cellular automata and agent swarm techniques based on cytoskeletal dynamics, is also fully introduced and described in Chapter 4. The Cellanimat was designed to satisfy Objective Two. Morphology and behaviour in the Cellanimat are determined at every time step by direct environmental interaction rather than through gene expression. Consequently the Environment-Phenotype Map (E-P Map) framework is introduced and defined as the generator of morphology rather than the traditional genotype-phenotype map.

Results are given in Chapter 5 of the Cellanimat, with a single E-P Map, performing both chemotaxis and phagocytosis due only to a change in the environment, thus tackling Objective Three. It is shown that, through morphological plasticity, a single system can generate well-adapted morphology in a changing environment and adaptive behaviour through the body alone.

In Chapter 6 seven studies are detailed giving full insights into the Cellanimat model dynamics, properties and optimization, addressing thesis Objective Four. Redundancy, robustness, parameter sensitivity and evolvability are examined, and in some cases improvements to the original model functions are made. Results are given of a genetic algorithm optimizing the Cellanimat parameters for speed at a phagocytosis task.

Objective Five is addressed in the final chapters of the thesis, returning to the diatom morphogenesis case study armed with the Cellanimat test-bed environment. In Chapter 7 the context of the problem is set, introducing the MP involved in diatom colony formation and fully critiquing current theories on the mechanisms involved. This chapter also serves as further fulfilment of Objective One. In Chapter 8 the Cellanimat Colony Model is presented, as an aid at the hypothesis formulation stage, to further understanding of morphological plasticity in natural systems.

The use of simulations for hypothesis formulation in biology works as follows: 1) well-founded, proven aspects of the process in question are combined with new ideas to form a complete model; 2) the model is simulated and the new aspects refined until the observed behaviour can be generated; 3) predictions are made from the model for biological experiments to test the new hypothesized elements; 4) experiments then validate/counter the hypothesized aspects leading to new information to incorporate into the model. This simulate-predict-test cycle can be repeated until all aspects of the model are considered to be well-founded and understood.

The Cellanimat Colony Model consists of two Cellanimats back-to-back performing ArtCyto-driven interactive growth whilst a 3D extension of the Nature’s Batik Model deposits silica. It is shown that given a single E-P Mapping both morphologies associated with diatom colonies (and the associated adaptive behaviour) can be generated, due only to a change in the environment. The simulation is used

as a test bed to investigate aspects of the process, by no means fully understood at present, in order to stimulate further discussion.

Brooks (1991b) outlined three distinct levels in complete creature design: Micro (relationship between perception-internal-action), Macro (how all the micro level systems integrate into a complete creature) and Multitude (how lots of creatures interact). Brooks concluded that many, limited in scope, theories and methodologies towards complete creature architectures will be developed, but from them global unified theories can be developed using the experience. The Cellanimat colony model is an example of a system working at all three levels; it shows how local morphological plasticity in a single cell, generated by micro level processes, can result in a global gain for a collective system.

In Chapter 9 the advances and limitations of the work presented in this thesis, and the extent to which we have achieved the given objectives and proved the hypotheses, are discussed. Several avenues for future work are outlined. A basic introduction to generative algorithms commonly used for shape and pattern formation, as utilized by models described in this thesis, are given in Appendix A. A Glossary of the biological terms used throughout this thesis can be found in Appendix B.

## 1.2 Publications

The work in this thesis has been published in the following papers:

Bentley, K., Cox, E. J., Bentley, P. J. Nature's Batik: A Computer Evolution Model of Diatom Valve Morphogenesis. *Journal of Nanoscience and Nanotechnology* 5(1): 25-34. 2005.

Bentley, K and Clack, C. Morphological Plasticity: Environmentally Driven Morphogenesis. *In Advances in Artificial Life (Lecture notes in AI series) Proceedings of the Eighth European Conference on Artificial Life (ECAL '05)*. Capcarrere, M. et al. (eds). Pp. 118-127. Springer-Verlag. 2005.

Bentley, K and Clack, C. The Artificial Cytoskeleton for Lifetime Adaptation in Morphology. *In Workshop Proceedings of the 9th International Conference on the Simulation and Synthesis of Living Systems (Alife IX)*. Bedau, M., Husbands, P., Hutton, T., Kumar, S., Suzuki, H.(Eds.) Pp 13-16. 2004.

In addition the following papers are in preparation:

Bentley, K and Clack, C. The Cellanimat: dynamics and evolvability in an adaptive system with developmental plasticity.

Bentley, K, Cox, E. and Clack, C. A mechanism for diatom colony formation based on an *in silico* simulation study.

## Chapter 2

# Morphologies and AI: a review

In this chapter the question ‘*what does morphogenesis have to do with AI?*’ is answered. Starting at the beginning, the central concepts and goals of Artificial Intelligence (AI) research are introduced. The changing emphasis in AI from abstraction to embodiment, from controllers to morphologies, is discussed. The changing attitudes, landmark models, and past/present research directions are discussed, illustrating the progression of ideas towards the theme of this thesis: morphological plasticity for intelligent/adaptive behaviour in changing environments.

This review naturally arrives at a discussion of the biological concept of morphological plasticity, a new taxonomy of MP in AI is presented and the state of the art in situated, dynamic and plastic morphologies for the next generation of intelligent systems is discussed. A review of all generative design systems, applications and related AI work is however beyond the scope of this chapter. Instead, discussion is limited to research directly related to morphologies.

### 2.1 Intelligence, embodiment and philosophy: the rise of morphologies

AI began in the late 1950s. It is the interdisciplinary quest to understand cognition through computation, and ultimately to produce intelligent computer systems comparable in ability to humans (Floridi, 1999). As Floridi (1999) discussed, the early ‘good old fashioned AI’ (GOFAI) approach held that intelligence is body-independent and mind-independent. So, in principle intelligence was implementable in a computer, or more precisely by a “brainless, mindless and lifeless cognitive system enjoying no psychological or bodily experience nor any interaction with other similar systems” (Floridi, 1999). Intelligence was reduced to the processing of symbolic representations by syntactic rules, performed in isolation from the ‘real world’ (Fodor, 1975).

Traditionally, mind-independent intelligence is identified with *materialist monism*, where no distinction is seen between body and mind, mental events are considered nothing but neural events (Strawson, 2000). As Floridi noted, monism implies that intelligence is a direct manifestation of life and cannot be separated from the whole physical behaviour, bodily experience and natural interaction of a living organism with its environment (Floridi, 1999). GOFAI however, ignored this implication by claiming intelligence was also body-independent. Cognition was left completely abstract, severed from life, body

and environment and consequently AI systems remained far from achieving human-level performance.

'Nouvelle AI', pioneered by Brooks in the late 80's pulled AI back towards monism. (Brooks, 1991a) showed that intelligent behaviour could 'emerge' from lower level interactive behaviours of a system with its environment, such as movement and collision-avoidance. With Brooks' system there was no longer a need for complicated internal representations of the environment, as required by abstracted GOFAI models. With a body the system could simply exploit the real environment for information directly. High-level intelligent behaviour was shown to be achievable more simply in this manner, by the addition of lower level environment-system interactions rather than the design of a massively complex self-contained system. The aims of Nouvelle AI were considerably more modest however: to attain computational intelligence at the level of insects rather than human beings.

Intelligence was deemed inseparable from life and the bodily experience. Suddenly the body was centre stage in AI: *intelligence requires embodiment* (Varela, F. J. et al., 1993). Nouvelle AI, with its more monistic, matter-centred approach, began to have more in common with biology. Molecular biologists traditionally see no distinction between form (organisation) and matter (Emmeche, 1992). Physically instantiated systems in the 'real world' could potentially deliver next-level intelligent behaviour. Consideration now had to be given to materials and the morphological design of the system; bodies needed to be carefully constructed to maximize performance; the matter mattered.

Embodiment did not, however, necessarily imply that the abstract, *functionalist* approach to AI was dead. Functionalism is the philosophical doctrine that supposes psychological properties, such as intelligence, are *multiply realisable* (Emmeche, 1992). Although an object is a physical thing, the property of being that object is non-physical and can as such be realized in many different ways. So, embodiment itself could potentially be realized in abstraction from matter if the *organization* of the abstracted system and its environment satisfied requirements such that it was functionally similar to a physically embodied system (Quick, T. et al., 1999).

Functionalistic embodiment required a clear definition of embodiment, in terms of the *organization* of material with its environment, rather than the material or physics itself. Autopoiesis, introduced by Maturana, H. and Varela, F. J. (1980) holds still as the most reasonable definition of the organisation of life within an environment and forms the basis of most ideas of embodiment. "An autopoietic system is organised (defined as unity) as a network of processes of production (synthesis and destruction) of components such that these components: 1) continuously regenerate and realize the network that produces them and 2) constitute the system as a distinguishable unity in the domain in which they exist." Autopoiesis is achieved through *structural coupling* with the environment, where the organization of the system can be altered by the environment and vice versa.

Quick, T. et al. (1999) provided a clear functionalistic definition of embodiment, which could be used to generate non-physical instantiations of nevertheless embodied intelligent systems. It is based on environment-system coupling and goes as follows: *A system X is embodied in an environment E if perturbatory channels exist between the two. That is if for every time t at which both X and E exist, some subset of E's possible states have the capacity to perturb X's state, and some subset of X's possible states*

have the capacity to perturb  $E$ 's state.

So Cognition, in Nouvelle AI, is seen as the product of changeable systems structurally coupled with their environment: *embodied dynamical systems*. Embodied cognition as an approach moved the modelling of intelligent systems from a representation-rich study of control systems as the originator of behaviour to the study of coupling dynamics *between* system and its environment (Almeida e Costa, F. and Rocha, L. M., 2005; Beer, 2000). The dynamical systems approach to cognition was introduced as a real alternative to the computational approach (Van Gelder, 1998). As such, high-level artificial intelligence is deemed possible, instantiated in abstract by computational systems or physically in the real world, provided that the system's organization is coupled with its environment.

The blurring of cognition and life, of adaptive behaviour and intelligent behaviour, led AI research away from purely human-brain based models. Focus moved to the adaptive behaviour of embodied agents in specific environments, based on a plethora of natural living systems from single cells to humans. The conventional approach to understanding intelligence through embodied agents is the *animat* approach (Wilson, 1990; Guillot, A. and Meyer, J-A., 2001). As Pfeifer summarized: "The animat approach is by definition synthetic. The underlying slogan is understanding by building... The way we build our animats is a manifestation of our views of intelligence" (Pfeifer, 1996). Animats are comprised of the basic components: sensors, controller and effectors. They exist within, and interact with, a given environment to generate adaptive behaviour/intelligence. Generally, the 'morphology' of an animat is comprised only of the sensors and effectors, the controller, or processor, is abstracted, seen to control the morphology from somewhere within the body casing. See Fig.2.1.

The Animat approach was well suited to facilitate embodied intelligence studies through simulation and real-world robotics. Controller design and optimization, for a given morphology (usually a Kephra robot in evolutionary robotics studies (Mondada, F. et al., 1993)), dominated the field for many years, and is still a strong area of AI today, e.g. (Harvey, I. et al., 1996; Nolfi, S. et al., 1994). It soon became clear however, that optimization of the morphology itself, of the sensor and motor distributions and overall shape, weight and size could also improve performance. Naturally, Nouvelle AI arrived at morphological research, optimising the body, for the improvement of the system-environment coupling and thus of intelligent behaviour.

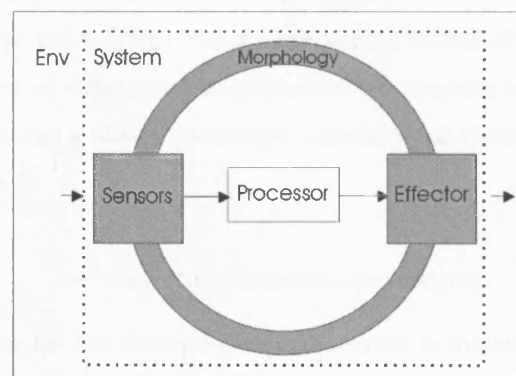


Figure 2.1: Schematic of the traditional animat design with morphological components shown in grey.



## 2.2 In the beginning: direct encoded morphologies

“The observation can be made, however, that evolution of a creatures controlling brain is just one part of the problem of artificial evolution of life — a creature that adapts to an environment needs an adequate body to inhabit.” (Funes and Pollack, 1998)

The hand design of optimal animat morphologies, physical or simulated, is a hard task. Evolutionary algorithms had been used to find optimal solutions to many other types of problem (Ogarty, 1994; Bentley, 1999a), so it was a natural first step to use them to generate optimized system morphologies. Design automation and optimization is a field in its own right with many applications, such as furniture design, artificial art and architecture, though discussion here is limited to animat based models (Bentley, 1999b, 2002; Coates, P. and Carranza, P. M., 2000; Bentley and Corne, 2002).

There are many different ways to represent a shape, e.g. with lines of different lengths and curvature, as a collection of smaller units or with equations. The simplest way to encode a shape as a string of numbers in a genotype is with a *direct encoding*. In a direct encoding each gene relates directly to an aspect of the shape, the morphology. The values could correspond to elements of the shape (where the genotype is the phenotype) as implemented by Chapman, C. D. et al. (1993) and shown in Fig.2.2. Or the genes could be parameters determining positions and sizes of the shape.

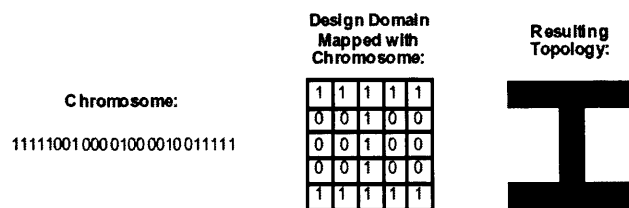


Figure 2.2: Direct genotypic encoding of shape, reproduced from (Chapman, C. D. et al., 1993) with permission.

The inspired Golem project (Lipson, H. and Pollack, J., 2000) used direct encoding to generate the brain and body of robots that were subsequently printed out using a 3D printer (rapid prototyping), see Fig.2.3. Morphologies, and controllers, were evolved to optimize a given task: locomotion ability on an infinite plane. The genotype was a string of values representing packets of direct information as below. Where, bars connected vertices with a given length and stiffness, neurons had associated thresholds and coefficients of connections, and actuators could move a specified bar according to the output of a given neuron within a certain range.

$$\langle vertices \rangle \langle bars \rangle \langle neurons \rangle \langle actuators \rangle. \quad (2.1)$$

This was by no means the first instance of neural network evolution, nor of structure evolution, but it was one of the first and clearest examples of the evolution of both morphology and controller in simulation with successful, and mostly automated transfer to the real world. The generation of complete creatures as discussed by Brooks (1991b) has fast become a major stream of Nouvelle AI research. The

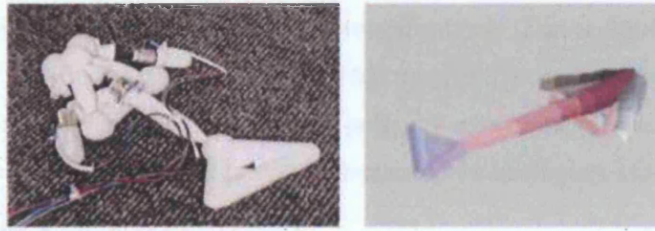


Figure 2.3: Evolved morphology and controller as part of the Golem Project, left shows the printed out robot, right shows it in simulation. Reproduced from (Lipson, H. and Pollack, J., 2000) with permission.

recognition of bodily and environmental importance in intelligence meant that a cognitive system had to have all bodily aspects considered in the design process, not just features of abstracted networks. The golem project followed the view that embodiment requires a physically instantiated body in the real world - the simulated creatures were only a means to an end.

Though the design stage of the project was automated, it should be noted that the actual building of the golem robots still had to be finished by hand. Actuators and circuitry had to be implanted within the printed out structure as technology for this was not yet in place. However, this work showed in principle that embodied intelligent systems could be designed and generated by non-human means; through the evolutionary algorithm, design could be optimized for a given task and environment in ways that may not have occurred or been comprehensible to a human or been possible to manufacture by conventional methods (Lipson, H. and Pollack, J., 2000).

## 2.3 Importance of development: indirect encodings

The direct encoding approach was limited. It did not scale-up, with more complex morphologies the genotypic complexity also increased, resulting in combinatorial explosion for highly complex phenotypes (Roggen, D. and Federici, 2004). The bio-inspired approach of *indirect encodings* followed, addressing the scalability issues in morphological design.

In nature, highly complex phenotypes are produced by comparably small genotypes through the process of *development*. In nature, genes do not specify morphological features directly, but rather, through genetic regulation, they determine protein synthesis regimes which then generate a hierarchy of structural organisations. Protein-protein interactions produce higher-level structures within and between cells. Cells, within multicellular organisms, display a further level of morphological organization, as they adhere, move, divide and die. Thus the morphology of a creature can only be indirectly attributed to the genotype: the intermediate processes in the organisational hierarchy are essential to the resultant morphological complexity. Development increases the phenotypic complexity possible from small gene strings, by reuse of genes and hierarchical self-organization of produced components.

### 2.3.1 Developmental Algorithms and Computational Embryology

Developmental algorithms indirectly map genotype to phenotype. Although development, as a term, can refer to the growth of a morphological feature at any point in the life-cycle, most developmental algo-

rhythms are in fact *embryogenies*, modelling early development only (Kumar, 2004). An Embryogeny is defined in (Bentley and Kumar, 1999) as having the following two properties: 1) an indirect correspondence between alleles and phenotypic effects and 2) polygeny, where multiple genes act in combination. Bentley and Kumar (1999) defined three types of computational embryogeny, as follows:

- **External:** hand-designed and not evolved.
- **Explicit:** Evolved but every step of the growth process is explicitly specified by the user.
- **Implicit:** Evolved, growth process generated by interaction of low-level components.

Most developmental algorithms to date are explicit embryogenies (Bentley and Kumar, 1999). The main problem with explicitly defined algorithms is that once again human design of a complex system is required. Instead of the morphology, now the growth process must be defined, but the same problems exist: the more complex the required morphology is, the more difficult the task of designing the developmental algorithm becomes (Kumar, 2004). The aim of this thesis is to explore a more implicit method of growth, utilizing low-level rules based on real biological systems, to generate growth without human design bias or limitations.

### 2.3.2 Virtual creatures

A number of full reviews of work in this particular area, using evolution and developmental algorithms to optimize simulated/real robot morphologies and controllers have already been made (Taylor, T. and Massey, C., 2001; Pfeifer, 2004; Lungarella, M. et al., 2004) so discussion here is limited to a selection of classic examples.

Karl Sims's Virtual Creatures (Sims, 1994a,b) are the classic example of an evolved, explicit embryogeny for the development of brain and body in physically simulated animats. Directed graphs were used as the genetic representation, giving instructions for the iterative building process of body and brain. This type of representation allowed reuse of instructions to generate recursive structural components, similar to L-systems (see Appendix A.2 for an introduction to L-systems).

The morphologies were composed of articulated 3D rigid parts connected together with joints of various types. A body part could contain a contact sensor, joint angle sensor or photosensor. Internal neurons, not associated with any part of the body were evolved to perform certain functions on the sensor inputs and return values to the effectors. The effectors then exerted a force, on the associated joint, moving the body.

Creatures were evolved for a single task, either walking, jumping or swimming within a physically simulated world with aspects such as articulated body dynamics, collision detection/response and friction. Some of Sims's evolved creatures can be seen in Fig.2.4. The diagram in Fig.2.5 is taken from the same paper and highlights the inbuilt division in many developmental models between the body, physically instantiated in the world, and the brain, abstracted from the body but fundamentally orchestrating the intelligent behaviour.

Sims's creatures, as noted by Funes (2001), behaved according some physical laws but lacked other reality constraints. E.g. blocks overlapped and movements were not motor generated. Funes's

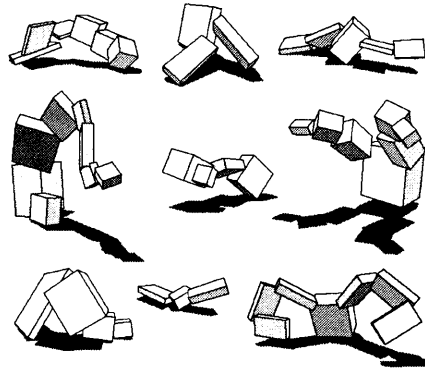


Figure 2.4: Evolved morphology of Karl Sims Virtual Creatures for walking, reproduced from (Sims, 1994a) with permission.

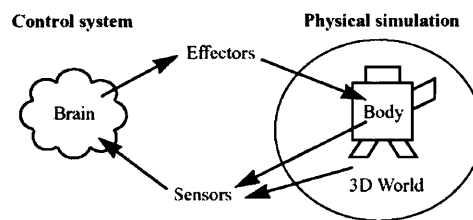


Figure 2.5: The relationship between brain, body and world in Sims work, indicating the division between brain (abstract) and body (physical), reproduced from (Sims, 1994a) with permission.

work represented the first attempt at reality constrained evolution of brick based structures using indirect encoding. The morphologies were simulated then built in the real world, for such tasks as bridging gaps and holding external loads. Funes and Pollack (1998) presented their morphologies as ‘adaptive physical designs for robots’. However, adaptation in form only occurred across evolutionary timescales, the morphology remained static in design over the ‘lifetime’ of the system, and was more architectural in function rather than animat/robot based. However, principles in crossing the ‘reality gap’ in morphology design, useful to robotics, were discussed.

Hornby and Pollack’s work using L-systems as the generative encoding for evolved morphologies for locomotion tasks (Hornby, G. and Pollack, J., 2001b) and later co-evolved brains and bodies (Hornby, G. S. and Pollack, J. B., 2001) showed the power of indirect encodings with recursive elements. L-systems were used to encode for the different joints and positionings within the creatures morphology. The structures were evolved for motility across given surfaces in simulation. The grammatical, developmental encoding meant that the creatures obtained a far more natural look and a great many more parts than in previous research (Hornby, G. and Pollack, J., 2001b).

The Hornby and Pollack model once again followed a ‘grow then test’ methodology where growth occurred before the creatures entered the environment and the morphological design remained set for the rest of its ‘lifetime’. The same is true for many of the other landmark models in developmental algorithms research, e.g. Delleaert and Beer’s multicellular based model of morphogenesis involving cell division (Delleaert, F. and Beer, R., 1996, 1994) and Bongard’s memorable sphere-based creatures for

block-pushing tasks (Bongard, 2001, 2003). Computational Development (Kumar, 2004) is an umbrella term that subsumes what was previously known as Computational Embryology. This distinction was made to avoid implications that the field only researches *early* development without environmental input. Development is an ongoing process spanning the entire lifetime of an organism. *Lifetime* adaptation in form is therefore one of the key aims of Computational Development, yet it has not been realized by current models.

### 2.3.3 The POE model

Sipper, M. et al. (1997) defined the POE model in order to partition work in bio-inspired hardware. POE stands for the three axes: Phylogeny, Ontogeny and Epigenesis. They define Phylogeny as the evolution of speciation, Ontogeny as the developmental process of a multicellular organism and Epigenesis as the combination of the system with its environment, resulting in learning and plasticity.

Epigenesis allows the small scale genotype, together with ontogeny, to define the large-scale complex phenotypes exhibited in nature. Epigenesis is the modification of systems within the organism (*innately* specified), through lifetime interactions with the environment (*acquired* specification of the system) (Sipper, M. et al., 1997).

This model betrays the non-plastic stance of the developmental algorithms movement. Ontogenies are used to grow more complex morphologies from small genotypes, without environmental input, and epigenesis is not often implemented as far as morphologies are concerned. But, in reality all developmental processes are plastic to some degree: as will be discussed in Section 2.6, the stages of ontogeny and epigenesis are far more blurred. Environmental interaction for example, cannot correctly be defined as occurring only after the formation of the individual. Throughout this thesis it will be shown that environmental interaction occurs at many stages of development and life to the adaptive benefit of the system.

Neural networks are the main example of models that do use epigenesis as defined here - learning reshapes the network structure, weights and connections e.g. (Floreano, D. and Urzelai, J., 1999). But, generally this stage is not modelled in terms of the morphology itself, i.e. in an 'embodied robot' only the neural network controller adapts to the environment, not the morphological 'casing'.

### 2.3.4 Advances and Limitations

Hornby, G. and Pollack, J. (2001b) performed a comparison between direct and indirect encodings. They showed that increased morphological complexity can be generated with indirect encodings. In this study evolution with a developmental algorithm (L-system) outperformed evolution with a direct encoding at an automated design problem. Indirect encodings have also been shown to be superior in terms of genotype size and convergence, precision and efficiency (Eggenberger-Hotz, 2004). They are more scalable and evolvable due to the reduction in dimensionality of the search space. The following list is a summary of the advantages of indirect encodings as laid out by Bentley (1999a):

- Reduction of search space - smaller gene sets
- Increased repetition in structures

- More complex forms
- Adaptation - fault tolerance

The benefits of developmental algorithms reach further than simply improving on morphology optimization methods. Development as a process has many interesting properties, in addition to scalability and evolvability, it has been shown to improve the robustness of designs through adaptability and self-repair (Miller, 2003; Ozturkeri, C. and Capcarrere, M. S., 2005). As Miller (2003) discussed, robustness is a big problem in the human design of hardware and circuitry. As technology becomes more complex it can become more costly in maintenance due to bad human design. Natural design processes, such as development, have in-built fault tolerance mechanisms which can and should be harnessed. Indeed the intrinsic robustness of morphogenesis mechanisms has been the subject of discussion for some time (Goodwin, B. C. et al., 1993).

The major limitation of developmental algorithms when applied specifically to animat morphologies, as exposed by the POE model, is the lack of *lifetime* development of morphologies where plasticity to the environment is possible. This can of course be justified by the short time span that the field has been in existence. Allowing developmental processes to continue throughout a creature's lifetime could increase performance and robustness, by allowing it to actually exploit the identified properties of self-repair and adaptation. Plasticity in morphology through situated lifetime development is seen to increase survivability in nature, as will be discussed in Section 2.6, and could be the next step towards animats capable of coping in more complex environments.

Research in developmental systems has remained, on the whole, controller-centric, or at least controller-dependent, following the original animat plan to the last where sensor and effectors, embedded within the morphology are controlled by an abstract 'brain' like network. The 'intelligence' of the system is seen to emanate from the controller and the morphology is seen more as a 'facilitator of cognitive powered adaptive behaviour' than as its producer (Paul, 2004). But the balance of roles for brain and body is shifting.

## 2.4 Shift in control: cheap design

"Now there is a trivial meaning of embodiment, namely that "intelligence requires a body". In this sense, anyone using robots for his or her research is doing work on embodiment... However, there is a non-trivial meaning of embodiment, namely that there is a tight interplay between the physical and the information theoretic aspects of an agent...By information theoretic implications of embodiment we mean the effect of morphology, materials, and environment on neural processing, or better, the interplay of all these aspects." (Pfeifer, R. and Iida, F., 2005)

In recent years the emphasis has started to shift away from controller-centric models in the favour of morphologies. Investigations focus more on the physical properties and dynamics of bodies coupled with the environment than on controllers coupled to the environment. Iida (2005) noted that this shift comes with a change in aims in robotics: from precise and separable modelling of body, environment

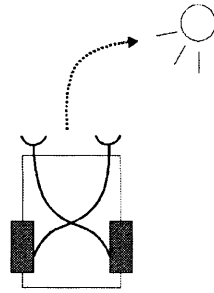


Figure 2.6: Schematic of a Braitenberg vehicle, the light sensors were connected directly to the opposite wheel motor. If the right sensor triggered the left wheel moved, leading the robot towards the light source.

and control architectures for reliable behaviour in static environments to adaptive, dynamical systems able to cope with changing environments.

It is clear from some of the models discussed in the previous section e.g. (Sims, 1994a; Hornby, G. and Pollack, J., 2001b; Bongard, 2001) that the evolved morphology may actually be doing some of the work, be *responsible* for whole or part of the intelligent behaviour (Pfeifer, 2000). This is the notion of *cheap design* (Paul, 2004; Iida, 2005) that well-adapted bodily design reduces the complexity and energy needed for control and power: controller complexity and the well-adaptedness of the morphology are inversely proportional. For further discussion of the controller-morphology tradeoff see (Pfeifer, R. and Scheier, C., 1999).

Taken to its logical conclusion: a morphology could be so well adapted that a controller is no longer required. In nature, many creatures survive without nervous systems, such as single cells. A seminal example of ‘no brainer’ cheap design, from the early days of Nouvelle AI, are Braitenberg vehicles (Braitenberg, 1984). Braitenberg vehicles had a morphology so well adapted to the task in hand (phototaxis) that they required no controller, see Fig.2.6. Indeed, cheap design was implied much earlier by Brooks (1991c), where he showed that embodiment would enable the use of simplified controllers requiring little or no representations.

#### 2.4.1 Passive Dynamic Walker

Through studies in robot motion ideas of cheap design emerged, where motion could be generated through the exploitation of physics alone. The passive dynamic walker is the classic example of cheap design, as shown in Fig.2.7, a passive dynamic walker, in its simplest form, is comprised of bars connected with knee joints, different weights are strategically attached which cause the structure to ‘walk’ when placed on a slope. It exploited the environmental physics and gradient, together with the body design to accomplish the seemingly complex task of human-like walking without the need for a controller.

The environmental dependence of the passive dynamic walker, the need for a slope, was overcome by the addition of a neural network controller which powered motion along flat surfaces (Endo, I. et al., 2002). Passive dynamic walkers are energy efficient and simple. As they are bio-inspired they are capable of producing very life-like behaviour and are potentially more adaptable to unpredictable terrain

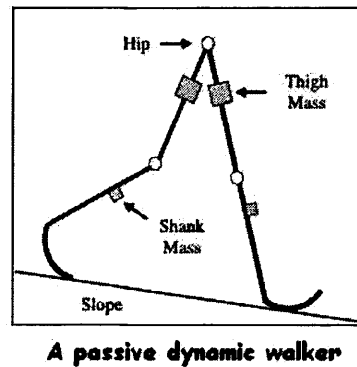


Figure 2.7: Schematic of the passive dynamic walking exploiting physics to generate realistic walking motion. Reproduced from (Vaughan, E. et al., 2004) with permission.

and changing environments. (Vaughan, E. et al., 2004) showed that gait changes, controlled by a Central Pattern Generator (CPG) regulated by sensor information, as in humans, could allow the walker to continue as terrain and gradients changed.

Though controllers were added to increase the potential of passive dynamic walkers control systems alone, without the crucial body design, could not have produced such realistic and efficient movement.

### 2.4.2 Morphological Computation and the XOR robot

Going beyond the idea that an embodied cognitive system can be decomposed into two distinct functional parts, where the controller performs computation and the body is physical, implies that the body can also be computational. This is the idea of *morphological computation* as introduced by Paul (2004).

Paul in (Paul, 2004) describes the XOR robot, it is a clear example of a morphology capable of computation, beyond the capabilities of its controller. Briefly, the XOR robot has one wheel and two motors. Motor A spins the wheel and motor B lifts the wheel off the ground. The robot controller is a perceptron network which classically cannot solve the non-linearly separable XOR problem. The OR output of the perceptron is linked to Motor A (output 1 causes it to lift) and the AND output is linked to motor B (output 1 causes it to spin). This means that if the two inputs to the perceptron are (0,0) then the wheel will not lift nor spin.

All possible inputs, outputs and robot motions are shown in Table 2.1. Through the *combination* of AND and OR outputs instantiated in the actual morphology, rather than in an extra layer of neural network nodes (as usually required to solve the XOR problem), the robot gave stationary or motile responses to the inputs in the correct order, solving the XOR problem.

The Fernando, C. and Sojakka, S. (2003) 'brain in a bucket' was a similar illustration of how material properties can generate the equivalent of a hidden layer in the perceptron, allowing it to solve the XOR problem. The bucket held water, again two motors representing the outputs of logical operations were used. The motors rippled the water and the four possible resulting interference pattern gave the solution of the XOR problem.



Input 1	Input 2	OR	Motor A	AND	Motor B	XOR	Robot
0	0	0	still	0	Ground	0	Stationary
0	1	1	spin	0	Ground	1	Motile
1	0	1	spin	0	Ground	1	Motile
1	1	1	spin	1	Lift	0	Stationary

Table 2.1: Summary of activity in Paul (2004) XOR robot.

### 2.4.3 Limitations

One major criticism frequently levelled at cheap design (Iida, 2005; Paul, 2004), is that it is environment-dependent. The argument runs: if the system exploits the environment to function then it is dependent on that environment and as such cannot cope with environmental changes and is not an adaptive system. This is indeed true for some cheap design systems, such as the basic passive dynamic walker, without the slope it would have no motion. However it was shown by Vaughan, E. et al. (2004) that cheap design combined with control can generate motion in changing gradients. The counter-argument put forward by Iida (2005) highlights the importance of cheap design to adaptive systems research in terms of cost, simplicity and for improving active exploration of environments by the incorporation of sensorimotor coordination.

The approach of designing task-specific systems through evolution in a single environment will inevitably incur problems if the environment changes. This is not a problem limited to cheap design. Indeed the method of designing/evolving a morphology that is structurally static throughout evaluation, i.e. cannot grow or change in response to the environment may inhibit adaptation to changing environments more than the cheap design principle itself, as with the grow then test methodology adopted by developmental algorithm studies.

Development is not often used in the design process for cheap design systems. They tend to be hand designed, requiring detailed engineering knowledge and/or physical robot building. Again, scalability becomes an issue and developmental encodings may need to be used in combination with the cheap design approach. One route to growing cheap design systems could be by evolving developmental algorithms to achieve a set task, in different environmental settings, whilst minimizing a cost function, ensuring efficiency and exploitation of the environment.

The dependence on environment of cheap design systems could be turned around to be an advantage. Dependence on the environment means that environmental information is in some way being passed to the morphological system and could be used to inform reorganizations of the morphology such that the system maintains performance in the face of changes. E.g. if the passive dynamic walker had morphological plasticity it could alter the weights on its legs in response to environmental input such that it could cope with different slope gradients, further reducing the controller's role.

With an ability to adapt morphology over a lifetime could come a reduction in the role for conventional, abstracted controllers altogether. *Fully embodied* agents may become the norm, where the 'controller', similar to a neural network only in function, is actually part of the morphology. Just as it is

accepted that morphology can compute, it also must be accepted that controllers can be physical.

## 2.5 Morphological Plasticity: future direction for AI?

“A research methodology is proposed for understanding intelligence through simulation of artificial animals (“animats”) in progressively more challenging environments.” (Wilson, 1990)

This thesis is concerned with the design of agents able to survive in complex and changing environments, in line with the overall aim of animat research as stated in the above quotation. Interest lies in the potential of morphological solutions for the improved adaptability of animats. Focus is centered on the generation of efficient well-adapted morphologies, in natural and artificial systems, rather than on increased controller complexity. In particular mechanisms for lifetime adaptation in morphology, rather than controller plasticity, for increased performance in changing environments.

There are two logical options for designing a morphology well-adapted to a changing or complex environment, which contains many factors that the animat must cope with. Either:

1. it can have a multi-functional morphology, i.e. its form has duality and is well-adapted to many different tasks. Or, more likely, it is comprised of appendages for each possible task, rather like a Swiss Army knife.
2. It can change between different forms as new environmental challenges present themselves, it needn't have an appendage for every eventuality, it can be changed, rather like building many different forms with lego bricks.

In Nature, examples of both types of morphology are seen. Organisms grow and change shape, some, as will be explored in this thesis, adapt their shape to extraordinary degrees. More permanent areas of morphologies are also seen, which are seemingly reserved for single functions, such as bacterial flagellum for swimming. If a large amount of the organism's time is to be spent on a particular task, evolutionary arguments can be conceived for the development of specific functional areas of morphology. If however, a task is less often performed, but still of importance, it could be argued that the development of a more universal on-the-spot growth mechanism would be more energy efficient. The functional morphological area could be grown or altered on-demand saving energy in the maintenance of a permanent feature. As the environment an animat inhabits becomes more complex it becomes infeasible to constantly maintain an appendage or design to cope with all eventualities, indeed different environmental factors or tasks may require morphological designs which are mutually exclusive.

Many physiological studies have investigated morphological plasticity, the changeability of form in relation to environmental factors, however evolutionary biology has tended to focus on developmental plasticity and not *lifetime* morphological dynamics (Piersma, T. and Drent, J., 2003). Reversible transformations in physiology and morphology over short time spans can incur selective advantages, they are adaptive responses that increase survival; thus they are now considered an important topic for evolutionary biologists (Piersma, T. and Drent, J., 2003); this trend should continue into Nouvelle AI research.

A wide variety of protozoa, plants and animal cells respond to mechanical and chemical signals in the environment with rapid morphological changes, for example: grazers induce defensive colony formation in freshwater green algae (Lürling, M. and Van Donk, E., 1999). Plants use phytochrome pigments to sense the red:far-red radiation ratio in the environment, they then modify their growth and morphology accordingly in a shade avoidance technique (Meyers, L. A. and Bull, J. J., 2002). The magnitude of body size decrease of the marine iguanas on the rocky shores of the Galapagos islands, when algal stocks are low, has been shown to be positively correlated with the likelihood of survival, due to lower maintenance costs; similarly sea cucumbers and several bird species such as the Japanese quail have been shown to have reversible size changes of the gut with food availability and diet change (Piersma, T. and Drent, J., 2003). A flexible morphology permits organisms to survive in fluctuating niches. Indeed, genotypes which incorporate lifetime morphological plasticity to the environment have been shown to potentiate rapid evolutionary adaptation, accounting for genetic assimilation (Behera, N. and Nanjundiah, V., 2004).

### 2.5.1 Dynamic Morphologies: a definition

The idea of an on-the-spot adaptive growth mechanism could illuminate new adaptive and indeed intelligent properties in artificial agents for the next-level of complex, changing environments. The mechanisms behind such morphological plasticity in nature could give insights into how a fully embodied *adaptive* agent, not limited by environment-dependence, could be realized. For such morphological plasticity an animat would have to have a Dynamic Morphology. A more formal definition of a Dynamic Morphology follows:

**Definition: Dynamic Morphology (DM)** A morphology that is capable of change (by which is meant specifically altering sub-component connectivity) in active response to the environment.

In a DM system, genetic information relating to morphology continually combines with the wealth of information in the environment. So with increased MP, genotypes become more scalable, morphologies are kept relevant to current environmental conditions, and adaptive behaviour can be morphological, not solely controller-based. The stipulation is made that response must be *active* which means internal components must be stimulated to cause the resulting morphological change by a force from *within* the animat, as opposed to morphological change caused by a force from the environment alone, which would be classed as a *passive* response. For example, hitting a robot with an axe and splitting it in two would be a passive morphological change, the robot did not actively cause the change from within. Whereas, cell division, for example, can be stimulated by local environmental gradients of growth factors, but the ultimate force for division is generated from within the cell by activity in the cytoskeleton Alberts, B. et al. (1994).

Returning to Quick's functional definition of embodiment, Section 2.1, only a DM, with the capacity to affect its environment, is a true example of an 'embodied morphology' (EM), where *morphological* structure is coupled to the environment. Static morphologies, even with controller coupling to the en-

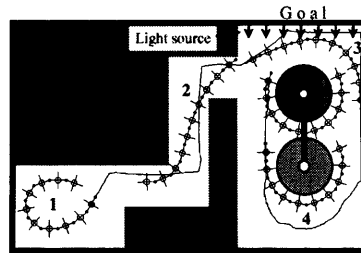


Figure 2.8: Schematic of Kawai's linear cluster robot MfM 'changing its shape' in performing phototaxis and 'baggage carrying'. Reproduced from (Hara, F. and Pfeifer, R., 2000).

vironment, do not themselves satisfy the criteria for embodiment, they are neither DMs or EMs. DMs exploit environmental dependence to generate adaptive behaviour.

### 2.5.2 Morpho-functional Machines and connectivity

There are as yet very few examples of true DMs in AI. Morpho-functional machines (MFM) are animats, often robots, where intelligent behaviour emerges from a balanced interplay between morphology, materials and control (Pfeifer, 2003). More generally they are machines that can change their morphology while performing a task. Though similar in premise to Dynamic Morphologies there is a crucial difference: the perspective from which the morphological 'change' has occurred.

To qualify as an MFM a system is not required to alter the fundamental organisation of components, but only to appear changed. For example, the linear-cluster robot 'morpho-functional machine' presented by Kawai, N. and Hara, F. (1998), see Fig.2.8, classes as a static morphology rather than a DM. Though its 'straight form' and 'clustered form' are different to the external observer, they are nevertheless structurally isomorphic: the connectivity of subcomponents cannot change. Similarly, snake movement through grass is not an example of morphological plasticity, even though different body positions are observed as it moves.

This is an important difference between morpho-functional machines and Dynamic Morphologies. Logically, morphological plasticity requires that sub-component connectivity change in relation to the environment, that structural changes can occur. Otherwise, if no change could occur in a morphology at the fundamental level, then environment induced variation in growth or development would not be possible, indeed no growth and development would be possible at all. Only DM class animats satisfy this criteria, therefore only DMs are capable of morphological plasticity by definition. Of course a DM can be called a morpho-functional machine, but not necessarily vice versa. Therefore also, MFMs are not examples of EMs only of embodied controllers.

In MFMs, the extent of a morphology's adaptability is measured in the degrees of freedom of its actuator joints, which permanently connect the subcomponents in some arrangement. With more degrees of freedom comes a greater potential for morphological adaptation (Hara, F. and Pfeifer, R., 2000). Through morphological plasticity mechanisms comes the potential for even greater adaptability, beyond the dictation of actuator joints in a static design. Continuous growth and development could pave the way for emergent morphological features, open-ended design beyond the initial designer's configuration:

autonomous, adapted novelty in form.

### 2.5.3 Self-assembly, Collective and Modular Robotics

There are examples in collective and modular robotics of systems that do allow the alteration of sub-component connectivity. However, re-organisation does not always occur in direct response to the environment, rather it can be controller dependent (Murata, S. et al., 2000; Chirikjian, G. S., 1994). Modular robotics is an interesting example of Nouvelle AI which offers a more dynamic approach to morphology determination.

Yim (1997) presented a self-assembling robotic system capable of approximating arbitrary 3D shapes utilizing the Rhombic Dodecahedron Shaped primitives. The basic idea of modular robotics is to have a collection of robotic modules which act together to perform a given task. There are various applications: locomotion over a variety of terrains for delivery, inspection or exploration and dynamically forming structures like bridges, walls and chairs (Yim, 1997). In Yim's work the modules are all of one type and made to fit together with minimal gaps. Structural change is achieved by modules maneuvering around one another. Each of their components contains a mechanism for transfer of power between adjacent modules, defining a robot whole to be all the modules in one connected component.

Penrose (1959) investigated the exploitation of form, without the need for complicated control systems and sensors, in his work on self-replicating chains. Penrose decided to avoid the encumbrance of prefabricated units such as photoelectric cells and wheels. His idea was to build simple units or bricks with properties such that a self-reproducing machine could be built out of them. They were cleverly made blocks of plywood each about 4ins long and a quarter inch thick standing end to end along the long side of a shallow rectangular box. When shaken the pieces moved in one dimension knocking into each. They would connect if a seed structure, of two connected units, was present. It was an example of a DM polymerising machine.

O'Grady, R. et al. (2005) presented a collective robotics system which utilized blue and red LED communication for navigation through rough terrain. The robots attempted phototaxis as individuals but if the terrain became too rough they grouped together through LED based communication. Through this functional self-assembly they achieved the phototaxis task, not possible as individuals in such unpredictable terrain. Though this is not an explicit example of morphological plasticity in an AI system, as dynamics work at the society level rather than on the individual level, nevertheless the results show that plasticity in structures can improve performance.

A swarm-bot is defined as an artifact composed of simpler autonomous robots, called s-bots (Trianni V. et al., 2006). Limited in sensory and computational abilities as individuals, s-bots achieve high locomotory performance in rough terrains including hole avoidance (Trianni V. et al., 2006; Groß, R. et al., 2006). S-bots as individual robots have static, controller-centred conventional morphologies with the important feature that they can link with other s-bots, see Fig. 2.9. and as with DMs it is in this dynamic connectivity that their strength lies. However a swarm-bot can only be defined as a DM if the aggregate is seen as an individual organism. They seem to relate more to a social aggregate and as such work at a higher level of organisation than is required to be called morphological plasticity. The



Figure 2.9: Swarm bots, reproduced from <http://www.swarm-bots.org/> with permission.

individuals of the system cannot alter form.

These robotic systems highlight the need for a hierarchy of elements for adaptive shape, just as proteins, cells and multicellular organisms are at each level capable of connectivity changes and morphological plasticity. At some point in the future self-organization in structure can be expected to apply to all elements in collective or modular robotic systems, not just the aggregate as a whole. This could be the future for AI, intelligent systems composed of adaptive, fully embodied, morphological hierarchies with structural plasticity at all levels. However, this thesis is not only concerned with how to build adaptive robots, but in all types of adaptive system and indeed the aim is to uncover truths about the process itself, as it occurs in reality; understanding adaptability through a constructivist framework.

#### 2.5.4 Dynamic Morphologies in AI

Within other research areas some clear examples of Dynamic Morphologies exhibiting MP can be found. For example, Marée, A. F. M. and Hogeweg, P. (2001) and Savill, N. J. and Hogeweg, P. (1997) cellular automata based modelling of slime mold. Cells aggregate upon starvation, via chemotaxis, forming a differentiated higher-level slug-like organism. This work showed clearly an algorithmic environment-driven multicellular MP mechanism. Rieffel, J. and Pollack, J. (2005) included plasticity in their developmental algorithm for growing brick-based structures. Though not an example of animat MP it is one of the few examples of plasticity in developmental algorithms.

Open L-systems are an approach for the generation of recursive branching structures designed to incorporate environmental information. Examples using open L-systems for growing artificial plants discussed in (Mech, R. and Prusinkiewicz, P., 1996) certainly class as DMs.

Suzuki, K. and Ikegami, T. (2004) developed an Artificial Chemistry cell system that could also be classed as a DM due to the transport of new molecules across the membrane from the environment which are then able to combine with other molecules, changing connectivity within, though the morphologically plastic aspects were not the emphasis of this work. Indeed Artificial Chemistry as a modelling approach offers a flexible and abstracted method for investigating low-level connectivity changes and membrane morphology self-organization (Hutton, 2002) and greatly inspired the later work of this thesis. Basing a model on the cell immediately removes the role of a conventional neural network controller and provides the opportunity to study how adaptive behaviour can be purely morphological.

Fully embodied DM systems, allowing morphological responses to the environment, could provide

solutions to the increasing challenges of complex environments, providing increased adaptability and efficiency, through cheap design, growth, morphological computation and plasticity.

## **2.6 A Taxonomy of Morphological Plasticity in AI**

Table 2.2 shows the varying degrees and types of morphological plasticity in AI models, based on the framework for natural systems defined by Piersma, T. and Drent, J. (2003). Here it is extended to include instances of 'no morphogenesis' and 'no plasticity' (no possibility of morphological change via environmental input) as this is where most animat models currently belong. However, in biology, there are conspicuously no instances of living systems without growth or plasticity.

	Change is reversible	Change within a lifetime	Change over a generation	Change periodic with environment	Biological example	AI example
No Morphogenesis	No	No	No	No	None	Most AI Work e.g. (Harvey, I. et al., 1996)
Non-Plastic Embryogenesis	No	No	No	No	None	Most developmental algorithms e.g. (Sims, 1991)
Irreversible MP	No	No	Yes	No	Temperature/sex determination (Azuma, T. et al., 2004)	e.g. Cellanimat Colony Model, Chapter 8, also (Mech, R. and Prusinkiewicz, P., 1996)
Reversible MP	Yes	Yes	No	No	cell chemotaxis (Bray, 2001)	e.g. Cellanimat chemotaxis, Chapter 5, also (Suzuki, K. and Ikegami, T., 2004)
Life-cycle staging	Yes	Yes	No	Yes	Seasonal Plumage (Piersma, T. and Drent, J., 2003)	None
Polyphenism	No	No	Yes	Yes	Arthropod seasonal offspring (Piersma, T. and Drent, J., 2003)	None

Table 2.2: Taxonomy of morphological plasticity in AI compared with natural systems. See text for definitions.



*Non-plastic embryogenesis* encompasses most developmental algorithms to date, as described in Section 2.3. *Irreversible MP* describes the environmentally influenced, initial growth of morphological attributes, which once grown cannot be altered further. *Reversible MP* is the large array of morphological adaptations that occur across an individual's adult lifetime, influenced by the environment. It can include any context-based variation in morphology as well as the morphogenesis of specific new attributes. Growths of this kind can be altered at a later date.

Open L-systems class as a DM with irreversible MP: once branches of the plant have grown, using environmental information, they cannot be changed. The Cellanimat Colony Model described in Chapter 8 is an example of irreversible MP. The Cellanimat Model performing chemotaxis and phagocytosis, described in Chapter 5, is an example of a DM with reversible MP; the morphological features can change shape further.

*Life-cycle staging* is a sub category of reversible MP describing cyclic or periodic morphological changes correlated with periodic environmental changes. It occurs across the lifetime of an individual. *Polyphenism* is a subcategory of Irreversible MP. It is the cyclic production of generations with discrete phenotypes related to seasonal or other periodic changes, it occurs across generations rather than the individual. The definitions here are more flexible: polyphenism and life-cycle staging are allowed to be correlated with *any* periodic environmental change, not just the seasons as described in (Piersma, T. and Drent, J., 2003), as seasons are rarely included in AI models.

Behera, N. and Nanjundiah, V. (2004) noted that morphological plasticity has Lamarckian implications. They verified that MP can 'speed up evolution' by using an evolutionary algorithm model with haploid genotype strings: one of 'structural genes' which cause the phenotype and one of 'regulatory genes' which determined the functioning of the structural string. Initial environmental triggers caused the canalization of regulatory proteins to favour certain phenotypes over short numbers of generations. Such quick, assimilated MP may be crucial to the characteristic phenotypic modifications of major evolutionary transitions (Behera, N. and Nanjundiah, V., 2004). Open-ended evolution (whether agents can become increasingly adapted to an environment that offers increasingly complex challenges) is a crucial question in the field of Nouvelle AI (Holland, 2003). The challenge of becoming increasingly adapted is greatly reduced if MP offers a method for quick morphological adaptation.

## 2.7 Thesis Stance: A Summary

In this thesis a functionalist monist approach is followed, within the field of Nouvelle AI. This means that understanding, of how the bodily experience within an environment can produce adaptive behaviour, is strived for through a constructivist approach using simulated computational models. The aim is to contribute to both understanding of intelligence and the design of intelligent systems. This work fits in neatly at the cutting edge of both streams of AI research detailed within this chapter: morphology optimization (development) and embodied cognition (cheap design). The key advance investigated, relevant to both streams, is the addition of morphological plasticity mechanisms. MP allows the morphology to continually develop, in relation to the environment, throughout its 'lifetime', maintaining an optimized morphology even with environmental changes. MP also provides a body-dependent mechanism for com-

1. Optimizing Morphology	2. Embodied Cognition	Morphology
evolved direct encoding	brain separate from body	static
developmental algorithms	cheap design	static
<b>situated development (MP)</b>	<b>fully embodied cognition (MP)</b>	<b>dynamic</b>

Table 2.3: Brief overview of research progression (top to bottom = past to future) within the two morphological research streams: optimizing morphology automation and increasing the embodiment of cognition. The Morphological plasticity (MP) work in this thesis contributes to both streams (shown in bold type) by utilizing Dynamic Morphologies.

putation, producing fully embodied cognition: adaptive behaviour through the morphology alone. See Table 2.3.

MP is particularly useful for coping in complex, changeable environments. This is an open problem in intelligent systems research and indeed one of the stated aims of animat-based research is to simulate agents able to cope in increasingly difficult environments (Wilson, 1990). As described throughout this chapter, most AI systems are task-specific and require tightly controlled environments, since small changes could stop the behaviour working, e.g changes in terrain. Therefore this investigation is focused around single-celled organisms that live within fluctuating niches; they cope without a brain, so the ‘body’ is doing all the work. One particular organism, the diatom, was chosen as a case study. Diatoms are bio-indicators which means their morphology is tightly linked to the environment, and changes as the environment changes.

Returning to the quote at the beginning of this chapter, Section 2.1: “The way we build our animats is a manifestation of our views of intelligence” (Pfeifer, 1996). It is clear that views of intelligence within Nouvelle AI are shifting from a human brain-centred idea of intelligence to a general morphology-centred intelligence. The cutting edge of AI animats today has the majority of emphasis on the organization of the body, on morphological computation, adaptive design and dynamics. Within this progression towards ‘fully embodied intelligence’, the ability of animats to alter morphology on a lifetime basis could be the next inevitable step towards systems that can cope in increasingly complex environments — next level intelligence. The goal of this thesis is to investigate, at a ground level, mechanisms for morphogenesis and morphological plasticity in natural systems, and algorithmic formulations for artificial systems, through the simulation of fully embodied animats.

## Chapter 3

# Nature's Batik

“In spite of received dogma that diatom valve morphology is constant with species, experimental work has shown that in addition to size related variation, changes in the environmental conditions can modify the valve morphology.” (Cox, 1997)

It is difficult to grasp ideas about morphogenesis mechanisms and behaviours without focusing research on a particular case study or model organism. This chapter will introduce the model organisms of this thesis: the diatoms. Diatoms are a good choice for studying morphological plasticity mechanisms and adaptations because they show diverse phenotypic variability and plasticity correlated with temporal environmental composition. There are many open questions in diatom research related to morphogenesis, so as a model organism they offer an opportunity for contributions to both bio-inspired computing and biology.

The latter part of this chapter will describe experimentation with a tailor-made Cellular Automata model combined with a Genetic Algorithm, aimed at understanding the interacting processes involved in diatom valve morphogenesis. First understanding of these basic mechanisms is needed, before considering how the environment may be affecting the course of morphogenesis. Subsequent experiments to investigate mechanisms of morphological plasticity in diatoms, detailed in Chapters 7 and 8, relied heavily on the model described here.

### 3.1 Introduction to Diatoms

Diatoms are single celled photosynthetic protists that thrive in many environments such as seas, lakes, and damp soils. With over 200,000 species, they are the second most diverse group of photosynthetic organisms and produce approximately 20% of the world's carbon fixation (Mann, D. G. and Droop, S. J. M., 1996). Most interestingly they possess an external shell or frustule of amorphous silica that functions as a cell wall. Organisms that incorporate inorganic material into their morphology offer a rare and exciting opportunity to learn, from nature, efficient mechanisms for the manipulation of materials for technology and as such there has been considerable interest in diatoms for nanotechnology (Gordon, R. and Parkinson, J., 2005).

The silica frustule is made up of two halves, each comprising a valve and a number of girdle bands. Diatom valves are often beautifully patterned, with regularly arranged pores perforating the



Figure 3.1: SEM image of diatom *Mastogloia*. Reproduced with permission from the ADIAC, CEC contract MAS3-CT97-0122, online image database.

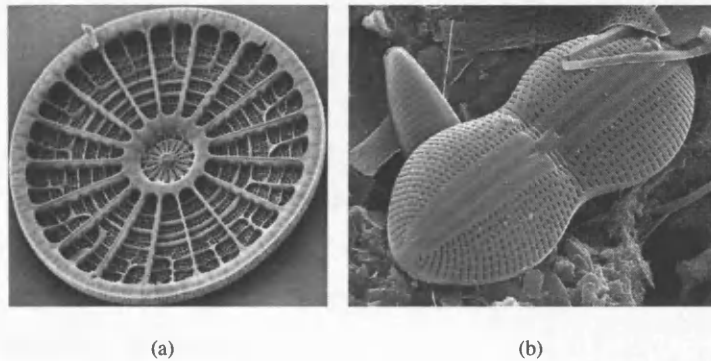


Figure 3.2: (a) Centric diatom *Arachnoidiscus* sp, (b) pennate diatom *Diploneis heemskerkiana*. Reproduced with permission from the ADIAC, CEC contract MAS3-CT97-0122, online image database.

valves (Round, F.E. and Crawford, R. M. and Mann, D. G., 1990). See Fig. 3.1. As a cell wall, the frustule is structurally very strong and resistant to enzyme attack and also functions as a defense against grazing and infection. However, some diatoms are susceptible to parasitism by chytrids, oomycetes and protozoa, and variation in susceptibility within species has been observed (Canter, 1979; Canter, H. M. and Jaworski, G. H. M., 1982, 1983; Mann, 1999) although it is unclear whether there is a consistent point of entry for the parasites. Diatom cell walls confer rigidity and precise shape to the enclosed protoplasts. However, they must also allow the transport of small molecules to and from the protoplast and allow for its expansion during the mitotic cell cycle (Schmid, 1986).

Two major symmetry groups of diatoms can be recognized: centric and pennate. Centric diatoms usually exhibit radially symmetrical valves, with an annular pattern center, whereas pennate diatoms have approximately bilateral symmetry and an elongate pattern center (Round, F.E. and Crawford, R. M. and Mann, D. G., 1990), see Fig.3.2. Within the pennate group, raphid diatoms are characterized by the possession of a double-slit (raphe) system, which is the elongate pattern center and has an intrinsically asymmetrical mode of development (Cox, 2002).

Diatoms reproduce predominantly by mitosis, each daughter cell producing one new valve (the hypovalve) after cytokinesis but retaining one of the parent valves as the older valve (epivalve) of each daughter. Because the new valves are formed within (and are constrained by) the parent frustule, there is often (but not invariably) a gradual decrease in average cell size over a series of mitotic divisions (MacDonald, 1869). Within a certain critical size range, diatoms can be induced to reproduce sexually (meiotic division results in either an ovum or a monoflagellate sperm) and thereby to restore the max-

imum size for that species by auxosporulation (formation of a full sized *auxospore* offspring) (Mann, 1999).

### 3.1.1 Diatom Phenotypic Plasticity

Many algae are notoriously plastic in morphology, growth and biochemical composition (Lüring, M. and Van Donk, E., 1999). Species specific form is variable depending on the interaction between the cell and the environment. Diatoms react very sensitively to the environment, for example they convert to resting spore morphology (vegetative, 'hibernation' state) and back again depending on environmental conditions, or even taking on the form of another species when put in a different environment (Paasche, E. et al., 1975; Cox, 1994; Schmid, 1979). Diatom taxonomy is based on the presumed invariability of valve structure, but as autotrophic organisms, diatoms are closely dependent on the environment in their reactions. *Thalassiosira rotula* valve morphology has been observed to change to that typical of a separate species: *T. gravida* with a temperature decrease (Syvertsen, 1977). Cox (1994) put forward the concept of 'Ecotypes': where alternate 'species' may actually be from the same taxa but in a different environment, the opposite of this is the traditional view that all distinct forms belong to a series of ecologically and genetically discrete taxa.

Trobajo, R. et al. (2002) tested morphological change against changes in salinity, Nitrogen to Phosphorus ratio and water movement. They showed that these three conditions often co-vary in an environment, i.e. not just one will alter, so the effect of a single factor can only be separated under controlled conditions. They showed that valve width decreased with increased salinity and length increased with salinity. However, other studies showed the converse to be true with different diatoms: that width *increased* with salinity. So no consistent pattern change can be correlated with salinity effects. There is definitely a difficulty in determining the correct trigger from field data, or trusting the determined trigger.

Morphological variability within a taxon could itself be used as a bioindicator provided the variability is a clear response to environmental conditions (Trobajo, R. et al., 2002). Cox (1994) backs up this idea: understanding the environment-induced phenotypic plasticity could improve the predictive power of diatoms in water-monitoring paleoecological and climate change studies. However, this may not be so possible as some morphological changes may be the result of a combination of factors in the environment, not an isolated factor.

Certain species of diatom do not live as independent single cells. Instead they have developed a complex set of interactions during morphogenesis, which allow them to form and disband colonies, triggered by environmental cues and giving them a greater chance of survival. Colony formation in such diatoms is an explicit and interesting example of phenotypic plasticity, of morphological adaptation to environmental changes. There has been a large amount of interest and speculation as to the adaptive quality of the response and the possible underlying mechanisms, however, there are no current solid theories and very little data on *exactly* how and why certain species of diatom form colonies.

Diatom colony formation is therefore a good system to model in order to further understanding of the adaptive systems that underlie morphological plasticity and also to contribute to current understanding within diatom research. The work described in this chapter, modelling valve morphogenesis forms

the basis of the much broader investigation into colony formation described in the final chapter of this thesis.

## 3.2 Diatom Valve Morphogenesis

Despite a variety of studies over the last few decades (Pickett-Heaps, J. et al., 1990), the fine control of nanometre to micrometre-scale pattern during diatom valve morphogenesis remains poorly understood. Transmission electron microscopical (TEM) studies reveal that the cytoskeleton is intimately involved in valve patterning and may also incorporate the use of cytoplasmic organelles or other inclusions as molds for different valvar components (Edgar, L. A. and Pickett-Heaps, J. D., 1984; Edgar, 1980; Pickett-Heaps, J. et al., 1990). Schmid (1980) suggested that the process of using material to block the deposition of silica is comparable to the negative-technique used in batik, where the outline of an image is drawn with wax and the dye only soaks into the cloth where there is no wax. Thus colour is incorporated where wax was absent. The model is similarly based on the premise that silica is deposited around organically produced templates, the protoplast effectively generating a negative imprint of the valve pattern (Schmid, 1980). The model explores the evolution of a negative space mechanism for the manipulation of silica, to produce a functional, patterned shape, similar in form to a raphid pennate diatom valve.

Parkinson, J. et al. (1999) presented a theoretical model, based on diffusion limited aggregation (DLA), which produced centric-like patterns. However, cell biologists would argue that observed patterns are not explicable by the physics of diffusion alone (Schmid, 1986, 1980; Pickett-Heaps, J. D. et al., 1979, 1988; Cox, 2002), but that cytoplasmic components and processes are modulating valve morphogenesis. The model, described in the remaining part of this chapter, focused on the morphogenesis of raphid pennate diatoms, which had not previously been the subject of computer models.

### 3.2.1 Valve morphogenesis in raphid diatoms

Here the stages of valve morphogenesis in the diatom *Craspedostauros australis* will be described. Fig.3.3 shows the nearly completed valve and Fig.3.4 is labelled to show which parts terminology, used in the following description, refer too.

During formation of diatom valves, silica is transported to the silica deposition vesicle (SDV) where it diffuses in and adheres to already consolidated silica in an accretive manner (Schmid, 1980). Valve formation occurs in a series of stages, which always occur in the same order, although taxon specific patterns are also observed (Cox, 1999). The variation in valve morphology between species and the consistency of morphology within species together indicate that morphology is genetically controlled.

Silicification begins with the raphe sternum (central spine), first forming a longitudinal rib that curls around as it approaches the cell apices and meets the extending shorter ribs on the secondary side (Round, F.E. and Crawford, R. M. and Mann, D. G., 1990; Pickett-Heaps, J. et al., 1990; Cox, 2002), see Fig. 3.5. The initial position of the SDV and of the raphe system seems to be controlled by the position of the microtubule centre (MC) (Schmid, 1980; Cox, 2002) whose orientation also sets that of the valve pattern (Schmid, 1980). After enclosure of the raphe slits, ribs of silica (virgae) that will ultimately lie between the striae (rows of pores), grow out in a transapical direction (Fig. 3.6(a)), with the

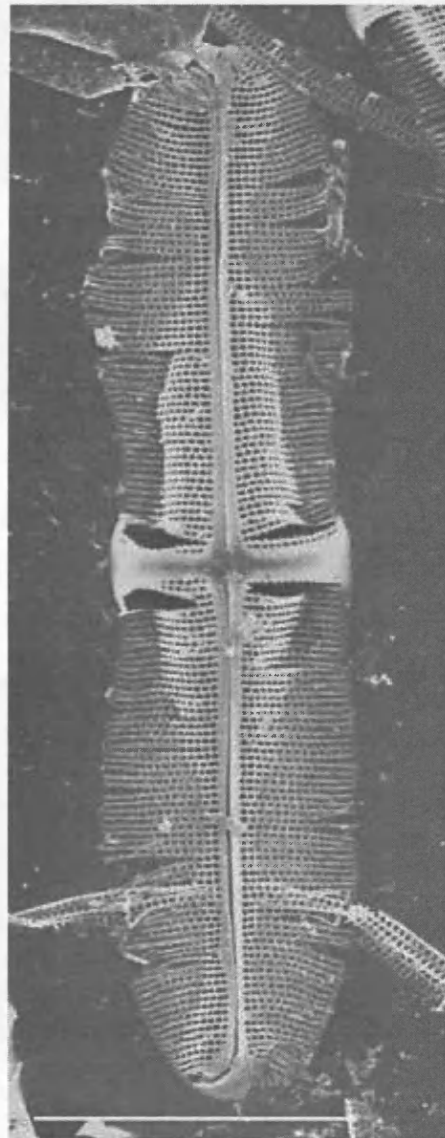


Figure 3.3: *Craspedostauros australis*, external view of almost complete valve. Scale bars represent 10  $\mu\text{m}$ , courtesy of Eileen Cox.

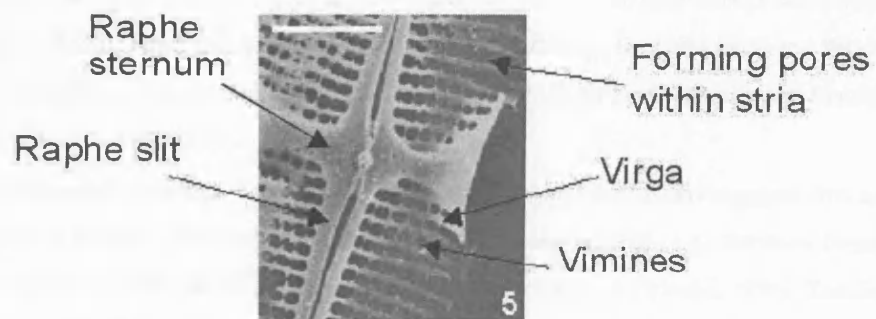


Figure 3.4: *Craspedostauros australis*, with morphological features labelled. Scale bars represent 2  $\mu\text{m}$ , courtesy of Eileen Cox.

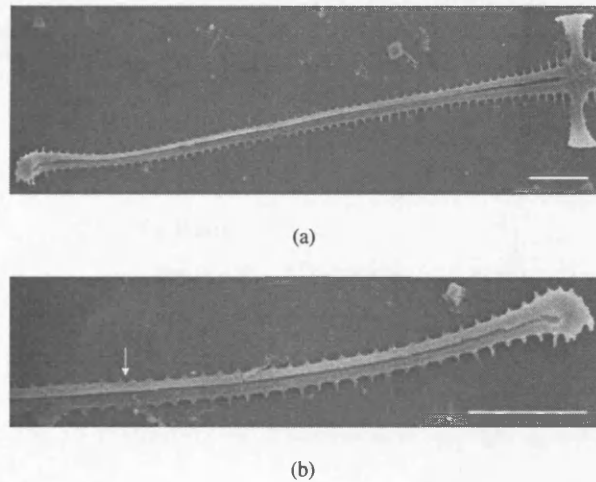


Figure 3.5: *Craspedostauros australis* (a) Raphe slit showing very early virga development. Valve centre to right hand side of picture. (b) Detail of other end of raphe system. Point where secondary side of raphe is completed indicated by arrowhead. Scale bars represent  $2\ \mu\text{m}$ , courtesy of Eileen Cox.

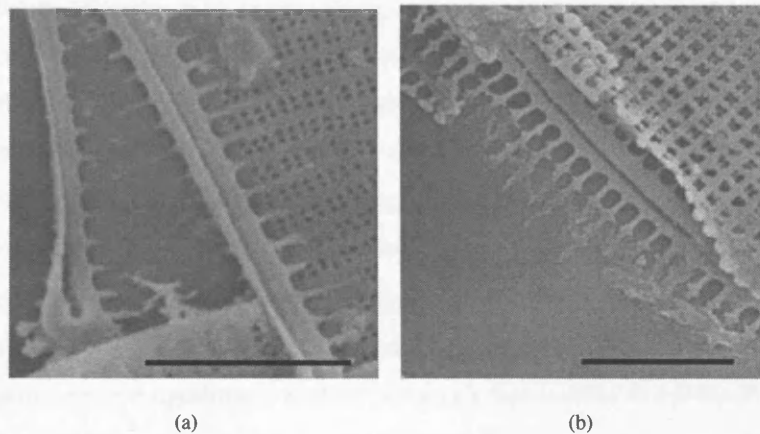


Figure 3.6: *Craspedostauros australis* (a) Early raphe overlying part of mature valve, showing identical spacing of forming virgae and mature striae. (b) Vimines beginning to form near raphe slit. Scale bars represent  $2\ \mu\text{m}$ , courtesy of Eileen Cox.

cross connections (vimines) developing later to define the pores often between  $0.1$  and  $0.5\ \mu\text{m}$  diameter, Figs.3.6(b) and also shown in 3.4, (Cox, 2002; Cox, E. J. and Ross, R., 1980; Brett and Waldron, 1996). As silica polymerizes onto the enclosed forming valve the SDV expands apically and transapically (Li, C. W. and Volcani, B. E., 1985).

The sequential formation of virgae, vimines and fine pore occlusions suggests that areas where silicification is initially prevented by the presence of organic material, e.g. between forming virgae, must subsequently be opened up to allow silicification of the vimines (Schmid, 1986). Tubulin and actin have been implicated in pattern formation, as microtubules and microfilaments are variously associated with the SDV during morphogenesis (Edgar, L. A. and Pickett-Heaps, J. D., 1984; Li, C. W. and Volcani, B. E., 1985; Chiappino, M. L. and Volcani, B. E., 1977) and their inhibition affects the raphe position and pore spacing respectively (Schmid, 1980; Blank and Sullivan, 1983; Cohn, S. A. et al., 1989).



Cell State	Material Represented	Class (0= Organic, 1 = Siliceous)
0	Nothing	
1	Raphe	0
2	Silica	1
3	Epitheca	1
4	Striae	0
5	Pore centre	0
6	Pore	0

Table 3.1: Possible states for grid cells and their classes.

### 3.3 The Nature's Batik Model

The novel computer simulation described here uses evolution to design functioning raphid pennate diatom valves and was published in the paper "Nature's Batik: A computer evolution model of diatom valve morphogenesis" (Bentley et al., 2005). The model of valve morphogenesis was constructed based on current theories that highlight the importance of cytoskeletal elements in valve development. An 'organic' negative imprint was grown in a grid-based system, using both local and global rules to dictate grid cell states. 'Silica' then diffused out into all remaining grid cells. This model was shown to generate simulated raphid pennate diatom valves capable of functioning as cell walls. At every stage of development the generated valves were consistent with observations of real diatom valve growth.

In the model, the valve was grown in several distinct stages, employing both local and global rules. The parameters involved in these stages, which ultimately governed the shape and patterning of the valve, were evolved using a genetic algorithm to explore the valve's functionality as a cell wall. The model was highly abstracted, the Cellular Automata had only seven possible states during growth. These states were classed as either 'organic' or 'siliceous' and so, once the valve had grown, it could be further reduced to a two-state system. The possible states and the class to which they belong are detailed in Table 3.1. All parameters of the model discussed in this section are shown in italics in parenthesis and relate either to initial model settings or to genes (Tables 3.2 and 3.3).

#### 3.3.1 Valve Growth

The valve was grown on a grid of size ( $2xMAX \times 2yMAX$ ) where  $xMAX$  and  $yMAX$  were set at the beginning of each experiment. The CA grid had all cells initialised in state 0, meaning 'nothing present'. This is shown in Fig. 3.7(a), where  $xMAX$  and  $yMAX$  equal 10.

##### *Defining epitheca shape*

Hypovalve growth in diatoms is almost invariably restricted by the shape of the epitheca, as shown by SEM observations of developing virgae. Virgae are forced to curve and thus form the valve mantle when they impinge upon the epitheca (Cox, 1999). Epitheca shape must therefore first be defined, although for the purposes of the model an arbitrary shape could be chosen. In order to model the epitheca

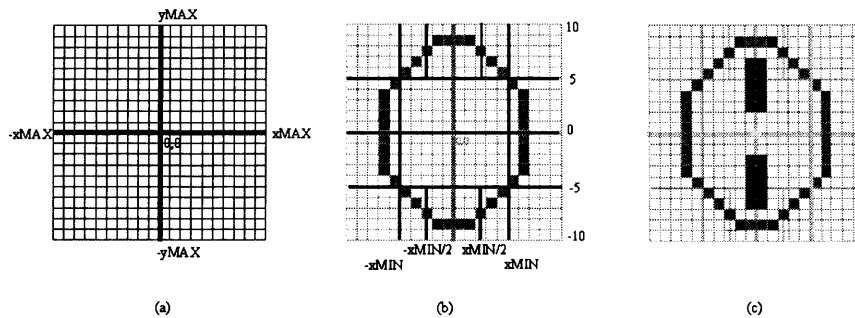


Figure 3.7: (a) Initial grid, all cell states set to 0, shown in white. (b) Control points shown in black, there are 4 on the left, which are mirrored on the right. Control points and the cells joining them shown in grey, are denoted by state 3 meaning 'epitheca'. (c) Raphe slit material is denoted by state 1 and shown in dark grey.

simply and effectively, epitheca shape was described by a number of points (*controlpoints*), between which lines are drawn, analogous to placing a rubber band around a set of pins. A more complex shape can be generated by the use of more points.

Because many raphid pennate diatoms are both isopolar and bilaterally symmetrical, only the *controlpoints* in the bottom left quadrant of the grid were specified in the genotype. These were then reflected in the  $x$  and  $y$  axes by a translation algorithm enforcing symmetry, to produce the full epitheca outline. The parameter  $xMIN$  determined where the  $x$  coordinate of a control point could lie. For the bottom left quadrant control points had to lie between, but not including  $-xMAX$  and  $-xMIN$ , in Fig.3.7(b)  $xMIN$  was set to 5. The first and last third of the control points lay between, but not including, 0 and  $xMIN/2$ . Thus  $xMIN$  constrained the width of the epitheca and also prevents the epitheca having tapered-out ends.

The  $y$  axis was divided into equal segments according to the number of control points. The control points each lay in one of these segments. This was essentially a way of generating endlessly different elliptical shapes. In practice, the locations of the  $x$  and  $y$  coordinates were given by a decimal value between 0 and 1 specifying, when scaled to the size of the segment, how far from the bottom and away from the  $y$  axis the point lay, within the segment. For example (Fig. 3.7(b)), the first control point was specified by (0.6666, 0.8) in the genotype, which given that the segment was sized  $3 \times 5$ , translated as (2, 4) within that segment. Due to the position of the segment, this translated finally as (-2, -9).

#### Setting the position of the raphe

It has been suggested that the presence of a raphe fibre prevents silicification where the raphe slit is forming (Schmid, 1980). The model therefore postulates that raphe slit material (= raphe fibre) grows along the  $y$ -axis in both directions, starting a certain distance (*RapheGap*) from a given start point ( $MC$ , representing the microtubule centre) and within a given width (*RapheWidth*). Cells within this area with no radius 1 neighbours of state 3 (i.e., not close to the epitheca) had their state changed to 1 meaning 'raphe slit material' (Fig.3.7(c)).

*Simulation of SDV growth and Silica Deposition*

All silica deposition occurs within the SDV, and the SDV expands as silica diffuses in and is accreted (Schmid, 1986; Pickett-Heaps, J. et al., 1990; Schmid, 1980). For the model, the SDV was modeled simply as a rectangle with initial corner vertices defined by the following equation, where the vertices were labeled *a* to *d* clockwise from the top left hand corner.

$$a = (MC_x - 2 \times RapheWidth, MC_y + RapheGap) \quad (3.1)$$

$$b = (MC_x, MC_y + RapheGap) \quad (3.2)$$

$$c = (MC_x, MC_y - RapheGap) \quad (3.3)$$

$$d = (MC_x - 2 \times RapheWidth, MC_y - RapheGap) \quad (3.4)$$

Only cells of state 0 within the SDV box could be changed to state 2 (silica), i.e., class 0 and 1 material (organic and siliceous) in a CA cell within the SDV prevent silica deposition. State 0 cells within the SDV could only become state 2 if there was a state 2 cell in its radius 1 neighbourhood. The SDV was initiated with all state 0 cells changed to state 2, i.e. full of silica. The SDV increased in size if 70% of the empty cells in the SDV had been filled with silica. The SDV expanded along the *y* axis until it reached the epitheca, then along the *x* axis, until it abutted the epitheca laterally.

*Delimitation of striae*

The scenario presented by Schmid (1986) invokes the use of spacer vesicles and organic matter to set the position and form of pores that form striae. A certain number (*Striae*) of blocks of material that mark out the striae were placed at a certain distance (*StriaeRapheGap*) from the raphe slit and were grown outwards from the *StriaeRapheGap* ( $\equiv$  sternum) along specific trajectories. This was based on the observation that many pennates have radiating striae. These trajectories were calculated as follows: start points: (*x*<sub>1</sub>, *y*<sub>1</sub>) of the stria trajectory lines were equally spaced along the *y*-axis at a given distance from the raphe slit (*StriaeRapheGap*) on both sides. The end points (*x*<sub>2</sub>, *y*<sub>2</sub>) were calculated in polar coordinates (*r*,  $\theta$ ), where *r* equalled 300 for all experiments. Theta was calculated for each stria by dividing the given  $2\pi$  radians into *Striae* equal segments. Then  $x_2 = r \cos \theta$ ,  $y_2 = r \sin \theta$ . Stria material was grown at a given thickness (*StriaeWidth*) along each line between the respective (*x*<sub>1</sub>, *y*<sub>1</sub>) and (*x*<sub>2</sub>, *y*<sub>2</sub>) until neighbours of radius 2 contained a cell of state 3 (it approaches the epitheca)(Fig. 3.8(a)). For the model, this process has to be initiated almost simultaneously with the SDV to ensure the formation of striae.

*Delimitation of pores within striae*

Pores were defined within striae by the outgrowth of vimines, once the virgae had reached a particular length, depending on the species (Cox, 1999). For each diatom taxon, mature pore diameter falls

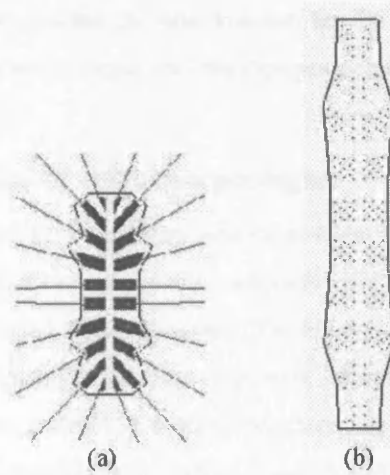


Figure 3.8: (a) Radiating striae. (b) Pore centers placed within striae.

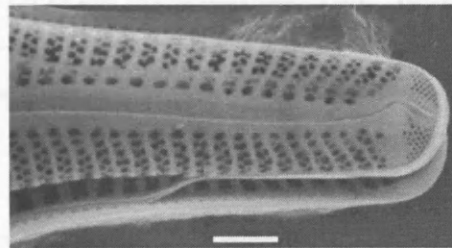


Figure 3.9: *Gomphonema truncatum*. Vimines fusion creating offset pores within the striae. Scale bar represents  $2\mu\text{m}$ , courtesy of Eileen Cox.

within a particular range and pores show consistent spacing along a stria. For the purposes of the model, pore centres were set using a simplified packing algorithm, to generate pore position as in Fig.3.9. The pore centres were placed at a given distance (*PackingDist*) from each other along the first vertical line nearest the  $y$  axis of cells in all striae, then at equal *PackingDist* and *PackingDist*/2 intervals from those along the stria trajectory gradient. Similarly, to attain a consistent size for each taxon, pores were assumed to have an ideal radius (*radiusIdeal*) as the end point of their developmental trajectory. Pores were initialised with size  $\text{radiusMAX} = \text{radiusIdeal} + 10$ , for all experiments, and pore radius decreased as the amount of silica in the cell's local neighbourhood increased. The number of cells  $N$  of state 2 in the neighbourhood of a pore centre with radius  $r = 2 \times \text{radiusMAX}$  was calculated every third time step (to save on computation time). This specified by how much the pore material reduced, at each assessment, in accordance with equation 3.5.

$$r = \begin{cases} \text{radiusIdeal} + \frac{50(\text{packingDist} \times 0.1)}{1+N}, & \text{if } N > \frac{\text{radiusMAX}}{4}; \\ \text{radiusMAX}, & \text{otherwise.} \end{cases} \quad (3.5)$$

Once all pore radii were calculated, any cell within the stria that was situated within a pore radius was set to state 6 (pore material). Pore centres however remained as state 5. To aid calculation at the next evaluation, remaining state 4 cells (= stria material) were reset to 0. This meant that half pores

could occur, where the centre was within the stria boundary but the radius traversed it. The conversion from decimal distance calculations to integer cell state changes incurred a non-perfect pore arrangement, tantamount to noise (Fig.3.8(b)).

### 3.3.2 Computer evolution of valve morphologies

A genetic algorithm is an evolutionary algorithm used for problem solving or for modeling natural evolution (Holland, 1975). Populations of individuals, each individual comprising a genotype and a corresponding phenotype, are maintained by the computer. The fitness of each individual is measured using a fitness function to assess the quality of the phenotype with respect to some objective or environment. "Better-adapted" individuals are selected as parents that then give rise to the next generation of offspring, inheriting their parents' genes through random crossover and mutation operators. Over a number of generations, the evolutionary algorithm creates individuals with higher fitnesses.

A standard generational GA was used to evolve parameters of the model to investigate the relationship between valve morphology and functionality/behaviour. The model was exposed to an 'environment' involving molecules transporting across the membrane and grazers trying to attack the cell to see if the morphogenesis model would be able to evolve valves able to function in such an environment. Illustrating that 1) the model can produce functionally similar valves to real diatoms and is therefore plausible and 2) there is a link between morphology and behaviour in even the most rigid of structures.

Genotypes were initialised randomly, with evolution running for one hundred generations using population sizes of 100. Each genotype consists of the eighteen genes shown in Table 3.3, relating directly to the parameters for growth shown. Each member of the population was grown and then assessed by the fitness function described below. The top 10% of the population became the parents of the next generation. The highest scoring member genotype was transferred unchanged into the next generation (elitism). The other ninety-nine members of the next generation were produced using crossover at a random point in the genotype of two randomly chosen parents (with replacement). All ninety-nine were then subject to creep mutation with a probability of 0.08888. On average 1.6 genes were mutated per member of the population, which was usual for a standard GA.  $MRATE_i$  was the creep value subtracted from integer genes.  $MRATE_f$  was the creep value subtracted from decimal encoded genes (Table 3.2).

#### 3.3.2.1 Fitness Function

Diatom cell walls, while protecting the enclosed protoplast against infection, must also allow molecular exchange with the external environment. Circular molecules and pathogens with radius  $MRADIUS$  and  $PRADIUS$  respectively, were placed with their centres in each CA cell on the valve. Molecules were allowed to move randomly a set number of times ( $MTIME$ ) whereas the pathogens remained static. This reflected the probability of molecules moving along concentration gradients and diffusing through pores, while pathogen attacks usually occur at much lower frequencies. If no class 1 material (silica) or state 0 (nothing) in all the CA cells in a molecule's or pathogen's radius was encountered, passage through the valve was permitted. (The rule about state 0 precludes the formation of impossible valves). Points,  $m$  for a molecule or  $p$  for a pathogen, were then awarded. The fitness was a function of the two processes shown in equation 3.6. Fitness was thus higher for a valve that did not allow pathogen

Static parameters	Setting
xMAX	40
yMAX	160
controlpoints	10
MC(x,y)	(0,0)
PRADIUS	2.1
MRADIUS	1.2
MTIME	5
MRATEf	0.4
MRATEi	20

Table 3.2: Static parameters and their usual setting in experiments

	Gene	Possible Range for Gene G
0	packinDist	$0 < G < xMAX - 1$
1	xMIN	$0 < G < xMAX - 1$
2	RapheWidth	$0 < G < xMAX - 1$
3	StriaeRapheGap	$0 < G < xMAX - 1$
4	Striae	$0 < G < yMAX/4$
5	striaeWidth	$0 < G < 2yMAX$
6	RapheGap	$0 < G < yMAX$
7	radiusIdeal	$0.00G < 10.00$
8	controlpoint0(x)	$0.00 < G < 1.00$
9	controlpoint0(y)	$0.00 < G < 1.00$
10	controlpoint1(x)	$0.00 < G < 1.00$
11	controlpoint1(y)	$0.00 < G < 1.00$
12	controlpoint2(x)	$0.00 < G < 1.00$
13	controlpoint2(y)	$0.00 < G < 1.00$
14	controlpoint3(x)	$0.00 < G < 1.00$
15	controlpoint3(y)	$0.00 < G < 1.00$
16	controlpoint4(x)	$0.00 < G < 1.00$
17	controlpoint4(y)	$0.00 < G < 1.00$

Table 3.3: The genes, their order in the genotype and the possible ranges for each.

entry but allowed the maximum amount of molecular movement.

This was a highly simplified model of cell wall function, but was used so that the resulting pattern emerged from the interaction of two necessary functions of the valve. It precluded enforcing or unwittingly ‘pre-programming’ the pattern by selecting for a certain arrangement and size of raphe, striae and pores. This approach to fitness by functionality has since been implemented in (Paulin, 2004). The penalty conditions that set fitness to -20000000 were set in order to ensure that impossible valves did not grow or propagate through subsequent generations. To save on computation time, if these penalty conditions were met, valve growth was not allowed to start, analogous to an organism possessing an expressed lethal gene (Equation 3.6).

$$fitness = \begin{cases} -20000000, & \text{if } packingDist < 2radiusIdeal; \\ -20000000, & \text{if } radiusIdeal > fracstriaeWidth2; \\ -20000000, & \text{if } Striae \times striaeWidth > valveLength; \\ \sum m - attacked, & \text{otherwise.} \end{cases} \quad (3.6)$$

$$moved = \sum m \quad (3.7)$$

$$attacked = \sum (p\pi PRADIUS) \quad (3.8)$$

### 3.4 Results and discussion

The model was programmed in C++, all experiments were performed on a standard 1.8 GHz PC workstation with graphics programmed in OpenGL. In 15 evolutionary runs of the model to maximize the fitness function, the static parameters were set as in Table 3.2 (type A runs). The mean fitness was 2093, with standard deviation of 892.13. In a further 10 runs (type B runs),  $MRATE_i$  was set to a random integer between 1 and 100 and  $MRATE_f$  was set to a random decimal between 0 and 1. Mean fitness rose to 5184, with standard deviation of 1740. Improving the mutation operators allowed populations to reach a higher fitness. A typical evolutionary run took 8-12 hours.

#### 3.4.1 Evolved Valves

A cross-section of evolved valves is shown in Fig.3.10, and their respective genes and fitnesses are given in Table 3.4. Both high and poor scoring (low fitness) valves are shown to illustrate the full effects of the evolutionary algorithm.

#### 3.4.2 Growth patterns

Setting the initial SDV box slightly to the left of the MC meant that the growth of the primary silica rib (Fig.3.11) was consistent with EM observations. This emerged from the interaction of silica diffusion local rules, the SDV initial box placement and the prior placement of raphe material. Gradual decrease in the size of the pore material within the striae allowed the characteristic sequence of virga growth followed by vimen growth to occur. Fig.3.11 shows the growth of the virgae and vimines, while Fig.3.12 shows the decrease in size of pore material as silica accumulates around it. An enlarged section (Fig.3.13) shows the pore size decrease in more detail. The model produced growth patterns comparable to those observed in raphid diatoms by EM (Figs.3.5 to 3.3).

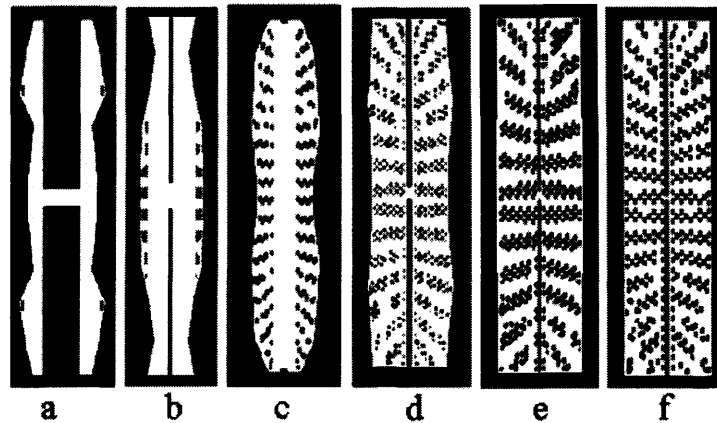


Figure 3.10: Evolved valves. Valve a is an example of a highly unfit valve, it was the highest scoring valve in the first generation of a type B run. The wide raphe leaves it open to attack by pathogens. Valves b, c and d are final generation valves from type A runs. The lower scoring ones are thinner ( $x_{MIN}$  being smaller) and have not grown an effective raphe slit. Valve d has a better score as it has a larger surface area due to a greater  $x_{MIN}$  value, it has also grown pores that allow molecular movement but not attack by pathogens ( $radius_{Ideal}$  is between 1.2 and 2.1). Valves e and f are both final generation valves of type B runs. They have far higher scores as the surface area has been maximized whilst pore size and raphe slit width have been minimized. The number and width of striae is also maximized while gaps between striae and raphe have been minimized.

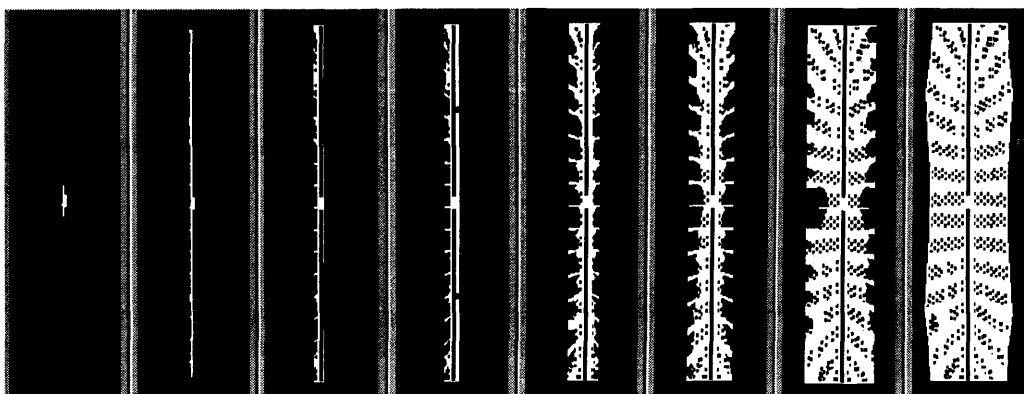


Figure 3.11: Frames showing the growth of valve *d*.



Valve	a	b	c	d	e	f
<b>Fitness</b>	<b>-40718</b>	<b>1843</b>	<b>2136</b>	<b>4038</b>	<b>6258</b>	<b>6685</b>
packinDist	38	4	6	6	7	8
xMIN	23	16	13	32	37	37
RapheWidth	31	3	15	3	2	3
StriaeRapheGap	18	20	8	3	2	2
Striae	18	16	20	16	14	18
StriaeWidth	19	15	10	17	22	17
RapheGap	8	12	154	6	4	2
radiusIdeal	9.265175	1.198767	1.786889	1.214118	1.587725	1.779229
controlpoint0(x)	0.179052	0.267885	0.066463	0.239570	0.278939	0.539293
controlpoint0(y)	0.447951	0.012336	0.512589	0.385418	0.194739	0.568163
controlpoint1(x)	0.853450	0.190313	0.641316	0.885647	0.442885	0.593188
controlpoint1(y)	0.189459	0.486837	0.682882	0.454176	0.661061	0.598743
controlpoint2(x)	0.457076	0.547197	0.499161	0.394147	0.814783	0.533769
controlpoint2(y)	0.527757	0.107358	0.345067	0.168523	0.150304	0.117862
controlpoint3(x)	0.093081	0.048347	0.009485	0.023353	0.058443	0.265664
controlpoint3(y)	0.371258	0.189740	0.080178	0.001025	0.542070	0.591907
controlpoint4(x)	0.195929	0.085885	0.214515	0.628376	0.262612	0.093600
controlpoint4(y)	0.499649	0.498434	0.502548	0.157860	0.524644	0.018738

Table 3.4: The sample of evolved valve's fitnesses and genotypes

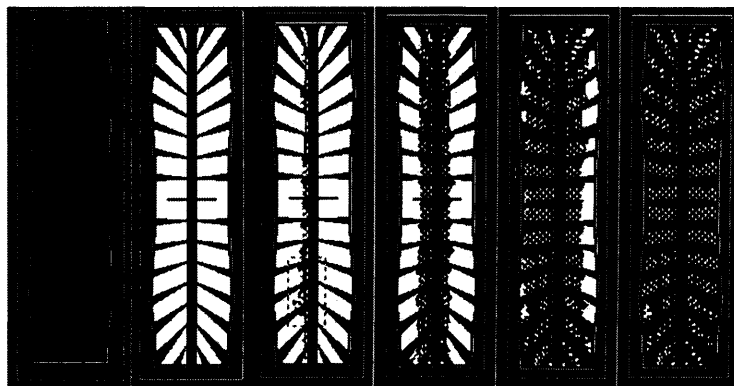


Figure 3.12: Frames showing in white the epitheca outline and the shrinking of organic material to form pores during growth of valve *d*. Silica is diffusing as in Fig.3.11. The dotted box in the third frame is the section whose growth is shown enlarged in Fig.3.13.



Figure 3.13: Three stages in the growth of the section enlarged from Fig.3.12 showing the organic material in the striae (shown in white) reduce down to the radiusIdeal to form the pores, as the amount of silica around it increases, the silica is not shown

### 3.4.3 Areas for improvement of the model

This was a preliminary model and could therefore benefit from further exploration and development in a variety of directions. There was no realistic selection pressure on valve outline so the fittest shape for the epitheca was a rectangle, which is of course very rarely seen in nature. However, an extra component could be added to the fitness function to reward for shear drop shapes, which would cope better with flow, as detailed by Gordon, R. et al. (1996). More streamlined shapes may also favour moving over surfaces or through sediments, the typical habitats of most raphid diatoms. Stria trajectories and pore arrangements were similarly oversimplified. They failed to account for the occurrence of parallel, or intercalated shorter striae, and for the uniseriate rows of pores within striae, seen in many raphid diatoms. This could be overcome by the use of a variety of packing algorithms, for example that new striae could emerge where there is space, rather than being globally positioned. The CA model would also allow the substructure and pore occlusions seen in many diatom pores to be simulated, but would require a larger CA grid. xMAX and yMAX were relatively small, the number of control points was fixed at 10, the packing algorithm was the same throughout runs and the MC was set to (0,0) to minimize the program run time. However, larger grid sizes allow for more intricate patterning as one cell is translated as one pixel and alternate packing algorithms can be implemented to great effect (Fig.3.14).

It did prove possible to simulate valves in which the raphe does not lie centrally along the long axis, mimicking the situation observed in cymbelloid diatoms, although the model has not modified valve outline. Offsetting the MC offsets the patterning without the need to recalculate or change the model. Fig. 3.14(b) shows a valve grown with an offset MC where all parameters were set by hand. It would be interesting to investigate these properties in further experiments using evolution.

Although there is currently much interest in the biochemistry of silicification and the nanofabrication of consolidated silica in diatom valves (Kröger, N. and Sumper, M., 2000, 1998) variation in the form of silica deposited occurs at a finer scale than the valve features with which this chapter has been concerned. Similarly, it has been assumed that the position of the SDV (within the confines of the parent cell) reduces the direct influence of the external medium on silica deposition.

There are several other aspects in which this first model simplifies wall morphogenesis. It was assumed that morphology was primarily controlled by genetics, rather than attempting to incorporate the effects of environmental variables on morphology. However, it could also be argued that until a clearer

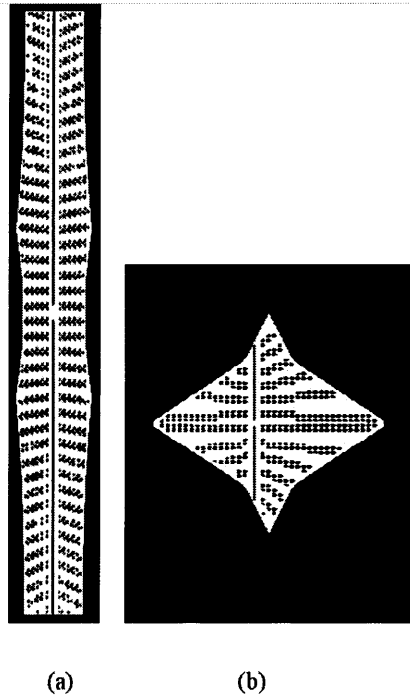


Figure 3.14: Valves grown using hand specified genotypes, (a) Increased resolution,  $xMAX = 70$ ,  $yMAX = 320$ . (b) offsetting the MC offsets the entire process in a realistic manner, MC at  $(-10,0)$ . Both use an alternate packing algorithm where pore centers were set in horizontal rows.

understanding of the interaction between the environment and diatom valve morphology is obtained, it is difficult to set up suitably realistic hypotheses to model. There are relatively few experimental studies of the effects of varying environmental regimes on morphology (Schultz, 1971; Cox, 1994; Trobajo, R. et al., 2002). Similarly, the fitness function tested does not represent the only factors that affect morphology. Other factors such as locomotion and buoyancy (Pickett-Heaps, J. et al., 1990) could be incorporated, but the fitness function could easily be extended to include these. Further simulations could also be carried out where the various static parameters are changed. Arguably, the use of developmental genetic encoding would be more biologically plausible than the current genetic encoding and should be explored. It has also been shown that symmetry arises spontaneously in such systems (Dellaert, F. and Beer, R., 1996, 1994).

### 3.5 Summary

The case study organisms of this thesis, the diatoms, have been introduced and a simple model of valve morphogenesis, involving only the interaction of silica and organic material, has been presented. This chapter has satisfied thesis Objective One, as detailed in Chapter 1. It has also provided a starting point for the biological inspiration needed to test the primary hypothesis.

## Chapter 4

# Cell and Cellanimat

In order to develop new ways to design artificial systems, with increased abilities to adapt and survive in changing environments, an understanding of morphological plasticity is strived for. How it is facilitated by single cells, allowing them to perform adaptive behaviour without a brain and have such well-adapted designs, is of primary concern. Mechanisms of diatom valve morphogenesis were discussed in the previous chapter, in a simplified un-situated way. But this clearly is not the whole story. To build on this model the question was asked: how might environmental information signal this system to generate different valve morphologies as the environment changes? Focus centred on the organic material that blocks silica deposition. How does the cell know where to place this? As discussed previously, the cytoskeleton has been implicated in this process (Schmid, 1980). Thus, the next step was to investigate how the cytoskeleton may be able to achieve such a feat.

It became clear that the cytoskeleton may be the underlying mechanism that, if harnessed in artificial systems, could generate adaptive behaviour, and design, through environment-morphology interaction. Extending biological inspiration beyond diatoms, to all eukaryotic cells, it is possible to understand how the cytoskeletal-generation of variety and adaptation in morphology is achieved, owing to the large volume of cell-physiology research. This knowledge can then be used to both create artificial systems with similar adaptive capabilities and gain greater insights into the mechanisms that may be controlling diatom valve morphogenesis.

This chapter is comprised of two halves: first the basic biology of eukaryotic cells will be introduced, focusing only on the problem in hand, rather than detailing the wide array of cellular components and properties. Only the particular cellular subsystems involved in morphological change and environmental signalling will be discussed. The biology has been reformulated into more computational terms. Identifying key, functional, system features was a crucial stage in forming the sound basis for the novel artificial adaptive system: the *Cellanimat*. The *Cellanimat* is then introduced, step by step, in the latter half of this chapter, along with the novel framework for characterizing the environment-system interactions generating its morphological plasticity: the *Environment-Phenotype Map*.

## 4.1 The Cell Basics

Cells belonging to the different kingdoms, e.g. animal, plant and protista, exist in many shapes and sizes with specialized features and functionalities. However, all cells have certain features in common. The most fundamental, ubiquitous and important feature of cells is that they are in a semi-fluid state. The dynamic adaptability of cells can be attributed fundamentally to this fact, that constituent parts are flexible: they can move with ease, alter state and produce new components through chemical reactions. Indeed, cellular membranes have been described as a *fluid mosaic* due to the free and often rapid diffusion of the phospholipid molecules comprising them (Singer, S. J. and Nicolson, G. L., 1972). There are two classes of cell: eukaryotic and prokaryotic. The fundamental difference is that eukaryotes have a double membrane encapsulating genetic material within the nucleus, enhancing their evolvability. Focus will centre on eukaryotic cells.

A cell is made up of four classes of macromolecule: nucleic acids, proteins, complex carbohydrates and lipids. The shape of a macromolecule is determined by its physical properties, the shape also determines the interactions possible *between* macromolecules. This is because a macromolecule's shape affects which binding sites are exposed. In shape changes, due to changes in substance properties, e.g. through binding, macromolecules can alter which binding sites are exposed affecting the course of future interactions. Shape also affects the electrostatic field around the macromolecule generating a guidance system for potential binding partners; a strong attractive force on one particular side of the macromolecule can pull appropriate neighbouring macromolecules in for binding, indeed this property has evolved in cells to accelerate, and increase the accuracy of, the binding process as discussed in (Smith, G. and Sternberg, M. J. E., 2002). Macromolecules can be viewed as 'autonomously dynamic agents' involved in a low level of a dynamical hierarchy, where they decay, unfold, refold, form new proteins or catalyze reactions (Lenaerts, T. et al., 2002). Shape is an essential concept throughout the hierarchical levels in cells and crucial when considering the structure of the higher level system (Widnell, C. C. and Pfenninger, K. H., 1990).

Macromolecules organize into higher level structures: networks and *organelles* (so called as they resemble organs in a multicellular organism). Although organelles first appeared to be relatively permanent in early electron microscope experiments, they have since been shown to be dynamic, both metabolically and structurally (Widnell, C. C. and Pfenninger, K. H., 1990). A brief introduction to the cellular organelles and systems that seem necessary for morphological plasticity follows, see also Fig.4.1.

- **Nucleus:** the nucleus is the defining feature of eukaryotic cells, which contains DNA and associated proteins. Gene expression in the nucleus results in protein synthesis at the ribosomes, studded along the endoplasmic reticulum (ER).
- **Endoplasmic Reticulum (ER):** continuous with the outer membrane of the nucleus, the ER is the cell's own body-part manufacturing station (Widnell, C. C. and Pfenninger, K. H., 1990). Its large span means that it acts as a large scale delivery system of newly synthesized proteins. The ER cisternae (membrane sacks) act as a storage and release site of  $\text{Ca}^{2+}$  ions, which can play an

important role by affecting the behaviour of proteins in the cytoskeleton.

- **Cytoskeleton:** the cytoskeleton is a complex network of dynamically assembling and disassembling protein filaments within the cytoplasm (semifluid, translucent substance within cells, outside the nucleus, composed of primarily of proteins and fats) that coordinate changes in cell shape and movement.
- **Membrane:** a membrane is a self-organizing structure of lipid bilayers. Lipids have a hydrophilic head and a hydrophobic tail, thus the most energetically stable arrangement is for them to form into bilayers where the tails face each other, blocking out water. The ability of all living systems to adapt their morphology relies heavily on the fluidity of membranes. The plasma membrane (also called the plasmalemma) defines an interface between the cell and environment; intracellular membranes compartmentalize the cell.
- **Mitochondria:** a mitochondrion contains an inner membrane folded to form cristae enclosed within an outer membrane. The major function is adenosine triphosphate (ATP) synthesis. ATP is required for any cellular chemical reaction to take place, it is the energy store of the cell. When it loses a phosphate group energy is released leaving adenosine diphosphate (ADP). ADP must reattach a phosphate before it can return to the ATP state and provide further energy. Thus ADP-bound macromolecules are inactive and ATP-bound macromolecules are active — capable of activity. The cell is not the 'basic unit of life', the cell is itself seen as a symbiosis of subcellular components, which were once autonomous living systems; the mitochondria is the most obvious example of this: it was once a free living prokaryotic cell (Rizzotti, 2000).

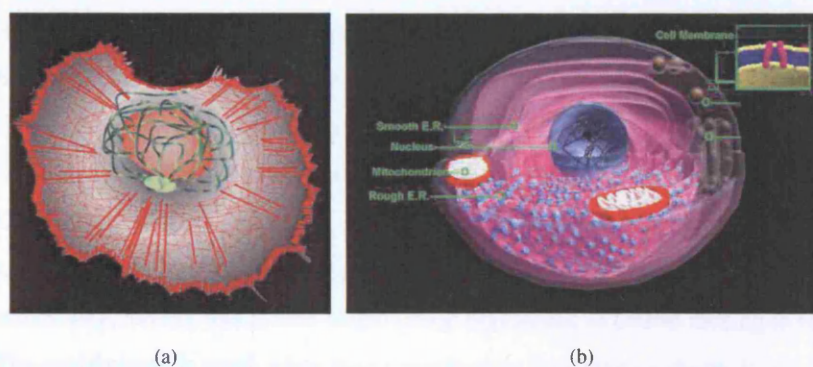


Figure 4.1: (a) The cytoskeleton: actin filaments and actin cortex shown in red, microtubules in green sprouting from the centrosome (microtubule organising centre) around the nucleus. Reproduced from [www.helios.mol.uj.edu.pl](http://www.helios.mol.uj.edu.pl). (b) Basic cellular components: nucleus shown in blue; endoplasmic reticulum shown in purple; mitochondria in red and white; all encapsulated by the cell membrane (plasma membrane). Adapted from <http://www.ibiblio.org/virtualcell/index.htm> with permission.

The ability of eukaryotic cells to execute coordinated, directed movements and rapid, sometimes massive, changes in shape depends crucially on the cytoskeleton: the complex network of protein filaments that extends throughout the cell's cytoplasm (Alberts, B. et al., 1994). The above listed cellular

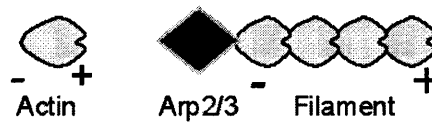


Figure 4.2: the opposing binding sites on an actin monomer give it polarity; as minus sites always bind onto a plus site the filament as a whole also has polarity, with monomers only able to polymerize onto the plus end. Arp2/3 is a complex needed to start filament polymerization.

components have been singled out for discussion as they are all directly involved in cellular MP and are thus included in the Cellanimat model to some degree or other. The nucleus contains genetic material which determines the levels of, amongst other things, cytoskeletal proteins to be synthesized in the ER. These levels, combined with the changing levels of energy produced by the mitochondria, and signals from the environment, generate changing structures and networks of filaments in the cytoskeleton. The dynamic cytoskeletal structures can affect membrane shape and behaviours, facilitating the morphological plasticity of the cell.

## 4.2 The Cytoskeleton

The cytoskeleton is a major system within cells. It is involved in the transport of molecules and small vesicles carried, in a directed fashion, along filament lengths rather than left to travel by haphazard diffusion. It determines cell shape and controls cell shape changes. Muscle movements and movements within non-muscle cells are orchestrated by the cytoskeleton — it is capable of contraction. It is involved in cellular ingestion of particles (phagocytosis) and is the brawn, and organising power, behind cell division. In short, it is crucial for cellular travel, ingestion, reproduction and structure.

Though it can be described as the brawn of the cell, the structure and muscle system, it is not always simply sent instructions from a 'decision maker' as might be imagined by an advocate of traditional, neural network based animats (of the format: sensors → processor → effectors), though muscle cells do follow this structure (Alberts, B. et al., 1994). The cytoskeleton itself interacts directly with the environment, as will be seen, allowing it to process, regulate and control cell structure and behaviours in an autonomous way; indeed, this is how single celled organisms, of course lacking in brains, are able to survive. The cytoskeleton is much more than a mechanism for changing shape, it is a fundamentally different way of executing and processing adaptive behaviour.

The cytoskeleton consists of *structural* and *accessory* proteins. Actin and tubulin are structural proteins, of which the cytoskeletal filaments are made. Actin monomers (single macromolecules) polymerize into long chains called microfilaments. Thirteen tubulin polymers combine to form cylindrical 'microtubules'. The cytoskeleton also contains intermediate filaments with varied protein composition from cell to cell. The long chain morphology of filaments is possible only because the protein monomers that comprise them are polar (they have opposing binding sites: labelled minus and plus sites) allowing them to form chains rather than clusters. Filaments themselves are polar, as the monomers within always join minus sites to plus sites, the two ends of a filament are similarly labelled minus and plus. Monomers

add on at the 'plus' end and fall off at the minus end. A nucleating complex, such as Arp2/3, is needed to initiate actin filament polymerization, see Fig. 4.2. Arp2/3 is an interesting complex, it not only nucleates filaments it also has a binding site for F-actin (actin in a filament) meaning it can stick to an already formed filament and nucleates a new filament as a branch offshoot. This results in actin filaments being part of a branched, tree-like structure and also reinforces polymerization within a small area. See Fig.4.2.

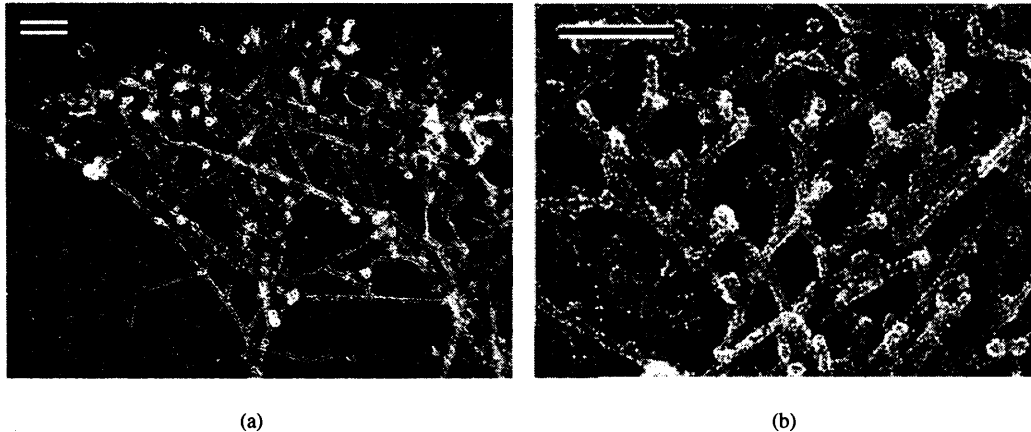


Figure 4.3: Arp2/3 sticks to actin filaments then nucleates a new filament branch generating tree-like structures composed of actin filaments. EM image of actin branching within lamellapodia (sheet-like membrane protrusions) during fibroblast chemotaxis. Reproduced with permission from (Svitkina, M. and Borisy, G. G., 1999).

Structural proteins are recruited from large 'subunit pools' of monomers within the cytoplasm. For perspective: eukaryotic cells typically contain a billion or so protein molecules, there are around 10,000 different types and their diameter is typically 2000 times smaller than the cell ( $10\ \mu\text{m}$ ). In non-muscle cells actin comprises about 15% of the total protein content. Thousands of structural proteins can polymerize together into filaments, which can be long enough to span the entire cell (Alberts, B. et al., 1994).

#### 4.2.1 Focus

In this thesis, focus lies on modelling only the structural protein actin and microfilaments, see Fig.4.4. The cytoskeleton consists of massive numbers of proteins and it would not be feasible or useful to attempt to model all protein types. Each actin molecule is a single polypeptide 375 amino acids long that has a molecule of ATP tightly associated (ATP is the energy currency of the cell). Actin has been chosen over tubulin for two reasons. 1) The actin cortex exists at the cell's periphery, as shown in Fig.4.1(a) and so can quickly alter the cell's outer membrane morphology and function. Microtubules on the other hand are less dynamic; though they can still disassemble, they give fundamental structural support rather than executing quick morphological changes (Alberts, B. et al., 1994). 2) Actin, and not tubulin, has been indicated in diatom valve formation (Pickett-Heaps, 1998) so further study and inclusion of an actin based model could give greater insight, not only into algorithmic methods for MP for artificial applications but also into the process as performed in the chosen model organisms: the diatoms.



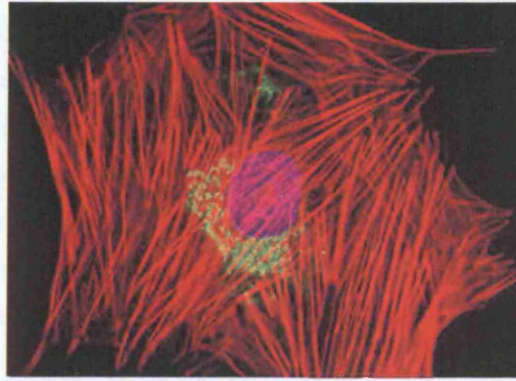


Figure 4.4: Human fetal lung fibroblast cell, actin filaments shown in red using fluorescence staining, nucleus in blue. Reproduced with permission from <http://www.olympusmicro.com/primer/techniques/fluorescence/gallery/cells/mrc5/mrc5cellslarge3.html>

### 4.2.2 Dynamics

Actin filaments are highly dynamic, they can be assembled in one place and then rapidly disassembled, ready to be rebuilt in a more advantageous position. Filaments rarely occur in isolation but rather in much stronger cross-linked aggregates or bundles. The arrangement and behaviours of filaments are regulated and controlled by the cell through the strategic release, distribution and removal of *accessory* proteins. Barbieri (2001) concluded that accessory proteins are 'true adaptors' for this flexible role in regulating the cytoskeleton. There are a multitude of accessory proteins, see Fig.4.5(a); their combined use results in a complex system of cooperative/competitive interactions, generating a rich diversity of filament behaviours and structures. See Fig.4.5(b).

Filaments are very efficient; actin monomers are recycled through them due to ATP loss, and through interactions with accessory proteins, see Fig.4.6. The activation and binding of actin to a filament and then the subsequent loss of affinity for the filament provide both the 'on' and 'off' mechanisms needed for filament assembly and disassembly, which are tweaked and controlled by the accessory proteins to perfectly suit a given situation. Without loss of affinity, filaments would extend indefinitely and monopolize all available actin, and space, inside the cell. For balanced, productive, behaviour, disassociation must be considered with as much importance as the binding events themselves.

### 4.2.3 Environment and the Transduction Pathway

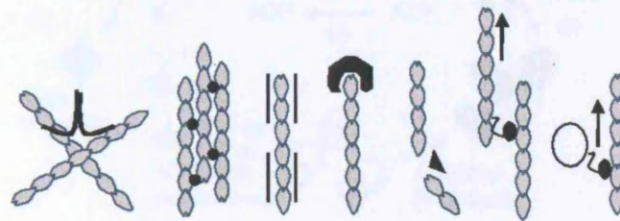
Accessory proteins regulate cytoskeletal filaments, but how are they controlled? Accessory protein levels are ultimately controlled by signals from the environment. There are three ways for the environment to affect cytoskeletal behaviour: 1) direct effects on local accessory protein levels; 2) direct effects on structural proteins. 3) indirectly via effects on genetic regulation and protein synthesis. Focus will centre on mechanisms involving the first two types, which involve signals from the environment filtering through into the cell via the *Transduction Pathway* (TP), a complex cascade of reactions among specific proteins, triggered by a change at the cell's periphery.

The flow diagram shown in Fig. 4.7 shows the generalized sequence of events as a cell processes environmental information and then morphologically responds via TP signalling of the cytoskeleton. Many upstream pathways in the TP are *multifunctional* and can be triggered by different receptors; PIP2, Rho, WASP and Cdc42 are indicated as involved in many different responses. Focus will lie on just two to keep things simple.

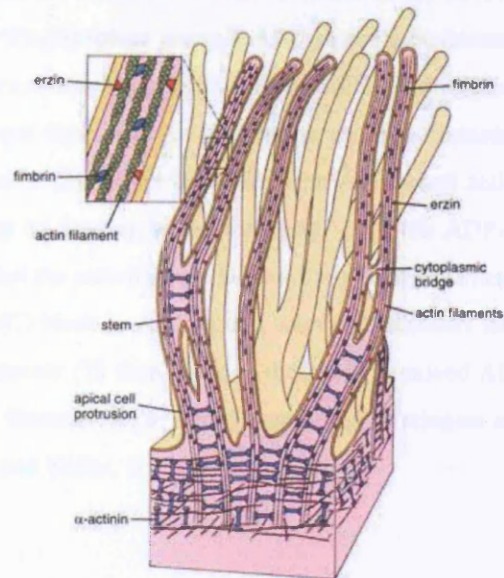
PIP2 (phosphatidylinositol, 4,5-bisphosphate) is a membrane-bound protein complex activated when a signal is detected by certain membrane receptors. Profilin, the cytoskeletal 'activating' accessory protein binds to inactive PIP2 and is released upon PIP2 activation. Deactivation of PIP2 causes profilin in the vicinity to re-bind to it (Bray, 2001). Thus it can be seen how the environment, through the manipulation of PIP2 has a direct route to affect actin polymerization.

The WASP (Wiscott-Aldrich Syndrome Protein) family are membrane-associated, proline-rich proteins. When activated by a receptor they undergo structural changes, resulting in the exposure of a previously hidden binding site for Arp2/3 and ATP-bound actin (i.e. profilactin) (Holt, M. R. and Koffer, A., 2001; Miki, H. and Takenawa, T., 2003). Once bound to WASP Arp2/3 also changes form, 'activating it' and exposing an actin-binding site, meaning it is ready to start a filament. WASP and PIP2 are crucial, and impressive, for their funneling of structural proteins to the exact, correct locality in the cell, and activating them, such that they will polymerize into filaments and make needed changes to the membrane shape (Holt, M. R. and Koffer, A., 2001).

It is worth noting that 'sensors' in living systems need not be membrane embedded, specific receptors. Changes can be triggered by indirect links to external influences. For example, lowered nutrient or light intake can result in lowered overall energy causing changes in behaviour, though there are no 'membrane sensors' for nutrient levels, the cell is still able to respond to environmental conditions. Cells have a variety of perceptual pathways at their disposal, they needn't have evolved a specific receptor for



(a)



(b)

Figure 4.5: (a) A selection of cytoskeletal accessory proteins, shown in black, affecting actin filament behaviour. From left to right: filamin cross-links filaments; fimbrin bundles filaments in parallel; tropomyosin strengthens filaments; gelsolin is a capping protein, blocking further addition to the plus end; cofilin is a severing protein; myosin I is a motor protein, its head domain 'walks' along the filament towards the plus end. Myosin I can have either a filament, vesicle or cell membrane attached to its tail domain causing contractile motion or transporting cellular material around the cell along the actin filament network. (b) Actin filaments combine into higher level structures, which can cause local protrusions of the membrane, regulated by accessory proteins. Here long parallel bundles of filaments are held together by fimbrin and  $\alpha$ -actinin which hold them apart at different distances. Erzin, a plasmalemma protein, anchors the filament bundles to the membrane as they extend outwards. Reproduced from (Alberts, B. et al., 1994).

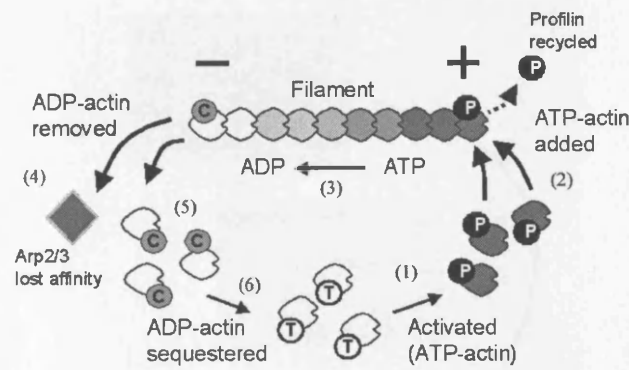


Figure 4.6: Actin monomers are recycled through filaments in the following stages. (1) Profilin (P) facilitates the reattachment of a phosphate group in ADP-bound actin (monomers shown in white) giving ATP-bound actin (monomers shown in grey). Profilin and ATP-bound actin together form the complex: profilactin. (2) Profilactin can bind onto the plus end of an actin filament, releasing the profilin back into the system in the process. (3) Whilst in the filament ATP-bound actin hydrolyzes to ADP-bound actin (the energy is used up by binding to the filament). (4) Both ADP-bound actin and arp2/3 (the macromolecule needed to start the actin filament) lose affinity for the filament and disassociate, only from the minus end. (5) Cofilin (C) binds to ADP-bound actin and increases its likelihood of disassociating from the filament. (6) Thymosin (T) then binds to the newly removed ADP-bound actin, rendering it unable to bind back onto a filament (sequestering) until profilin releases it and begins the cycle again. Adapted from (Holt, M. R. and Koffer, A., 2001).

each environmental factor.

### 4.3 The Cellanimat: an overview

The Cellanimat is a prototype computational model designed for the investigation of MP capable systems and based wholly on the biology presented in the previous section. It will be thoroughly introduced in this overview section. Rule-by-rule instructions for re-implementation are detailed in the next section. It is ostensibly an agent-based model, though some aspects are modeled within Cellular Automata rules for efficiency. It can be thought of as a game where ‘agents play on a CA board’. The major component facilitating MP within the Cellanimat is the Artificial Cytoskeleton (ArtCyto). However, all components were seen as minimally necessary to generate MP (see Section 6.2 for a full investigation into this claim).

The name ‘Cellanimat’ derives from the model’s adaptive abilities based on cellular mechanisms (literally cell - animat). However, it holds interesting new properties differing from the traditional animat (described in Chapter 2) due to the unique cell-based design, where having a separate controller to the body no longer holds meaning. Instead, the ArtCyto can be seen to play dual roles — there is less modularity in function, see Fig.4.8.

This observation is consistent with it being a highly biologically inspired model, rather than predominantly human-designed, as discussed by Paul in (Paul, 2004). Paul highlighted the following difference between human design and biological architectures: there is a human tendency to design compo-

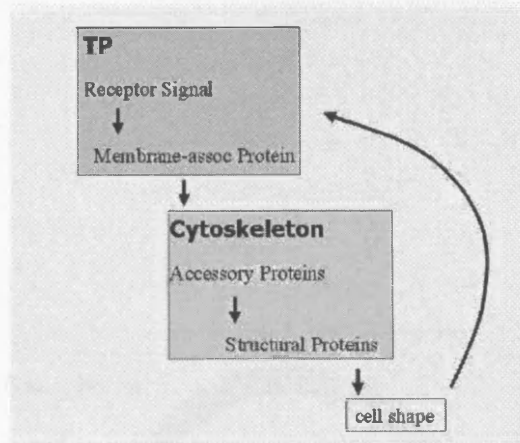


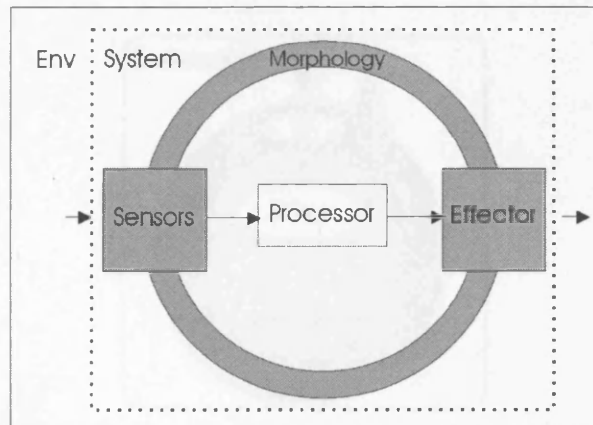
Figure 4.7: Flow diagram showing how a cell can morphologically adapt to environmental changes through TP signals affecting the cytoskeleton. When a receptor in the plasma membrane is triggered by the environment, membrane-associated TP proteins are affected. Changes in TP reactions affect the behaviour of cytoskeletal accessory proteins (e.g. profilin) which in turn affect structural proteins and, ultimately, filament dynamics. Rearrangements in the filamentous structures within the cell can alter cell membrane shape. Any alteration in cell membrane shape could then cause the environmental inputs to receptors to change.

nents with single functions whereas in Nature much *duality* in function is seen, where single components play many roles.

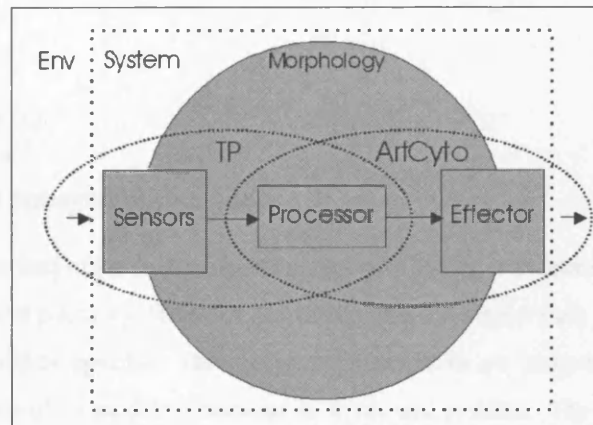
The Cellanimat is intended as a system capable of ‘morphological computation’, as introduced by Paul, and the duality inherent in the model is the mechanism by which this is possible — growth and decision making, movement or processing of external information can all be performed by the same subsystem of the model, allowing for greater computational weight — or indeed all computational weight — to be taken by the morphology rather than a separate controller.

The Cellanimat is designed as an *implicit* developmental algorithm, as described in Section 2.3.1. The progress of growth depends on the self-organization of proteins together with the environment rather than following an explicitly defined route. It should in this way, be capable of generating a variety of changing forms.

The Cellanimat is a Dynamic Morphology for autonomous morphological design and adaptive behaviour. Morphology is determined at each time step through interaction with the environment. The Cellanimat is a dynamical hierarchy, modelling real cells at three levels: 1) the cell as a whole, in its environment; 2) the cells subsystem interactions (membrane, transduction pathway, cytoskeleton, cytoplasm); 3) each subsystem’s macromolecular interactions. The Cellanimat and its environment are implemented as a 3D voxellated world. It is an idealized model of Nature (partially inspired by artificial chemistry techniques (Hutton, 2002) and the Glazier and Graner cellular automata approach to cell modelling Glazier, J. A. and Graner, F. (1993)) that concentrates on the computational process of morphological adaptation; macromolecular interactions in the Cellanimat are faithful to the biology but it is



(a)



(b)

Figure 4.8: (a) Traditional animat architecture, where processing is performed by a separate module to the physical body. (b) Cellanimat architecture, where processing is performed by the body itself. The Cellanimat exhibits duality, the ArtCyto component performs both processing and effecting. Similarly the TP can be considered as bearing some processing responsibility along with sensor signalling.

Subsystem	Description
<b>M</b>	Membrane; the Plasmalemma, the outer membrane of the Cellanimat
<b>C</b>	Cytoplasm; contains concentration gradients of diffusing proteins
<b>ArtCyto</b>	Artificial Cytoskeleton; consists of structural and accessory proteins
<b>TP</b>	Transduction Pathway; consists of membrane-associated signalling proteins

Table 4.1: The subsystems of the Cellanimat.

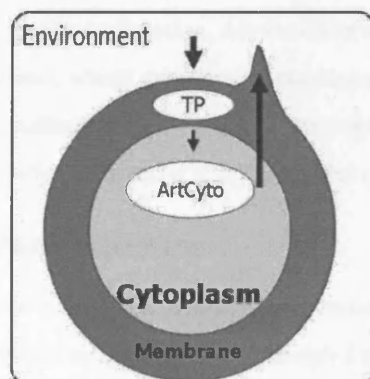


Figure 4.9: Schematic of the Cellanimat's nested subsystems generating environmentally driven membrane shape change.

not an exact model of a cell.

### 4.3.1 Cellanimat subsystem overview

The Cellanimat is comprised of the four subsystems shown in Table 4.1 as interest focused on only those relevant to morphological plasticity. However, the Cellanimat is designed such that the incorporation of further subsystems would be possible. The subsystems themselves are comprised of smaller units, the Cellanimat's macromolecules: modelled versions of lipids and proteins. The Cellanimat has fluidity; its component parts can move, interact, bind and change their state freely. The macromolecules interact across subsystems, giving rise to interactions between subsystems at a higher level and observable changes in shape and behaviour of the Cellanimat as a whole.

The subsystems are nested: the ArtCyto exists within the Cytoplasm subsystem and the TP exists within the Membrane subsystem, see Fig.4.9 for a schematic. This is because in real cells the cytoskeleton resides within the cytoplasm and the TP proteins included in the prototype were all membrane-bound. It would however be possible to include TP proteins that exist within the Cytoplasm in future experiments by nesting the TP within both the Membrane and Cytoplasm subsystems.

The subsystems are only distinguishable due to the self-organization of the macromolecules they contain. No extra rules have been overlaid to differentiate between subsystems, the subsystems are merely a way of classing groups of macromolecules together, in terms of function and role, as they are in biology. The system as a whole works from the interaction of the macromolecules alone.

### 4.3.2 Cellanimat macromolecule overview

The ArtCyto structural proteins are modelled as agents with a unique identity and internal knowledge (e.g. of their position, binding site activity); they are discussed in further detail in the next section. All other macromolecules are modelled within a Cellular Automaton. Further macromolecule types could be modelled as agents, for example if greater focus on their behaviour is required by a particular experiment. Agent numbers are set at creation and conserved.

All macromolecules (agents or CA) exist in single voxels and interact with their local Moore Neighbours (MNs), see Appendix A for further explanation. All voxels have sub-states, indicating the presence and properties of macromolecules and, where appropriate, concentrations contained. For simplicity, all proteins have the same diffusion coefficients (i.e. move only to neighbours within a radius of one voxel in a single time step), this could easily be altered if it is known that specific proteins can diffuse faster.

### 4.3.3 The Environment-Phenotype Map

The Cellanimat model needed to be considered within a new framework as the unique developmental process at the heart of the model would be generated not through a conventional genotype to phenotype mapping (G-P map), but rather through interaction with the environment. Therefore the growth process is explained in terms of the Environment-Phenotype Map framework (E-P Map), novel to this thesis. Of course a G-P Map could include information exchange with the environment, but as discussed in Section 2.3 the majority of developmental algorithms to date are non-plastic, taking the genotype to phenotype map idea literally and not including any information from outside of the system. The E-P Map concept was developed in order to highlight the importance of environment-system interactions in generating morphologies, not just genetics. It also highlights the level of plasticity and mechanisms for morphological adaptation during the 'lifetime' of the system.

The E-P Map is a general framework for understanding and classifying MP in Dynamic Morphologies. It is based on, and extended from, the open L-system approach for plant-environment interactions and classifications of morpho-functional machines, described in (Mech, R. and Prusinkiewicz, P., 1996; Pfeifer, 2003). It was also inspired by Hogeweg (2002b) which focused on the interplay of many lower mechanisms to generate the overall morphogenesis mechanism. It considers the generation of form, and growth-related behaviours, in terms of the system's structural coupling to the environment, rather than through purely internal processes. As such, a systematic measure of the DM environmental interface (the E-P Map) would not only provide a comprehensive framework for understanding and explaining morphogenesis mechanisms, but could help clarify, and indeed quantify, the level of embodiment of a system, as proposed by Quick, T. et al. (1999).

#### 4.3.3.1 Formal definition

An E-P Map is a set comprised of distinct environment-phenotype interactions, or 'EP functions', whose competitive/cooperative combination within a specific environment can be used to explain observed morphological behaviours and structural changes in the system. Three possible types of EP function can be defined:



- **Type 1:** the effect of a *global* environmental factor on the whole morphological structure.  
(e.g. gravity, temperature)
- **Type 2:** the effect of a *local* environmental factor on part of the morphological structure.  
(e.g. obstacles, gradients)
- **Type 3:** the *reciprocal* effect on the environment of a morphological-structural change.  
(e.g. depletion of environmental sources by uptake for growth)

We further classify an EP function as either passive or active: *passive* interactions do not cause or require the activation of *new* information-processing pathways in the DM. For example, a collision that simply blocks a DM's growth (addition of connected sub-components) is a *type 2-passive* interaction. A collision that triggers sensor activation, resulting in new sub-component behaviours and connectivity, is a *type 2-active* interaction.

#### 4.3.4 Example: The Protrusions E-P Map

To aid discussion of the Cellanimat the 'protrusions E-P Map', used in the experiments described in subsequent chapters, will be introduced and used as an example. However, other E-P Maps could be implemented by changing the rules of macromolecular interaction or their properties or by adding/removing macromolecules. The protrusions E-P Map closely models the first stage of chemotaxis, the formation of a protruding 'leading edge' facilitating movement of a cell towards a diffusing chemoattractant signal (Bray, 2001). Actin filaments, induced to assemble by the environmental signal, push out the membrane locally (creating the membrane protrusions). These protrusions change the cell's overall morphology and behaviour, allowing it to move to the stimulus when combined with other stages of the processes (a fuller description of chemotaxis can be found in the next chapter). The protrusions E-P Map consists of the three EP functions below, which determine the Cellanimat's morphology and behaviour at each time step.

- **EP<sub>1</sub>:** 'Filament formation'                      *type 2-active*
- **EP<sub>2</sub>:** 'Collision'                                      *type 2-passive*
- **EP<sub>3</sub>:** 'Redistribution'                              *type 3-passive*

See Fig. 4.10 for a schematic of EP<sub>1</sub>, the filament formation interaction and Fig. 4.11 for an overview of this in practice. EP<sub>1</sub> aims to model the environment-induced actin filament formation described in the previous section, hence its classification as *type 2-active* (local environmental factors induce activity within the Cellanimat). EP<sub>2</sub> defines a passive, local interaction where a solid object, such as the environment boundary, will block filament-driven membrane expansions. EP<sub>3</sub> allows filaments to push out the membrane through non-solid environmental factors, such as a chemical gradient. Instead of simply overwriting the environment's contents that the membrane has extended into, the contents are redistributed to all environment state MN voxels, conserving environmental factor volumes. EP<sub>3</sub> is therefore a *type 3-passive* function: the Cellanimat has a reciprocal affect on the environment.

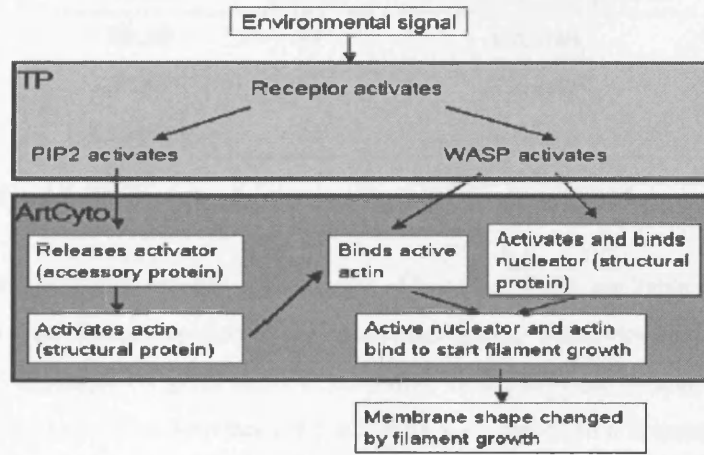


Figure 4.10: Filament formation EP<sub>1</sub> function from the protrusions E-P Map, abstracted from the biological pathway for fibroblast chemotaxis.

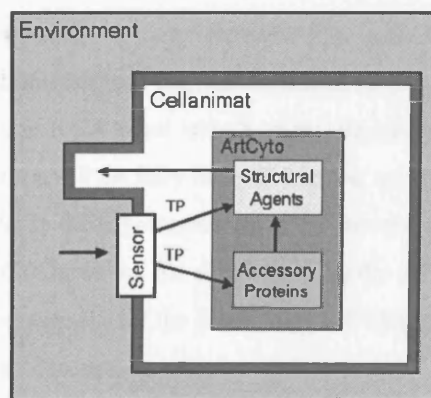


Figure 4.11: Filament formation EP<sub>1</sub> function in practice.

Macromolecule	Subsystem	Modelling scheme
Actin	ArtCyto	agent
Arp2/3	ArtCyto	agent
Profilin	ArtCyto	CA concentration gradient
WASP	TP	CA state
PIP2	TP	CA state
Receptors	TP	CA state

Table 4.2: The protein selection used in the Protrusions E-P Map example.

The protrusions E-P Map consists of a selection of just six proteins, see Table 4.2. The TP proteins only exist as CA state changes applied to the membrane voxels. Fuller descriptions of each macromolecule and its behaviours are given in the next section. In this example system, only one accessory protein (profilin) is used, which activates actin, allowing it to join on to a filament as previously discussed. The levels of profilin in the Cellanimat are raised and lowered by environmental interaction affecting PIP2 release/uptake. For simplicity, and to control variables, all other protein levels remain constant within the Cellanimat, i.e. Thymosin and Cofilin are realized by static parameters and attributes of actin agents only, as an ‘inactive state’ or loss of affinity parameter respectively.

Of course in real cells all protein levels constantly fluctuate in relation to the environment, recycling, degrading or by genetic regulation. The protrusions E-P Map is used only as an example here; the Cellanimat could work with many different versions of this mapping, involving different protein selections for the ArtCyto and TP, or indeed completely different E-P Maps such as internal transport of material in relation to external stimuli.

## 4.4 The Cellanimat: Rules of Play

Evaluation of the Cellanimat occurs in the order shown in Fig. 4.12, at the end of each evaluation the time step  $t$  (initially zero) is incremented and the evaluation repeats as desired. First the world is created, then, throughout the time steps each CA voxel and all agents are assessed and states are updated. Each stage of the Cellanimat algorithm will be fully described in the sections that follow. The Cellanimat was implemented as a 3D model in the experiments described in subsequent chapters (and published in (Bentley and Clack, 2004, 2005)), however, for simplicity here the 2D case will be described <sup>1</sup>. Table 4.3 contains all the threshold parameters for the protrusions E-P Map that will be used, and more fully described, throughout this model description.

These parameters, together with those shown in Table 4.4, constitute the genotype of the system, they are a small set of unchanging parameters whose predefined setting, along with specified environmental factors, affect the course of growth as determined by the implicit interactions between proteins. Results from evolutionary experiments with these parameters are described in Chapter 6; it is clear that the size of the genotype is small, though it will be shown that it can be used in conjunction with the E-P

<sup>1</sup>For 3D, there are simply twenty-six Moore Neighbours (MNs), instead of eight, for macromolecules to interact with.

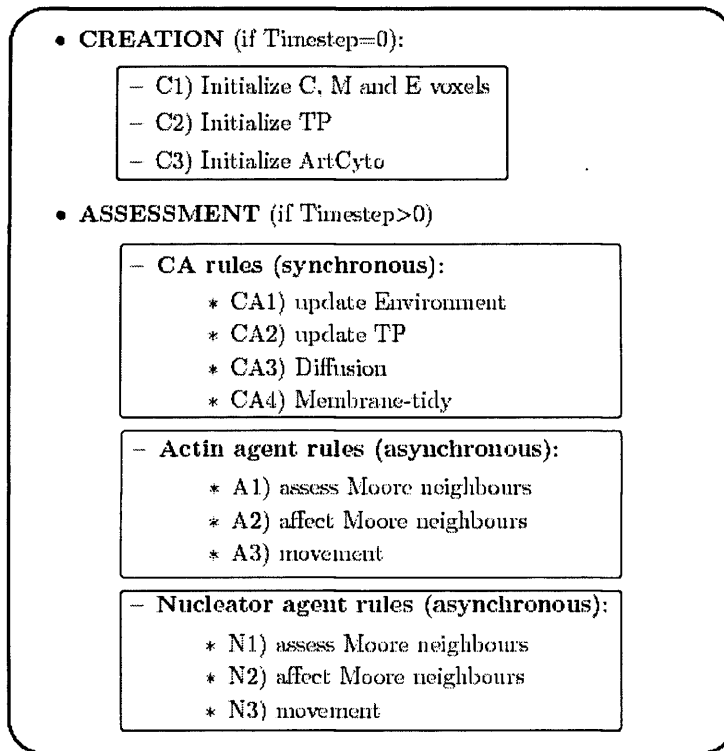


Figure 4.12: The Cellanimat model evaluation performed at each time step. Details of each rule given in text.

Map to generate complex, adaptive forms and behaviours.

#### 4.4.1 Creation

At the start of a run, the Cellanimat and its environment need to be initialized. A variety of initial shapes can be assumed; for example in the experiments described in the next chapter a 3D cylindrical form is used. In this description for simplicity a 2D square is used. See Table 4.4 for details of the parameters needed in creation.

##### *C1) Initialize C, M and E voxels*

Creation rule C1 initializes the basic E (environment), C (cytoplasm) and M (membrane) voxels. The environment, with size (columns, rows), has all voxels set to voxel-state E (environment). The Cellanimat Cytoplasm voxels are then initiated as defined by the the L, W, and position (x,y) parameters. The membrane is initialized to satisfy the simple rule that no cytoplasm can be exposed to the environment in any of its MNs, see Equation 4.1. Note that the total length and width of the Cellanimat, once the membrane has been initialized, is L+2, W+2.

$$\forall E, \quad \text{if } \exists C \in MN, \quad E \rightarrow M \quad (4.1)$$

E, M and C voxels had type specific substates as detailed in Fig.4.14. The stored values in the substates reflected the presence and properties of macromolecules which altered through the update rules

Acronym	Description
RECth	concentration of stimulant in environment needed to activate a receptor
CHEMth	diffusion rate of chemoattractant
PPlume	plume of profilin released by PIP2
Pth	diffusion rate of profilin
PAth	Concentration of profilin needed to change actin state (SA $\rightarrow$ PA)
Precycle	amount of profilin bound and released by actin in the rules PrUptake and PrRelease
FTH	time an agent must have spent in a filament before it starts to lose affinity
FINT	time interval at which a filamentous agent's affinity for a filament decreases

Table 4.3: Cellanimat threshold parameters.

Parameter	Definition
(columns, rows)	size of environment
(x,y)	cellanimat centre
L	cytoplasm length
W	cytoplasm width
#A	no. of Actin agents
#N	no. of Nucleator agents
P(REC)	probability of M voxel containing a receptor
chemPlume	amount of chemoattractant initialized in a voxel

Table 4.4: 2D Cellanimat creation parameters.

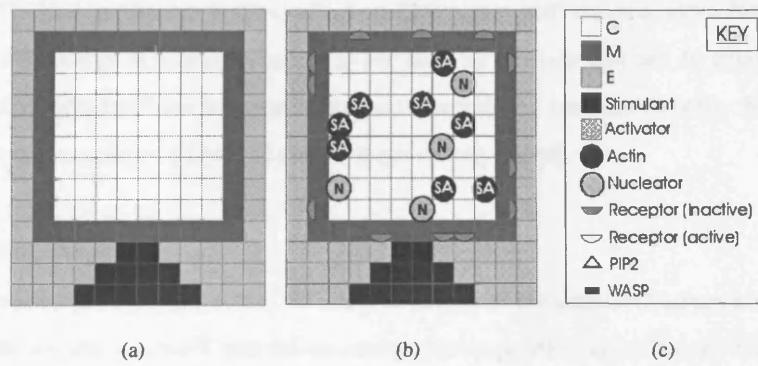


Figure 4.13: (a) Creation rule C1 initializes the basic E (environment), C (cytoplasm) and M (membrane) voxels, a small plume area of stimulant has also been initialized in the environment. (b) Creation after rules C2 and C3: the proteins residing within the three voxel types are shown. (c) Key for all similar diagrams.

described in the coming assessment section. For a specific experiment various things could be initialized in the environment, for example, a chemoattractant plume. A plume of set amount (chemPlume) could be initialized in a single voxel, or a group of voxels, by setting E.chemo in each to chemPlume. See Fig. 4.13(a) and 4.13(c) for an example view of the Cellanimat's world after stage C1 has been executed.

#### C2) Initialize TP

3 Voxel types	Sub-states
Membrane -TP	-rec (0, 1 or 2) -WASP (0 or 1) -PIP2 (0 or 1)
Cytoplasm -ArtCyto	-actin (int) -nucleator (int) -profilin (float)
Env	-chemo (float)

Figure 4.14: Voxel types and substates. E.g. if M.rec = 1 then a receptor is present, if M.rec=2 then the receptor is active; if C.actin=4 then the actin agent with identifier 4 resides in that voxel. If no agent is present then C.actin = #A+1 and C.nucleator=#N+1.

In the protrusions E-P Map only the front and back end TP proteins are modelled, i.e. those that are directly affected by the environment (Receptors) and those that directly affect the ArtCyto (PIP2 and WASP). This greatly improved model efficiency. The voxel substate M.rec could be in one of three settings: absent (0), inactive (1) or active (2). All membrane voxels had the same probability, P(REC) of containing a receptor (M.rec was set to 1 with probability P(REC)).

PIP2 and WASP are represented by the substates M.PIP2 and M.WASP respectively, they could be in two possible states: active (1) or inactive (0). In creation both substates were initialized as zero for all M voxels.

Altering P(REC) can have a marked affect on Cellanimat performance, more fully investigated in Chapter 6, as the number of receptors relates to the scale of reaction that can be triggered. In the protrusions E-P Map receptors have no movement across membrane surfaces directly, though distribution does change as the membrane shape and size changes during growth.

### C3) Initialize ArtCyto:

In the protrusions E-P Map the ArtCyto consists simply of the structural agents actin and nucleators (representing the nucleator Arp2/3) and the accessory protein profilin (an activator). Only one agent was allowed per voxel and profilin could only diffuse through ‘empty’ C voxels — not containing an agent. C.profilin was initialized as zero for all C voxels.

Agents are initialized in randomly chosen C voxels to mimic the widely dispersed synthesis of proteins by the Endoplasmic Reticulum, which extends throughout the cell. Agent internal knowledge initial settings are given in Table 4.5.

Actin agents cycle through the states SA, PA, WA and FA representing their binding activity. SA is the inactive state, representing sequestering by thymosin; they are unable to form into filaments when in this state. PA is the active state, when the agent has bound to profilin. The WA state is held when active actin binds to WASP and FA when it joins onto a filament. It can then fall off from the filament returning to state SA. The state changes are fully described in the next subsection. As profilin levels are initialized as zero in all voxels actin agents are initialized in the ‘inhibited’ state SA.

Nucleator agents play the role of the Arp2/3 complex from real cells. They cycle through the states N, WN and FN. They are ‘inactive’ (unable to start filaments) in state N. WN is the active state, when bound to WASP. FN state nucleators have nucleated a filament and are still bound to it. They then fall off the filament and return to stated N. As WASP are all initialized as inactive all nucleators begin in the inactive state N. See Fig. 4.13(b) for an example view when stages C2 and C3 have been executed.

## 4.4.2 Assessment: CA Rules

First, all components modelled within the CA are evaluated synchronously then the agents are each updated in turn (asynchronous updating).

### CA1) Assess Environment

$$\begin{aligned} &\text{if } V.P = Dth + \delta, \quad \text{where } \delta > 0 \\ &\quad \text{then } V.P := Dth, \quad \text{and} \\ &\quad \forall V \in MN, V.P := V.P + \frac{\delta}{x} \end{aligned}$$

Depending on the environment’s contents, different rules can be implemented here. For a diffusing chemoattractant, or ‘stimulant’, a method similar to Miller’s described in Miller (2003) is used. In their CA model of diffusion all voxels in the correct state are evaluated at each time step, according to a specified diffusion threshold and initial plume value. The equation above shows this for a general diffusible protein  $P$ , within voxel  $V$ , with diffusion threshold  $Dth$  and  $x$  being the number of MNs also in state  $V$ .

Agent internal state	Knowledge contained	Initial setting
$A_i.(x,y)$	x,y coordinate position	random
$A_i.minusSite$	identifier of agent bound to at minus site	none
$A_i.plusSite$	identifier of agent bound to at plus site	none
$A_i.orientation$	orientation of binding sites	none
$A_i.Fcounter$	time spent in current filament	0
$A_i.state$	current state	SA
.....	.....	.....
$N_i.(x,y)$	x,y coordinate	random
$N_i.bindingSite$	identifier of actin bound at binding site	none
$N_i.branch$	if forming a branch	none
$N_i.Fcounter$	time spent in current filament	0
$N_i.state$	current state	N

Table 4.5: Agent internal knowledge attributes and initial settings for actin agents (A) and nucleators (N).  $i$  is the agent's unique identifier.

#### CA2) Assess TP:

Environmental factors, such as the diffusing stimulant, can trigger the Cellanimat's receptors to activate. Fig.4.15 shows the exact rules for receptor, WASP and PIP2 state changes in pseudo code; every membrane voxel is evaluated using this rule in a time step. PIP2 when activated, and only upon activation, releases a plume of profilin (of size PPlume) into each neighbouring C voxel not containing an agent.

If no active receptor exists in an active WASP's MNs, the WASP is deactivated within the Membrane-tidy function (rule CA4 described later). Without such a tidy-up function WASP could be left stranded when receptors are moved around during the agent rule 'Mchange'.

As described in the previous section, profilin binds to inactive PIP2 and is released upon its activation. So in the model, at each time step, if  $M.PIP2=0$  then all neighbouring profilin is removed. The removal of profilin is an important feature of real cells, it allows the cell to concentrate cytoskeletal activity into just the area needed, rather than activity being triggered throughout the cell as profilin diffuses. The chain of events in the TP, and subsequent regulation of profilin levels allows the environment to 'contact' the ArtCyto and trigger shape changes. Figure 4.16(a) shows the activation of TP receptors in the example Cellanimat shown in Fig.4.13(b), resulting in local state changes.

#### CA3) Diffusion

Any accessory proteins modelled as concentration gradients within the Cellanimat are diffused within this stage of the algorithm. In the protrusions E-P Map only profilin is present as a concentration gradient, its diffusion is calculated using the method as described in the CA1 rule above. Figure 4.16(b)



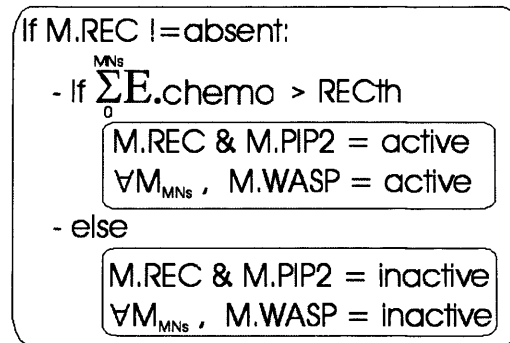


Figure 4.15: pseudo code for rule CA2) environmental control of TP activations.

shows the sample Cellanimat after profilin diffusion has taken place.

#### CA4) Membrane-tidy

At every time step a 'tidy up' function is implemented for the following two reasons.

1. To maintain the membrane as a continuous barrier, with single-voxel thickness, between the E and C voxels. Any membrane voxel that does not have both C and E MNs is overwritten as state E, see Fig. 4.22(b). This is a very simple model of membrane lipid assimilation and self-organization, which in reality is due to the progression towards an overall low-energy state by lipids possessing both hydrophilic head and hydrophobic tail domains as discussed previously.
2. To maintain integrity in the WASP activation system, an M voxel will have WASP deactivated if no active receptor can be found in its MNs. This is implemented because receptors can be overwritten and 'moved' during the agent rule 'Mchange' (described in Section 4.4.3) and so active WASP would otherwise become stranded.

#### 4.4.3 Assessment: actin agent rules (asynchronous)

When a protein agent binds to another its own state changes, but it also changes the state (and possibly the position) of the other protein involved; this means that when a single agent is being assessed, fundamental changes can occur in another agent (and its local environment) before or after (but not during) the other agent's turn to be assessed, thus the agents update *asynchronously*. All agents are assessed in turn, in numerical order, based on their identifiers. There are three stages to agent assessment:

1. **Assess Moore neighbours** consists of state and attribute changes in the agent resulting from assessment of the current local neighbourhood. The agent, and also a neighbour agent if two are binding together, change state and update their internal attributes.
2. **Affect Moore neighbours** involves changes made to the local CA environment by the agent. Rules for the new or persisting state are implemented which may alter the local environment.
3. **Movement** finally, the new agent position is calculated based on its current state.

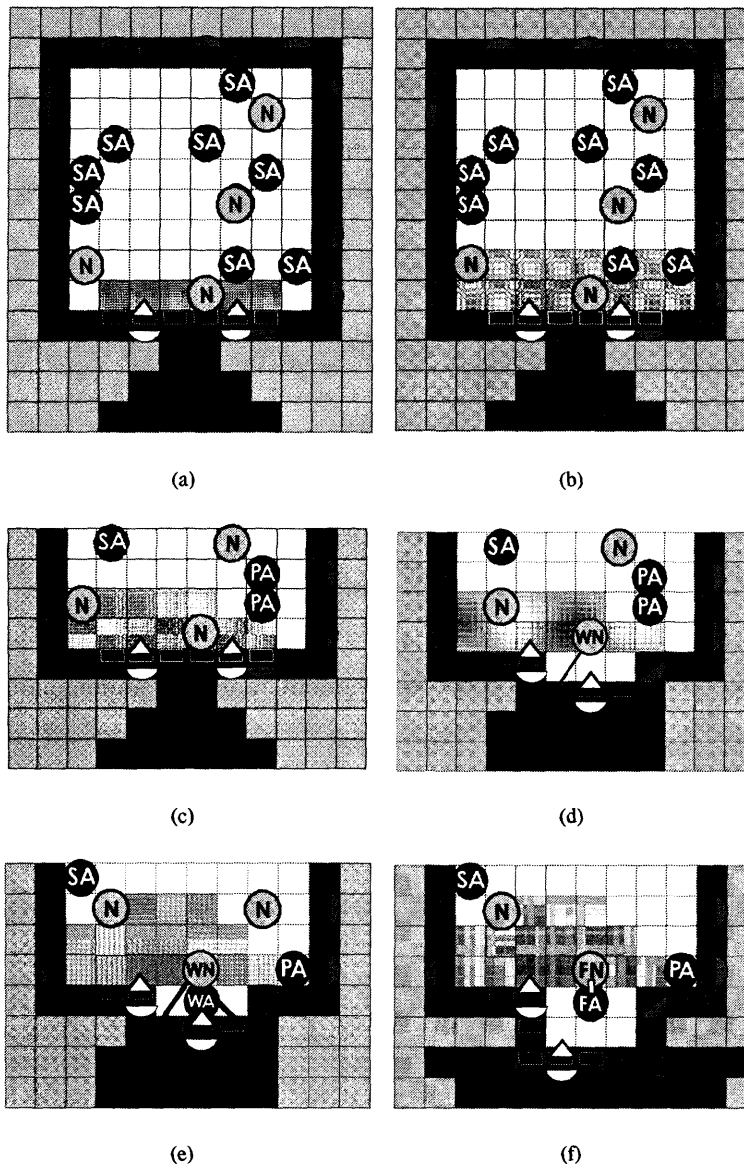


Figure 4.16: refer to Key in Fig 4.13(c). (a) Rule CA2 'Assess TP': two receptors neighbouring the environmental stimulant have become activated. WASP and PIP2 have subsequently also been activated and PIP2 has released profilin. (b) Rule CA3 'Diffusion': profilin has diffused into nearby empty C voxels. (c) 'Actin agent rules': two actin agents have changed state to PA as they encountered local profilin levels over the PAth threshold (rule A1). Amount 'Precycle' of profilin has been removed from their MNs (rule A2). All SA and PA state actin agents move to a randomly chosen MN (rule A3). (d) The bottom N state nucleator has changed state to WN and pushed out the local membrane (Mchange rule), as it had WASP in its MNs (rule N1). WN agents cannot move, the other N state agents move randomly (rule A3). (e) A few time steps later it can be seen that random movement has landed one of the PA state actin agents next to WASP, causing it to change state to WA. (f) The WN and WA have bound together forming a filament - their states change respectively to FN and  $F^+A$ . This triggered the Mchange rule, where the local membrane is again pushed out (rule A2). A new receptor and WASP distribution was initiated and the stimulator in the environment has been redistributed ( $EP_3$ ).

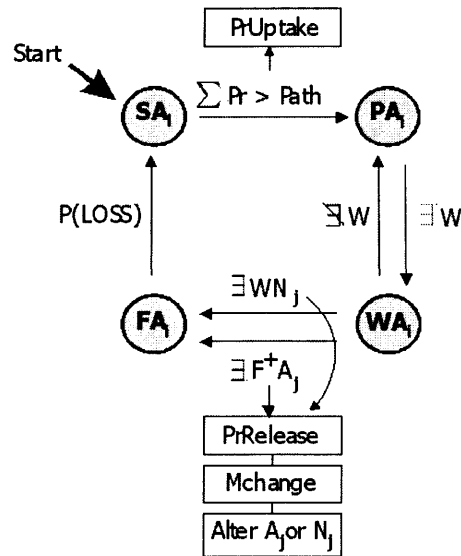


Figure 4.17: Actin agent state changes, reflecting the macromolecule the agent is bound to, see Table 4.6 for acronyms, here Pr means C.profilin and W means active WASP. State changes can only occur in this sequence, reflecting the biological case. Certain state changes provoke a reciprocal affect on the agent’s environment, these are shown in boxes and described in Section 4.4.3.

Acronym	Protein	In Voxel	movement
SA	Sequestered-actin (inactive)	C	RM
PA	active actin (Profilin bound)	C	RM
WA	active actin (WASP bound)	C	WM
F <sup>+</sup> A	Filamentous-actin (+site free)	C	None
F <sup>-</sup> A	Filamentous-actin (-site free)	C	None
FA	Filamentous-actin (fully bound)	C	None
N	Nucleator (inactive)	C	RM
WN	active Nucleator (WASP bound)	C	None
FN	Filamentous-nucleator	C	None
<b>Profilin</b>	activator accessory protein (Profilin)	C	Diffusion
<b>WASP</b>	WASP	M	None
<b>PIP2</b>	PIP2	M	None

Table 4.6: Cellanimat protein Acronym descriptions, the voxel type they belong to and their types of movement RM denotes random movement, WM - WASP-bound movement described in text.

*A1) Assess Moore Neighbours*

Agents first assess the contents of their MNs and change state if necessary. The local rules for agent state changes are shown in Fig.4.17. Each state change represents a change in connectivity of components, the forming of new macromolecules, and so agent attributes are updated to reflect binding changes.

Actin agents are initialized as sequestered (**SA** - bound to inhibitor). When the sum of profilin in an SA agent's MNs exceeds the threshold  $P_{A_{th}}$  the agent's state changes to **PA**, as if it has bound to profilin and become active. Actin is restricted from joining onto a filament in the Cellanimat (becoming **FA**) until it has first bound to WASP (**WA**), mimicking the WASP related funnelling of structural proteins to the membrane, in real cells, see Figs 4.16(e) and (f).

A filament is started when a **WA** agent detects a **WN** nucleator in its MNs, i.e. when WASP has brought an active nucleator and an active actin to the same location, close to the source of stimulation by the environment. See Figs.4.18(a) & 4.16(e). The cycling of actin through filaments is characterized by the **FA** substates, full details shown in Fig.4.19.  $F^+A$  identifies the agent at the plus end of a filament, that has its plusSite (see Table 4.5) free. Fig.4.18(a) shows that the first actin agent in a filament is assigned this state, signifying to neighbouring **WA** actin that they can bind to it, joining the filament, see Fig.4.18(b). To generate only straight, rigid filaments, when agents bind together their orientation attribute is set, maintaining the direction of growth. Fig. 4.21 shows the set orientation function.

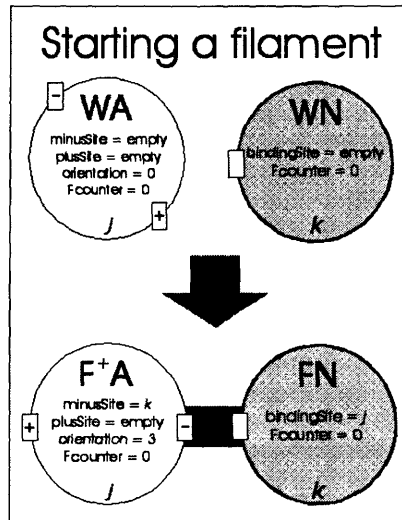
State  $F^-A$  indicates the agent is at a filament's minus end due to the nucleator, or actin agent, originally bound to its minusSite disassociating, see Fig.4.20. An agent in this state has its minusSite free and is next to disassociate from that filament. When actin disassociates from a filament it returns to the inactive, sequestered state **SA**. Disassociation, or 'Loss of affinity' is implemented as a simple probabilistic function,  $P(LOSS)$ , which increases with time, rather than directly modelling ATP-ADP hydrolysis. Increasing  $P(LOSS)$  is akin to increasing levels of a severing protein, such as cofilin. As  $P(LOSS)$  increases average filament length decreases. When an actin agent is in any of the **FA** substates its internal filament counter ( $F_{counter}$ ) increments with each time step spent in the filament. When, and only when, an actin agent is in state  $F^-A$  can it disassociate. When  $A_i.F_{counter} > F_{TH}$  the probability of disassociation is activated and increases with time, inline with the set interval  $F_{INT}$ , as shown in Equation 4.2.

*A2) Affect Moore Neighbours*

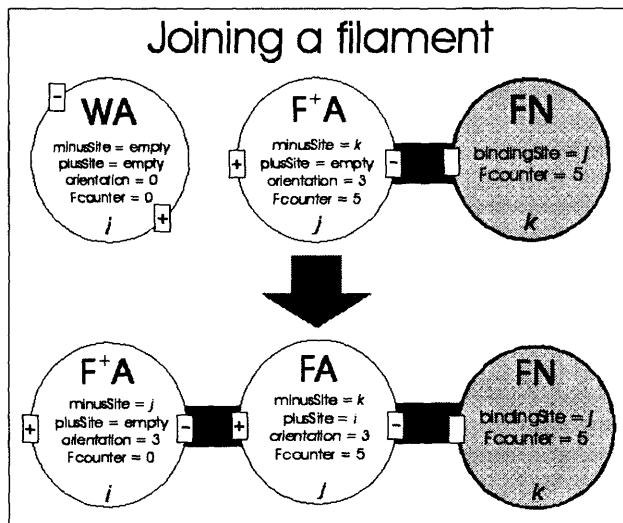
$$P(LOSS) = \begin{cases} \frac{A_i.F_{counter}}{100 \times F_{INT}}, & \text{if } A_i.F_{counter} > F_{TH}; \\ 0, & \text{otherwise.} \end{cases} \quad (4.2)$$

Certain agent state changes, or binding events, effect important changes back onto the agent's local environment. Fig.4.17 shows when the following rules (shown in boxes) are implemented.

**PrUptake:** This rule is called when an actin agent is activated by profilin. A small amount of profilin (less than or equal to *Preycle*) is removed from the system, as if it has actually bound to the agent. Specifically one random C state MN voxel is chosen and its profilin content is removed. If



(a)



(b)

Figure 4.18: Agent state and attribute changes during filament formation. Actin agents shown as white circles, nucleators shown in grey. When a state change occurs, agent attributes are overwritten, ensuring agents bind to the correct number of neighbours and that the neighbour knows which agent *they* are bound to, eliminating incorrect disassociation events. Orientation values are obtained by the 'set orientation' function, detailed in Fig.4.21.

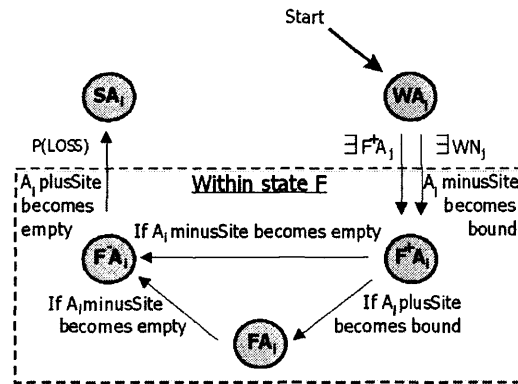


Figure 4.19: As Actin agents have two actin-binding sites, the FA state can be further divided into the three states shown. This extra F state change sequence models the polarity of filaments, so that new agents join onto only the filament's plus end and fall off at the minus end. An agent can go straight from  $F^+A$  to  $F^-A$  if it joined a filament and loses affinity before another agent had time to join onto its plusSite.

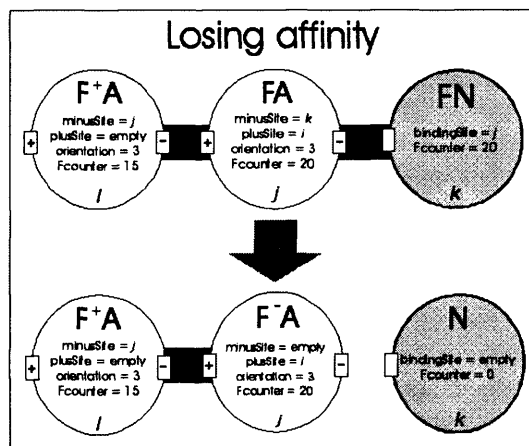


Figure 4.20: Agent state and attribute changes during loss of affinity from the filament's minus end. Actin agents shown as white circles, nucleators shown in grey.

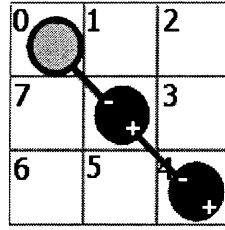


Figure 4.21: The actin agent's 'orientation' attribute ( $A_i$ .orientation) denotes the orientation of binding sites. Orientation is set when binding to another agent. If an actin agent  $A_i$  in state **WA** (shown in black in the central voxel) is next to a nucleator **WN** agent (top left) then they bind. The MNs of the binding agent are numbered with position values ( $Pv$ ) clockwise in the way shown.  $A_i$ .orientation is set to zero (the nucleator's  $Pv$ ). For a further actin agent  $A_j$  to bind to the forming filament its position value  $Pv$ , from the perspective of  $A_i$  must satisfy:  $Pv \equiv_8 A_i$ .orientation + 4; here, its  $Pv$  is 4 so the condition is satisfied and the two bind together. In binding agent  $A_j$ .orientation is set to zero, as from its perspective this is  $A_i$ 's  $Pv$ .

$C$ .profilin > Precycle then only the amount Precycle is taken.

**PrRelease:** This rule represents the release of profilin, when active actin (state **WA**) binds onto the end of a filament. When a **WA** agent changes state to **FA** a random **C** state MN is chosen to receive the extra Precycle amount of profilin. Combined with the PrUptake rule this simulates the recycling of profilin, at the leading edge, observed in real cells. Profilin is hindered from diffusing too far from the membrane by this recycling, thus reinforcing the *local* activation of actin, with no wasted effort too far from the desired site (Holt, M. R. and Koffer, A., 2001).

**ClearContents:** This rule represents the movement of all profilin from a voxel as an agent moves into it, so that profilin concentrations are conserved during agent movements, see rule A3 'movement' below. The contents are distributed fairly to all **C** MNs not containing an agent. This rule adds realism to the diffusion of profilin as the number of other Cellanimat proteins moving will further affect profilin distribution.

**Mchange:** This rule occurs in two stages, to allow a filament to alter membrane shape whilst conserving Cellanimat cytoplasm volume, see Figs.4.16(d) & 4.16(f).

$$\forall M \in MN, \quad M \rightarrow C \quad (4.3)$$

$$\forall \text{new } C, \quad \text{if } \exists E \in MN, \quad E \rightarrow M \quad (4.4)$$

1. **Push-out:** as an agent changes from **WA** to **F<sup>+</sup>A** the membrane is moved outwards locally, using the exact rule detailed in Equation 4.3 above.  $M$  voxels newly generated by this rule have probability  $P(\text{REC})$  of containing a receptor, as in creation rule **C2**. This represents the migration of receptors laterally on the membrane as membrane shape changes, and also the production of new receptors during a cell's lifetime.
2. **Contract:** To conserve cytoplasm volume a crude contraction function is used, modelling ba-

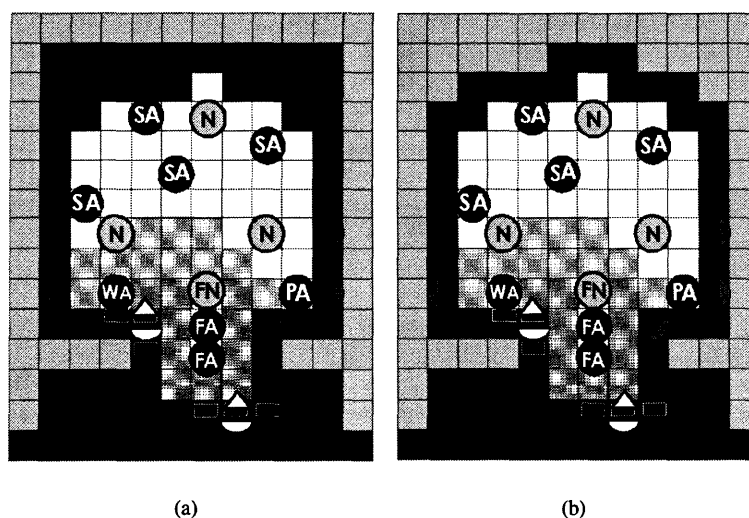


Figure 4.22: (a) for each new cytoplasm voxel created by the push-out stage of the Mchange rule, the furthest C voxel is simultaneously ‘contracted’ (changed to an M voxel) to conserve cytoplasm volume. This leaves the membrane with areas of higher density. (b) Membrane thickness is kept constant by the assimilation of surplus M voxels back into the uniform thickness, using the membrane-tidy rule (rule CA3).

sic surface tension properties. In chemotaxis and phagocytosis complicated cytoskeleton-powered mechanisms control contraction at the rear of the cell which were beyond the scope of the model and experiments performed so far. The contract rule does the following: for each new C voxel created during push-out, the furthest C voxel not containing an agent in a filamentous state (dC) is found. If dC contains profilin, then the ClearContents function is called to redistribute it. If dC contains an agent, that agent is moved to a randomly chosen MN; if no free MN exists, the agent would be re-initialized in a randomly chosen free C voxel, representing the decay and re-production of proteins. Once cleared of its contents dC is then changed to state M as if the membrane has pulled into the Cellanimat at that point, see Fig.4.22(a).

### A3) movement.

There are different forms of movement associated with each state, shown in Table 4.6.

- **Random movement (RM):** the agent has (arbitrarily) ten tries to randomly pick a free C MN to move to, otherwise it remains still. The ClearContents rule is called upon a successful move. The new C voxel acquires the agent’s identifier, the agent’s position data is updated (actin.(x,y)) and the old C.agent substate is reset to empty.
- **WASP Movement (WM):** the biological concept of ‘recruitment’ of proteins, to a specific protein such as WASP, is modelled as follows: an agent in state WA can only move such that a WASP is still in its MNs. If there is no WASP MN, e.g. if the adjacent WASP has deactivated, then actin.state changes back to PA with random movement.



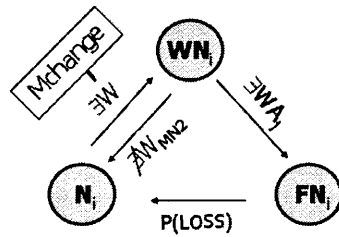


Figure 4.23: Nucleator agent state change rules. W stands for active WASP, MN  $r=2$  stands for radius 2 Moore neighbourhood.

#### 4.4.4 Assessment: Nucleator Agent Rules

##### *N1) Assess Moore neighbours*

Figure 4.23 shows the nucleator state change rules. Nucleator agents are active only when bound to WASP (WN). When active they are able to start a filament, if a similarly active actin agent is present to bind to. When an actin agent binds to an active nucleator its state changes to FN and other attributes are overwritten as in Fig.4.18(a). N changes to WN if there is an active WASP in its MNs. To allow room for actin agents, bound to WASP at the membrane, to move in front of the nucleator and start a filament the Mchange rule is called here and the membrane is pushed out locally, whilst contracting at the back. See Fig.4.16(d). WN agents return to state N if an active WASP can no longer be found in its radius 2 MNs (given that the Mchange causes the WASP to move out to the radius 2 MNs this is allowed to still activate it). A nucleator in state WN can become state FN if a WA state actin agent is present in its MNs, see Figs.4.16(e) & 4.16(f). The WA agent then also changes state (to FA) and the two agents, now bound together, can no longer move. With probability P(LOSS) the state FN agent will disassociate from the FA agent and return to the inactive, unbound state N, shown in Fig.4.20.

**Branching:** nucleator agents in state N and not already 'stuck' to a filament, check their MNs for a filament to stick to in order to form a branch, as observed in real cell and described in section 4.2. If an FA state actin agent exists in its MNs, bound to another FA agent, then the nucleator changes its N.branch state from zero to one and abstains from random movement for one turn. This gives it more of a chance to form a filament next to another in a branch. If it does not nucleate a branch in this next time step then it returns to random movement and tries elsewhere. This avoids nucleators becoming permanently stuck in unviable positions.

##### *N2: affect Moore neighbours*

In the protrusions E-P Map nucleators could only have the effect on their environment of redistributing the profilin gradient during movement, through the clearContents rule as described previously in Section 4.4.3.

##### *N3: movement*

Table 4.6 shows the type of movement associated with each nucleator state. The movement types

are described in Section 4.4.3. See Figs. 4.16(d) and 4.16(f) for examples of these rules in situ.

## 4.5 Pseudo code overview

In this section a brief overview of the Cellanimat algorithm is given, as described above.

- CREATION

- C1) Initialize C, M and E voxels

- \* set all voxels to state E
- \* set voxels within length L, width W centred on (x,y) to state C
- \* set all C voxels with E neighbours to state M

- C2) Initialize TP in M state voxels

- \* initialize an inactive receptor with probability P(REC) otherwise set to none present
- \* set WASP and PIP2 to zero (inactive) in all M voxels

- C3) Initialize ArtCyto in C state voxels

- \* initialize #A actin agents in random positions (in state SA)
- \* initialize #N nucleator agents in random positions (in state N)
- \* set profilin level to zero in all C voxels

- ASSESSMENT

- CA Rules (synchronous)

- \* CA1) Update environment (if voxel is state E)

- diffuse excess chemoattractant to E state MNs

- \* CA2) Update TP (if voxel is state M)

- if sufficient stimulus in E state MNs and voxel contains a receptor: activate receptor and PIP2. Activate WASP in all M MNs
- otherwise: deactivate receptor and PIP2. deactivate WASP in all M MNs

- \* CA3) Diffusion (if voxel is state C)

- diffuse excess profilin to C state MNs

- \* CA4) Membrane-tidy (if voxel is state M)

- change state to E if does not form part of minimal barrier (does not have both E and C MNs)
- deactivate WASP if no active receptor in MNs

- Actin agent rules (asynchronous)

- \* A1) Assess Moore neighbours

- SA actin: change to PA if sufficient profilin,
- PA actin: change to WA actin if  $\exists$  WASP MN

- WA actin: change to FA actin if  $\exists$  an active nucleator or  $F^+ A$  in MNs. Or change back to PA if no WASP in MNs
- FA actin: change to SA with probability  $P(\text{LOSS})$
- \* **A2) Affect Moore neighbours**
  - PrUptake: as SA changes to PA remove amount 'Precycle' of profilin from one C state MN
  - PrRelease: as WA changes to FA release amount 'Precycle' to one C state MN
  - ClearContents (conserve profilin): distribute profilin contents of voxel to all C state MNs not containing an agent, before moving into it.
  - Mchange (as WA changes to FA): 1) Push-out (filopodia extension), overwrite all M state MNs to C, overwrite all E MNs, for each new C voxel, to state M; 2) Contract (conserve cytoplasm), for each new C voxel created during push-out, overwrite furthest C voxel to state M.
- \* **A3) Movement**
  - Random movement: SA and PA agents try ten times to randomly pick an empty C MN to move to.
  - WASP movement: WA agents can only move if the new voxel has a WASP MN
- **Nucleator agent rules (asynchronous)**
- **N1) Assess Moore neighbours**
  - \* N: change to WN if  $\exists$  WASP MN
  - \* WN: change to N if no WASP in radius 2 MNs. Change to FN if  $\exists$  WA in MNs
  - \* FN: change to N with probability  $P(\text{LOSS})$
- **N2) Affect Moore neighbours**
  - \* ClearContents (conserve profilin): distribute profilin contents of voxel to all C state MNs not containing an agent, before moving into it.
- **N3) Movement**
  - \* state N agents perform random movement

## 4.6 Summary

In this chapter basic cell biology and the cytoskeleton have been introduced. The Cellanimat, powered by the Artificial Cytoskeleton, has been presented in detail as a model addressing Objective Two of this thesis. It is a loyal yet abstracted model of the cytoskeleton within a cell generating morphological plasticity to the environment. Due to the many local rule interactions of the cytoskeleton that have been modelled it is hypothesized to be capable of powering a similar level of morphological plasticity in the Cellanimat to real cells. The aim was, through careful close modelling, to harness the ability of real cells

to generate large arrays of different, well-adapted morphologies through environmental interaction with many small component parts of dynamic structures.

Certain aspects have been simplified and scaled down, part of the aim of the model was to create a small, efficient model that could run on a single workstation providing a viable mechanism for powering adaptive behaviour in a simulated animat. As such the cell:filament:monomer scale was not maintained, instead filaments are much larger in size. This greatly improved model efficiency and was hypothesized to be powerful enough as a mechanism to generate visibly, and functionally, similar morphological plasticity and behaviours to real cells. Increasing the accuracy of cell:filament scale was presumed to add only greater resolution in the complexity of forms generated, rather than extra system features. To reduce the realism of the scale further however could result in lost ability to generate complex forms, e.g. if only one filament could fit within the Cellanimat.

The Cellanimat is reasonably complex as a first-incarnation model, simulating the generative process reasonably accurately, for two reasons: 1) to avoid loss of information and ability in the early stages of creating an MP mechanism for an AI system and 2) to remain useful as a biological model for the investigation of diatom morphogenesis and MP. The Cellanimat was based on real low-level production rules involved in cellular morphogenesis. This allows it to be useful for actually *understanding* morphogenesis rather than just as an abstract, unrealistic mechanism for growing life-like looking AI systems. For example L-systems (Lindenmayer, 1968), though simple, effective and able to produce life-like tree structures, cannot tell us how and why a branch in a tree actually is generated. Conversely, basing the Cellanimat growth process on realistic 'perception-action loops' (EP functions) does give an explanation of how and why certain morphological features occur and as such could be of more use in understanding morphological plasticity in natural and artificial systems.

The cytoskeleton is able to perform incredible feats of structural plasticity due to the many physical properties of the component parts, the sheer numbers of proteins involved and the interactions between them. To lose these aspects in the first version would have denied the model, and future incarnations, the very attributes it needs to produce rich behaviours. However, starting with a more detailed model allows us to pick and choose aspects that are useful for particular applications: simplifying and pruning the complex model to create a simplified, refined model is a preferable task to attempting to improve the realism and detail of a highly simplified model for an application, refer to the schematic shown in Fig.1.1. Indeed in coming chapters it will be shown that some rules can be further simplified, and even omitted, to create a more simplified version and applied to a particular modelling problem in diatom morphogenesis.

To test these hypotheses the Cellanimat was subjected to several experiments concerned with judging its ability to produce similar morphological plasticity to real cells, detailed in the next chapter. To investigate the inner workings of the model, uncover any hard to detect problems, investigate parameter optimizations for increased efficiency and rule simplifications seven studies were performed, detailed in Chapter 6.

## Chapter 5

# Cellanimat multifunctionality: from chemotaxis to phagocytosis

In the previous chapter the Cellanimat model was introduced and a small scale 2D example of the Cellanimat, growing membrane protrusions in response to an environmental stimulus, was described. In this chapter results from full scale experiments will be discussed, as published in (Bentley and Clack, 2004, 2005).

To validate the protrusions E-P Map, by showing a qualitative similarity between Cellanimat behaviour and cytoskeletal driven cell behaviours, the Cellanimat model was tested at chemotaxis (Experiment A), a well-defined biological case involving the cytoskeletal generation of membrane protrusions.

This thesis is concerned with adaptive systems for *changing* environments, where morphological plasticity can prove to be a distinct advantage. As such the ArtCyto was designed to be capable of powering many different forms of adaptive behaviour, and not be designed in a task-specific way. The expectation was that by basing the model on the cytoskeleton it would indeed have the qualities necessary to cope with a variety of problems that a changing environment might throw at it; that, through situated morphogenesis it would design itself in such a way that would be beneficial for the prevailing conditions.

With this in mind a comparison test was performed (Experiment B), discussed in the latter half of this chapter, where a single change in the Cellanimat's environment — from a chemotactic cue to a foreign particle — was shown to cause a change in observed morphology and behaviour, from chemotaxis to phagocytosis. No change was made in the system itself. This was an important experiment that highlighted the *multifunctionality* of the Cellanimat with the protrusions E-P map and highlighted the level to which the environment can determine morphology as well as behaviour in an artificial system.

### 5.1 Experiment A: chemotaxis

As previously discussed, the unicell exhibits morphological dynamics that surpass those of multicellular organisms. Due to its fluid nature, a unicell can rapidly reorganize its entire inner structure, outer body shape, transport organelles from one side to the other and even split itself in two; all in direct response to environmental changes. All these behaviours are executed by the cell's cytoskeleton (Alberts, B. et al., 1994).

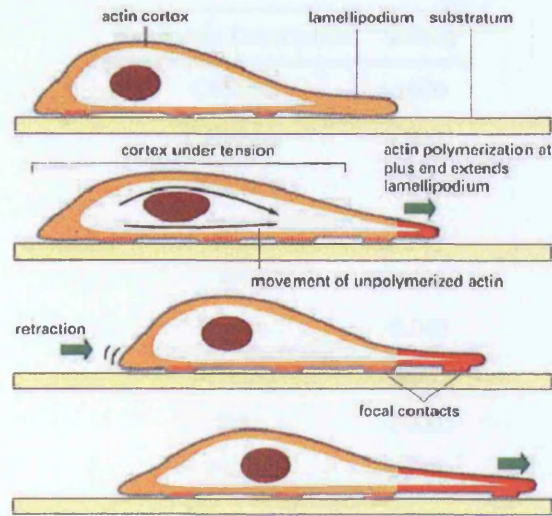


Figure 5.1: The stages of chemotaxis, reproduced from (Bray, 2001). First actin-driven membrane protrusions form into a leading edge lamellapodium towards the stimulus. Focal adhesions attach the cell to the substratum and cortical tension increases. Contraction at the rear and disassembly of focal adhesion sites, combined with newly forming focal adhesions at the front move the cell forward.

Fibroblast cell chemotaxis is a reasonably well defined example of lifetime morphological adaptation as it involves no obvious locomotory organelle, such as a flagellum. Instead, the cell undergoes transformations in form. In the first identified stage *protrusions* extend forward in a 'leading edge' formed of *lamellapodium* (large sheets of extended membrane) and microspikes (finger-like extensions comprised of bundles of actin filaments in parallel). In the next stage *attachment*, actin-driven *focal adhesions* connect the cell to the substratum and in contraction the cell's cortical tension pulls it forward, along with other actin-driven mechanisms, the focal adhesions disassemble and new ones form as the cell crawls forward. The further stages of *attachment* and *traction* involve less well defined biological and physical mechanisms and exceed the scope of this experiment. Thus, only the first stage of chemotaxis has been modelled in the protrusions E-P Map (Alberts, B. et al., 1994; Bray, 2001). See Fig.5.1 for a schematic of chemotaxis and Fig.5.5(a) for an SEM image of a fibroblast cell during chemotaxis.

The aim was to validate the protrusions E-P Map, as it was based in the molecular dynamics during the chemotactic protrusions stage, by testing the Cellanimat at chemotaxis. Its ability to generate a leading edge was judged and, with the simplified contraction mechanism, its success at motility towards the chemoattractant source was measured. The aim was to show that morphologically and functionally the Cellanimat simulates, qualitatively, the morphological plasticity of fibroblast cells. That the Cellanimat was capable of exhibiting adaptive motile behaviour through situated morphogenesis.

### 5.1.1 Experimental Set Up

A cylindrical Cellanimat, radius 25, height 10 voxels was placed on the base, in the centre, of a 3D environment with dimensions:  $250 \times 75 \times 20$  ( $l, w, h$ ). Table 5.1 shows the parameter settings for the experiment. For simplicity these were set by hand. In the next chapter these parameters are comprehen-

Parameter	Description	Setting
CPlume		1000
CHEMth		0.0001
P(REC)		1/5
#A		6000
#N		1500
RECth		0.005
PPlume		0.005
Pth		0.0005
PAth		0.008
Precycle		0.0001
FTOP		10
FINT		2

Table 5.1: The parameters used in experiment A: chemotaxis

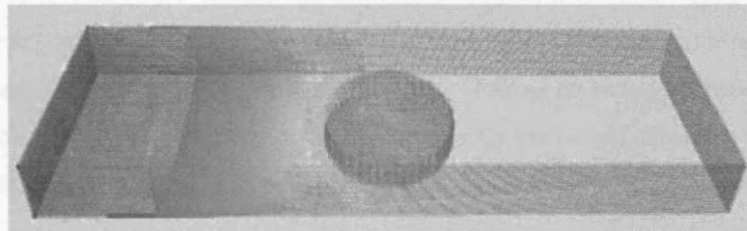


Figure 5.2: Initial Cellanimat in its environment, chemoattractant gradient featured left.

sively investigated and optimized. A plume of chemoattractant (CPlume) was dropped, in voxel (37,0,0), 2000 time steps previous to the start of the test during which it diffused creating a gradient. The plume drop site was 120 voxels from the Cellanimat's centre, meaning that to reach it the Cellanimat would have to travel a distance twice its length. See Fig. 5.2. The model as described in the previous chapter was run 40 times in this environment. Each run lasted 800 time steps. The experiment was performed on a standard 1.8 GHz PC workstation programmed in C, with graphics programmed in OpenGL. Each run took approx 7 minutes.

**Null Hypothesis A:** the Cellanimat will not show any significant, sustained, directed movement towards the chemoattractant source.

**Null Hypothesis B:** the Cellanimat will not behave in such a way as to maximise its exposure to the chemoattractant.

**Null Hypothesis C:** the Cellanimat's morphology throughout the process will not be similar to real fibroblast morphology during chemotaxis.

The aim of this experiment was to falsify the above three null hypotheses. The expectation was

that the ArtCyto/TP protein selections and the protrusions E-P Map will allow the Cellanimat to adapt its morphology by forming membrane protrusions into a leading edge increasing its exposure to the chemoattractant by moving the Cellanimat's centre of mass towards the source.

### 5.1.2 Motility results

The cellanimat's centre of mass was defined as the average position of its voxels. As such the centre of mass could in theory reside outside of the actual structure. The mean distance left, between the Cellanimat's centre of mass and the chemoattractant initial plume drop, after 800 time steps was 84 voxels, averaged over the 40 runs. The progression of the mean distance between the two through the time steps is shown in Fig.5.3. The Cellanimats accelerated at approx. time step 230 and then more gradually crept nearly twice their radius towards the initial plume drop site.

The Cellanimat was not expected to travel the entire distance to the initial plume drop site, as the high concentration of stimulant at this point would have dispersed after 2000 time steps of diffusion. However, the Cellanimat was expected to sense the areas of highest concentration and travel into them. This it did, travelling in an almost straight line towards the original source, see Fig.5.5. Bearing in mind that the original radius of the Cellanimat was 25 voxels, it can be said that, though the radius had changed through the changes in form, it had a distance, on average, of about 60 voxels left between its periphery and the initial plume drop site, and that it travelled in exactly the correct direction, i.e. a significant, sustained and directed movement in response to the environmental stimulus, falsifying null hypothesis A.

### 5.1.3 Chemoattractant exposure

To see if the Cellanimat satisfied the requirement for increasing exposure to the chemoattractant, the concentration of chemoattractant experienced at its periphery, at each time step ( $[C]$ ), was calculated. This was calculated by summing the E.chemo values in all E voxels with state M voxel MNs. On average, this value increased from 0.5 at the start of the run to 12.1 at time step 800, see Fig.5.3. The average value increased steadily over the run. However, an unexpected peak occurred in every run, not captured by the averaged plot, as the peaks occurred at varying times and averaged out. The variance around the peak varied from an average 1.85 to 3.99. The peak of one typical run can be clearly seen in Fig.5.3. See Fig. 5.4 for an explanation of the peak phenomena using other data collected during run A.

### 5.1.4 Morphological change

The Cellanimat had three distinguishable morphologies during a run: 1) the initial cylindrical form; 2) a leading edge lamellapodia with protrusions during accelerated movement (Fig.5.5(b) & 5.5(c)); 3) finally, a skewed cylinder with short protrusions in most directions (Fig.5.5(d) & 5.5(i)). See Figs.5.5(e) to 5.5(i) for images of protein distributions during chemotaxis; active proteins are situated more densely at the leading edge (left) and inactive ones to the rear (right). Further images of Cellanimat chemotaxis are shown in experiment B and in the next chapter.



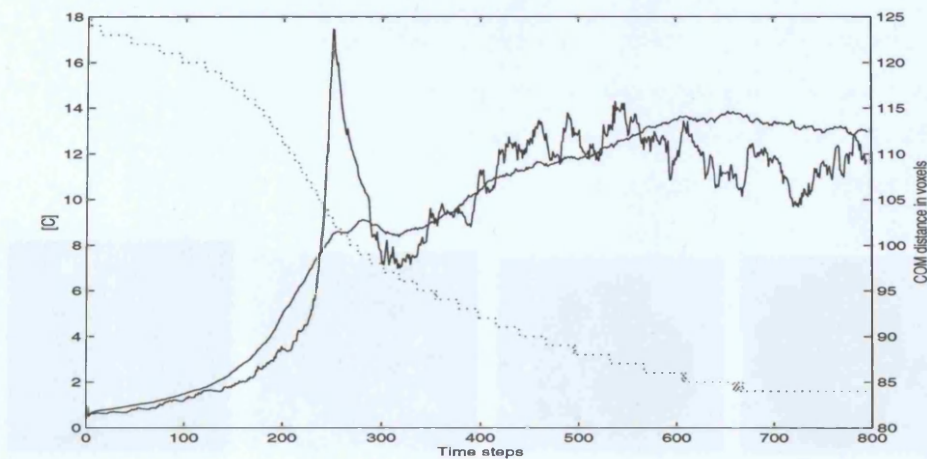


Figure 5.3: dotted line: the average distance of the Cellanimat's centre of mass from the chemoattractant plume drop site at each time step (right hand axis) averaged over 40 runs. Thick, peaked line: the concentration of chemoattractant  $[C]$  (left hand axis) that a Cellanimat in one typical run (run A) was exposed to (sum of chemoattractant in E voxels neighbouring membrane voxels). Thin line: the average exposure of  $[C]$  over all runs.

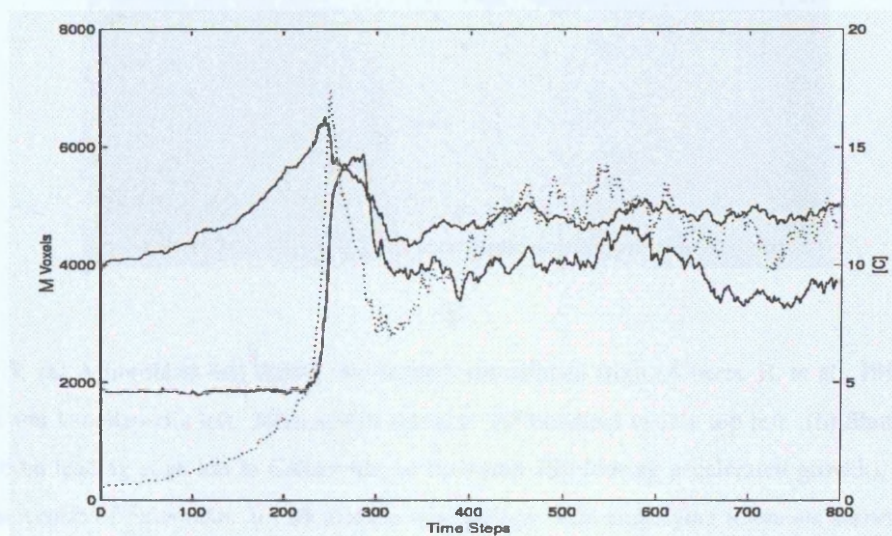


Figure 5.4: Data from run A. Dotted line: the concentration of chemoattractant  $[C]$  at the Cellanimat's periphery as shown in Fig.5.3. Upper thick line: the number of exposed M voxels (those with E state neighbours) decreased rapidly just before the peak in  $[C]$ . Lower thick line: the no. of M voxels touching the environment boundary (with no E MNs, e.g. those on the base and those touching the environment ceiling) rapidly increases at this point. This implies, given that the Cellanimat is initiated with non-exposed M voxels at its base and the sides of the environment are far from the Cellanimat, that *vertical* protrusions increase the cell's exposed surface area until they abut the environment roof, suddenly, and significantly, decreasing the cell's exposed surface area, causing the observed peak in  $[C]$ .

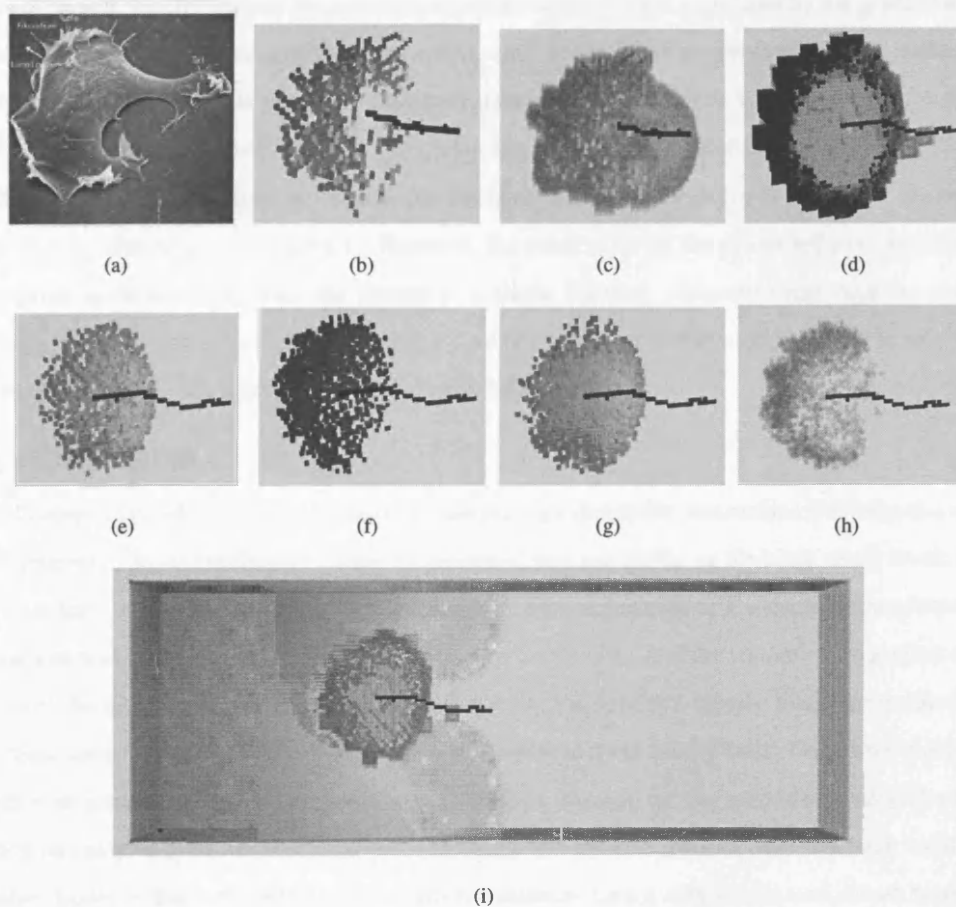


Figure 5.5: (a) A fibroblast cell during chemotaxis, reproduced from (Alberts, B. et al., 1994). Leading edge and lamellapodia left. Microspikes (parallel AF bundles) visible top left. (b) filaments form lamellapodia leading edge left in Cellanimat, at time step 230 (during accelerated growth), black line shows the centre of mass path. (c) Membrane morphology with underlying filaments shown,  $t = 230$ . (d) Membrane morphology, black units contain active WASP, time step 800. Distribution of: (e) inactive nucleators (state N); (f) actin agents in state PA; (g) SA state actin; (h) profilin gradient (only in non-agent voxels); (i) view from top during chemotaxis, note redistribution of chemoattractant gradient as the Cellanimat has moved through it.

### 5.1.5 System effects on the environment

The Cellanimat could affect its environment; EP<sub>3</sub> (described in Section 4.3.4) called within the morphology push-out rule allowed the Cellanimat to locally redistribute the chemoattractant in its environment, as shown in Fig.5.5(i). This in itself generated interesting phenomena. As actin filaments created outward membrane protrusions, pockets of chemoattractant became trapped between protrusions and continually reinforced growth locally. Indeed the peak that occurred in Fig.5.3 was generated by the gradual trapping of chemoattractant against the environment ceiling, until the Cellanimat grew too tall and pushed all of it out to the sides, reducing its exposure. Similarly internally, profilin could become trapped, as filament formation further compartmentalized the cytoplasm space within, also resulting in positive feedback.

Due to the lack of filament movement, the filaments could not align correctly to form microspikes (unless they by chance grew in parallel). However, the small scale of the model led to morphologically similar protrusions occurring from the growth of a single filament. Of course real cells are enormous in relation to the size of an actin filament, but it was not necessary in the model to stick to this scale in order to show functionally and qualitatively similar behaviours.

### 5.1.6 Conclusions

The Cellanimat exhibited *lifetime* adaptation in morphology due to the protrusions E-P Map as a situated growth process. The morphological plasticity exhibited was *reversible*, as the body could revert back to its original form, or change to another — the changes were not permanent. Exposure to the chemoattractant gradient was increased through the activity in the Cellanimat, and the Cellanimat travelled towards the source: the task was achieved. The major subsystem, the ArtCyto, closely modelled on the eukaryotic cytoskeleton, exhibited qualitatively similar dynamics to those in real cells. Due to the connectivity changes that occurred between sub-components (binding changes of the macromolecules) the Cellanimat can be called a dynamic morphology. Therefore, the protrusions E-P Map has been validated as a feasible model of the actin-driven protrusions mechanism during chemotaxis and shown to generate adaptive behaviour through morphological computation alone.

## 5.2 Experiment B: phagocytosis vs chemotaxis

The aim in this experiment was to test the multifunctionality of the cellanimat with the protrusions E-P Map, to see if the system could cope and perform new behaviours if the environment changed, with no change to the system itself. The expectation was that this would be possible as the biological process that the protrusions E-P Map was based on had itself been evolved over millions of years to allow an organism to survive in a changing environment. By coupling the Cellanimat with a different environment the aim was to show, through a simple comparison experiment, that the *environment* can be a major player in determining morphology and that morphogenesis can generate behaviours without the need for external controllers, due to the plasticity of the underlying systems. As such the aim was to motivate further study of environment-morphology interactions, for well-adapted design and adaptive behaviour.

As the same proteins involved in the protrusions stage of chemotaxis have been indicated in the early stages of phagocytosis (engulfment of a foreign particle), it was hypothesized that the Cellanimat with the

protrusions E-P Map would be able to perform phagocytosis if the chemical gradient in the environment was simply replaced with a foreign particle. Experimental results will be provided, demonstrating that with this single E-P Map a bifurcation in morphology did indeed occur, caused only by the environmental difference. The inter-relation of observed morphologies, behaviour and environment will be discussed using the E-P Map framework.

### 5.2.1 The process of phagocytosis

In macrophage cell phagocytosis (to ingest foreign particles), cell surface receptors trigger and bind to the particle, tethering it; this causes reactions involving the same proteins downstream as in fibroblast chemotaxis, but leads to a different morphology — in this case an enclosing concave morphology called the ‘phagocytic cup’ (Castellano, F. et al., 2001). Chemotaxis (movement morphology) and phagocytosis (ingestion morphology) are distinct both topologically and functionally yet are controlled by the same underlying mechanism of *continual* environment-morphology interaction, thus the environmental difference causes the bifurcation in morphology.

Macrophage cells (white blood cells), dendritic cells, neutrophils, *dictyostelium discoideum* and many other cell types use the process of phagocytosis to engulf, internalize and degrade large particles (over  $5\mu\text{m}$  in diameter), it is a quite universal cell function relying on profound rearrangements of the actin cytoskeleton and the plasmalemma. It is used to intake food, foreign particles in the immune system and for the engulfment of apoptotic ‘corpse’ cells (Niedergang, F. and Chavrier, P., 2004; May, R. C. and Machesky, L. M., 2001; Castellano, F. et al., 2001). The process of phagocytosis can be summarized in the following four stages:

1. The engagement of receptors on the surface of the cell is triggered after recognition of ligands on the particle. The receptors then bind to the surface of the particle, tethering it and starting the ‘phagocytic cup’ formation, independent of actin activity. This is due to the ‘zippering effect’, where the binding of one ligand, pulls the next ligands closer to the particle allowing them to bind, repeating the process (May, R. C. and Machesky, L. M., 2001). See Fig.5.6(a).
2. The receptor activation initiates reactions in the transduction pathway, involving the same proteins downstream (e.g. WASP, PIP2) as in chemotaxis. This triggers large-scale actin filament formation at the edge touching the particle, which causes the observed ‘phagocytic cup’ morphology. See Fig. 5.6(b).
3. Through ‘focal exocytosis’ the particle is fully engulfed, forming the ‘phagosome’. This may require the recruitment of internal membranes (recycled from the Endoplasmic Reticulum) to add to the plasmalemma along cytoskeletal tracks utilizing myosin motors (accessory proteins) (Niedergang, F. and Chavrier, P., 2004), or it may involve myosin based contractile activity (May, R. C. and Machesky, L. M., 2001). Specific proteins that initiate phagosome maturation are also delivered. See Fig. 5.6(c).
4. Phagosome maturation occurs after full engulfment. Enzymes are delivered to the phagosome. During maturation the phagosome, still at the periphery of the cell, is carried along microtubules

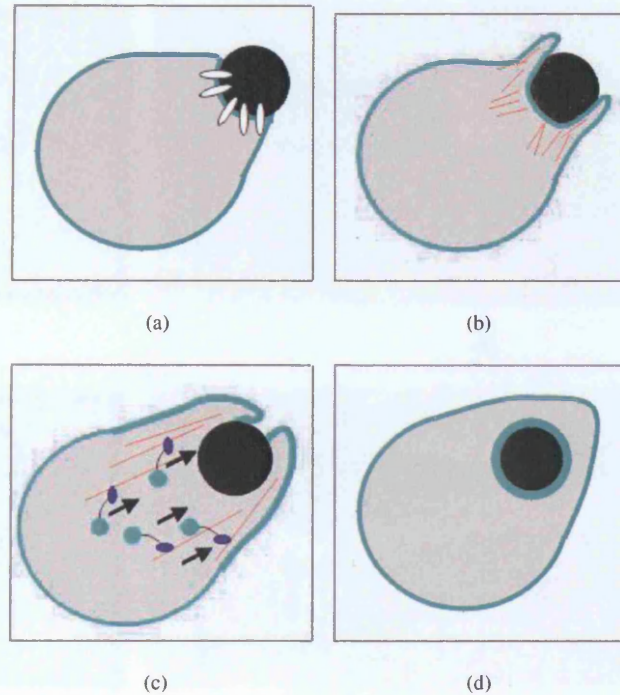


Figure 5.6: The four stages of phagocytosis, the engulfment of a foreign particle by a cell. See text for explanation.

Aspect	Chemotaxis	Phagocytosis
example cell	fibroblast	macrophage
environmental stimulus	chemical gradient	foreign particle
characteristic morphology	convex leading edge	concave phagocytic cup
behaviour	movement	ingestion

Table 5.2: The default Cellanimat parameter settings.

to the cell centre (perinuclear location) whereupon antigen presentation degrades the ingested material. See Fig. 5.6(d).

Table 5.2 summarizes the main differences between chemotaxis and phagocytosis in terms of morphology and behaviour.

### 5.2.2 Experimental setup

The aim was to test the multifunctionality (in behaviour and morphology) of the protrusions E-P Map. The primary investigation therefore used the protrusions E-P Map first in an environment with chemoattractant (Env A) and then in an environment with a foreign particle (Env B). Two further investigations were then performed: (i) improving the E-P Map, where improvements were made and the Cellanimat was re-tested in each environment and (ii) exploring the limits of phagocytic cup morphology within just environment B. All together five tests were performed, each run 100 times to gain averaged results.

For all experiments the Cellanimat was cylindrical (cytoplasm radius 20 voxels, height 6 voxels). The environment had dimensions (100,100,10) the Cellanimat's base was centred at (50,70,1) (before

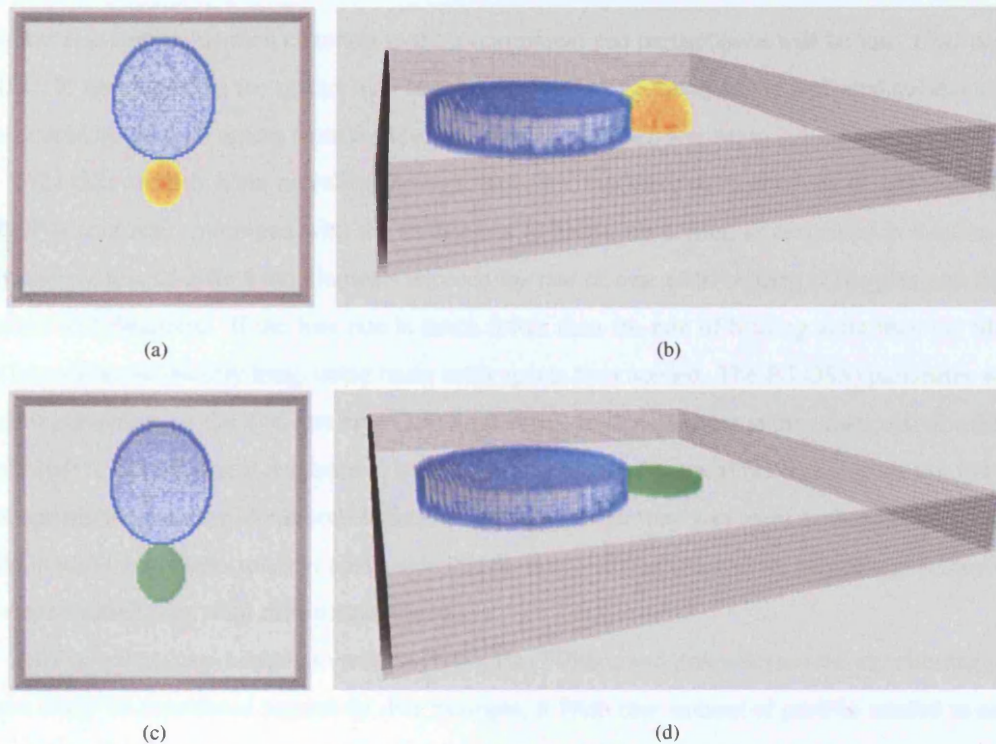


Figure 5.7: (a) Top view of Cellanimat in Env A at  $t=27$  when chemoattractant has diffused to reach Cellanimat (b) side view, Env A,  $t=27$  (c) initial top view of Cellanimat in Env B  $t=0$  (d) Env B side view  $t=0$ .

the membrane was created around it using rule C1, see Section 4.4.1). The chemoattractant plume, or particle centre depending on the environment chosen, was initialized 30 voxels south of the Cellanimat center at  $(50, 40, 0)$ . The chemoattractant was permitted to diffuse for a short number of time steps until it came into contact with the Cellanimat: the particle was initialized already in contact. See Fig.5.7 for views of the initial set up with both environments.

### 5.2.3 Default parameters

For the following experiments, in this section and in the next chapter, a default parameter set was used, shown in Table 5.3. These parameters were again hand designed for simplicity though alterations were made to improve on the performance in Experiment A; the following chapter fully explores parameter optimization.

Logically, increased agent quantity corresponds to increased response. However, over-crowding could impair agent movement and profilin diffusion, leaving agents inactive and stuck. Therefore the total number of agents (actin and nucleators) was set to 75% of the cellanimat's total cytoplasm volume (6565 voxels given the Cellanimat dimensions). As only one nucleator is needed to start a filament, the 75% of agents was not divided 50:50 between the two types, but 65:35 in favour of actin (which gave 3,201 actin and 1,723 nucleators).

$P(\text{REC})$ , the probability of a newly created membrane voxel containing a receptor, controls the strength of communication between the environment and the system. If  $P(\text{REC})$  is low then the Cellan-

imat has less communication channels to the environment and performance will be low. Conversely if P(REC) is very high then the system may become overloaded, too many newly activated nucleators (WN state) could block actin agents from the leading edge. So, P(REC) was set to 0.5.

P(LOSS) controls actin recycling through filaments, modeling the hydrolysis of ATP-bound actin to ADP-bound actin combined with the severing of filaments by cofilin, as described in Section 4.2.2. If the rate of loss of actin from filaments exceeds the rate of new actin binding at the plus end then the filament will disappear. If the loss rate is much lower than the rate of binding actin then the filament will become unnecessarily long, using more actin agents than needed. The P(LOSS) parameter was set to a low percentage of the total test time (250 time steps), so that an agent at the minus end of a filament would start to fall off after it had been in the filament for ten time steps. FINT was also set to a low value (2) to greatly increase the likelihood of disassociation as further time was spent in the filament. This was found in preliminary tests to allow for sustainable filaments with efficient actin recycling, i.e, they would not extend indefinitely with little disassociation.

All four parameters relating to profilin (PAth, Pth, PPlume and Precycle) are closely interlinked, and cannot really be considered separately. For example, if PAth (the amount of profilin needed to activate actin to state PA) were to be much higher than PPlume (amount of profilin released by PIP2) and Pth (diffusion threshold of profilin), then the occurrence of PA agents is unlikely, as it would exceed the average amount of profilin in each voxel. The relationships between these parameters, detailed in the equations below, were upheld. In the CA model of diffusion as described in Section 4.4.2 a low value for the diffusion threshold (Pth) will give a wide but low spread of profilin; a high value produces a small but intense spread. So in setting the four profilin parameters a medium diffusion spread and low PAth setting were used to ensure activation of sufficient actin agents by profilin. Precycle (the amount removed and released through actin activation and actin binding to a filament) was kept small so that only low levels of profilin were removed from the system in recycling, to avoid jeopardizing future actin activation.

$$PPlume < 1, \quad (5.1)$$

$$Pth \leq PPlume \times 8 \quad (5.2)$$

$$PAth \leq PPlume \times 8 \quad (5.3)$$

$$Precycle \leq PAth \quad (5.4)$$

#### 5.2.4 Multifunctionality

Within experiment B five tests were performed (denoted Exp 1 to 5). The Cellanimat was first tested at chemotaxis (Exp 1) with the setup and parameters as described above. The distance covered by the Cellanimat to reach the plume drop site was calculated as its 'movement behaviour'. Fig. 5.8(a) shows that by 100 time steps ( $t=100$ ) the Cellanimat had, on average, moved its centre of mass 78% of the distance towards the plume site. See Fig.5.9 for example screen shots of Exp 1. The leading edge morphology is shown in Fig. 5.9(b). The morphology returned to a cylindrical form towards the end of the run, as observed in Experiment A. This morphology and the subsequent lack of further

Parameter	Default setting
#A	3201
#N	1723
FTOP	10
FINT	2
P(REC)	1/2
Pth	0.5
PPlume	0.5
PAth	0.01
Precycle	0.01

Table 5.3: The default Cellanimat parameter settings.

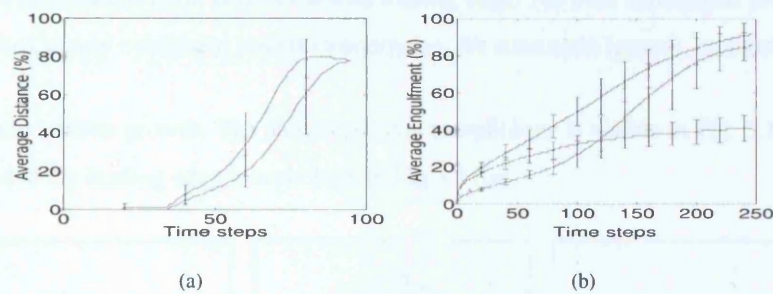


Figure 5.8: (a) Average distance (%) covered at each timestep over 100 runs of chemotaxis: Exp 1 (lower) Exp 3 (upper) (b) Average engulfment (%) at each time step over 100 runs of phagocytosis: Exp 2 (lower) Exp 4 (upper) Exp 5 (middle).

distance covered was due to the  $EP_3$  redistribution function being of 'type 3': redistribution caused the Cellanimat to become completely submerged in chemoattractant triggering  $EP_1$  (filament formation) in all directions, evening out the form and inhibiting movement. See Fig.5.10 for close up views of the filamentous actin structure within the leading edge and submerged forms.

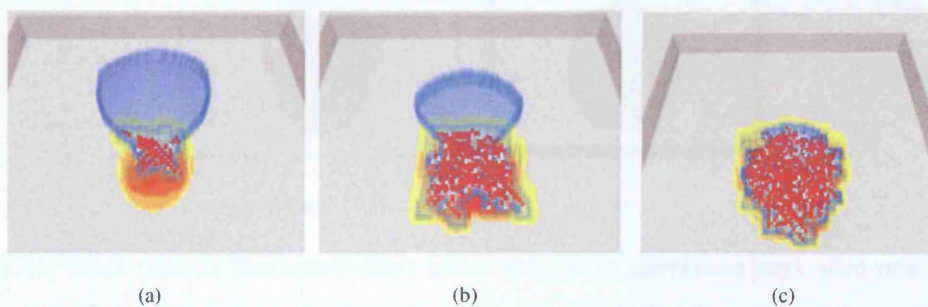


Figure 5.9: Screen shots of one run in Exp 1 chemotaxis. Actin filaments (red) and nucleators (white). Membrane (blue) becomes submerged in chemoattractant (yellow-orange) due to its redistribution of the gradient.

The Cellanimat with the same E-P Map was then tested at phagocytosis in Env B (Exp 2). The 'engulfment behaviour' was measured as the number of external particle voxels (its exposed surface, not including the base) with membrane MNs. The particle had radius 10, height 3 voxels. Fig. 5.8(b) shows that the behaviour reaches a plateau, resulting from the competition of  $EP_1$  and  $EP_2$ ; particle P



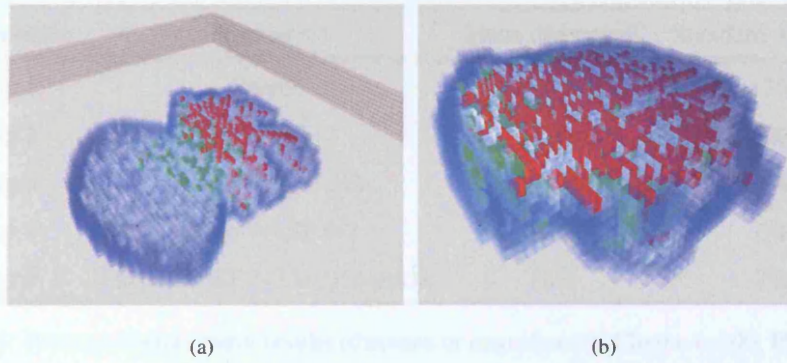


Figure 5.10: (a) filamentous actin network within leading edge. (b) final submerged form. Actin (red), nucleators (white), empty cytoplasm voxels (white/grey), PA state actin (green), membrane (blue).

both activates and inhibits growth. The phagocytic cup morphology is visible in Fig. 5.11(b) and can be easily compared to the leading edge morphology in Fig.5.11(a).

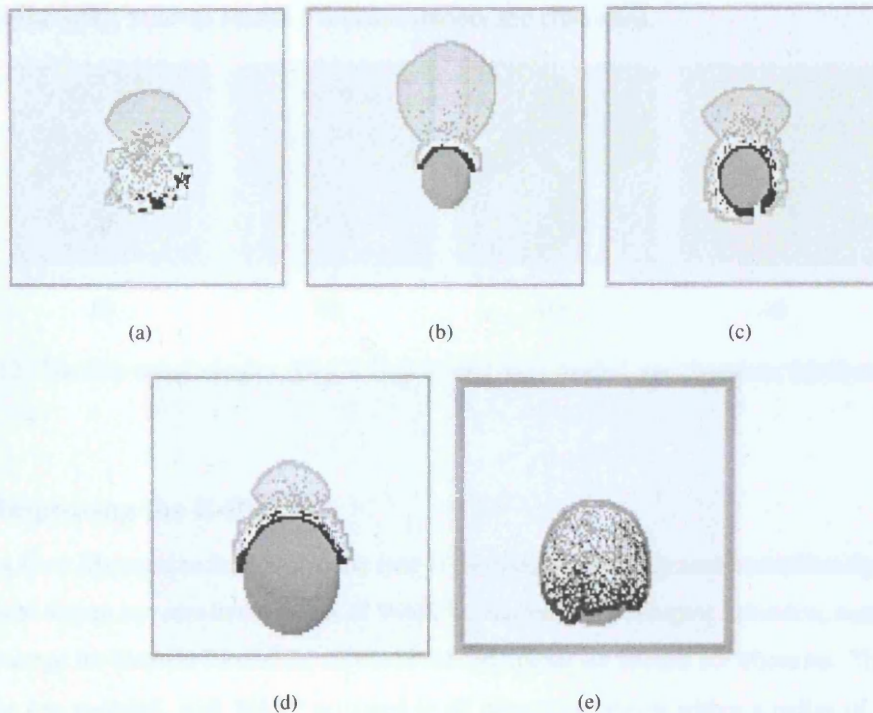


Figure 5.11: WASP (Black); filaments (white); active actin (grey); membrane(grey). slice view of first 3 layers only (a) Exp 1: chemotactic leading edge, white voxels outside cell contain C, timestep  $t=90$  (b) Exp 2: Phagocytic cup  $t=250$  (c) Exp 4:  $t=250$  (d) Exp 5:  $t=125$  (e) Exp 5: full top view  $t=250$ .

### Morphometrics

A clear difference in observable morphology is evident from Figs. 5.12(a) and 5.12(c), the chemotaxis morphology (Morph 1) is convex, whereas the phagocytosis morphology (Morph 2) is concave. In a convex morphology advancing membrane voxels assist the advance of neighbouring membrane voxels. By contrast in the concave Morph 2, leading membrane voxels are prevented from moving ahead by the particle itself ( $EP_2$ ). A cup morphology is thus intrinsically more difficult to achieve. The difference

Experiment	Description	Mean dist/engulf	Standard deviation
Exp 1	Chemo	78%	12%
Exp 2	Phago	41%	7%
Exp 3	Chemo WASP $r=2$	78%	3%
Exp 4	Phago WASP $r=2$	92%	6%
Exp 5	Phago WASP $r=2$ large particle	86%	7%

Table 5.4: Averaged behavioural results (distance or engulfment); Chemo  $t=100$ , Phago  $t=250$

can be quantified by calculating a Medial Axis Function (MAF)<sup>1</sup> (Lee, 1982) for both morphologies as Clack described in (Bentley and Clack, 2005); see Figs. 5.12(b) and 5.12(d). In Morph 1, the illustrated medial axis contains a middle “body” section, whereas the Morph 2 medial axis has none. Furthermore, the radius functions of circles forming the medial axis “legs” in Morph 1 are four times Morph 2’s. A further difference results from EP<sub>3</sub> in Exp 1, chemoattractant is eventually displaced so Morph 1 starts to grow haphazardly, whereas Morph 2 remains smooth and controlled.

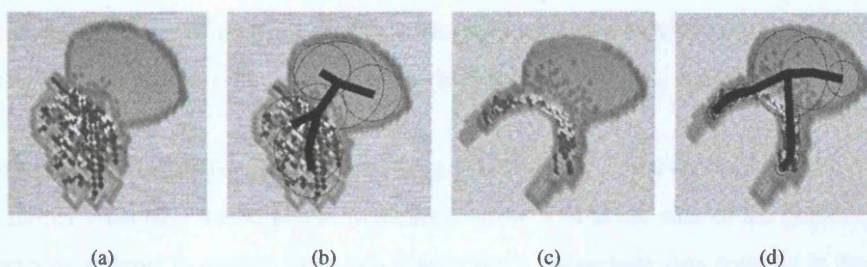


Figure 5.12: The two morphologies (Exp 3, Exp 4) and their medial axis functions (environment omitted).

### 5.2.5 Improving the E-P Map

In order to allow filaments to form just to the side of the particle, and thus avoid inhibition by EP<sub>2</sub> it was hypothesized that an increase in the radius of WASP activation, upon receptor activation, would increase the viable range for filament formation, as WASP-bound agents are needed for filaments. Therefore the Cellanimat was re-tested, with WASP activated in all membrane voxels within a radius of two voxels (rather than one) from an activated receptor, in Exp 3 (chemotaxis) and Exp 4 (phagocytosis). See Table 5.4. Increasing the WASP radius only had a small effect on chemotaxis as EP<sub>2</sub> inhibition was never a problem, but it greatly increased engulfment in Exp 4, see Fig. 5.11(c) for full cup morphology and Fig.5.13 for screen shots of a run of Exp 4.

Wider WASP activation in Exp 4 increased the range of viable locations for EP<sub>1</sub> (filament formation), as EP<sub>2</sub> inhibited growth into the particle. However, engulfment ability in real cells is more likely

<sup>1</sup>The Medial Axis Function (known variously as the median axis, medial axis, symmetric axis, or line skeleton) is defined as the locus of points, which lie in the interior of the form exactly equidistant from the border of the outline. This procedure allows the collapsing of a 2-D outline onto a curve. The approach consists of embedding a series of overlapping circles that touch the outline in such a way that they are tangential to the borders of the form. The centres of each of these circles define a point on the MAF. Paraphrased from (Lestrel, 2000)

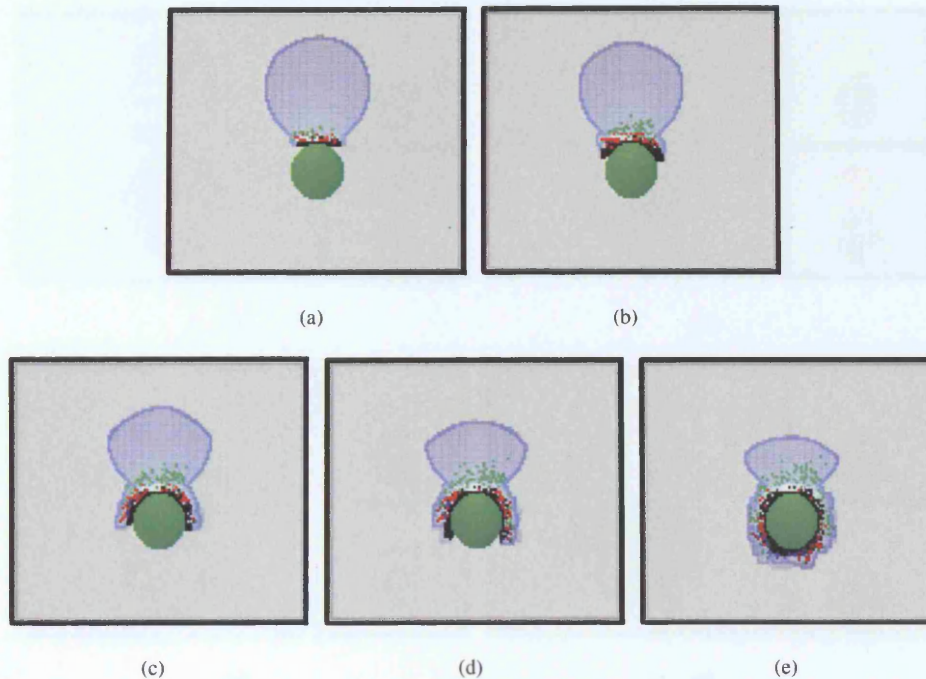


Figure 5.13: Screen shots of one run in Exp 4 phagocytosis with WASP radius 2 activation. Actin filaments (red) and nucleators (white). Membrane (blue) particle (green), active WASP (black).

due to two factors: 1) increased filament branching potential and 2) the flexibility of filaments. Flexibility and further branching would allow filaments to grow around the side of the particle, rather than stubbornly trying to grow in straight lines into it and failing. Branching was possible in the protrusions E-P Map, but nucleators deactivated when disassociated from WASP, thus branching was actually very rare, only occurring if the branch point also neighbored active WASP. It is not known whether nucleators stay active after WASP disassociation in real cells; this would seem worthy of further investigation. Increased WASP radius was a simple way to fully achieve engulfment with the model as it stood.

### 5.2.6 Extreme ingestion

In the paper 'How to Eat Something Bigger Than Your Head' Aderem (2002) showed that a cell can engulf a particle larger than itself through the recycling of internal membranes. In Exp 5 the improved system was tested against a particle equal in radius to the Cellanimat, as the Cellanimat had no limits imposed on membrane stretching. For this test, so that the particle and Cellanimat did not overlap, but were initialized in contact, the particle centre was placed a further ten voxels south, at (50,30,0). See Table 5.4 and Figs. 5.11(d) and 5.11(e); the Cellanimat stretched its entirety around the particle engulfing an astonishing 86% on average. See Table 5.4 for a breakdown and comparison of all results. See Fig.5.14 for screen shots during one run of extreme ingestion.

### 5.2.7 Summary

In this chapter, with experimental results the Cellanimat's effectiveness as a 'no-brainer' adaptive system, able to cope with different tasks in a changing environment, through MP has been shown, addressing the overarching primary hypothesis of this thesis and Objective Three specifically. With a single E-P Map

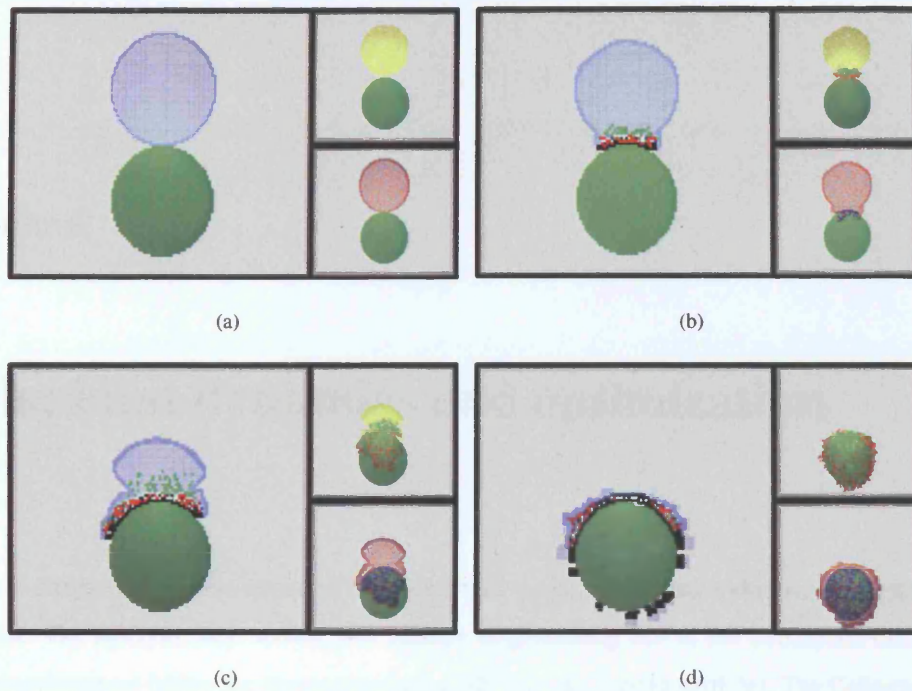


Figure 5.14: Screen shots, top view, of one run in Exp 5 extreme phagocytosis with WASP radius 2 activation. Large image in each sub-figure shows a slice through view of first three layers; actin filaments (red), PA actin (green), and nucleators (white), membrane (blue), active WASP (black), particle (green). Each small top right image shows: actin agent distribution in full top view; SA actin (yellow) and FA actin (red), PA actin (green). Each bottom right image shows: receptor distribution in full top view; inactive receptors (red), active receptors (dark blue).

a bifurcation in morphology, and behaviour, has been shown to occur, caused only by a difference in the environment. The Cellanimat displayed functionally similar adaptive behaviour and morphologies to chemotactic and phagocytic cells. This validates it as a model and shows it to be a multifunctional adaptive system where many forms can be assumed and functions performed, as required by a changing environment.

## Chapter 6

# Cellanimat dynamics and optimization

In the last chapter two instantiations of the Cellanimat model, embedded within an environment, were discussed. The ArtCyto, as it stands, was capable of generating MP in the Cellanimat once coupled with the environment (either the chemoattractant gradient or the foreign particle). The Cellanimat shares many working features of real cells e.g. actin recycling through filaments, profilin diffusion and recycling and membrane fluidity and assimilation. These features have been modelled qualitatively: not anchoring the model to the experimental data of one specific cell type permits exploration of parameter variation effects on behaviour, system dynamics and optimization for specific tasks. It is this pursuit, of dynamical analysis and optimization for a specific task, that this chapter is concerned with.

When the array of Cellanimat features all work together they can combine to produce the higher level behaviours of movement and ingestion, as shown in the previous chapter. But, what are the dynamics of each of these lower features during the behaviour? How do they combine and which ones dominate? Are any of the defined features actually redundant? Is the system robust to the stochastic elements in the model? How do perturbations in the model's parameters effect the overall behaviour? To what extent is the Cellanimat a DM, how does protein connectivity change over time?

Through a meticulous investigation of Cellanimat dynamics deeper insights into the inner workings of the system, and its many interesting interdependent-features, are revealed. This allows improvements on the model to be made: optimizing performance, speed and fidelity to biology. The Cellanimat's parameters are scrutinized, in order to optimize the default parameter set described in the previous chapter along with specific functions. This is done methodically with 1D and 2D projections into fitness space. The projections are plots of the average fitness when one or two parameters are co-varied between a range of values whilst all other parameters remain constant. This permits a fuller understanding of why parameter variants have certain affects. The results of the dynamical investigations are then validated by comparison with an evolved parameter set optimized for speed and engulfment ability. A parameter set was not simply evolved alone, as the primary goal was to have a deep understanding of the workings of the model and its parameters, in terms of efficiency, robustness, redundancy, dynamics and self-organization *together with* optimization and evolvability.

## 6.1 Overview of studies

The following list summarizes the seven studies detailed in this chapter. For all studies, the Cellanimat was tested at either chemotaxis or phagocytosis, as indicated, and the model, parameters and environmental set up were exactly as described in Section 5.2.4 in the previous chapter, unless otherwise stated.

- **Study One. Redundancy and compositional dynamics.** An overview and comparison of macromolecular dynamics and compositional changes in the Cellanimat during chemotaxis and phagocytosis is given. Also, the effects of removing each subsystem/protein on Cellanimat behaviour and protein activity are discussed. This results in a stricter definition of the WASP-nucleator interaction to improve biological fidelity.
- **Study Two. Agent volume: optimization and robustness.** An investigation, using a 2D projection, where the ratio of actin and nucleator agents to the total cytoplasm volume is varied to indicate optimal settings of the #A and #N parameters. Robustness of the system is tested for the range of ratios investigated, indicating how the sensitivity of the system to stochastic elements varies with agent volumes. Interesting new issues are raised linking low robustness to the release of profilin in systems with high agent volumes, resulting in a revision of the PIP2 release function for such systems.
- **Study Three. The role of profilin: recycling or saturation?** First, the dynamics of profilin in each related function are observed, leading to optimization of the profilin system. Then the role of profilin recycling in the Cellanimat is investigated leading to conclusions concerning links between the over-saturation of the diffusible signal and high performance.
- **Study Four. The role of cofilin: actin recycling in the Cellanimat.** An assessment of the effects on overall performance of agent recycling through filaments. The P(LOSS) function determines, stochastically, the off-rate of proteins from filaments, modelling cofilin-severing of actin filaments together with the natural disassociation of agents from filaments. It is recast as a deterministic function to aid investigation of optimal parameter settings. A 1D projection varying P(LOSS) is detailed and the saturation of actin compared to cofilin-related recycling is discussed.
- **Study Five. The extent of an optimal TP.** A comparison of radius 1 and radius 2 WASP recruitment regimes, during phagocytosis, using the improved functions from previous studies. The optimal number of receptors is investigated by varying P(REC) in a 1D projection. Issues relating P(REC) to profilin saturation are discussed.
- **Study Six. Compositional dynamics with the optimized model.** Composition dynamics, with all the new improved functions and optimized parameters, during chemotaxis and phagocytosis, are compared.
- **Study Seven. Saturation GA, evolution of an optimal parameter set.** Genotypes (parameter sets), that maximize engulfment and speed, are evolved and saturation is shown to be exploited

rather than recycling mechanisms. A complementary, future GA is discussed which would apply a cost function to over-saturation, inducing exploitation of the more realistic recycling mechanisms.

## 6.2 Study One. Redundancy and compositional dynamics

In this study the dynamics of protein composition in the Cellanimat during chemotaxis and phagocytosis are first compared. The Cellanimat was tested at chemotaxis, as in Section 5.2.4 for 200 time steps in an environment with a diffusing chemoattractant plume, WASP was recruited to radius 1 MNs only. The Cellanimat was then tested at phagocytosis for longer (300 time steps) with WASP recruited to radius 2 MNs, as it has been shown, in the previous chapter, to be an intrinsically harder task than chemotaxis. Each state of actin was treated as a different macromolecule. SA and PA, for example, represent the binding of actin to thymosin (sequestering protein) and profilin respectively which constitute different macromolecules. Monitoring how volumes of the system proteins, in the various states, changed indicated how connectivity between proteins changed throughout the Cellanimat's lifetime. At each time step the volume of each protein state was recorded throughout a sample run.

### 6.2.1 During chemotaxis

Figure 6.1 shows the Cellanimat's compositional dynamics during chemotaxis. See Fig.6.2 for screen shots of the protein distribution changes during chemotaxis. Fig.6.1(a) shows that the Cellanimat's centre of mass (at creation it was 30 voxels) came closest to the initial site of the chemoattractant plume at around  $t=95$ , and as with the examples in the previous chapter, the distance then increased slightly as the plume itself has moved since the initial plume was dropped. The number of membrane voxels increased as the Cellanimat accelerated towards the chemoattractant (Fig.6.1(b)); this stretching ability of the membrane facilitates the development of the leading edge. Once the Cellanimat reached the original plume drop site the high membrane volume then decreased. Interestingly, a regrowth of the membrane is observed after this point due most likely to the Cellanimat following new gradients all around it, created by its own displacement of the chemoattractant, see Figs.6.2(v) and 6.2(x).

Profilin concentration increased as the Cellanimat travelled, reaching a peak when the plume site was reached, Fig.6.1(c). The levels are notably high however, and will be discussed in the next section. The number of inactive (SA state) agents decreased rapidly, coinciding with the growth of PA and FA state agents and the acceleration of the Cellanimat towards the chemoattractant, Fig.6.1(d). The number of WA agents stayed low and remained near constant after the initial bloom. This results from limited amount of room at the membrane for WA agents as compared to the full space inside the Cellanimat for the other agent states to exist in.

Fig. 6.1(e) shows that a relatively low percentage of nucleator agents become involved in the activity at the leading edge, and once the source of the plume was reached, the number of FN agents gradually decreased, though it still remained higher than expected. This can be explained by Fig. 6.1(f) which shows that the density of WASP within membrane voxels continued to rise (to around a third of the number of membrane voxels) after the source had been reached and only slightly declined towards the end of the run. This related to the submersion of the Cellanimat, such that instead of a leading edge,

the entire periphery was recruiting WASP in most directions, particularly above, where chemoattractant was trapped between the environment roof and the Cellanimat. See in Fig. 6.2 the distribution of WASP at  $t=125$ .

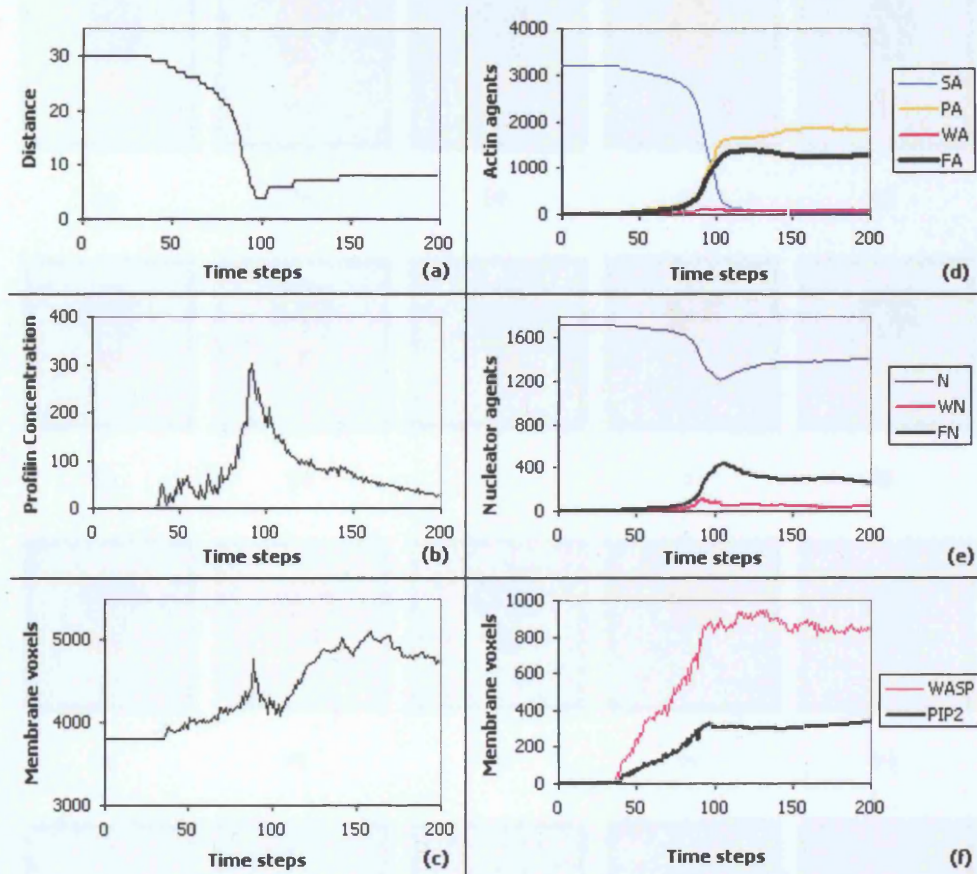


Figure 6.1: Cellanimat compositional dynamics over one run of chemotaxis for 200 time steps using the original model and default parameters. (a) change in distance between Cellanimat's centre of mass and the initial plume drop site (b) profilin levels (c) number of membrane voxels (d) number of actin agents in the different states (e) number of nucleator agents in the different states (f) number of membrane voxels containing active WASP and active PIP2.





Figure 6.2: Screen shots of chemotaxis. Rows top to bottom show:  $t=30, 50, 88, 100$  and  $125$ . Columns left to right: first column shows Membrane (blue) and chemoattractant (yellow); second shows receptor distribution, active=purple, inactive=orange; third WASP distribution (black); fourth actin distribution, SA=red, PA=green, WA=blue, FA=white; finally, nucleator distribution, N=blue, WN=black, FN=white.

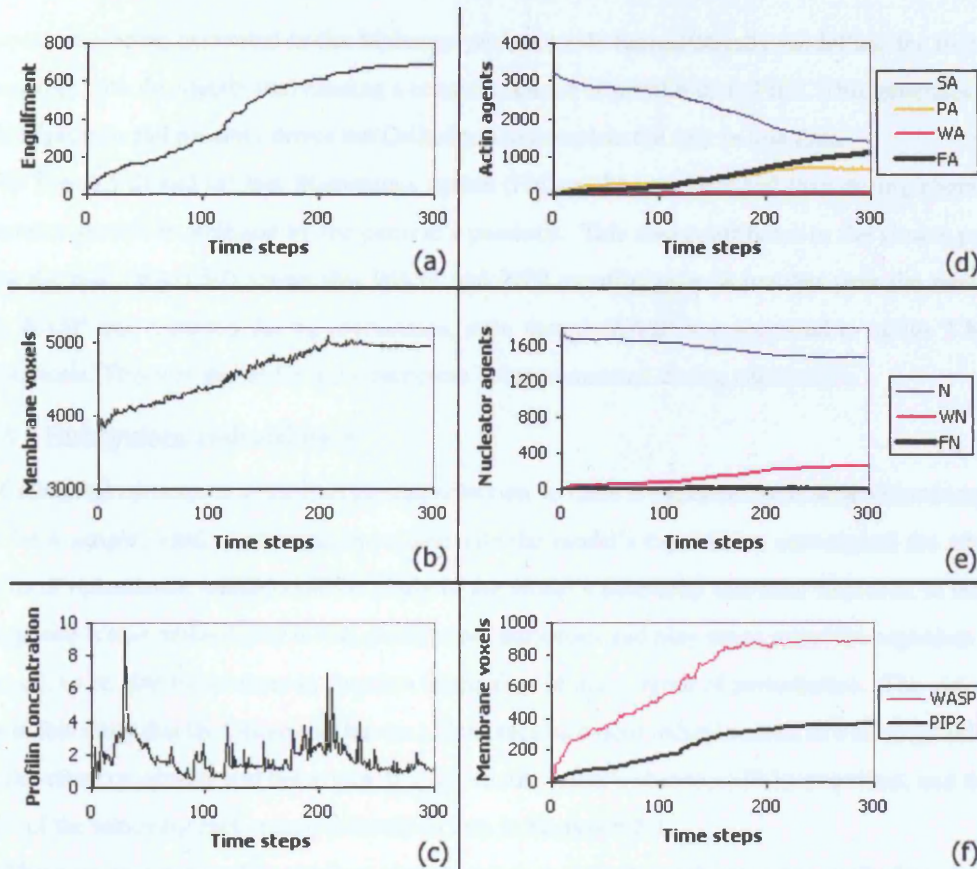


Figure 6.3: Cellanimat compositional dynamics over one run of phagocytosis for 300 time steps using the original model and default parameters: (a) engulfment score, number of membrane voxels neighbouring the particle; (b) number of membrane voxels (c) profilin concentration (d) number of actin agents in the different states (e) number of nucleator agents in the different states (f) number of membrane voxels containing active WASP and active PIP2.

### 6.2.2 During phagocytosis

The results are shown in Fig.6.3. Figure 6.3(a) shows that the maximum engulfment achieved during this sample run at  $t=284$  was 98.2% (701 is the maximum possible and it achieved a maximum of 689). The dynamics of composition for phagocytosis were different from those collected during chemotaxis. One reason is that even after 300 time steps the Cellanimat's engulfment has not passed its maximum, as it did in chemotaxis at  $t=95$ . In Fig.6.3(b) the number of membrane voxels, on average, increased throughout phagocytosis and begins to plateau at  $t=200$  as less of the particle is left to engulf so there is less chance of a filament growing in the right place.

Fig 6.3(c) shows that profilin concentrations were overall far lower in phagocytosis than in chemotaxis. The  $EP_b$  function 'obstruction' within the E-P Map meant that the particle blocked the Mchange rule as it tried to push-out the local membrane. Profilin plumes are released by PIP2 if and only if a receptor activates, not during its active period. In phagocytosis all receptors that are active remain so for the whole run, only releasing a single plume of profilin upon activation. In chemotaxis, the receptors

are constantly being generated in the Mchange push-out rule (unrealistically modelling the movement of receptors with the membrane) causing a constant release of profilin from PIP2. This generates higher levels of profilin and possibly drives the Cellanimat to complete the task in less time.

In Figs.6.3(d) and (e) less filamentous agents (FN and FA) are detected than during chemotaxis, as filament growth is inhibited by the particle's presence. This also contributes to the slower progress during the task. Fig.6.3(f) shows that WASP and PIP2 steadily grow in number over the whole run. More WASP was recruited during chemotaxis, even though WASP was recruited to radius 2 MNs in phagocytosis. This was due to far more receptors being stimulated during chemotaxis.

### 6.2.3 Subsystem redundancy

The Cellanimat consists of a minimal protein selection so there is expected to be little redundancy. The need for a simple, small, first selection to illustrate the model's capabilities outweighed the advanced benefits of redundancy, which could be costly to the model's simplicity and size. However, in real cells the opposite is true: redundancy is rife, proteins are numerous and play many roles; the organism needs, above all, to be able to continue to function in the face of many types of perturbation. The aim was to show in this study that the Cellanimat has no redundancy as it does indeed consist of a minimal selection. First the effect on activity and behaviour of a whole subsystem's absence will be described, and then the results of the removing each macromolecule in turn in Section 6.2.4.

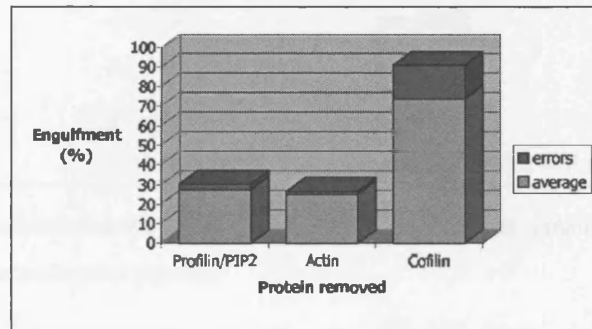
There are no functionality overlaps of subsystems as a whole, each plays an equally important role and if any are knocked out there is a total system failure: no behaviour can be generated. Without the TP a message cannot reach the cytoskeletal proteins; without the ArtCyto no structural changes can be made; without the Cytoplasm subsystem, there is nowhere for the ArtCyto to exist in; without the Membrane subsystem there is nowhere for the TP to reside in and there would be no coherent boundary between the environment and the internal cellular components. Some activity would of course still occur in the Cellanimat when certain subsystems are knocked out: without the Cytoplasm or ArtCyto activity and compositional changes would still occur in the TP.

In real cells no morphological behaviour (in chemotaxis or phagocytosis) would be observed without the transduction pathway, and similarly, without the cytoskeleton, membrane or any cytoplasm. These subsystems are all necessary. However, a failure *within* the transduction pathway of a real cell would most likely be overcome, as it maintains a high level of redundancy, many proteins within it can play the same role. Similarly if certain cytoskeletal proteins failed the behaviour might still be possible. However actin, filament nucleators (such as Arp2/3) and proline-rich proteins (such as WASP) have been shown to play a central role in chemotaxis and phagocytosis and so a total system failure could be expected upon their removal (Castellano, F. et al., 2001; Holt, M. R. and Koffer, A., 2001).

### 6.2.4 Macromolecular redundancy

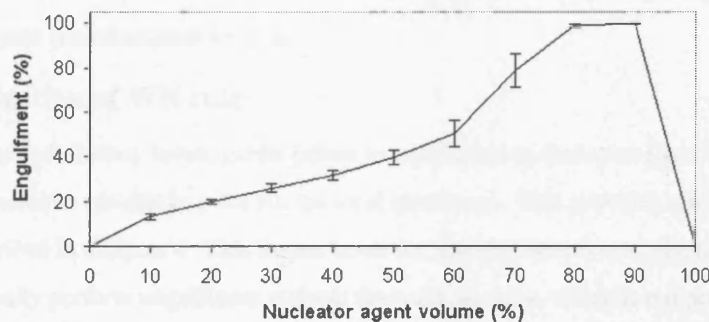
The effects of removing each macromolecule in turn from the system (with replacement), on Cellanimat behaviour and internal activity during phagocytosis, are shown in Table 6.1. In contrast with the biological case, if actin is absent, the behaviour is still possible. Fig. 6.4(a) shows that, on average, engulfment of 25% is still possible without actin. Indeed, if profilin or PIP2 are absent the behaviour

also still occurs due to the ability of nucleators to push-out the membrane when they bind to WASP. PIP2 provides profilin and profilin simply enables actin to reach its activated state and then bind to WASP as profilactin (state PA). Absence of profilin/PIP2 manifests as equivalent to a failure of actin, the only difference being that actin agents are still present, taking up valuable space in the cytoplasm.



(a)

Actin agent volume = 0%



(b)

Figure 6.4: (a) Effect on behaviour of certain protein absences averaged over 20 runs with original model and parameters. (b) Results of 1D projection varying number of nucleators with zero actin agents. Averaged over 20 runs. Original model and parameters for 200 time steps.

Fig.6.4(b) shows the results of a 1D projection, with #A set to zero — no actin agents. The number of nucleator agents was varied, between 10% and 100% of the total Cellanimat cytoplasm voxel volume, in 10% jumps. The total volume of cytoplasm voxels was 6565. Results were averaged over 20 runs of phagocytosis, each for 200 time steps. The model appears to deviate significantly from the biological case. If there is a sufficient number of nucleator agents then high levels of engulfment can be achieved even in the absence of actin, though phagocytosis is an actin-driven process — actin should not be redundant.

Cofilin also has a level of redundancy, Fig. 6.4(a) shows that its absence had little effect on engulfment ability. Cofilin allows the cell to control filament length, increased cofilin can increase the recycling of actin through filaments, increasing efficiency. It stimulates the rapid disassembly of filaments in one area so they can be reused quickly in another region. In real cells the level of cofilin would

Macromolecule removed	Activity	Engulfing behaviour
actin	yes (N to WN)	yes (nucleators still push out membrane)
nucleators	yes (SA to PA to WA)	no
profilin	yes (N to WN)	yes (nucleators still push out membrane)
cofilin	yes (all)	yes (full)
Receptors	no	no
WASP	yes (SA to PA)	no
PIP2	yes (N to WN)	yes (nucleators still push out membrane)

Table 6.1: Effects on macromolecular activity (viable state changes that remain) and overall engulfment behaviour of each macromolecules absence.

rise and fall as needed in different areas of the cell, in the Cellanimat it is modeled as a constant in the P(LOSS) parameter. If the cell is over saturated with actin, recycling becomes redundant. In the default parameter set, although the parameters relating to recycling (FTOP and FINT) imply good efficiency, the high volume of actin agents renders this mechanism obsolete. The issues of recycling and saturation are more fully investigated in subsequent sections.

### 6.2.5 Optimization of WN rule

The outcome of the redundancy investigation points to an interesting deviation from the biological case. New WN state nucleators are able to push out the local membrane. This provides room for a WA actin to bind to it, as described in Chapter 4. This means however, that the system can, given an overabundance of nucleators, actually perform engulfment without the need for actin, which is not possible in real cells. To eradicate this artifact of the simplified model two simple changes were made to the WN rule: 1) that nucleators cannot call the Mchange rule, they can no longer push-out the membrane; 2) They bind to WASP found only in its radius 2 MNs (not in its radius 1 MNs). See Fig.6.5 and compare Figs.6.6 to the old versions shown in Fig.4.16(d) in Chapter 4.

The optimized WN rule is based on the biological insight that WASP is a long protein with several different binding regions along its length, the arp2/3 binding region being located at the ‘C-terminus’, the end farthest away from the membrane (Miki, H. and Takenawa, T., 2003; Holt, M. R. and Koffer, A., 2001). It binds nucleators far enough from the membrane for actin to join on to them without the need to push out the membrane first.

A simple model, where all radii for binding and assessment are set to one, is obviously not going to maintain fidelity to biology on close scrutiny, the question is when is it necessary to lose some simplicity to gain increased performance? It may not always be beneficial to use the optimized WN rule, and in fact the new rule has little impact on engulfment ability overall as shall be seen. But here, within the context of a dynamical and redundancy assessment of the model, it is worth defining a more life-like function so any projected/evolved optimal parameters can be appreciated and increase the biological fidelity of the model.

To validate the new WN rule the effects of macromolecular knock-outs were re-assessed when

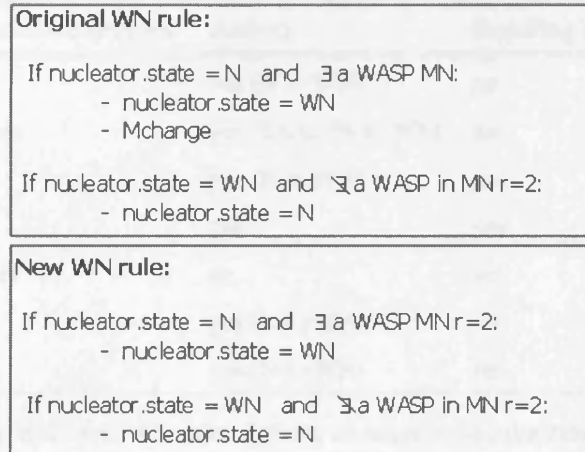


Figure 6.5: Pseudo code for the original and new WN rules relating to Nucleator state WN activity. Mchange is not called in the new WN rule so nucleators cannot affect Cellanimat form directly.

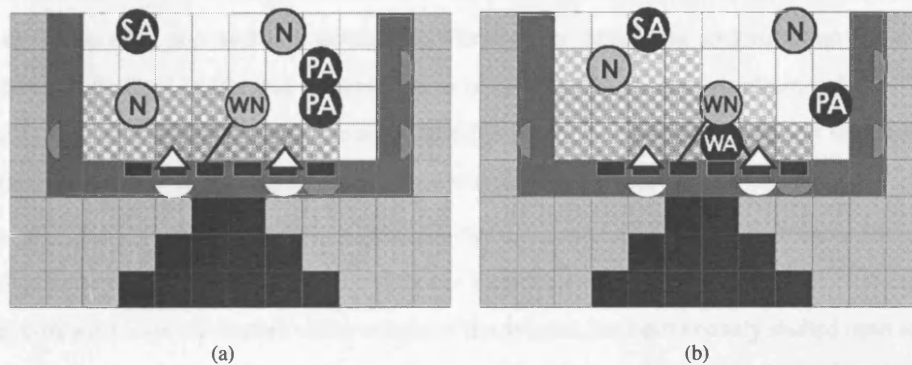


Figure 6.6: The new WN rule in practice: (a) a nucleator at a distance of 2 voxels from an active WASP can bind to it, changing state to WN. There is no local membrane push-out and (b) enough room is left for a WA agent to bind to it and form a filament.

the new WN rule was implemented. See Table 6.2. It is clear that now macromolecular redundancy is consistent with expectations, based on the biological literature. There is less redundancy with the new WN rule but greater emphasis on a minimal realistic model. The decision to implement the new or original WN rule will depend on which factor (fidelity/redundancy) is more important in a given application.

### 6.3 Study Two. Agent volume: optimization and robustness

The main aim of this study was to discern the optimal number of agents required to perform the phagocytosis task. The aim was also to test how robust such 'optimal' settings were, given the stochastic nature of the model, and to assess any correlation between robustness and agent volume. A 2D projection into engulfment space was performed, where the number of actin and nucleator agents in the system were varied. The number of agents, #A and #N, were given as a percentage of Cellanimat cytoplasm volume (6565 voxels in total) and varied in 10% jumps between 0 and 100% of the total Cellanimat volume.

Macromolecule removed	Activity	Engulfing behaviour
actin	yes (N to WN)	no
nucleators	yes (SA to PA to WA)	no
profilin	yes (N to WN)	no
cofilin	yes	yes
Receptors	no	no
WASP	yes (SA to PA)	no
PIP2	yes (N to WN)	no

Table 6.2: Redundancy with new WN rule. Effects on macromolecular activity and engulfment behaviour when each macromolecule is removed, with replacement

The optimized WN rule, as defined in section 6.2.5, was used. Results were averaged over 20 runs; each run lasted 250 time steps. Certain combinations were not included in the study and were allocated a zero score. These were impossible combinations where either there were no actin or no nucleators or if the combined volume of agents was greater than or equal to 100% of the cytoplasm volume. With zero actin/nucleators, the redundancy study showed, that this would generate no behaviour; with 100% of the Cellanimat composed of agents there would be no way for them to move.

Fig. 6.7(a) shows that, on average, performance increased as actin agent volume increased and nucleator volume decreased. The results reflect the inclusion of the new improved WN rule, which of course favours actin over nucleators as the weight of the process has been entirely shifted onto actin. This kind of combination — high-actin with low-nucleators — is what was logically expected in a biologically loyal model, as a greater quantity of actin, compared to arp2/3, is needed for filament formation. This again reaffirmed the use of the new WN rule for increased biological fidelity. The agent projection gives a valuable insight into striking the right balance between ‘room to move’ and ‘enough activity’: a tradeoff is required. As the number of nucleator agents rose a drop off in engulfment ability was observed. The nucleators can be seen to have ‘taken up valuable space’, which could have been better occupied by actin, or left free to improve agent movement.

The errors (standard deviation over the twenty runs) on the agent projection were higher than would be expected for a robust solution, see Fig.6.7(b). Though the results were only averaged over a relatively small number of runs, it became clear that there was an inconsistency in engulfment ability affecting the errors greatly, that would not have been ironed out by increasing the number of runs. Instances where no behaviour was recorded occurred when on most other runs it would achieve near full engulfment. This resulted in the high errors, note that the long high peak on the errors graph occurs when the combined agent volume is close to the total cytoplasm volume.

It was found that the Cellanimat was dependent on initial conditions when a high percentage of agents was used, specifically the initial locations of receptors and agents. The PIP2release function, which releases profilin into the cytoplasm when a receptor activates, was designed with simplicity in mind, and lower agent volumes. An amount (PPlume) of profilin would be released to any available

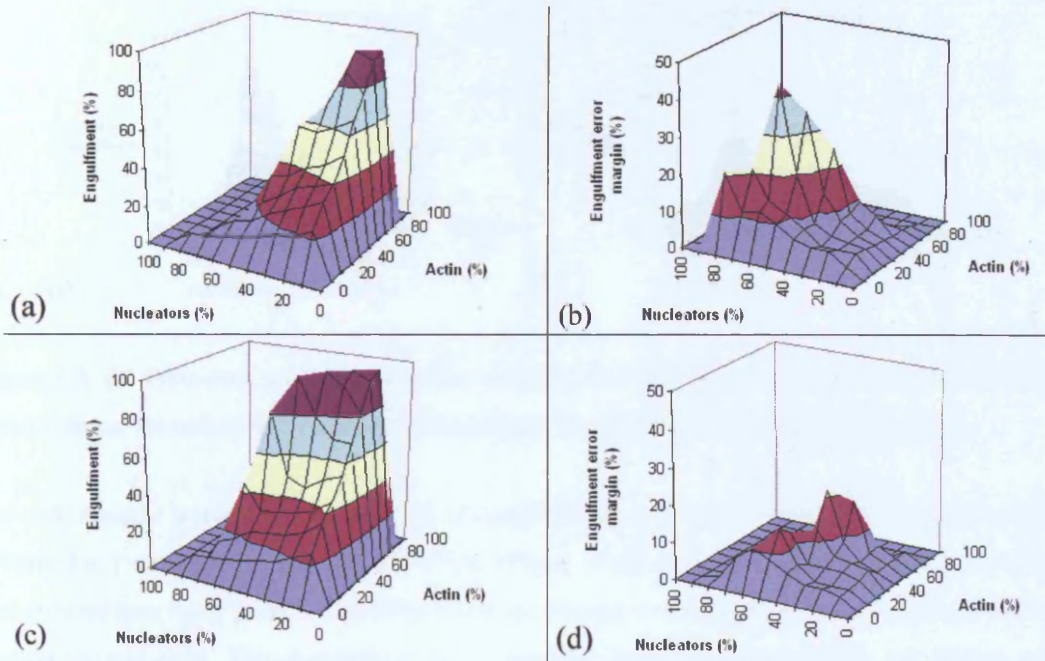


Figure 6.7: (a) 2D projection results showing the average effect on engulfment of varying actin and nucleator agent volumes (agent volumes given as a percentage of the total cytoplasm voxel volume (6565 voxels)). (b) Error margin on the averaged results shown in (a). (c) 2D projection results varying agent volumes with the optimized PIP2 release function. More agent combinations achieve high engulfment. (d) Error margins on projection shown in (c), errors have been considerably reduced by the PIP2 release function.

cytoplasm MNs upon PIP2 activation (receptor activation). This of course was fine with the original, lower volumes of agents. But when agent volumes are high, there becomes a real chance that all the initially active receptors (touching the particle) will have no cytoplasm voxel MNs to release profilin to, as they all contain agents, resulting in the absence of profilin and thus no further behaviour or activity. Interestingly, this phenomena would not have occurred when tested at chemotaxis. If the receptors initially exposed to the required amounts of chemoattractant could not release profilin due to high agent density, other receptors would activate as the chemoattractant diffused. See Fig.6.8(a) for a graph detailing the frequency of 'no behaviour' runs. Note that when no behaviour is generated by the system the engulfment score is not zero but 5%, as some membrane voxels are initiated in contact with the particle.

### 6.3.1 Optimization of PIP2-profilin functions

In the light of the projection results, that higher overall volumes of agents yield better performance, a new more biologically plausible version of the PIP2 release function is presented. Simplicity must be sacrificed, if robustness of behaviour to initial conditions and stochastic elements is desired, when using high agent volumes.

Instead of the PIP2 release function releasing profilin to any available cytoplasm voxels, meaning the released amount varies from receptor to receptor, it was decided to define a set amount that every



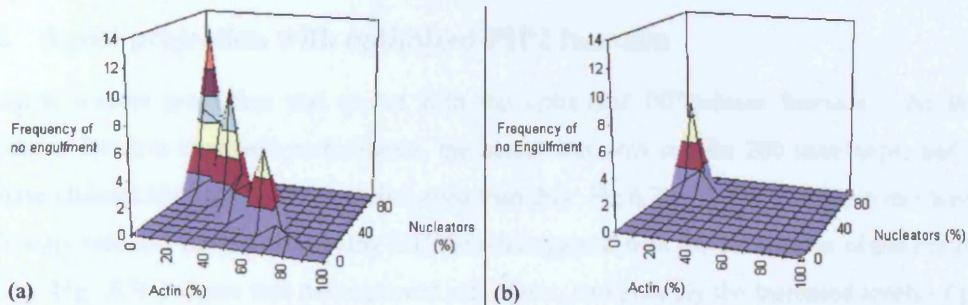


Figure 6.8: (a) Frequency graph showing that instances of no behaviour generated correlate with high agent volume. (b) reduction in instances of no behaviour with optimized PIP2release function.

activated receptor would release, in packets of size (PPlume), over time. Arbitrarily, this new parameter (PPlumeFull) was set to be eight packets of size PPlume. Each receptor voxel was given a new substate that counted how many packets of profilin had been released, and stopped all further attempts once the counter reached eight. This slow-release mechanism may also aid the phagocytosis task further, when high agent volumes are used, as it will maintain a constant supply of newly released profilin at the site where active actin is most needed, rather than releasing a single larger packet and allowing it to diffuse back into the cell too early. In addition to this the PIP2uptake of profilin, by inactive receptors (containing inactive PIP2), were restricted to taking only the amount PPlumeFull in total. Inactive receptors utilized the new counter to achieve this. See the pseudo code in Fig.6.9 for the old and new PIP2release/uptake functions.

#### Original PIP2 rule:

```

- if M.rec = inactive and ∃ Particle in MNs
M.rec = active
M.PIP2 = active

∀ C in MNs:
    C.profilin = C.profilin + PPlume

- if M.PIP2 = inactive
    ∀ C in MNs:
        if C.profilin > PPlume
            C.profilin = C.profilin - PPlume
        else
            C.profilin = 0
  
```

#### NEW PIP2 rule:

```

- if M.rec = inactive and ∃ Particle in MNs
    M.releaseCounter = 8
    M.rec = active
    M.PIP2 = active

- if M.PIP2 = active and M.releaseCounter > 0
    ∀ C in MNs:
        C.profilin = C.profilin + PPlume
        M.releaseCounter - 1

M.uptakeCounter = PPlume x 8

- if M.PIP2 = inactive and M.uptakeCounter > 0
    ∀ C in MNs:
        if C.profilin > PPlume {
            C.profilin = C.profilin - PPlume
            M.uptakeCounter - PPlume
        }
        else {
            M.uptakeCounter - C.profilin
            C.profilin = 0
        }
  
```

Figure 6.9: Pseudo code for the original and new PIP2 release and uptake rules relating to the release and uptake of profilin by PIP2.

### 6.3.2 Agent projection with optimized PIP2 function

The agent volume projection was re-run with the optimized PIP2release function. As the new PIP2release function improved performance, the model was only run for 200 time steps, and indeed may have attained high fitness much earlier even than this. Fig.6.7(d) shows that the errors have been significantly reduced, the top error being half the errors gained with the old version of the PIP2release function. Fig. 6.7(c) shows that the improved robustness, and possibly the increased levels of profilin released (investigated in the next study), allow more combinations of agent volumes to achieve high performance.

Compare Fig.6.8(b) with Fig.6.8(a), the PIP2release function does indeed appear to have reduced the instances of ‘no behaviour’ due to high agent volume no longer blocking profilin release. Some instances when actin levels are low are still encountered, but this could be due to an actual lack of ability, on the Cellanimat’s part, when actin levels are low rather than a blockage of agents. Indeed, the average score for a Cellanimat with an actin:nucleator ratio of 10:80 was 7.52% (error =2.54%), so the ‘no behaviour’ score (5%) did not significantly deviate from the average score — it was within one standard deviation of the mean.

From these results the optimal settings for #A and #N, for robustness and performance, were found to be #A=70% (which gives 4596 actin agents) and #N=20% (which gives 1313 nucleator agents). These are far higher than previously suspected. However both the 80:10 and 60:30 volume combinations also reliably yield near 100% engulfment. So as long as the number of actin agents stays over 50%, and the total number of agents fill 90% (or possibly more) of the Cellanimat’s cytoplasm voxels it will achieve near full engulfment. Of course this result is task dependent, and dependent on the settings of the other static parameters. To gain a parameter set optimal over all parameters a GA is recommended, details given in study 7. The Cellanimat’s increased production of profilin, due to the optimized PIP2release function, meant that the original balance in the parameters has now been upset. A projection into profilin dynamics was conducted to understand more precisely the effects that profilin levels have on performance, and to suggest profilin-related parameter optimizations.

## 6.4 Study Three. The role of profilin: recycling or saturation?

Profilin is a cytoskeletal accessory protein, in the Cellanimat it is a crucial component, it is the diffusible signal linking the ArtCyto to the external environment. To understand the role of profilin in the Cellanimat, in terms of efficiency and optimization, a thorough investigation of all profilin related mechanisms, and their dynamics, was performed. Based on insights from this investigation, improvements to the system are outlined and then validated. In real cells profilin recycling can be seen as a very efficient method of maintaining high profilin levels at the leading edge (Holt, M. R. and Koffer, A., 2001). A 2D projection was performed, varying the two profilin parameters P<sub>ath</sub> and P<sub>recycle</sub>, to gain insights into the necessity of a profilin recycling mechanism within an artificial setting, and to define optimal parameter settings. Profilin dynamics are determined by the following four functions in the Cellanimat, as previously described in Chapter 4:

- **PIP2 release/uptake:** profilin is released/uptaken by PIP2 upon receptor activation/deactivation.
- **diffusion:** all profilin is diffused through empty cytoplasm voxels.
- **PrUptake:** in real cells profilin activates sequestered actin (state SA) and binds to it forming profilactin. In the Cellanimat this is represented by the removal of a small quantity of profilin local to the actin agent concerned.
- **PrRelease:** In real cells, when profilactin binds onto the end of an actin filament the profilin is released back into the cytoplasm. In the Cellanimat, this is represented by a release of profilin when state WA actin changes state to FA, by joining a filament.

There are just four parameters, given below, that relate to profilin. The amounts are given in arbitrary, abstract units and do not relate to actual concentrations found in real cells. Default settings are given in square brackets.

- **PAth** [0.01]: amount of profilin needed, in an actin (state SA) agent's MNs, to activate it (change state to PA).
- **Precycle** [0.01]: approximate amount of profilin taken, and subsequently released, during profilin recycling (through the PrUptake and PrRelease functions).
- **PPlume** [0.5]: amount of profilin released by PIP2 into each available Cytoplasm MN upon, and only upon, receptor activation.
- **Pth** [0.5]: the profilin diffusion threshold.

#### 6.4.1 Dynamics of profilin recycling

Before finding optimal parameter settings related to profilin it was necessary to take a deeper look at how the profilin recycling mechanisms were implemented within the model. Investigation into how each of the stated functions, relating to profilin, affected profilin levels was performed. Areas for improvement were searched out, in terms of simplicity and accuracy. A higher degree of transparency, and improved accuracy, of the profilin recycling *mechanisms* sheds greater light on the definition, and importance, of optimal parameters, and will lead to greater insights into the role of diffusible signals and recycling systems during morphological plasticity in the artificial system as a whole.

Using all original versions of functions, and the default parameter set, the Cellanimat was tested for 250 time steps at phagocytosis with WASP radius 2 recruitment. The following data was collected at each time step: the average amount of profilin *detected* by an SA actin agent upon activation; the average amount of profilin actually *removed* per agent in the PrUptake function; and the average amount of profilin *released* per agent in the PrRelease function. This gave a fuller picture of the role of profilin in the original model, as used in the previous chapter, and the recycling/activation 'strategy' implemented by the default parameter set.

#### 6.4.1.1 Profilin detected during PrUptake

On average, over the whole run, 0.043 (with error 0.085) profilin was detected when state SA actin agents changed state to PA, which is 4.3 times the default P<sub>ATH</sub> setting. Fig.6.10 shows that over the time steps a wide range of profilin levels were detected as can be expected. A small number of peaks can be distinguished in this graph, where much higher levels of profilin were detected, possibly by agents close to a newly released plume of profilin, that has not yet diffused.

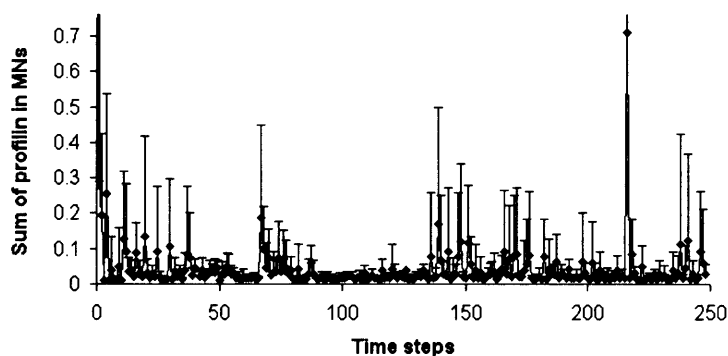


Figure 6.10: The average sum of profilin detected by an SA agent in its MNs (whilst being activated by profilin and changing state to PA). Averaged over all SA agents with enough profilin ( $\sum ProfilinMNs > P_{ATH}$ ) to activate in each time step.

#### 6.4.1.2 Profilin removed by PrUptake

Fig.6.11 clearly shows that throughout a run the amount removed from the system via the PrUptake rule is rarely the full amount of the Precycle parameter (0.01), and on average, the amount taken is less (the overall average value for this run is 0.00191, which is 19.1% of the Precycle parameter, with standard deviation 0.0014). Indeed sometimes the amount taken is zero. As the model was not initially designed to optimize efficiency, but rather to perform a desired task optimally (chemotaxis or phagocytosis), the functions relating to profilin recycling were quite relaxed and simplified. Conservation of profilin was not given high priority. The PrUptake function removes all profilin from a single, randomly chosen cytoplasm voxel (neighbouring the actin agent changing state), not containing an agent up to the value of the Precycle parameter. So, if  $C.profilin < Precycle$ , then the amount removed would of course be less than Precycle, and may even be zero.

#### 6.4.1.3 Profilin released by PrRelease

The amount of profilin released with the PrRelease function, called when WA actin changes state to FA (as it joins a filament), over one run can be seen in Fig.6.12. 99.3% of the releases of profilin, in the PrRelease function, were of exactly the amount stated by the Precycle parameter (0.01). There were only 10 instances (out of 1323 calls of the function during one run) of actin being unable to find a C state MN to release the amount to, thus losing a small amount of profilin from the system. Were there more agents (with the default parameters only 75% of Cellanimat volume was occupied by agents) the expectation is that the number of instances where no C state MN could be found, to release to, would rise.

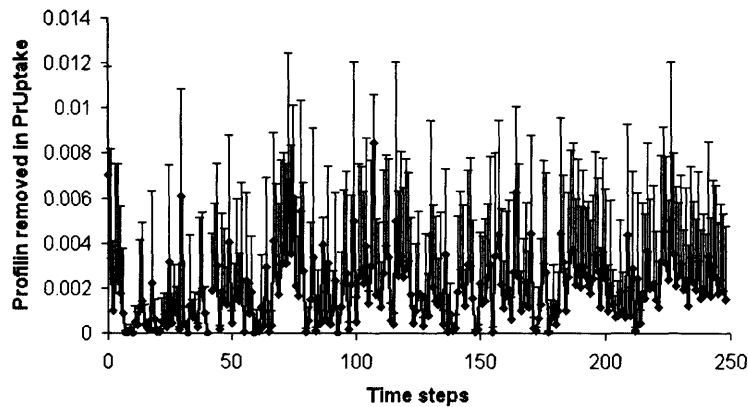


Figure 6.11: The average amount of profilin removed in PrUptake, when actin changes state from SA to PA, in each timestep.

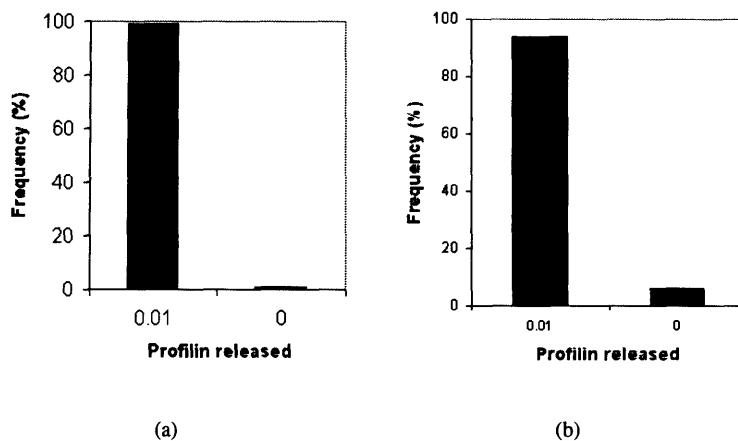


Figure 6.12: (a) Frequency charts showing how often PrRelease fails to release profilin as actin.state changes from WA to FA. (b) Frequency when the NEW WN and NEW PIP2 rules are used with agent volumes at 70:20.

To test whether release failures would increase with agent volume the study was re-run using the updated WN rule and the updated PIP2 rule (as defined in sections 6.2.5 and 6.3.1 respectively). The optimal agent volume of 90% of the total cytoplasm volume was used, divided into the ratio 70:20 (actin to nucleators). This high agent volume left less Cytoplasm voxels available for profilin release during the PrRelease function. Fig.6.12(b) shows that surprisingly, a similar frequency to Fig.6.12(a) was found. Over the vast majority of cases PrRelease managed to locate a free Cytoplasm voxel for profilin release, in the Moore neighbourhood of the agent in question (changing state from WA to FA). So, the amount of profilin lost over a run was only a tiny proportion and further complication of this rule to restrict loss, though trivial, was deemed unnecessary, given the current level of abstraction of the model from biology.

#### 6.4.1.4 Summary

Overall, on this sample run, 3,682 (arbitrary units) of profilin were removed from the system by the PrUptake recycling function, whilst 14.13 units were released by the PrRelease recycling function. It

is clear why the default parameter set yielded high engulfment: the Cellanimat was benefiting from the simplicity of the PrUptake rule and actually generating more profilin to the system with the recycling mechanism. This increased actin activation beyond the amount that should have been generated by the influx of profilin from PIP2 release alone.

An extension to the PrUptake function, so that it searches through all available neighbours until the full amount *Precycle* has been removed, could be implemented to rectify the advantageous anomaly observed in the recycling system and to improve conservation of profilin. An extension such as this would shift importance back onto the parameter settings rather than there being intrinsic benefits in the mechanism. This change could initially have a detrimental effect on the Cellanimat's engulfment ability. However, it can be seen that the extra amount released by the recycling system (10.448) if spread over the 300 time steps may have been negligible, it would have only been enough to activate three extra SA-state actin agents in a time step, as it becomes 0.03 (2.d.p) extra per time step.

The Cellanimat was over-saturated with profilin in the original version, as used in Chapter 5, due to the simplicity of the recycling system. Saturation of profilin allowed it to perform well at the cost of efficiency. An efficient system would minimize the energy cost of protein production, recycling mechanisms in real cells represent one of the ways natural systems implement efficiency. But as task performance rather than efficiency was the main criterion for success in the chemotaxis and phagocytosis studies, the cost of protein production did not matter. For integrity however, improving the PrUptake function is suggested.

#### *Optimized PrUptake function*

To improve on profilin conservation and efficiency the PrUptake function can be amended, as shown in Fig.6.13, such that the uptake of exactly the amount specified by *Precycle* is enforced. For full profilin conservation, the PrRelease function could be extended so that if no empty C voxel exists in the agents MNs to release the previously removed profilin to then it widens the search to radius two neighbours and so on until a suitable voxel is found. A more radical change could be to give profilin agent status. However, such a change would require more major, structural changes to the model. Profilin agents were originally discarded in favour of a gradient in the creation of the model as they 'took up valuable voxel space'; higher resolution (increasing Cellanimat voxelation), or doubling up of agents in voxels, would be necessary to sustain a greater density of agents. No such extensions to improve the PrRelease function were implemented within this thesis as the benefits did not out way the extra memory and calculation time required.

#### 6.4.1.5 Validation

To validate the optimized PrUptake function, to show that it does indeed improve conservation of profilin the new function was implemented and data collected on profilin levels over one typical run. The Cellanimat was tested at phagocytosis for 200 time steps with WASP radius two recruitment using both the previously optimized WN and PIP2 release functions and the optimal agent ratio of 70:20 (see studies one and two). The Cellanimat achieved 100% engulfment by 200 time steps. Restricting the PrUptake

**Original PrUptake rule**

```

If  $\Sigma$  Profilin in C MNs > Path
go through MNs until a Cyto state voxel is found
remove 'Precycle', or less if not enough, from this voxel

```

**NEW PrUptake rule**

```

If  $\Sigma$  Profilin in MNs > Path
go through all MNs until amount 'Precycle' has been taken

```

Figure 6.13: Pseudo code for the original and new versions of the PrUptake rules. They are implemented by an actin agent in SA state as it changes to state PA.

rule had no detrimental effects on performance, however the over saturation of profilin due to the new PIP2release function must be taken into account. Figure 6.14 shows that the optimized PrUptake rule yields more realistic profilin removal/release levels. Now more profilin has been removed than released, 24.24 was released and 40.03 was removed in total. This is what was expected, as each actin agent in state PA or WA has removed profilin in PrUptake but has not yet re-released it in PrRelease, as it has not changed state to FA: the remainder of profilin removed from the system is caught up with agents that have not joined on to filaments.

### 6.4.2 Finding the Critical Saturation Point and optimized profilin parameters

Does the Cellanimat only function well when over-saturated with profilin or does recycling play a necessary part in activating actin? Is there a critical point, in parameter space, when recycling benefits the system? What is that saturation point? 1D and 2D projections into engulfment space were used to shed light on these questions.

A preliminary 1D projection into engulfment space was run for 200 time steps to give an idea of the effects of the optimized recycling mechanism on performance before optimization of the profilin parameter set began in full. The Cellanimat was tested at phagocytosis using all previously described updated functions (optimized WN, PIP2release and PrUptake rules) and the optimal agent volume ratio of 70:20. The task was repeated ten times varying Precycle in 10% jumps, between 0 and 100% of PATH. Fig.6.15(a) shows that, with the default profilin parameters, varying Precycle had no effect on behaviour. The Cellanimat was saturated with profilin and could reach full engulfment without recycling. The increase in profilin released by the optimized PIP2 function may have rendered the recycling mechanisms useless.

To test this, PATH was increased to 50% of PPlumeFull. Raising the amount needed to activate SA actin (PATH) reduced saturation as much more was needed for activation. Note that PPlumeFull is equal to eight times PPlume, which equalled four, so PATH was set to 2, rather than the original setting of 0.01, which is 0.25% of PPlumeFull. Precycle was varied in 10% jumps between 0 and 100% of PATH. With each new setting of Precycle the Cellanimat was tested ten times (so one hundred runs in total). It was hypothesized that, when profilin was a restricted commodity, increasing the amount recycled back to the membrane would increase performance. The expectation was to see that recycling could play an

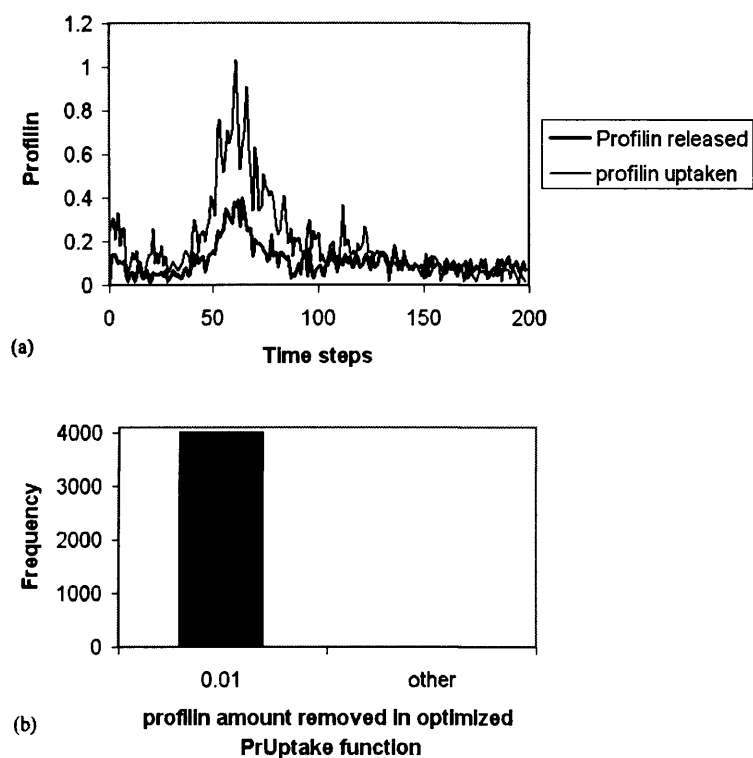


Figure 6.14: (a) Dynamics of profilin amounts released and removed at each time step with the new PrUptake rule. (b) Over the validation run only the amount Precycle (0.01) was removed using the new PrUptake rule.

important role in a profilin deficient, or at least under-saturated, system.

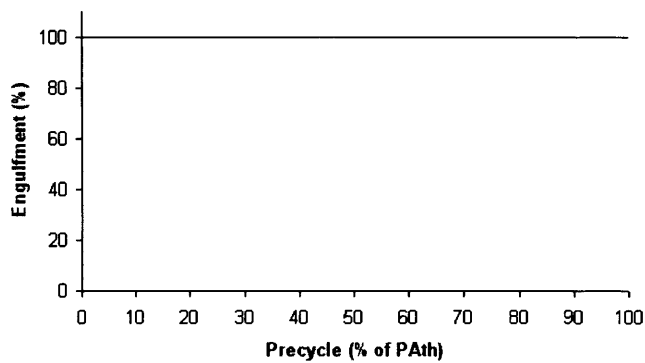
The highest fitness was indeed attained when Precycle was highest (equal to P<sub>Ath</sub>) see Fig.6.15(b). Setting P<sub>Ath</sub> to half the value of P<sub>PlumeFull</sub> put too much strain on the system, it was deficient in profilin and only achieved a top engulfment of 47.03% on average. The *Critical Saturation Point* (CSP) would be reached when the profilin parameters were such that the amount of profilin in the system was exactly the amount needed to yield high engulfment, no more no less. To find the CSP P<sub>Ath</sub> was varied together with Precycle in a 2D projection.

#### 6.4.2.1 Critical Saturation Point 2D projection

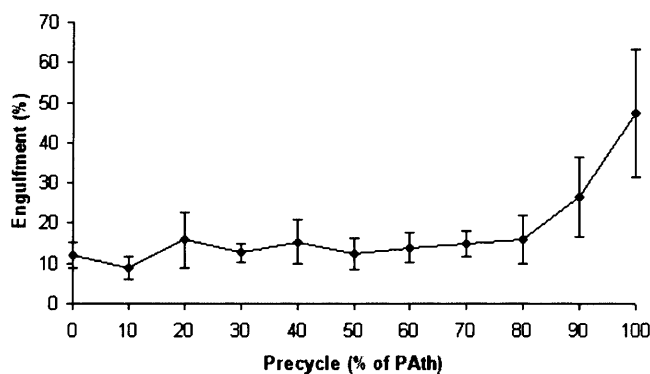
The Cellanimat was tested at phagocytosis 10 times for each pair of P<sub>Ath</sub> and Precycle parameter settings within the 2D projection, where P<sub>Ath</sub> was varied in 10% jumps between 0 and 100% of P<sub>PlumeFull</sub>, whilst Precycle was varied in 10% jumps between 0 and 100% of P<sub>Ath</sub>. Each test lasted 200 time steps. All optimized functions described in the previous studies were implemented (the new WN, PIP<sub>2</sub>release and PrUptake rules), WASP was recruited to radius 2 MNs, and the optimal 70:20 ratio of actin/nucleator agents was used.

See Fig.6.16(a), performance (engulfment) was on average above 50% when P<sub>Ath</sub> was less than 50% of P<sub>PlumeFull</sub> and highest with P<sub>Ath</sub>=10% of P<sub>PlumeFull</sub>, see Fig.6.16(a). The optimal setting for Precycle can be seen to be 100% of P<sub>Ath</sub>. If high performance is desired and are profilin recycling or





(a)



(b)

Figure 6.15: (a) Recycling had no effect on performance when PAtH was set to 2.5% of PPlumeFull; (b) with PAtH set to 50% of PPlumeFull, average engulfment increased as Precycle approached PAtH. This shows that recycling of profilin increases performance when the system is less saturated with profilin as expected.

efficiency are not a concern, then it is optimal, as shown in the first 1D profilin projection, to set PAtH less than or equal to 0.25% of PPlumeFull. But, if a Cellanimat optimized for efficiency and loyalty to biology is required, by avoiding over-saturation, the Critical Saturation Point must be found.

The Critical Saturation Point is located at on the 2D projection at the intersection of a high Precycle value (100% of PAtH) with a PAtH value which is high enough to define profilin as precious (improvements in performance are observed with increased recycling), yet also low enough that a useful number of actin agents can still be activated by it (indicated by high performance). If 'high performance' is defined as greater than or equal to 80% engulfment, then the Critical Saturation Point can be seen to lie at *approximately* PAtH = 10% of PPlumeFull (0.4) and Precycle = PAtH. Above this point, when PAtH is less than 10% of PPlumeFull, increases in Precycle does not appear to have any beneficial effects, so the system is over saturated. Below this point the engulfment level of 80% is not, on average, attained. Of course the Critical Saturation Point varies as the definition of 'high engulfment' varies, if only 50% engulfment is required then the point would lie at PAtH = 40% of PPlumeFull and Precycle = PAtH.

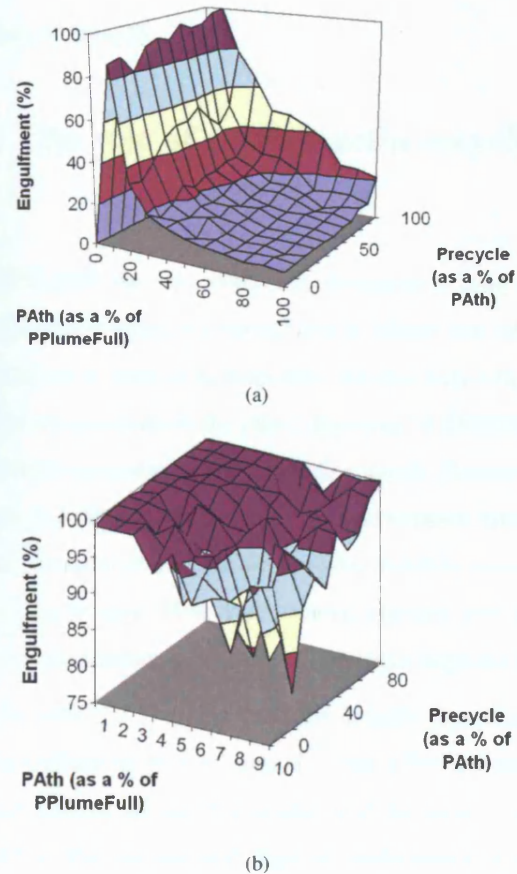


Figure 6.16: (a) 2D projection averaged results varying PPath and Precycle to find the Critical Saturation Point where recycling improves performance, and performance is also high. (b) Higher resolution 2D projection averaged results of the Critical Saturation Point area where PPath is between 0 and 10% of PPath.

For completeness, the resolution around the approximate Critical Saturation Point for 80% engulfment was increased, in order to define it more accurately. A further 2D projection was performed, this time varying PPath in 10% jumps between 0 and 10% of PPlumeFull and Precycle in 10% jumps between 0 and 100% of PPath. Each parameter pair, as PPath and Precycle were varied in the projection, was run ten times and results averaged. See Fig. 6.16(b). When PPath was less than 6% of PPlumeFull the system was saturated with profilin, as increased recycling yields no beneficial effects. However, when PPath is greater than 6% increased recycling began to cause improvements with the most striking improvement seen at PPath = 10% of PPlumeFull.

So, in an efficient and optimal Cellanimat, which strikes the right balance between over saturation and under activation utilizing the in-built recycling mechanisms, PPath should be set to be 10% of PPlumeFull (which is 0.4, when PPlume is 0.5) and Precycle to be 100% of PPath (0.4). With Precycle equal to PPath, all of the amount needed to activate actin (which represents the binding of a profilin molecule to actin forming profilactin) is recycled. Thus in this parameter set, the value 0.4 represents one molecule of profilin which is removed, during binding to actin, and released when the PA (then WA) actin loses the molecule and binds to a filament. If saturation is not a concern then optimal PPath would

be below 6% with any setting of Precycle.

## **6.5 Study Four. The role of cofilin: actin recycling in the Cellanimat**

Two parameters, within the P(LOSS) function, control the dynamics of actin recycling through filaments: FTOP and FINT. They simplistically model the natural loss of affinity that actin molecules exhibit for filaments, generating disassociation of actin from filaments, and thus recycling of actin through filaments, as actin joins at one end and disassociates at the other. Increases in P(LOSS) are akin to the effects of cofilin, a ‘severing’ cytoskeletal accessory protein, which controls filament length. In real cells ATP-bound actin hydrolyses back to ADP-bound actin whilst bound within a filament. ADP-bound actin has less affinity for the filament. So actin would lose affinity after a certain amount of time and disassociate without the need for a severing protein. However, severing proteins give the cell tighter control over average filament length, precisely regulating filament dynamics in response to the environment.

This study concerns the effect, if any, that variation in actin recycling speed (probability of loss of affinity/severing) has on Cellanimat performance, i.e. the effect of increasing/decreasing average filament length, and therefore also the volume of available actin for polymerization. The expectation was that greater recycling (high P(LOSS) values) will improve performance as more actin will be available at the active edge, and less will be needlessly tied up, bound in filaments far from the active edge. The default setting for P(LOSS) was high but not too high, with the argument that very high values would yield ineffectively short filaments that disappeared before further actin could bind to them exerting maximum extensions of the membrane. This argument will be tested in this study and optimal settings defined.

The ability to recycle actin improves efficiency in real cells. But, as energy was not modelled in the Cellanimat directly, the benefits of actin recycling, if any, would be of a different nature to energy efficiency. For instance it was expected that increased actin recycling could have a beneficial effect when actin agents were scarce, as displayed by the profilin saturation/recycling relationship in Study Three. If the system were saturated with actin, then recycling could result in no improvement in performance. So, the agent ratio from the default parameter set was used, instead of the newly found optimal combination, as there were less actin agents in the original parameters yet high engulfment could be achieved. In the agent volume projection (Study Two), with the optimized WN rule, the original agent settings (where 75% of the cytoplasm voxels were agents, 35% of which were nucleators, giving: #A=49%, #N=26% of the total cytoplasm volume) averaged 79% engulfment after 200 time steps.

A 1D projection was performed, varying the probability of an agent disassociating from a filament within a simplified, deterministic version of the P(LOSS) function, as described below. Optimal profilin parameters, as defined in Study Three, were used (P<sub>A</sub> and Precycle set to 0.4) all other parameters were taken from the default set. The engulfment was expected to be lower than 79% as the newly optimized profilin parameters reduce the Cellanimat profilin saturation apparent in the agent projection.

### 6.5.1 Deterministic P(LOSS)

The original P(LOSS) function dictates that after a certain point (FTOP) the probability of an agent, residing at the minus end of a filament (so only a FN or F<sup>-</sup>A state agent), losing affinity for that filament (unbinding and returning to the inactive state: N or SA respectively) *increases* by the interval (FINT). So for example, with the default parameter settings, when an F<sup>-</sup>A actin agent with  $\text{actin.Fcounter} = 10$ , the chance, P(LOSS), of it disassociating from the filament and returning to state SA, is  $\text{actin.Fcounter}/(\text{FINT} \times 100)$ , which is  $10/200 = 1/20$ . So there is a 1 in 20 chance of disassociating, however if it remains attached to the filament, on the next time step there will be a 1 in 18 (11/200) chance of disassociation and so on. Thus disassociation becomes more likely as the time spent bound to a filament increases.

Removing the stochastic element from this disassociation function gave a clearer picture of recycling effects with a projection. Determinism reduced noise. So, for the purposes of this experiment the P(LOSS) function was reduced simply to this: if the agent exists at the minus end of a filament and  $\text{agent.Fcounter}$  is equal to FTOP, then disassociate (unbind and change state to N or SA depending on agent type). This translation to a deterministic function can be implemented within the original function by resetting FINT to equal FTOP/100, this sets the probability of disassociation, when  $\text{agent.Fcounter} = \text{FTOP}$ , to 1.

### 6.5.2 Results

FTOP was varied between 0 and 150 (150 equalled the total time steps performed within each run). The results were averaged over 20 runs. The graph in Fig.6.17 shows that fast agent recycling through filaments (when FTOP was low) can be detrimental to the engulfment behaviour. If agents fall off filaments at a faster rate than they are polymerizing, then filaments were actually observed to disappear rather than persevering throughout a run. A relatively small range, in which the performance is heightened by recycling, is observed between FTOP = 10 and 40. After FTOP = 40 a performance plateau was observed, where increased filament length neither increased or decreased performance.

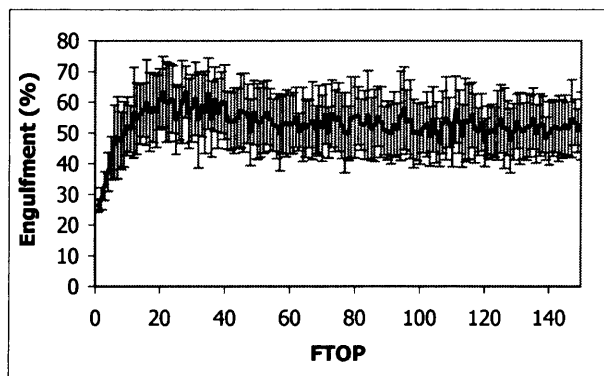


Figure 6.17: 1D cofilin projection using deterministic P(LOSS) function varying FTOP between zero and the top number of timesteps. Standard deviation over 20 runs shown in grey.

In real cells a balance is necessary, between the rate of polymerization and the rate of loss, within

filaments. When these are equal, the filament length remains constant, though the individual monomers comprising the filament are constantly changing. This phenomenon is called treadmilling (Alberts, B. et al., 1994). To achieve extending filaments, the rate of loss must be less than the rate of polymerization, for short but stable filaments, presumed to be the most efficient state, the rate of loss needs to be only slightly less than the rate of addition. Variation in disassociation rate during the run would allow the Cellanimat to chose between the different types of filament dynamics for different tasks. Variable disassociation would provide extra functionality and could prove to be an interesting addition in future work.

The role of cofilin and actin recycling deserves further, in depth, study. These preliminary results show that actin recycling affects overall performance and functionality, whilst holding interesting dynamic properties itself. Efficiency and further multifunctionality, indeed the overall complexity of possible Cellanimat behaviours, could be enhanced by the simple extension of variability in P(LOSS), giving the Cellanimat autonomous, and environmentally driven, control over filament length, dynamics and behaviour, a possibility for future work.

## 6.6 Study Five. The extent of an optimal TP

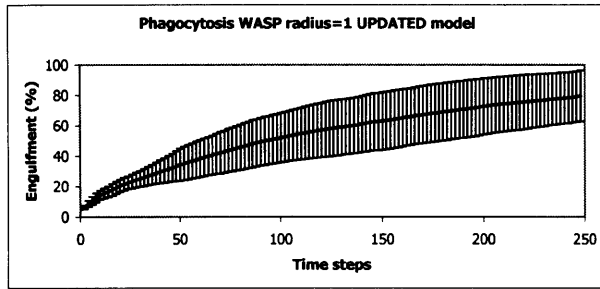
WASP recruitment to radius 2 neighbours, upon receptor activation, was found in Experiment B in previous chapter to more than double engulfment ability. To test if the model, with the parameter and function optimizations accumulated through the previous studies, had been so improved that WASP recruitment to radius 2 would now no longer be required for high engulfment, the Cellanimat was tested, with all optimizations discussed throughout this chapter, at phagocytosis with WASP radius 1 and then with WASP radius 2 recruitment, and results compared. A run lasted for 250 time steps and results were averaged over 50 runs. The optimal parameter settings used were (70:20 agent volume, P<sub>Path</sub> = 0.4, P<sub>recycle</sub> = 0.4) along with all improved functions (WN, PIP2 and PrUptake).

Fig.6.18 shows that WASP radius 2 recruitment still played a key role in engulfment and displayed less variability in performance than with WASP radius 1 recruitment, due probably to less dependence on initial conditions. However, with WASP radius 1 the optimized model gained an average of 80% engulfment by  $t=250$ , greatly surpassing the original model and parameters, which managed just 41% on average (Experiment B in previous chapter).

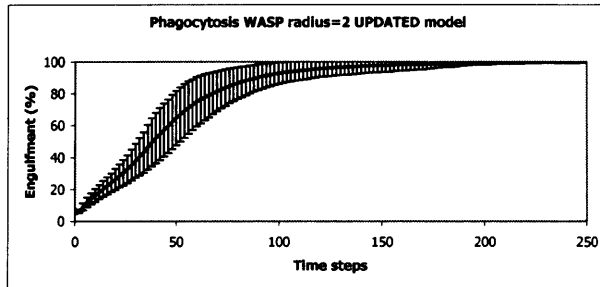
Indeed, these graphs highlight another important fact; with the improved model and optimized parameters, on average, full engulfment is actually achieved by time step 150, and in many cases much earlier. This is markedly faster than the 250 time steps it took on average to reach 92% engulfment with the original model and parameters in the previous chapter.

### 6.6.1 Receptor density optimization

To find out the optimal number of receptors for the phagocytosis task, P(REC), the probability of a new membrane voxel containing a receptor, the following experiment was repeated 50 times. P(REC) was varied between a zero and a 100% chance of placing a receptor in a new membrane voxel, in 10% intervals, and the Cellanimat was tested at phagocytosis for 150 time steps (as results described above



(a)



(b)

Figure 6.18: (a) WASP radius 1 activation still yields low performance at phagocytosis even with the improved model functions (b)WASP radius 2 activation still yields higher performance with the improved functions.

show that full engulfment can be achieved by  $t=150$  with  $P(\text{REC})=50\%$ , with WASP recruited to radius 2 MNs, 70:20 agent volume,  $P_{\text{Ath}}=0.4$ ,  $P_{\text{recycle}}=0.4$  and all other parameters as in the default set. The test was performed to give insights into the sensitivity of engulfment to  $P(\text{REC})$ , and the stochastically determined distribution of receptors.

Fig.6.19 shows that as  $P(\text{REC})$  increased there was a sharp rise in performance followed by a plateau at near full engulfment after approx.  $P(\text{REC})=30\%$ . The performance plateaus at approx. 95% engulfment. There was greater variability recorded in performance with low  $P(\text{REC})$  values, as the response was sensitive to the stochastic initial, and prevailing, receptor distribution.

The initial parameter setting of  $P(\text{REC})$  (50%) was found to be appropriate. But initial concerns suggesting that high  $P(\text{REC})$  values would cause the system to be overloaded and thus performance would degrade were shown to be false. Of course, as  $P(\text{REC})$  increases so does PIP2 volume, so high  $P(\text{REC})$  values are linked to profilin saturation. An efficient Cellanimat, especially one that has any kind of cost function associated with generation of receptors or other proteins, would need  $P(\text{REC})$  to be low.

## 6.7 Study Six. Compositional dynamics with the optimized model

In this study the compositional dynamics of the optimized model were compared to those of the original model, detailed in Study One. The Cellanimat was tested at Phagocytosis with WASP recruitment to radius=2 for 300 time steps and at chemotaxis with WASP radius 1 recruitment for 200 time steps. The optimized WN, PIP2 release and  $P_{\text{rUptake}}$  functions were used along with the optimal parameters: agent volume 70:20,  $P_{\text{Ath}}=0.4$ ,  $P_{\text{recycle}}=0.4$ . All other parameters were taken from the default set.

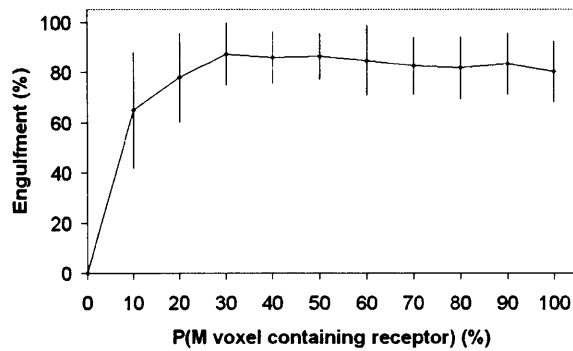


Figure 6.19: Varying P(REC), the probability of a membrane voxel containing a receptor, affects performance.

### 6.7.1 Phagocytosis

See Fig.6.20. The run displayed reached almost full engulfment by just 150 time steps, concurring with results from the WASP recruitment radius investigation in Study Five. In comparison with the compositional dynamics using the original model, a higher overall level of profilin is now observed. These graphs betray more about what happens after full engulfment is reached than the original model data as full engulfment was achieved earlier in the run. The number of FA agents rose higher than with the original model, related possibly to the earlier achieved engulfment creating more active WASP sites for filament formation earlier. The number of WN agents continued to rise whilst the number of FN agents decreased, validating the claim that WASP-bound agents take up the only available room at the particle-membrane periphery. The number of membrane voxels barely increased once full engulfment was reached as there was little filament growth in other directions as there is in chemotaxis.

### 6.7.2 Chemotaxis

The obvious differences between the dynamics shown in Fig.6.21 and the data collected with the original model, shown in Study One, was that the Cellanimat reached the source sooner. The number of nucleator agents in filaments (FN) actually exceeded the number inactive at one point. A higher level of profilin overall was also recorded, as PIP2 was now always releasing PPlumeFull. This did not mean that the Cellanimat was more saturated with profilin, just that the value of a profilin unit had changed, due to the increased P<sub>Ath</sub> parameter.

## 6.8 Study Seven. Saturation GA, evolution of an optimal parameter set

This study concludes the investigations of optimization, efficiency, robustness and the inner workings of the Cellanimat. An optimal parameter set was evolved, so that all parameters were optimized in terms of the other parameters, rather than in isolation related to only their particular functions, as described within the earlier studies. A standard generational GA was used to evolve an optimal parameter set for phagocytosis, optimized for speed and engulfment. It was hypothesized that through evolution,

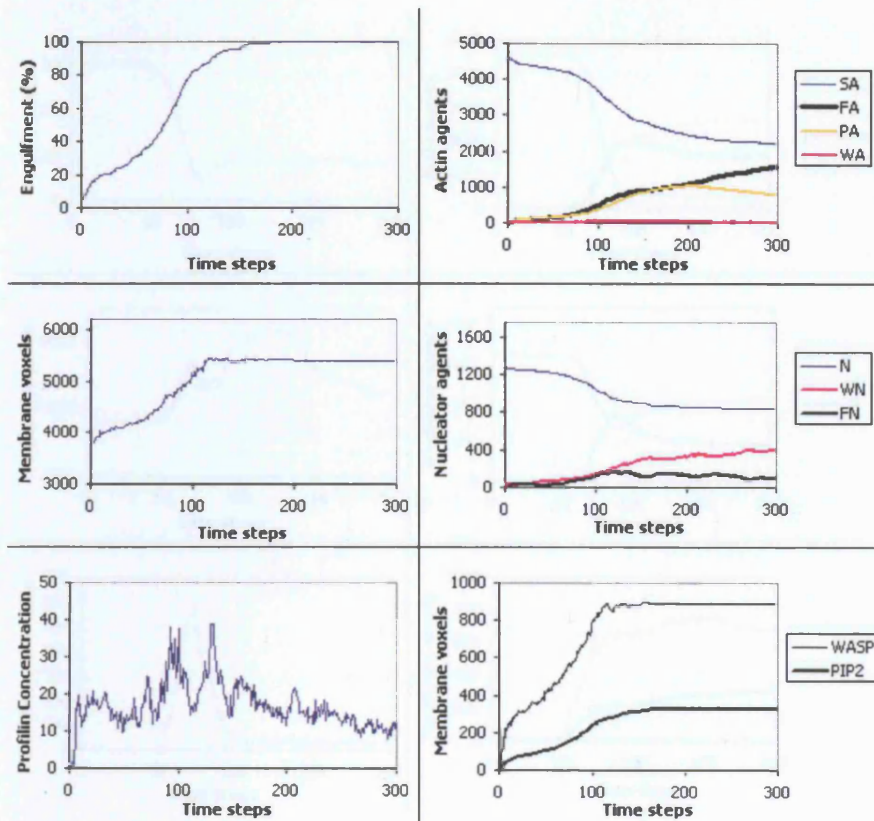


Figure 6.20: Compositional dynamics over one run of phagocytosis with the Updated Model.

saturation would be exploited leaving recycling obsolete: evolution would chose the easy, greedy, option if not directly encouraged to be efficient. As a result of the previous studies into recycling, it was expected that: agents would be seen to occupy a high proportion of Cellanimat volume, high receptor density and low PAth compared to PPlumeFull (profilin over-saturation) would be selected for.

Genotypes, initialized randomly within the ranges shown in table 6.3, were evolved over 50 generations with a population size of 50. Each member of the population was tested at phagocytosis for 200 time steps (experimental set up as in Experiment B in previous chapter) using the optimized functions from previous studies (the new WN, PIP2 release and PrUptake functions). Each genotype was assessed by the fitness function described in Equation 6.5. Parents were taken at each generation as the top 10% of the population. The highest scoring genotype was transferred, unchanged, into the next generation (elitism). The remaining population were produced using a crossover method that conserved the integrity of the genotype, given the interdependent value constraints, and were then subject to creep mutation, as described in the next sub-section.

### 6.8.1 Crossover and mutation

As some genes were interdependent, for example PAth depended on PPlume, crossover of two randomly chosen parents (with replacement) occurred at four distinct locations in the genotype only, see Fig.6.22. The top scoring parent was first entered into the next generation without crossover or mutation, but with replacement; it could also be chosen for crossover.



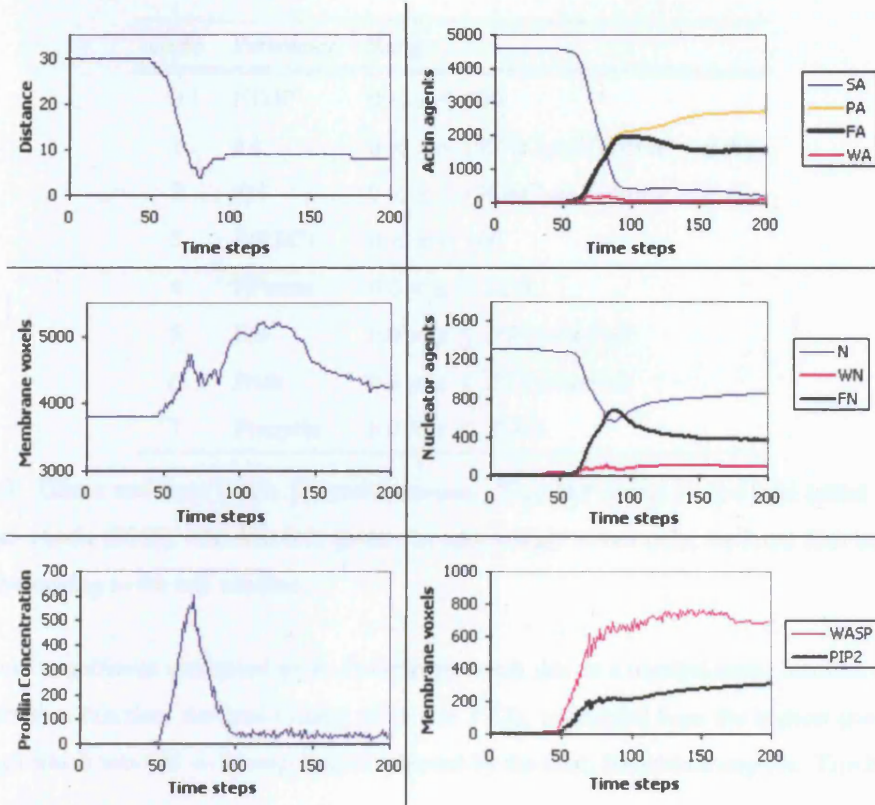


Figure 6.21: Compositional dynamics over one run of chemotaxis with the optimized functions and parameters from Studies One to Five.

Each new genotype in the population was then subject to mutation with a probability of 1 gene being mutated in each gene string ( $P(\text{gene mutation})=1/8$ ). See equation 6.1. A gene  $G$  was classified as either an integer or a float value and had the respective mutation operator applied to it. The mutation operator  $M_{int}$  was picked, upon mutation, from integers in the given range (eqn. 6.3) using a uniform distribution. Similarly for  $M_{float}$  but any float value could be picked. The sum was calculated within modulus  $r$ , ensuring the parameter remains within its viable range  $r$  as detailed in table 6.3.

$$G_{int} \equiv G_{int} + M_{int} \pmod{r} \quad (6.1)$$

$$G_{float} \equiv G_{float} + M_{float} \pmod{r} \quad (6.2)$$

$$0 < M_{int} \leq 1000 \quad (6.3)$$

$$0 < M_{float} \leq 1 \quad (6.4)$$

## 6.8.2 Fitness Function

In order to optimize for speed and engulfment the fitness function in equation 6.5 was used.  $T_G$  was the time step when engulfment of 700 or above was achieved. If this score was not reached  $T_G$  was the full time of the run (200). The highest engulfment value possible was 701 ( $E_{top}$ ) (see previous chapter for explanation of the engulfment metric).  $E_G$  was the actual engulfment achieved at  $T_G$ .  $FIT_G$  would

Gene	Parameter	Range
0	FTOP	$0 < x \leq 200$
1	#A	$0 < x \leq (95\%CytoVolume - \#N)$
2	#N	$0 < x \leq (95\%CytoVolume - \#A)$
3	P(REC)	$0 < x < 100$
4	PPlume	$0.0 < x < 11.0$
5	Pth	$0.0 < x \leq PPlumeFull$
6	PAth	$0.0 < x \leq PPlumeFull$
7	Precycle	$0.0 < x \leq PAth$

Table 6.3: Genes and their viable parameter ranges. ‘CytoVol’ refers to the total initial volume of cytoplasm voxels (6565). The first four genes can take integer values only, the latter four can take and number belonging to the real numbers.

decrease as engulfment and speed grew. In order to watch this as a maximization function rather than a minimization function, the final Fitness value was  $FIT_G$  subtracted from the highest possible score ( $FIT_{high}$ ) which was 901 — no engulfment achieved by the final, 200th time step (i.e.  $T_G=200$  and  $E_G = 0$ ).

$$FIT_G = T_G + (E_{top} - E_G) \quad (6.5)$$

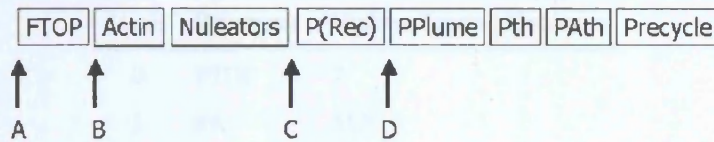
$$fitness_G = FIT_{high} - FIT_G \quad (6.6)$$

### 6.8.3 Results

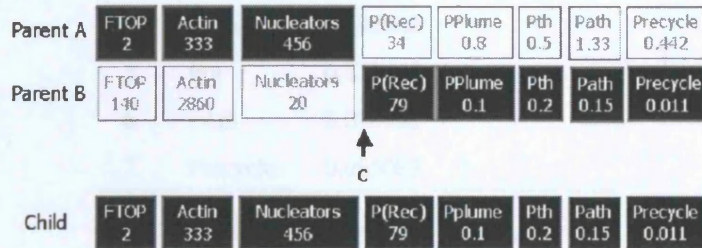
The evolution took approximately thirty hours although high fitness genotypes were discovered relatively early on, by around generation 10, see Fig.6.23 for the evolutionary dynamics. The top fitness in generation 50 was 847; engulfment of 700 was reached by time step 53. The mean fitness for the final generation was 711, meaning that, on average, full engulfment was reached by time step 190. The genotype for the final generation high scorer is shown in Table 6.4.

The evolved, optimal parameter set shown in Table 6.4 does indeed reflect and strengthen the findings of the studies performed in this chapter. A high proportion of membrane voxels contained receptors, 84% on average. The number of agents filled a high proportion of the cytoplasm volume (94%) corroborating the findings in Study Two. PAth was 0.5% (to 1.d.p) of PPlumeFull. This meant that the Cellanimat had indeed exploited the lack of constraints on protein production (e.g. an energy constraint) resulting in the complete over-saturation of profilin and actin.

The top scoring genotype achieved high engulfment extremely fast, but it was very inefficient. Precycle was very close to PAth which would indicate high recycling, however, as PAth was so low in comparison to PPlumeFull, it is clear that recycling would have had no effect on engulfment ability (from Section 6.4.2). Similarly the cofilin recycling of actin was ineffectual, given the over saturation of actin. The FTOP gene was 7 so filaments were kept very short, this would have been expected to



(a)



(b)

Figure 6.22: (a) The four viable crossover points in the saturation GA to conserve integrity in the parameter values due to interdependence. (b) Example of two parents crossed at point C.

be detrimental, from the results in Study Four, however the high density of agents may override any negative affects of short filaments.

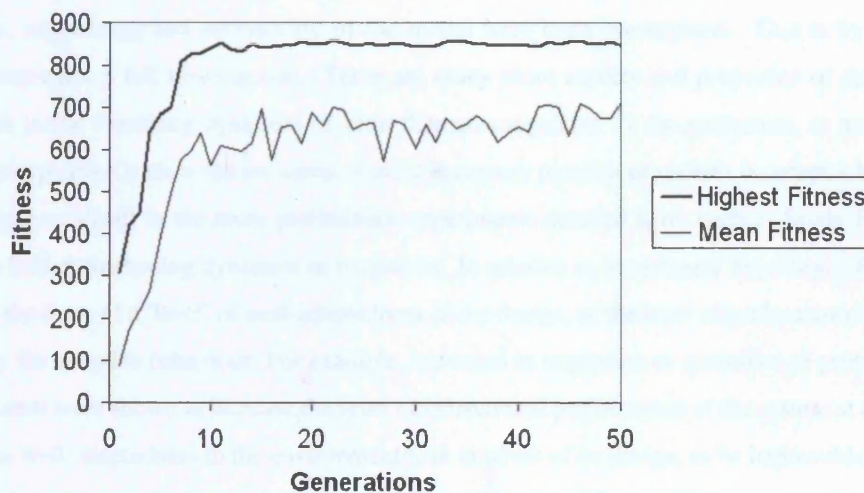


Figure 6.23: Evolutionary dynamics of the Saturation GA.

A complementary study to this Saturation GA could highlight a more realistic role for profilin recycling in the Cellanimat. The 'Starvation GA' could utilize a cost function, putting a price on each protein included. This would select for efficient, optimal parameter sets that minimize the number/concentration of macromolecules. In such a study, recycling mechanisms could be expected to become fully implemented by the selection of high Precycle, low PAtH, low agent volumes and medium P(LOSS) parameters. The cost function would represent energy in the system, a parameter set could be sought to optimize performance in harsh environments — under 'starvation' conditions. The expectation would be that the

Gene	Parameter	Highest Scoring Genotype
0	FTOP	7
1	#A	5120
2	#N	1052
3	P(REC)	84
4	PPlume	2.032882
5	Pth	0.870663
6	PAth	0.090932
7	Precycle	0.085083

Table 6.4: Highest scoring genotype.

system, evolved under these more stressful conditions, would more closely resemble real cells and give greater insight into the necessary mechanisms within the Cellanimat for different types of environment, harsh or rich in resources.

## 6.9 Summary

The seven studies described in this chapter were designed to address Objective Four of the thesis, investigating the properties of the artificial MP model created in Chapter 4. The dynamics, optimization, robustness, redundancy and evolvability of the model have been investigated. This is by no means meant to represent a full investigation. There are many more aspects and properties of the model to study, such as the branching dynamics of actin filaments regulated by the nucleators, or areas for improvement/expansion such as the inclusion of more accessory proteins or realism in receptor behaviours. Further depth or detail in the more preliminary experiments detailed here, such as Study Four, could illuminate further interesting dynamics or properties. In relation to the primary hypothesis, this chapter has raised the issue of a 'level' of well-adaptedness of the design, or the level of performance that can be reached by the adaptive behaviour. For example, increases in saturation or quantities of proteins within the Cellanimat were shown to increase the level of behavioural performance of the system at a task, also showing its well-adaptedness to the environment/task in terms of its design, to be improvable. Compare the original model's performance at phagocytosis (engulfment=98% at t=300), to the optimized model in Study Six where near full engulfment was reached by just t=150.

## Chapter 7

# A case study in morphological plasticity: diatom colony formation

Returning to diatom valve morphogenesis, armed now with a framework and optimized model for morphological plasticity investigation (the E-P Map and Cellanimat, Chapter 4), a full simulation study into the mechanisms involved in diatom MP can now be conducted in order to test the secondary hypothesis. As a case study the MP exhibited during diatom colony formation is explored here. The benefits of this exploration are two-fold: 1) furthering understanding of diatom colony formation mechanisms in biology by original review and qualitative modelling and 2) investigating algorithmic formulations and mechanisms for plasticity in morphological development of artificial, interacting creatures.

First, in this chapter, the phenomenon of diatom colony formation, involving valve plasticity to the environment, is introduced. The subtleties involved in determining the underlying mechanisms, along with a review of current theories, are discussed. This chapter represents a crucial stage in the development of the testbed simulation model. Without thorough, careful consideration of the related biology, current knowledge, theories and open problems, an accurate and useful model cannot be created. In the following chapter (Chapter 8) the Cellanimat Colony Model, which combines the earlier Nature's Batik Model (Chapter 3) with the Cellanimat (with the ArtCyto optimized and tailored to the new problem), based on the biology presented in this chapter, is described with results and implications discussed.

### 7.1 Background

Certain species of diatom do not live as independent single cells. Instead, they have developed a complex set of environment-related interactions during valve morphogenesis, which allow them to form and disband colonies. In tune with the environmental changes of their fluctuating niche, colony dynamics are presumed to give these diatoms a greater chance of survival.

As a diatom undergoes cell division it must generate two new 'sister' valves, back-to-back, in order for the two new daughter cells to be fully enclosed in silica, see Fig.7.1. In general, a colony forming diatom will, upon cell division, produce two new sister valves such that they interlock and hold the cells together, e.g. Fig.7.3(a). In certain species this continues until the colony reaches a certain average length, then a dividing cell, within the colony, produces different sister valves such that the cells are

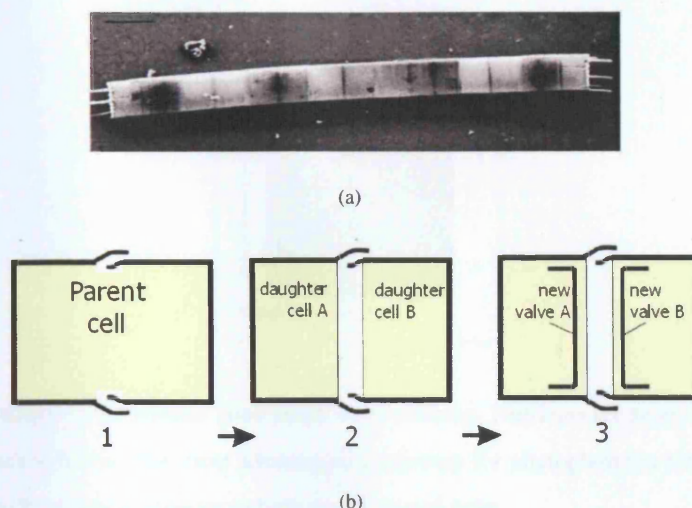


Figure 7.1: (a) *Aulacoseira granulata* colony of linked cells with separation spines delimiting the colony, reproduced with permission from (Crawford, 1979). (b) 2D schematic of a diatom dividing and forming new sister valves back-to-back.

able to slide apart ('separation valves'). Thus the separation valves provide a mechanism to divide the colony in two, giving the diatoms a mechanism for controlling colony length without loss of life through breakage, Fig.7.3(d).

It has been shown that all cells, within such colonial species, have the potential to form separation valves, but statistically the middle cell in the colony has been shown to exhibit the behaviour most prevalently (Davey, M. C. and Crawford, R. M., 1986). It is not clear how the cell 'knows' it is central (Davey, M. C. and Crawford, R. M., 1986). Conflicting evidence was however presented by Yakushin (1997), which found that on average colonies of *Aulacoseira subarctica* split with a 3:5 ratio. Colony formation has been implicated as beneficial in a number of ways, which will be discussed throughout this chapter, most distinctly as a mechanism to modify sinking rates in order to optimize nutrient and light exposure and to defend against grazers. The MP involved can be seen as a mechanism for executing adaptive behaviour at the individual level and society level.

Diatom Colony formation, in species able to develop both interlocking and separation valves (not all colonial diatoms form separation valves), is an explicit and interesting example of morphological plasticity to environmental change. There has been a large amount of interest and speculation as to the adaptive quality of the response and the possible underlying mechanisms, however, there are no current solid theories and very little data on *exactly* how and why certain species of diatom form colonies. Diatom colony formation is therefore a good system to model in order to further understanding of the adaptive processes that can underly MP and also contribute to current understanding within diatom research. Understanding the environmental cues which trigger/influence the morphological changes in diatom colonies has been highlighted as useful to understanding climate change through their use as bioindicators (Davey, M. C. and Crawford, R. M., 1986).

Most diatoms that form colonies are members of the phytoplankton, the assemblage of photoau-

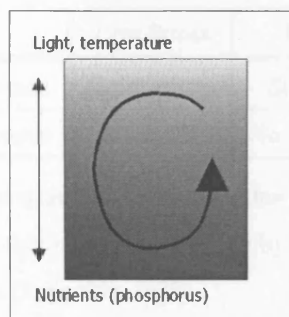


Figure 7.2: Schematic of the euphotic zone in the water column. Nutrients are more abundant below and light is more abundant above. The most advantageous strategy for phytoplankton is to cycle in the water column, benefiting from high exposure to both nutrients and light.

totrophs<sup>1</sup> that reside in open waters (pelagic zones) of seas, lakes, ponds and rivers for the majority of their life-cycle. They provide organic carbon to pelagic food-webs and as such are analogous to plants in terrestrial food webs, though not all photoautotrophs are true plants (Reynolds, 1994).

A mechanism to prolong suspension in the upper, illuminated layers of water (euphotic zone) is of great importance in phytoplankton. Adaptations to maintain this residence have functional relevance and it has been presumed that they have therefore been favoured by natural selection (Reynolds, 1984, 1988). Indeed marine phytoplankton's immense net carbon production of 1010 tons (annual net) is linked to their successful suspension within the euphotic zone (Smayda, 1970). However, continuous suspension is not always necessary or desirable (Reynolds, 1984).

A further characteristic of phytoplankton is the need to maintain a high exposure to essential nutrients such as phosphorus, which are more concentrated in the lower layers of the water column, see Fig. 7.2. Successful growth and survival require only that the mean daily residence time within the euphotic zone permits photosynthesis in excess of the total daily respiratory and secretory losses incurred within and below the zone. It has been suggested that temporary suspension mechanisms may be easier and more various than permanent suspension, granted that access must be at least periodic, though no justification for this suggestion was given by Smayda (1970).

Reynolds (1988) put forward the terms below to describe aspects of the phytoplanktonic environment. Above a critical range of disturbance, planktonic algae are vertically entrained (transported up through the light gradient). Stress/disturbance levels vary considerably between pelagic environments. Presumably, phytoplankton have evolved particular strategies and adaptations of morphology and physiological function to survive under one or other type of environment, shown in table 7.1. Colony formation can be seen as a response to a low stress/high disturbance environment. Colonial diatoms therefore usually fall into the ruderal category (see glossary for definition) and the large variation in colony morphology and dynamics between species may be seen as variation in strategy due to differences in stress and disturbance levels between their environments.

<sup>1</sup>photoautotrophs: microorganisms that synthesize their food from inorganic substances using light as an energy source

	Low Stress	High Stress
Low Disturbance	Competitors	Stress Tolerant
High Disturbance	Ruderals	No Viable strategy

Table 7.1: Table showing the adaptive strategies in the evolution of phytoplankton in freshwater pelagic environments. Competitors: exploit light/nutrient saturation by rapid growth and reproduction; Stress tolerant: can operate on low nutrients (Reynolds, 1988).

- **Stress:** when there may be insufficient essential nutrients available to match the supply of photosynthate
- **Disturbance:** the extent of wind-driven turbulent mixing

Reynolds (1988) also noted that many aspects of cell metabolism are related to cell morphology: efficiency of light interception and utilization, capacity to absorb and store nutrients, ability to alter rates of removal by grazers, susceptibility to loss by sinking and the manner in which they respond to temperature fluctuations. Motility can be a solution, allowing the individuals to migrate to depths with more favourable light and nutrient absorption. Most colonial diatoms are non-motile, so colony formation can be seen as a mechanism by a non-motile taxa to migrate, to cycle beneficially in the water column via morphological plasticity.

**Crucial open questions:**

- What environmental factor triggers/influences the change between linking and separation valves?
- What underlying organisation within the cell facilitates such morphological plasticity?
- Why does only the middle cell, on average, undergo the morphological transition?
- Does the difference in colony length affect the likelihood of being entrained?

## 7.2 Three example genera

There are a multitude of colony forming species each with its own particular morphology and behaviour. For example, there are diatoms that interconnect using organic material such as threads from strutted processes or by siliceous material such as interdigitating spines or fusion of structures; some attach in the girdle region (Round, 1972). The following are detailed descriptions of species within three distinct genera. The Cellanimat Colony Model, detailed in the coming chapter was based on the first example.

**1: *Aulacoseira***

*Aulacoseira* Thwaites is a cosmopolitan diatom genus of ecological importance (Edgar, 2003); the species are centric colony forming diatoms, displaying similar yet varied linking/separating valve morphologies. *Aulacoseira granulata* is one such species, occurring in freshwater habitats such as lakes, reservoirs and large rivers throughout the world (Davey, M. C. and Crawford, R. M., 1986). The linked valves of *A. granulata* have small interlocking spines and curved rows of pores, the separation valves



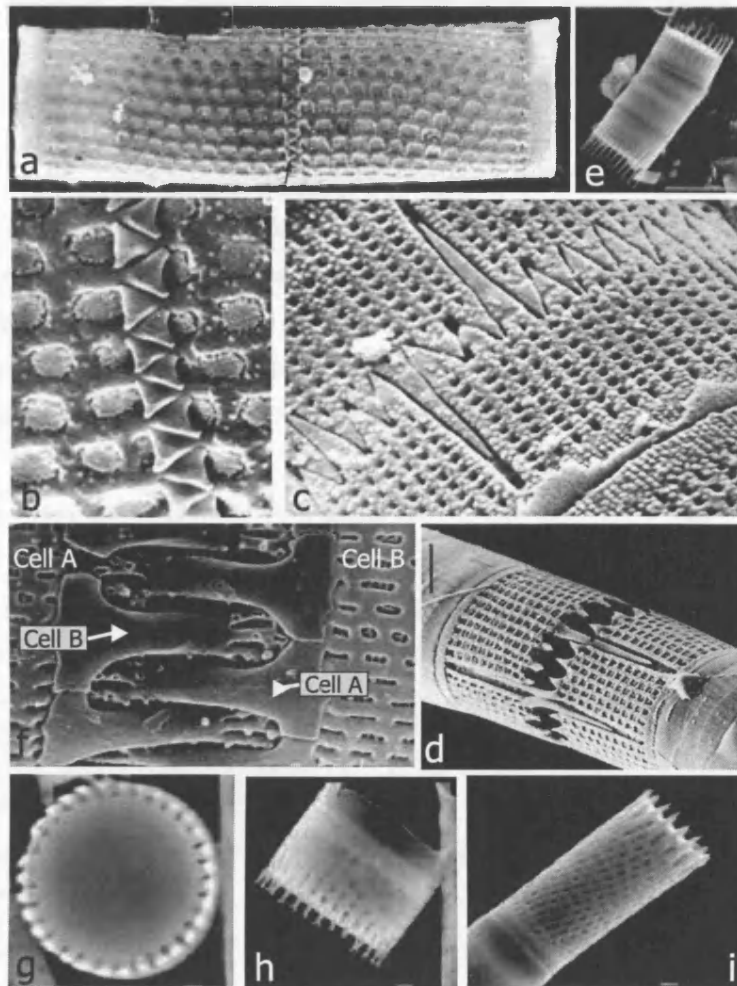


Figure 7.3: *A. granulata* SEM images (a-d reproduced with permission from (Crawford, 1979), e-i reproduced with permission from (Edgar, 2003). (a) Two linked cells, (b) linking valve morphology, (c) and (d) separation valve morphology. (e) *Aulacoseira* unidentified species SEM, separation spines visible on outer valves, (f) *A. Italica* interlocking morphology detail showing the spines from one cell grow past, then over, the sister spines. (g) and (h) valve face view and side view of unknown species of *Aulacoseira* showing that spines form only around the edge of the valve face (i) *A. ambigua* separation spines. Scale bar represents either 1  $\mu\text{m}$  or 10  $\mu\text{m}$

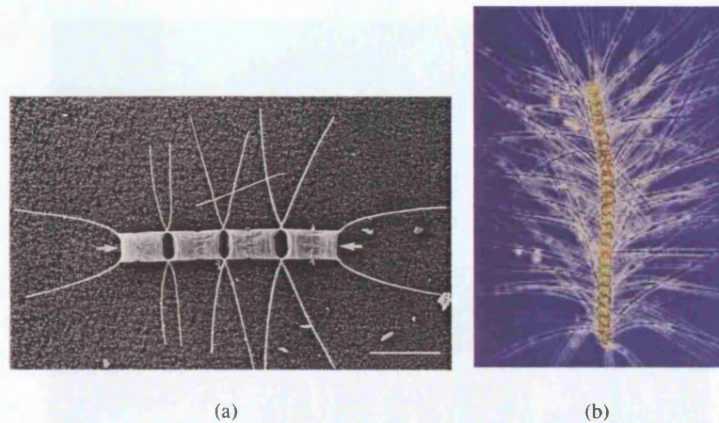


Figure 7.4: (a) *Chaetoceros decipiens* colony, bar = 50  $\mu\text{m}$ , the separation valves differing curvature is shown on the two end cells. Reproduced with permission from (Pickett-Heaps, 1998), (b) *Chaetoceros concavicornis* colony 1-2mm in length, of economic interest in the Pacific Northwest because their setae (spines) can cause the death of pen-reared salmon at Fish Farms. Reproduced from <http://thalassa.gso.uri.edu:16080/ESphyto/list/taxa/chconca.htm>.

have longer, flat spines and straight rows of pores. Fig. 7.3 shows example images of the linking and separation valve morphologies.

It has been suggested that colony length reflects the longer term environmental conditions, not day-to-day fluctuating conditions (Davey, M. C. and Crawford, R. M., 1986). Colony density has been shown to be inversely related to cell size, thus the cell wall thickness is the same regardless of cell size (Davey, M. C., 1986). Colony length on average, rarely exceeds 6-9 cells (Reynolds, 1984).

## 2: *Chaetoceros*

There are many species of *Chaetoceros*, all join by fusion of silica between long setae (protruding spines) see Fig. 7.4. Of the following two types: 1) *C.bacteriastroides* cells are joined together by seven 'pegs' as well as by two 'horns' that grow together and remain connected at their base. The separation valves have small spines and perforations. 2) *C.pseudocurvisetum* has curved, fused setae, valves also join at two areas, leaving a large aperture between the cells. It has curved chains and no small setae. It has specialized, deeply lobed, girdle bands which allow the setae of sibling valves to protrude outside the diameter of the chain during their formation, similar to those shown in Fig. 7.4, the large setae are joined by crossing over (Fryxell, 1978). *C.decipiens*, shown in Fig. 7.4(a), forms separation valves which are shorter, thicker and curve sharply, becoming almost parallel to the colony (Pickett-Heaps, 1998). This sharp change in curvature may prevent fusion as the sister setae no longer grow together in the same direction, allowing the cells to separate.

Fryxell (1978) proposed that the evolutionary direction between these two species was *C.bacteriastroides* to *C.pseudocurvisetum* with primitive colony formation involving cells tightly connected by valve surfaces, evolving to loosely connected cells allowing greater cell surface exposure. The spiral pattern of the chain has been proposed as advantageous for control of position in water column and orientation during sinking (Fryxell, 1978).

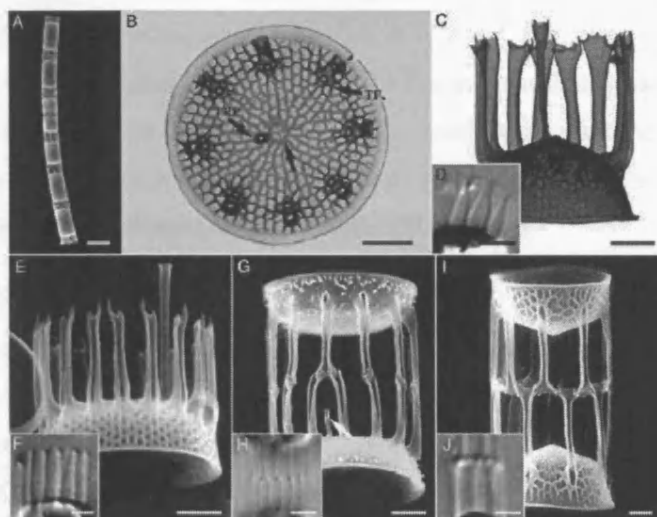


Figure 7.5: General morphology of the genus *Skeletonema* reproduced from (Sarno, D. and Kooistra, W. H. C. F., 2005). Light Microscopy: D,F,H,J. B,C show TEM valve face and side view. SEM: A,E,G,I show in turn a colony (scale bar 10  $\mu\text{m}$ ), separation valve, interlocking valves joined 1:1 apart from a single spine joined to two sister spines (both with scale bar 2  $\mu\text{m}$ ), interlocking valves joined 1:2 (scale bar 1  $\mu\text{m}$ ).

### 3: *Skeletonema*

*Skeletonema* is a morphologically and genetically diverse genus (Zingone, A. et al., 2005; Sarno, D. and Kooistra, W. H. C. F., 2005), see Fig.7.5. *Skeletonema costatum* is a coastal species that exhibits extreme variation in size and shape, and survives a wide range of salinities. It possesses strutted processes that facilitate colony formation (Medlin, 1991; Fryxell, G. A. and Miller, W. I. , 1978). Within *S.costatum* an isolate was identified as a new species due to its differing morphological behaviour (Sarno, D. and Kooistra, W. H. C. F., 2005). The usual isolates formed chains of twenty cells on average with robust processes between cells; the external tubes began at the valve surface, then interlocked and fused with the sibling cell's tubes; separation valves developed in the same way but did not fuse, see Fig. 7.5. The new isolate had chains of about ten cells under the same conditions (continuous light, 16°C, salinity 28‰ as artificial sea water) and weakly silicified strutted processes; the tubes were intact but trough-like with one side higher than the other, they met but did not fuse, the sibling cells remain connected due to the parent girdle bands remaining intact. As these differences have been observed for many years it is assumed that the difference in chain length is genetic (Medlin, 1991).

## 7.3 Possible reasons for colony formation

There are many possible reasons for colony formation to have evolved and environmental conditions that could be responsible for triggering the change in morphology between interlocking and separation valves.

### 7.3.1 Sexual reproduction

Colony formation could be an adaptation to increase the rate of population growth (Reynolds, 1988). It has been speculated that the close proximity of cells in colonies increases the likelihood of sexual reproduction as there is more opportunity for fertilization and a higher concentration of growth factors is maintained (Reynolds, 1988; Fryxell, G. A. and Miller, W. I. , 1978).

### 7.3.2 Fluid flow

Most cells experience an active and variable fluid environment. Flow has been shown to have a reversible effect on the morphology of *Ceratocorys horrida* (Peridinales, Dinophyta): in still conditions it grows six long spines, when agitated it produces shorter spines and reduces cell volume. resulting from a 39% decrease in vacuole size. When conditions reverse it reverts back to the long-spined form, sometimes within a single cell's lifetime. Sinking rates of the longer-spined form were shown to be lower than the short-spined form. It has been proposed that this could be an adaptation to escape from regions of high turbidity that can cause cell damage (Zirbel, M. J. et al., 2000). If sinking rate does indeed increase with colony length, then the fluid flow to which diatoms are subjected will also increase, and could affect spine morphology, perhaps resulting in separation valves. It would be interesting to test the effects of flow on diatom linking/separation valve morphology. However, cell size is unlikely to be affected in the same way as in Dinophyta.

### 7.3.3 Defence against grazers

Due to the pressures grazers exert on phytoplankton populations, colony formation has been regarded by many as an evolved defence (Davey, M. C. and Crawford, R. M., 1986; Fryxell, G. A. and Miller, W. I. , 1978). The colony chains may prove unmanageable to grazers due to awkward size, shape and extensions, they may clog filtering apparatus, they also may be unpalatable due to toxicity and indigestibility (Fryxell, G. A. and Miller, W. I. , 1978). Some species release extrametabolites to inhibit grazers and it has been pointed out that these would be concentrated in a colony (Fryxell, G. A. and Miller, W. I. , 1978), although it has been shown that size selection is more of a deterrent than taste (Porter, 1977).

Colony formation in *Scenedesmus acutus* (Chlorophyceae), a freshwater green algae, has been shown to be induced by the detection of chemical gradients from grazers; in the presence of *Daphnia* the unicellular *Scenedesmus* form colonies, reducing vulnerability (Lürding, M. and Van Donk, E., 1999). It would be interesting to analyze diatom colony dynamics with and without the presence of grazers, the shape may not only be a good defense, it could be a *consequence* of grazer presence. For instance, separation valves may only form in the absence of grazers. However, unlike *Scenedesmus*, colony forming diatoms do not live as unicells at any point, they are always in colonies, albeit of varying length, thus it is unlikely that grazers can be considered a sole cue.

### 7.3.4 Sinking rate increase or decrease?

Stoke's equation (Equation 7.1) suggests the most important factor affecting sinking rate is morphological change, rather than density change, due to the form resistance coefficient ( $\theta$ ).  $V$  is the sinking velocity of a particle,  $g$  is gravity,  $r$  is the radius of equivalent sphere (the term is squared here as resis-

tance is proportional to  $r$  and force is proportional to  $r^3$ ,  $\rho$  is the density of the particle,  $\rho'$  is the density of the medium and  $\eta$  is the viscosity of the medium. Particles remain in suspension when excess density equals zero or is positive, e.g. by water movement or motility (Davey, M. C., 1986). The form resistance coefficient cannot be derived, it has to be determined experimentally by comparing the sinking velocity of a particle with the sinking velocity of a sphere of equivalent density and volume, such as glass beads (Davey, M. C. and Walsby, A. E., 1985). This has important consequences when considering the calculation of sinking rates for artificial colonies, as a powerful physics simulator would seem to be the only possibility for calculating the form resistance.

$$V = \frac{2}{9}gr^2(\rho - \rho')\eta^{-1}\theta^{-1} \quad (7.1)$$

There have been various speculations as to whether the size, shape and other morphological attributes of diatom colonies help or hinder suspension in the water column (Smayda, 1970). Although an increase in the colony length:width ratio brings an increase in colony form resistance (Davey, M. C. and Walsby, A. E., 1985), colony elongation ultimately results in increased sinking rate rather than aiding flotation; *Skeletonema* has been highlighted as the only contrasting example, where micro-turbulent conditions between the numerous silica spines slow sinking (Smayda, 1970).

Reynolds showed that as density and volume of spheres doubled the rate of sinking increased approximately linearly, by on average  $20 \mu\text{ms}^{-1}$  whereas the sinking rate of *Melosira* colonies of equivalent volume and density increased by only  $2 \mu\text{ms}^{-1}$  as their length doubled (Reynolds, 1984). Thus for an individual, colony formation slightly increases its sinking rate. Form resistance of the colony keeps the increase low such that if the colony length increased to the average maximum of nine cells then the individual's sinking rate would only increase by on average  $4 \mu\text{ms}^{-1}$ . The increased sinking rate may be necessary to reach lower depths and increase exposure to nutrients as a greater volume of medium passes over the cells surface (Davey, M. C. and Walsby, A. E., 1985; Reynolds, 1988); this may also be necessary to avoid depleting nutrients in the higher levels of the water column with a static population; the low rate of the sinking increase may be necessary to avoid dropping out of the euphotic zone.

It has been noted that dead colonies sink faster than living ones, possibly due to a lack of mucilage strands adding to drag (Davey, M. C., 1986), so it is difficult to tell exactly what the sinking velocity effects are of elongating colonies as Reynolds' work used dead colonies. It may be necessary to test with living colonies, it could be found that living colonies have slower sinking rates. Indeed, non-siliceous protuberances under metabolic control might provide a more direct influence on suspension than other surface extensions such as the long tubular setae of *C. decipiens* which also incur an increase in density (Smayda, 1970).

Stoke's equation results in a 'flotation paradox' for diatoms. Suspension becomes the requirement to compensate by biological means the 'overweight' characteristic (self-regulated encrustation with dense material); cytoplasm density is approx  $1.05 \text{ g/cm}^3$ , water density is  $1.02 \text{ g/cm}^3$  and silica wall density is around  $2.6 \text{ g/cm}^3$ , so the silica cell wall actually hinders flotation (Smayda, 1970). The siliceous frustule seems counter adaptive to planktonic existence as it makes diatoms heavier and dependent on additional

nutrients, thus more prone to sinking. However, they are noted as being among the most successful taxa in freshwater and marine phytoplankton so the wall morphology must also incur benefits or at least be neutral (Sommer, 1988).

Sinking rate decreases with the age of the colony because the chain length decreases, due to separation valves (Smayda, 1970). The advantage of separation valves may be to reduce sinking rather than prevent it, it may give the colony a longer time in the euphotic zone and thus a higher probability of being entrained upwards. Assuming that the colony will have sunk in the water column when separation valves are initiated, it is conceivable that the altered local environment of the colony actually triggers the change in morphology, either the increased nutrient concentration, the decreased light and temperature gradient or their combination.

It can be concluded then, that linking valves may be advantageous as they allow individual cells to reach lower depths at slow rates and separation valves further slow the sinking rate to avoid loss from the euphotic zone. However, the increase in sinking rate due to colony formation in living cells may be negligible in which case it could be seen as a flotation device, and separation valves must perform a different function.

Separation valves do not directly result in vertical movement back to the higher layers in the water column unless shorter colonies are favoured by entrainment. So essentially, the mechanism for suspension in the euphotic zone remains unclear and further tests must be carried out to confirm the precise spatial dynamics of colonies in the water column before evolutionary and mechanistic conclusions can be drawn.

It is difficult to see the benefit for an individual diatom to reside in a colony in terms of sinking rates alone, given the inconsistencies surrounding colony suspension. It would seem that an individual planktonic diatom cell would fare better, in terms of suspension, if it were not in a colony. Thus, it is most likely that colony formation, and in particular separation valve formation, is the result of a trade-off between the benefits of grazer defence and suspension. Morphological plasticity is the necessary compromise response to multiple environmental concerns.

### **7.3.5 The null environmental hypothesis**

The null hypothesis must be that there is no environmental trigger/influence generating the morphological change. Morphological change would then be in response to internal cues, without any causal link to environmental changes. This relates to the idea of a coincidental synchrony between internal homeostatic mechanisms and environmental periodicity, which creates the illusion of adaptive behaviour, as detailed by Todd, P. et al. (1994).

### **7.3.6 Summary and environmental hypothesis**

The logical and possible colony dynamics with associated triggers are detailed in Table 7.2. The other conceivable permutations related to colony sinking rates would cause the colony to sink out of the euphotic zone and thus are eliminated as plausible theories. If the morphology of the colony is such that it achieves case A, permanent suspension, through the maintenance of colony length with separation valves, then it is unlikely that environmental changes in nutrients, light and temperature would trigger

	Separation valves slow	Separation Valve triggers
Linking valves slow	floating population (A)	grazers, sex, internal
Linking valves fast	cycling population (B)	light, nutrients, temp, flow, sex

Table 7.2: The logical possibilities for sinking rate dynamics and related triggers. Case **A**: linking valves do not cause a significant change in sinking rate, the colony is suspended, and separation maintains this suspension. Case **B**: linking valves cause significant increases in sinking rates, but separation valves reverse sinking via more probable entrainment, such that shorter colonies are found in higher concentrations in the upper layers of the water column and longer ones lower down.

separation valve morphology, as the environment is unchanged. Chain length could be maintained due to other factors previously discussed: grazers or even internal cues, unrelated to the environment.

If the colony morphology is such that it achieves case **B**, cycling through the water column, and there is indeed some mechanism for vertical movement in the water column related to shortened colony length (without this the colony would eventually drop out of the euphotic zone, so it is a necessary requirement) then it seems likely that the change in environmental levels of nutrients, light and temperature experienced at lower depths might cause the separation valve morphology, although the null hypothesis must still be considered.

Given that the phytoplankton colony forming diatoms can be considered to be ruderals, existing in a fluctuating niche, **B** is chosen, for the purposes of this study, as the more plausible case and thus the assumption is made that linking valves do indeed increase sinking rate and that plasticity is related to a perceived environmental difference.

Light, nutrients and temperature variation through the water column can all translate as changes in available energy for growth processes. This study will focus on light as the difference in environment experienced by diatoms between the top and bottom of the water column. There is an abundance of light at the top of the water column and a lack of it at the bottom. The availability of light can be equated with energy levels for morphogenesis in a similar way to growth rate being related to light. In high light environments growth rate increases (Yakushin, 1997). Growth rate can be calculated as the number of cell divisions performed by a population over a set time, i.e. how quickly the population divides and multiplies. This means that more light provides the energy for growth more quickly, i.e. diatoms in high light have more energy available for growth processes over a given time period.

## 7.4 Morphogenetic mechanisms

In order to understand how colonial diatoms are able to adapt their form so spectacularly to the environment the low-level mechanisms underlying silica spine formation need to be understood. Once a basic method is in place it is then possible to consider how environmental information may be able to affect progress, resulting in alternate morphologies. Consider the combination of morphogenesis mechanism examples discussed in this thesis, of chemotaxis/phagocytosis and diatom valve formation, described in Chapters 3 and 5, diatom spine formation is thought to be due to a combination of membrane and

cytoskeletal activity creating a mould for silica deposition, which is of course is open to environmental influence.

#### 7.4.1 Schmid's tricornate spine mechanism

Schmid (1982) proposed the following mechanism for spine formation in *Thalassiosira eccentrica* which it is hypothesized could account, at least in part, for the spines of certain types of colonial diatoms such as *Aulacoseira*.

During normal cell division, plasmalemma outfolds can be seen which cause a local lifting of the plasmalemma, creating moulds for the spines. The synchrony and coordination of these events have indicated that the two sister cells behave like a two-celled tissue, pulling themselves into position for stretching their surfaces. Schmid noted that contractions of the entire protoplast, or locally defined alterations of the cytoplasmic surface, are some of the more striking phenomena during morphogenesis. See Fig.7.6 for an outline of the process. Following Schmid's proposed mechanism the morphology of an auxospore (produced by sexual reproduction) should be very different to an asexually produced cell, as there is no interactive growth with a sister cell. The auxospore of *T. eccentrica* indeed has very different morphology, it is not flat but hemispherical and has no spines.

“The plasmalemma is an absolute necessity for valve shaping and completion, mediated by interaction with the cytoskeleton, secretion of swelling and adhesive mucilage and volume changes of the sister cells relative to each other. The mechanisms involved in gene expression, the biochemical and biophysical events as well as the cytomorphic interactions are far from understood.” (Schmid, 1982)

Due to this lack of knowledge surrounding the biochemical and biophysical events (see above), Schmid asks the question “if the silicalemma (SDV membrane) is the mould for the valve then what is the mould for the mould?” Cytoskeletal elements are generally found in a variety of other silica depositing organisms e.g. radiolarian skeletons and sponge spicules. *Thalassiosira eccentrica* is a good model system for illustrating the importance of the plasmalemma in valve and spine shaping, however to be applied to colony formation, the mechanisms *underlying* the plasmalemma modifications, and the environmental dependencies, need to be defined. Low doses of osmotic stress and microtubule inhibitors have been shown to cause fasciculation and a lack of spines in vegetative cells. Further research into the cytoskeletal influences on local plasmalemma morphology during colony spine formation would be desirable.

#### 7.4.2 Pickett-Heaps' seta formation mechanisms

“Valve morphology starts when the SDV expands across a cleavage furrow covered by an unidentified layer which may aid in its shaping.” (Pickett-Heaps, 1998)

Pickett-Heaps (1998) proposed two cytoskeletal mechanisms for seta formation in the diatom *Chaetoceros decipiens* (the long silica spines protruding from the colony shown in Fig.7.4(a)). A forming seta (long spine) is a hollow tube of silica, at the end of which is a bulbous, naked area of cytoplasm,



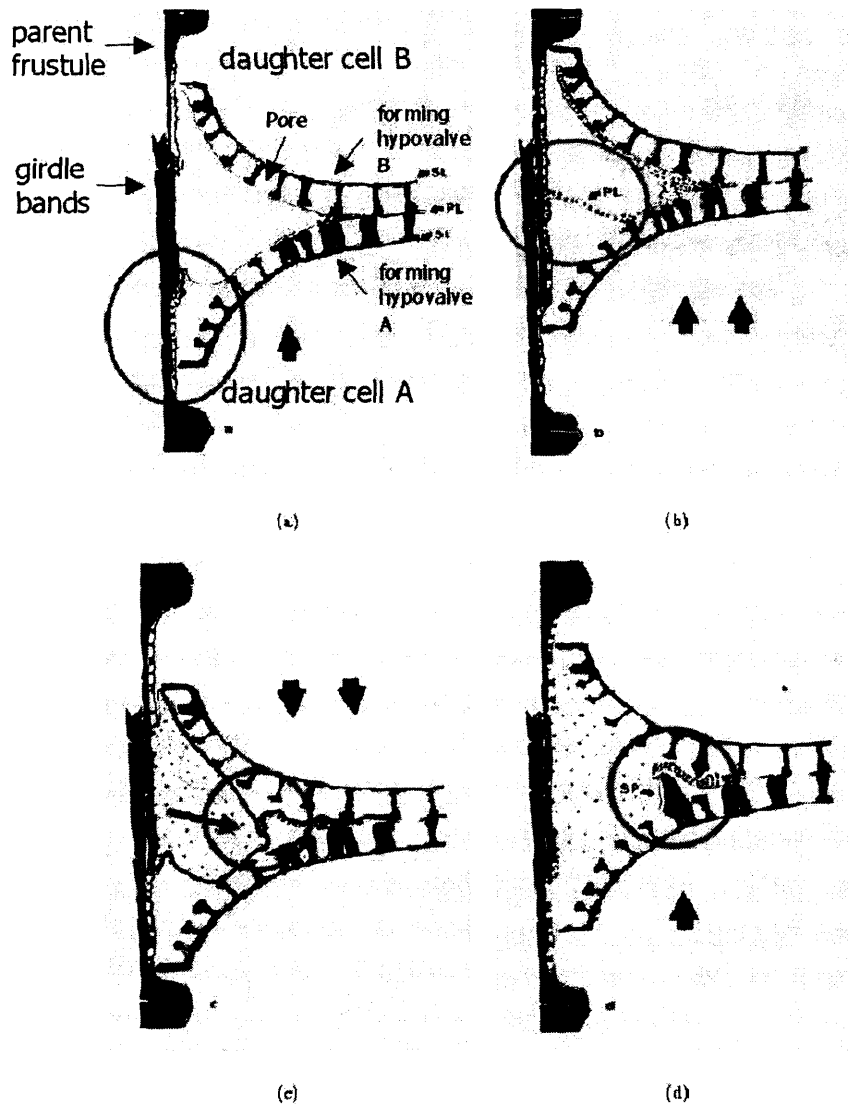


Figure 7.6: Diagram adapted from (Schmid, 1982) showing the major steps of spine formation. Thick arrows indicate the direction the daughter cell is shifting in, green circles highlight areas of interest, PL=plasmalemma, SL=silicalemma.(a) First the PL outfolds and adheres to the girdle bands.(b) There is further growth and outfolding of the PL, secretion of extracellular mucilage and adhesion of the two cell's PLs along the the girdle band, the PL detaches locally from the SL. (c) After establishing junctions between the PLs there is local contraction of the cytoplasm surfaces drawing it into conical shape, the PL also becomes less 'sticky'. (d) Conical PL outfold becomes the moulding surface for the spine (SP).

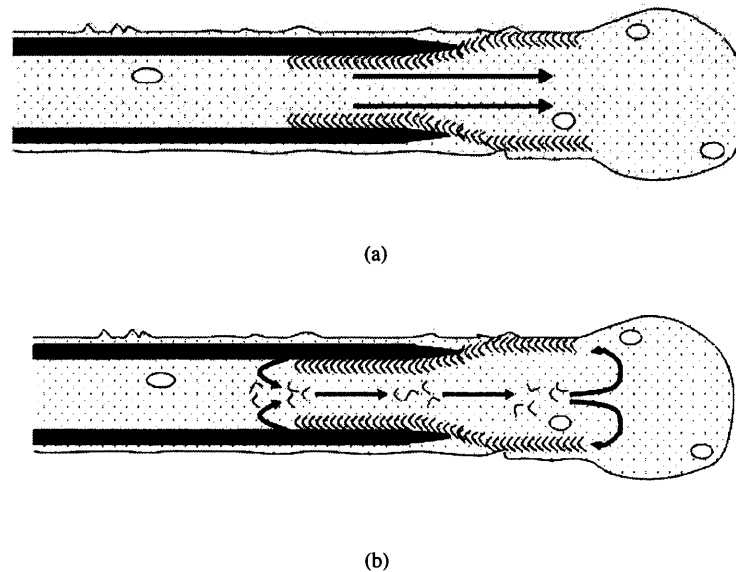


Figure 7.7: Pickett-Heaps's proposed models for setae formation by the cytoskeleton, redrawn with permission from (Pickett-Heaps, 1998), shown as a 2D cross-section, SDV containing silica shown in dark grey. (a) Molecular Ratcheting: The fibrous band could move forward as a single unit using molecular motility systems involving myosin. The band moulds the forming edge of the SDV just inside the plasmalemma. (b) Membrane ruffling: the fibrous band could be recycling or treadmilling where subunits disassemble at the left and reassemble at the right, as in filipodia.

containing a few vesicles. Immediately behind the soft end is a fibrous band whose morphology strongly suggests that it constrains the diameter of the seta. Close behind the fibrous ring is the SDV.

*Molecular Ratcheting* is the first mechanism Pickett-Heaps proposed, whereby the whole fibrous ring is steadily moved by some interaction with the just-formed wall by myosin motor proteins that can bind to the plasmalemma and actin filaments to move one against the other, see Fig.7.7(a). Therefore the fibrous ring concurrently drives and controls seta formation. Secondly Pickett-Heaps proposed a *membrane ruffling* mechanism, where the actin subunits in the fibrous ring are recycled, see figure 7.7(b).

No major roles for microtubules have been indicated in spine tip morphogenesis, although they are thought to govern the initial position of the seta. Although the fibrous ring is presumed to be actin, experiments to elucidate the precise role of actin in tip morphogenesis have been inconclusive, as anti-actin drugs and other physical/chemical disturbances inhibit seta growth. Pickett-Heaps ruled out turgor pressure (cell tension due to fluid contents, see glossary) driving the extension, although it drives extension in large vacuolated plant cells, such as root hairs, as it would not be sufficient to extend such low diameter tubes (the pressure required to extend the wall enclosing the tip is inversely proportional to the tube diameter, (Pickett-Heaps, 1998)).

## 7.5 Summary

This chapter has introduced some of the major concepts and theories surrounding MP in colonial diatoms, further satisfying Objective One and paving the way for fulfilment of Objective Five and testing of the

secondary hypothesis laid out in the next chapter. The subtleties and issues involved in understanding how such MP mechanisms might work have been specifically included in this thesis in order to highlight the intricate, complex nature of such adaptive morphological responses and the wealth of unanswered questions that remain. Careful consideration of all the facts are needed to ensure mechanism models are useful, in terms of actually furthering understanding of the complexities involved and harnessing the full potential of such mechanisms for future AI technologies.

## Chapter 8

# The Cellanimat Colony Model

The Cellanimat Colony Model was a simulation study of the morphological plasticity exhibited by colony forming diatoms, as described and discussed in the previous Chapter. It combined the earlier Nature's Batik model of diatom valve formation with the Cellanimat and E-P Map frameworks for exploring morphological plasticity in an artificial setting.

Building an artificial system from scratch to mimic, through only local interactions of the constituent parts, the generation of either interlocking or separation spines offered a unique opportunity to catalogue comprehensively the necessary and sufficient components and interactions for the colony-forming process. Simulation permits cheap and fast assessment of each element of the process in turn and in combination. The simulation methodology proved a useful tool at the hypothesis formulation level of the scientific process. Through close scrutiny of different versions of interacting processes, and the resultant unfolding of the morphogenetic process, the most likely processes and parameters that would generate the observed overall plasticity in morphology/behaviour, close to those seen in real diatom colonies, could be assessed and predicted.

The model was intended for use as a tentative, yet comprehensive preliminary basis: it was not intended as a final or fixed account. Using biological experiments either to validate or counter the various aspects of the model, it could be revised, improved or indeed completely overhauled in progression towards the truth of the process. It is easier to pursue evidence to validate or counter a proposed theory than to investigate without any clear theories in place (Rizzotti, 2000), so this work aims to provide the first compilation of a full, feasible model for the environment-dependent morphogenesis of diatom colony valves. In the final part of this chapter predictions and suggested future experiments for validation/counter-examples are discussed.

The aim was to show, using a specially created simulation, that the two morphologies exhibited by colony forming diatoms, interlocking and separation spines, could be generated by a single mechanism. The idea is that the evolution of colonial-diatom valve morphogenesis has resulted in a mechanism that will, through the incorporation of environmental information into the cytoskeletal-driven development, generate morphologies well-adapted to the two different environments experienced. It was hypothesized that the morphological bifurcation occurs as a result of changing environmental conditions between the top and bottom of the water column, such as variation in light levels.

A simulation of two Cellanimats, modelling the interactive growth of two sibling cells within a parent frustule, was developed to investigate this theory in the context of a Dynamic Morphology exhibiting *irreversible* MP (in Chapter 5 reversible MP was investigated). This provided an opportunity to observe the behaviour of a higher-level system comprising two interacting Cellanimats. During the model construction process, plausible interactions were examined and alternative ways of configuring components in order to assess viable elements that may be at work in the real process were explored, which will be discussed throughout.

The model was based on a combination of Pickett-Heaps' and Schmid's mechanisms, described in Section 7.4, and the original Nature's Batik Model described in Chapter 3. Considerable 'gap-filling' was necessary, as these theories are all qualitative, relatively speculative and lack the detail, quantification and substance needed for creating a large-scale realistic simulation. For example, Pickett-Heaps discusses actin dynamics but does not propose a trigger for cytoskeletal activity nor does he suggest the numbers of proteins involved. Attempts were made to fill gaps in the theory, such as these, with simple, generalized mechanisms, which were not intended to represent actual mechanisms in place, but merely facilitate the more solid aspects of the theorized mechanisms. Similar mechanisms to those explored in the chemotaxis and phagocytosis experiments were utilized in 'gap-filling' as they were simple, tested and, at least plausible. For example the cytoskeletal trigger utilized the TP proteins WASP and PIP2.

## 8.1 Overview of the Cellanimat Colony Model mechanism

The Cellanimat Colony Model is based on the fundamental idea that the cytoskeleton is needed to alter outer membrane shape, generating a mold within which silica can deposit to form spines, as encapsulated in both Schmid and Pickett-Heaps spine formation mechanisms (Section 7.4). The fact that the cytoskeleton can be affected by environmental conditions, either directly through cell signalling, as used in Chapter 5, or indirectly through changes in energy levels, as used in this model, allows the system to be morphologically plastic. The cytoskeletal mechanism could in theory generate either interlocking or separation spines, with the deciding factor being the environmental light levels, which provides differing amounts of energy for the process.

An E-P Map similar to the protrusions E-P Map described in Section 4.3.4 was used, which relied on the ArtCyto within each Cellanimat to generate local membrane protrusions protruding into the sibling cell. Silica continually deposited within a simple 'greedy algorithm' (stigmatically, into all available space) so a membrane protrusion would be the template for a silica spine to deposit in. As with the Nature's Batik Model, cytoplasmic material was placed by each Cellanimat in an initial configuration which blocked silica deposition. Interactions between the blocking material and silica generated the realistic stages of valve development and created pores. Silica was used as the trigger for the ArtCyto, activating WASP and PIP2 in neighbouring voxels of depositing silica.

A growing, actin-driven membrane protrusion could be blocked by silica in the sister Cellanimat. Thus each Cellanimat's developing silica structure acted as a template for the other. So the cytoskeleton created a dynamic membrane mold for silica deposition, whilst simultaneously the depositing silica created a template for the actin-powered membrane mold, and the whole self-organising system was

constrained by the parent frustule encasing the two Cellanimats. The important dual role of silica in this model, both activating and obstructing, was functionally similar to the role of the foreign particle in phagocytosis, Chapter 5. It is once again a Batik-based mechanism but this time reliant on a dynamical system of growing templates, generated and controlled by the cytoskeleton.

### 8.1.1 The Colony Environment-Phenotype Map

The following E-P Map defines the interactive growth of each Cellanimat with its environment. A Cellanimat's environment is comprised of the sister Cellanimat, the parent frustule and external light levels. Full descriptions of how these functions were implemented are given in Section 8.5. There were three distinct EP functions belonging to the E-P map as follows:

**EPa Activation** (type 2-active): Silica deposition triggers WASP recruitment, and ArtCyto activity, within the same Cellanimat

**EPb Obstruction** (type 2-passive): All silica, of the parent, sibling or same Cellanimat, blocks membrane protrusions driven by actin filaments

**EPc Redistribution** (type 3-active): a membrane protrusion redistributes the contents of the sister cell.

**EPd Energy** (type 1-active): light levels in the environment determine how much energy/time is available to the ArtCyto and cytoplasmic Blocks during the morphogenetic process.

### 8.1.2 Hypotheses

The Null Hypothesis of this work was that with this E-P Map a bifurcation in morphology, functionally and observationally resembling interlocking and separation spines, would not be generated by changes in environmental light levels only.

Specifically it was hypothesized that 1) a high light regime (called Env A), representing the top of the water column, would cause the ArtCyto to generate interlocking valves and 2) a low light regime (called Env B), representing the bottom of the water column, would cause the ArtCyto to generate separation valves due to the reduction in energy/time available for the ArtCyto agents.

## 8.2 Initialization

Two 3D rectangular Cellanimats were aligned face to face within a bounding box (CellA left and CellB on the right), representing a shallow cross-section through two sister cells containing only the edges of the valves, as shown in Fig.7.3(b). Each Cellanimat had, in addition to the usual three voxel types (C,M and E), new ones to simulate silica deposition: S voxels contained silica and could contain nothing else; C voxels had a new substate B (for blocking material) representing the cytoplasmic material positioned by the cytoskeleton to block silica deposition, as detailed in Chapter 3. If a C voxel were in substate B it could still allow agents and profilin to reside within it, but could not be changed to state silica. These additions, and the rules determining their behaviour described later in this section, were directly based on the Nature's Batik Model. The membrane represents the outer membrane or 'plasmalemma' of the diatom (PL). Once initialized the two sister PLs lay touching back-to-back, as the 'gap' parameter was

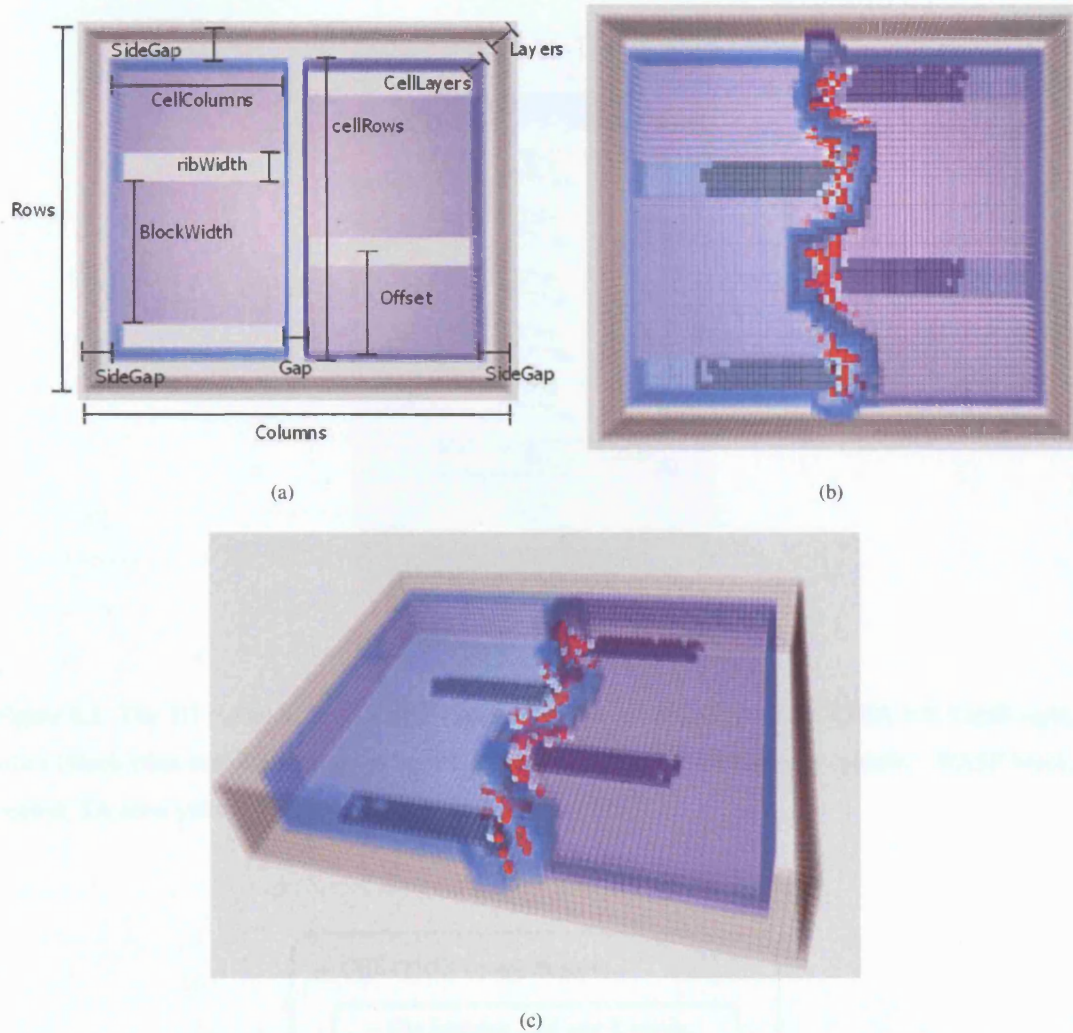


Figure 8.1: (a) The initial parameters defining sizes and spacing in the model. Viewed from above, showing two daughter cells within parent frustule boundary, CellA to the left and CellB right. (b) Top view with silica deposition and ArtCyto initiated, FA agents shown in red, FN agents shown in white, Blocks in pink, PL in blue, parent frustule in grey, silica in black. (c) Side view.

set to 2 and membrane, within the Cellanimat rule C1, see Section 4.4.1, is initialized in all E state voxels surrounding the cytoplasm voxels.

The Cellanimat's dimensions were configured to fit a desired number of ribs (virgae) into both cells, aligned with an offset, as detailed in Table 8.1 and shown in Fig. 8.1. Ribs in CellB were offset by a certain amount, which could of course be varied in future experiments, the initial alignment of ribs could indeed affect the outcome of interactive valve development. The model is 3D but can be thought of as a stack of 2D layers with interactions occurring across, and between, the voxels in each layer, see Fig.8.2.

The simulation followed the structure shown in Fig.8.3. This structure closely followed the form described in Chapter 4 for a single Cellanimat, it was simply extended to incorporate silica deposition and certain functions tailored to suit the new task. The updated model was implemented (with some simplifications to be described) following the optimization insights described in Chapter 6. Silica depo-



Figure 8.2: The 3D model as a stack of 2D planes (layers), viewed from front, CellA left, CellB right, silica (black ribs) only depositing on startHeight layer within the Cellanimats initially. WASP black, central; SA actin yellow, PA actin green, FA actin red.

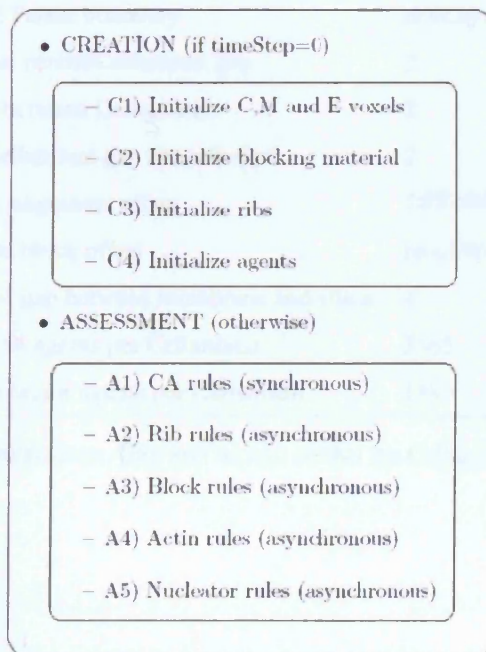


Figure 8.3: Simulation structure, all rules listed are implemented in a time step, after rule A1) the CA states are all non-agent voxel states are updated. For all following rules each agent and relevant voxels are updated in turn (asynchronously). After rule A5 the timeStep is incremented and the process repeats.



Parameter	Description	Default setting (voxels)
ribs	number of ribs	2
ribWidth	width of each rib	5
blockWidth	initial width of each block	$\text{ribWidth} + (\text{ribPLgap} \times 2) + \text{blockSize}$
blockSize	scalar added to blockWidth	$\text{ribPLgap} \times 2$
blocks	no. of blocks between two ribs	3
cellRows	width of each Cellanimat	$(2.5 \times \text{ribWidth}) + (1.5 \times \text{blockWidth})$
cellColumns	length of each Cellanimat	$(\text{blockWidth} \times (\text{blocks} - 1) - \frac{\text{blockWidth}}{2})$
cellLayers	height of each Cellanimat	7
Rows	width of Parent boundary	$\text{cellRows} + (\text{sideGap} \times 2)$
Columns	length of Parent boundary	$(\text{cellColumns} \times 2) + \text{Gap} + (\text{sideGap} \times 2)$
Layers	height of Parent boundary	$\text{cellLayers} + (\text{LayersideGap} \times 2)$
sideGap	horizontal parent/Cellanimat gap	2
Gap	distance between Cellanimats	2
LayersideGap	parent/Cellanimat gap above/below	2
offset	rib/block alignment offset	$\frac{\text{ribWidth} + \text{blockWidth}}{2}$
shift	horizontal block offset	$\text{blockWidth} - \text{ribPLgap}$
ribPLgap	horizontal gap between membrane and silica	4
#A	no. of actin agents per Cellanimat	3465
#N	no. of nucleator agents per Cellanimat	1485

Table 8.1: Model creation parameters. Gap was set to 2 so that the Cellanimat membranes touched once they were initiated.

sition on the valve face was assumed to have already occurred, this model was concerned only with the deposition involved in spine formation, around the edges of the valve.

Creation rules C1 and C4 followed the same format of initialization as described in Chapter 4. The only difference was that every Cellanimat voxel had a flag associating it with either CellA or CellB. Actin agents in CellA were numbered up to #A and initialized randomly within C voxels with the 'CellA' flag. In CellB they were numbered from #A+1 to 2#A and placed only in C voxels with the 'CellB' flag, similarly for nucleator agents.

### 8.3 Cellanimat

The Cellanimat and ArtCyto modelling methods only differed from the default model, described in Chapter 4, due to simplifications to fit the new scenario. There were no receptors, instead WASP and PIP2 were recruited to membrane voxels by the deposition of silica within the cell. WASP and the release of profilin triggered state changes in the agents, as in the default model, resulting in the formation of filaments. For simplicity, and as a result of the investigations into Cellanimat recycling mechanisms in Chapter 6, the PrUptake and PrRelease functions were not used, meaning that profilin was not recycled. Over-saturation of profilin was encouraged, in the absence of biological data, to speed up the membrane protrusions process, as shown in Chapter 6. So, high PPlume values were used and inactive PIP2 did not remove profilin from the system.

In the CA rules, the membrane-tidy function again replaced any excess membrane voxels (ones that had no environment or sister membrane neighbours) with cytoplasm, and assigned blocking material to it using the 'blockAssign' function, as described in Section 8.5.3. The only other CA function diffused profilin throughout each cell as in the default model. The contract membrane rule was not used, so cytoplasm volume was not conserved. This was because the Cellanimat does not represent the whole diatom cell, but only a section, so contraction of the membrane at the back would not be realistic.

The agent ratio (actin:nucleators) used was 35:15 per cent of the initial cytoplasm volume (which was 9856), giving 3465 actin and 1485 nucleator agents per Cellanimat. This ratio was selected after consideration of the results of the agent projection performed in Chapter 6 and the fact that the available cytoplasm for agents to occupy decreases with silica deposition. It was desirable to optimize performance through high agent volume yet also optimize their fluidity and movement within the Cellanimat. Indeed the speed and efficiency of the simulation was a factor, as increased agent volume increased the simulation time. So it was decided that a fifty percent total volume of agents per Cellanimat satisfied all criteria.

Agent state change rules featured only three differences: 1) a deterministic P(LOSS) function was used where  $P(\text{LOSS})=1$  if  $\text{agent.Fcounter} > \text{FTOP}$ , as described in Chapter 6. 2) No filament branching was used as a simplification. 3) a more realistic agent movement algorithm was used. The random movement algorithm described in Chapter 4 gave unrealistic protein distributions when protrusions were long. As a protrusion progressed the agents did not fill the newly created space as quickly as real concentrations of proteins would; the newly created cytoplasm voxels are meant to represent cytoplasmic material 'flowing in' behind the newly stretched membrane, which should bias agent movement. The

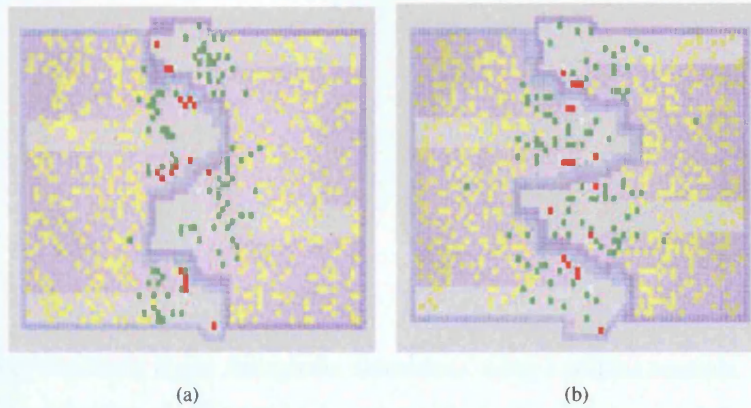


Figure 8.4: Types of agent movement affect protein distribution using 2200 actin and 1100 nucleators in each cell. 2D slice through views of layer  $\text{startHeight}+1$  at  $t=95$  (a) random movement gives unrealistic bunching of PA state actin (green) away from new cytoplasm, resulting in slowed progression of protrusions (b) gradient movement gives a more even spread of PA and SA (yellow) flowing into the newly created space, speeding up protrusion growth.

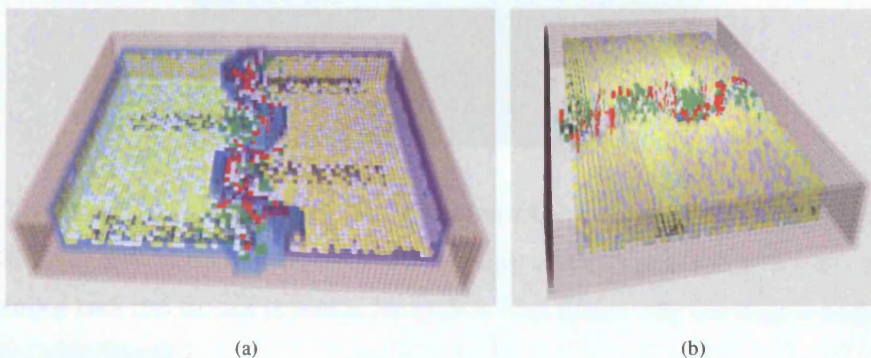


Figure 8.5: views from side showing agents present throughout the 3D layers.

chance of moving in the same direction, towards the new space, several time steps in a row was slim with the random movement algorithm. Instead a 'gradient movement' algorithm was used where each agent picked two random MNs and moved to the one with the greater number of empty cytoplasm MNs, i.e. agents flow down gradients in a space filling manner. Compare Figs.8.4(a) and 8.4(b). Fig.8.5 shows two 3D views of agents.

## 8.4 Silica deposition: re-implementing the Nature's Batik Model

As in the Nature's Batik Model certain stages of silica deposition, in terms of dimensionality, were predefined. In diatom valve formation, silica is first deposited along a 1D line on the valve face (for pennate diatoms), then in the full 2D plane (valve face) and finally in 3D as the ribs curve outwards back into the cell (and forwards into the sister cell in colony forming diatoms) whilst the valve face also thickens outwards, see Fig.8.6 (only stages 3 and 4 were modelled). First a particular 2D layer ( $\text{startHeight}$ ) had silica deposited, modelling the deposition along the valve mantle (side of the valve) in stage 3 rather than on the valve face (as with the original Nature's Batik Model).

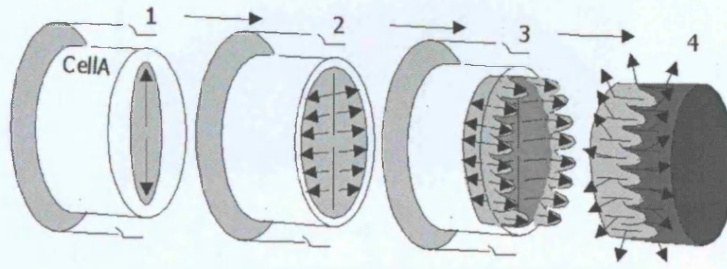


Figure 8.6: Silica deposition stages through the dimensions, using a pennate example. First along a 1D, then 2D along the valve face, the ribs curl backwards and forwards when they reach the edge of the valve face. Finally silica is deposited along all surfaces, building the surface structure out into 3D layers. In these experiments only stages 3 and 4 were modelled.

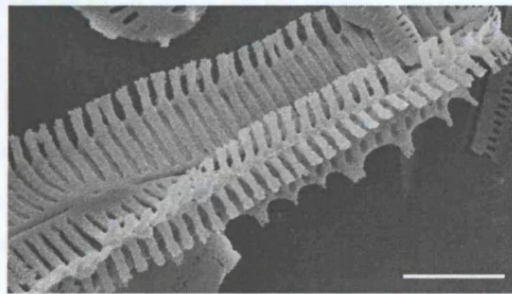


Figure 8.7: Dimensionality in growth process in SEM of *Diadesmis* reproduced with permission from (Cox, 2006). Ribs grow laterally along valve face until they abut the parent valve, then they grow out in third dimension back into the cell as well as forwards to form spines, only this stage is modelled in the Cellanimat Colony Model.

When the amount of silica in the current layer exceeded the set threshold ( $SDV_{expand3D}$ ) silica deposited on the next layer vertically upwards in the stack (modelling stage 4 of the process, where the valve thickens).  $StartHeight$  was set to layer 1 inside each Cellanimat for all experiments, see Fig. 8.8. When the amount of silica deposited in the new layer exceeded the threshold, deposition started on the next layer above and so on. Deposition in 2D and 3D was still a stigmergic process. As in the Nature's Batik Model, silica could only be deposited in a voxel that had at least one other S-state neighbour. Silica deposition was initialized as if it was curving round from the valve face to the valve mantle (side of the valve), as depicted in Fig.8.7.

#### 8.4.1 Blocks

The use of blocking material follows from the hypothesis outlined in Chapter 3, that the cytoskeleton transports vesicles and other cellular material to particular sites, which then block silica deposition and ultimately determine pore sizes and positions. Chapter 3 went further and suggested that the deposition of silica could be responsible for partially shrinking/pushing the cellular blocking material away, explaining the observed stages of growth, where ribs (virgae) form before the cross-connections (vimines) define the pores.

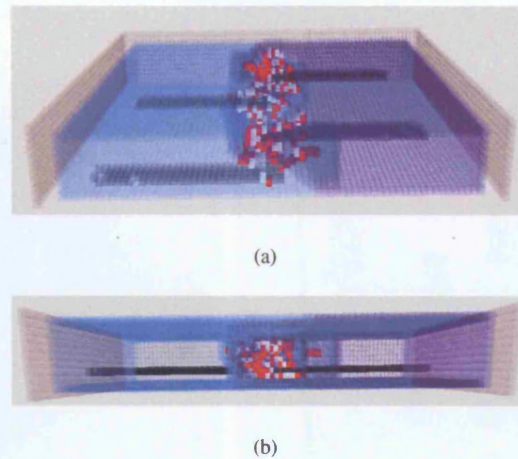


Figure 8.8: Side views showing silica deposition (black) only on startHeight layer (first layer up within Cellanimat) initially. Filament agents shown in red and white.

As with the Nature's Batik Model a set of blocks of a maximum size were used. Each block was treated as a 'stationary agent' with the following information associated with it: 1) a unique identifier 2) an unchanging set of coordinates defining the block's centre, 3) a radius (initially set to blockWidth/2) which reduced with increases in local silica levels, and 4) an incremental counter involved in block shrinking (initially set to -1). Each block could shrink in relation to its local silica volume. The empty space created between two shrinking blocks provided new room for silica to deposit. These newly deposited cross-connections, when fully deposited between two ribs, defined the pores.

**Initialization:** each block was initialized as a 3D stack of 2D squares with sides of length blockWidth. The base square of the pile was initialized on the startHeight layer within the Cellanimat, with the pile reaching up to the top of the Cellanimat as shown in Fig.8.9. The centre  $(x,y)$  coordinates for the block squares were determined for a particular block  $b$ , using Equation 8.1, where *Shift* determines how indented the block centres are from the side, determining how far back the first cross-connection will form from the valve edge. For a cross-connection to form on the valve edge (far right in Cella or far left in CellB), *Shift* would need to be set to zero, otherwise it would be positive, see Fig.8.10. The startHeight parameter determined the first layer of blocking material, to coincide with initial silica deposition on this layer and the eventual deposition on all layers above, see Fig.8.9.

**Shrinking:** though blocks were initialized as stacks of squares, when they were 'shrunk', as in Chapter 3, they became circles, hence the block radius attribute. This was a simplification of the method in the Nature's Batik Model where blocks were initialized as very large, overlapping circles appearing only within a rectangular, predefined space (Striae). Setting them to have flat sides to begin with precluded the need for a predefined space or extra, unseen shrinking stages, thus simplifying the algorithm. The resulting rectangular shape of a row of blocks represented the idea that silica deposition, as each rib turned the corner onto the valve mantle, had already pushed the blocking material into distinct streams leaving an open space in which the ribs could be deposited.

Each block shrank its radius, by amount  $R_{delta}$  (set to 1), if the amount of silica within a radial

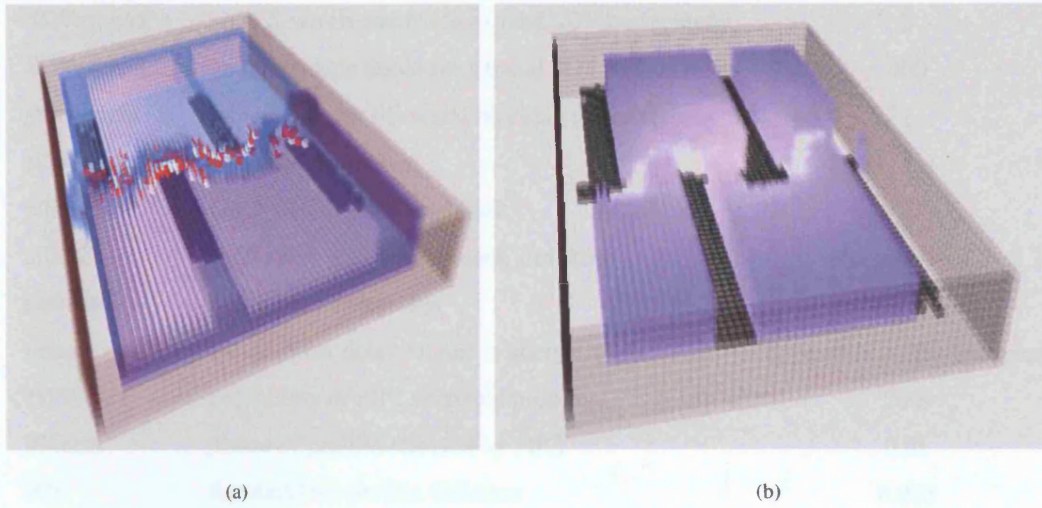


Figure 8.9: Side views showing silica deposition only on startHeight layer with block material (purple) present throughout the 3D layers, ready to block 3D silica deposition.

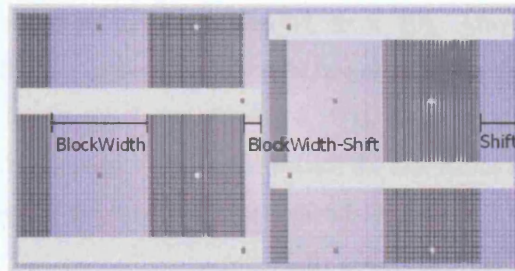


Figure 8.10: Slice through, view from top, of layer startHeight showing Block and rib centres, cellA left, cellB right, blocks with even identifiers shown in black, odd in blue. ribWidth=5 voxels, shift=blockWidth-ribPLgap, blocks=4

$$x = \text{sideGap} + D + S + (b \times \text{blockWidth}) \quad (8.1)$$

$$y = \text{sideGap} + \text{offset} + (b \times I) \quad (8.2)$$

$$I = \text{ribWidth} + \text{blockWidth} \quad (8.3)$$

$$D = \begin{cases} 0, & \text{if CellA;} \\ \text{cellCOLUMNNS} + \text{gap}, & \text{if CellB.} \end{cases} \quad (8.4)$$

$$S = \begin{cases} -(\text{blockWidth}) + (\text{shift} - 1), & \text{if CellA;} \\ -(\text{shift} + 1), & \text{if CellB.} \end{cases} \quad (8.5)$$

Parameter	Description	Default setting
SDVexpand	no of S voxels needed to expand SDV horizontally	3
SDVexpand3D	no of S voxels needed to expand SDV to next layer	400
startHeight	initial layer for silica and blocking material	1
rDelta	block shrink amount	1
silicaTH	block shrink silica threshold	10
silicaR	local silica radius from block shrinking	block.radius+1
radiusMIN	minimum block radius	$\frac{blockWidth}{2} - 2$
delay	block shrink delay related to energy levels	dependent on Environment
P(PPlume)	probability of PIP2 releasing profilin	20%
PPlume	plume of profilin released by PIP2	0.01
Pth	threshold for profilin diffusion	0.005
PAth	actin/profilin activation threshold	0.05
LOSS	time until agents disassociate from filament	10
WASPradius	radius of silica for WASP recruitment	ribPLgap+1

Table 8.2: Model assessment parameters

distance (silicaR) exceeded the set threshold (silcaTH, set to 10). After a set delay (delay) up to a minimum radius (radiusMIN) no further shrinks would be possible. See Table 8.2 for a full breakdown of all parameters used during the simulation. See Fig.8.11(b). By shrink it is meant that any cytoplasm voxels containing the block's identity, which reside outside the new radius from the block's centre, have the block's identity removed. If the voxel contains no block identities it is set to 'no-blocking material' state.

The delay setting is crucial and is one of two variables representing the effect of the external environment. If the delay is high, this means that the cell takes longer to form cross-connections between ribs, as if the cell resists for longer before being forced into changing shape by the depositing silica. This can allow sister spines to grow into the space between ribs before cross-connections form (as seen in Fig.7.3(c)). The effects of changing the delay setting will be discussed later in this chapter.

### 8.4.2 Silica

Each rib had a globally defined position and was again treated as a stationary agent with the following attributes: 1) unique identifier, 2) centre position ( $x,y$ ), 3) start time, 4) xFront value, and 5) xBack value. The rib centre ( $x,y$ ) was calculated for each rib  $r$  using the equations that follow; zLayer stored the current 2D layer for deposition, initialized as startHeight. Start time was set to 3 for all ribs, and determined when rib deposition would start. In future experiments this could be set differently for each rib allowing investigation of any effects on overall morphology.

$$x = sideGap + D + cellColumns - (ribPLgap + 1) \quad (8.6)$$

$$y = sideGap + \frac{ribWidth}{2} + offset + (r \times I) \quad (8.7)$$

$$I = ribWidth + blockWidth \quad (8.8)$$

$$D = \begin{cases} 0, & \text{if CellA;} \\ gap, & \text{if CellB.} \end{cases} \quad (8.9)$$

$$(8.10)$$

**Deposition rules:** each time step, each rib attempted silica deposition within two functions. First, within a backwards growth algorithm, each rib attempted to deposit (change state of voxels to S) in all cytoplasm voxels from its centre  $x$  coordinate back to its  $xBack$  position (the current local edge of the SDV), within a rectangle of width  $(ribWidth \times 2) + blockWidth$  in layer  $startHeight$ . Similarly for the forwards growth algorithm, it attempted deposition in voxels within the rectangular space, out from the cell to the  $xFront$  position. See Fig.8.11(a). The deposition would fail if the voxel had either a) no neighbours of state silica (the stigmergic rule), b) contained an agent (A or N), c) if it contained blocking material. On the next time step it would try again to deposit in all voxels regardless of the result on the previous timestep.

The  $xBack$  and  $xFront$  values were incremented, backwards one or forwards one respectively, if the amount of silica in the current  $xBack$  or  $xFront$  column of the rectangle exceeded the threshold (SDVexpand). This mimicked the method described in Chapter 3, which was meant to simulate the expansion of the Silica Deposition Vesicle (SDV) as more silica deposited within it. When the amount of silica over the current, whole 2D plane of a single Cellanimat exceeded the threshold (SDV3Dexpand) then silica would begin deposition in the next 2D layer up in any viable voxel with an S neighbour (stigmergy), whilst continuing forwards and backwards growth on layer  $startHeight$  and deposition in all layers below.

In forward growth there was a further stipulation: there must be a set amount of horizontal space (ribPLgap) between the voxel and PL for deposition to take place. A simple test was done to check the next few voxels ahead, if no M voxel was found then silica could be deposited. This ensured enough room was always available between the forming rib and the PL in which cytoskeletal agents could exist. The cytoskeletal process will be discussed below. Figure 8.11(b) shows blocks shrinking as ribs are deposited forward and backwards in the cells.

## 8.5 The EP functions

In this section a full explanation of the implementation of the three EP functions is given. The EP functions encapsulate the growth process and determine Cellanimat morphology, in relation to the environment, at each time step. A short discussion then follows of the implications, for the development of spines, of using the EP functions or slight variants on them.

### 8.5.1 EPa: Activation (type 2-active)

The cytoskeleton has been implicated in spine formation (Pickett-Heaps seta formation mechanism, section 7.4.2) and valve formation (Edgar, L. A. and Pickett-Heaps, J. D., 1984; Pickett-Heaps, J. et al.,



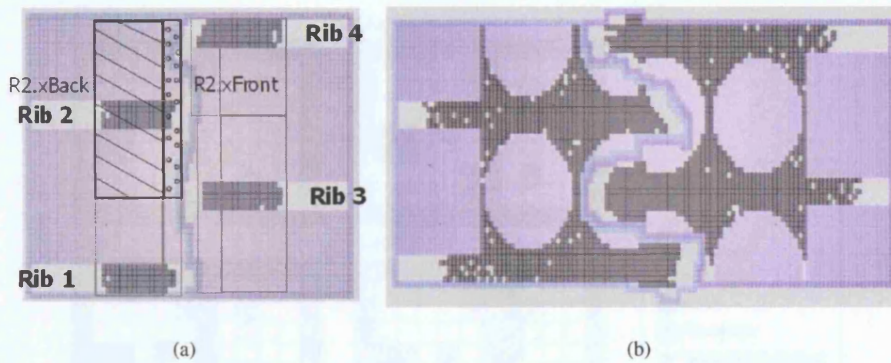


Figure 8.11: (a) The variable rectangles, which together represent the growing SDV. Hatched box shows the rib 2 SDV area associated with backwards growth, the stippled box shows the area for rib 2 forwards growth. (b) Ribs growing with blocks shrinking, delay set to 30. The blocks furthest out have not yet shrunk. Voxels containing agents have not yet been filled in with silica.

1990). As there is no clear experimental evidence of how the cytoskeleton is recruited a simple mechanism to activate the cytoskeleton was implemented. The suggestion is that something *functionally* similar must be taking place in diatoms. Following the Pickett-Heaps mechanisms, for a spine to grow out from the cell, the PL must be pushed forward in advance, allowing room for deposition. For the PL to be pushed-out ahead of a growing rib (ahead being out towards the sister cell) something must trigger the cytoskeleton to grow actin filaments at that point. There were a few options: filament growth could be stimulated along the edges where the sister cells touch; they could be triggered by the sister's silica deposition, or indeed by a totally unrelated event.

In the absence of experimental evidence, here this simple hypothesis is put forward: actin filaments are stimulated to grow only where new silica is depositing. This could generate Pickett-Heaps' mechanisms. Again no data has been collected on which proteins to stimulate the cytoskeleton are present, so the mechanism for generating membrane protrusions as used previously was used for simplicity, see Chapter 5.

### 8.5.2 EPb: Obstacle (type 2-passive)

This is a simple function that stops membrane protrusions growing into a space if any of the space is taken up with silica, be it the parent valve or otherwise. Silica, once deposited is permanent. It is too solid to be broken or moved by actin filament activity.

### 8.5.3 EPc: Redistribution (type 3-active)

As a growing actin filament in the ArtCyto tries to push out the local membrane (see description of the Mchange rule in chapter 4) it is able to redistribute certain types of sister cell material found in the local environment, as with the redistribution of chemoattractant described in Chapter 5. There were four steps to the Mchange rule, described through the 2D example situation shown in Fig.8.12, where a Cella state FA actin agent has joined a filament (not shown) and is trying to push-out the local membrane.

**Step one:** for all Cella M voxels neighbouring the FA agent, each CellB M MN was assessed. For

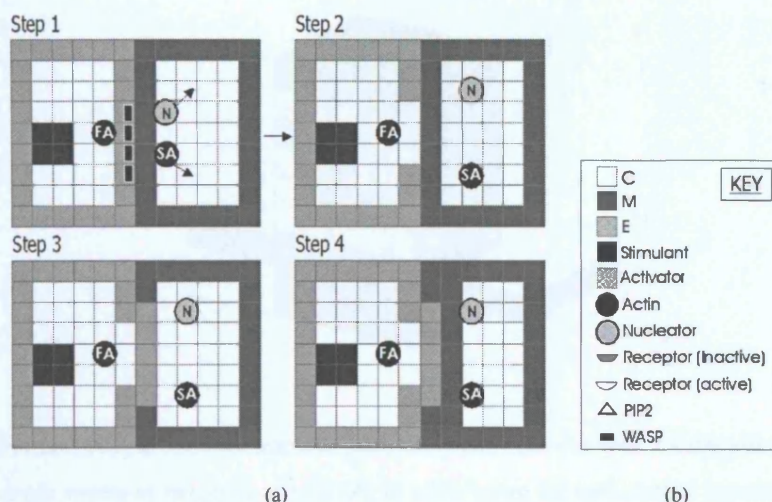


Figure 8.12: (a) Actin driven membrane protrusions: the four stages of the Mchange rule calling the EPc redistribution function. Cell A left. WASP shown as black rectangles within membrane, silica voxels black. (b) Key.

each Cell B M MN, all its agent MNs must be redistributed (EPc) to a randomly chosen MN, since all these voxels need to be overwritten to membrane in a following step. The process can fail at this point if: a) there is an F-agent (FA or FN) neighbouring the sister membrane, b) if there is no room in which to move an agent, or c) if silica neighbours any membrane voxels belonging to the parent or the sister (EPb). Sister profilin concentrations are also redistributed, though without being conserved, that is, if there is nowhere to move the profilin, this does not halt the process, that amount is simply overwritten. The non-conservation of profilin is justified by the initial over-saturation, by high PPlume values.

To increase the likelihood of step one succeeding, an extra 're-initialize' function was used. If no MN could be found to which to move an agent, during EPc redistribution, then it would be simply removed and re-initialized in the default state (SA or N for actin or nucleators respectively) in a random location in the cell. This function was introduced to combat the slowed progress of protrusions once the sister cell becomes condensed due to the small scale of the cells (they represent only a section of a bigger cell, though fully enclosed). The re-initialization function also represented the decay and synthesis of proteins occurring throughout the cell's lifetime.

**Step two:** if step one succeeded then there is enough room to overwrite the Cell A membrane and extend it into Cell B, pushing the Cell B membrane back into its cell. First the Cell A membrane voxels neighbouring the FA agent were overwritten to state 'cytoplasm'.

**Step three:** All MNs of the newly replaced cytoplasm voxels in state 'environment' or 'membrane' are replaced with membrane voxels with the Cell A identifier. The EPa function is called, upon the creation of each new membrane voxel, to assign WASP/PIP2. The ambiguity of this step allows Cell A to overwrite other Cell A membrane voxels if the membrane is not straight. This produced interesting and realistic assimilation of membranes. However it can be switched off by simply specifying that only sister membrane are to be overwritten, which would allow two similar membranes to line up along side

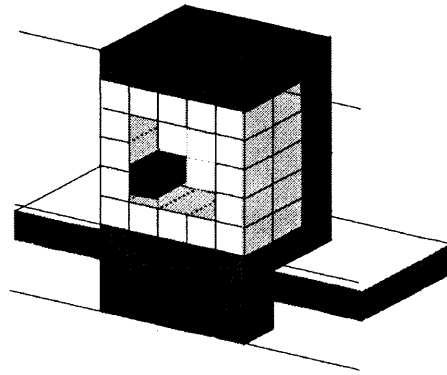


Figure 8.13: For an ArtCyto filament agent to push the membrane out over a sister silica rib there need to be at least seven voxels of height above the rib, to allow room for both sisters' membranes to be bent over the rib. Actin agent belongs to cellA, cellA membrane shown in white, cellB membrane in grey.

each other rather than wipe each other out.

**Step four:** Similarly, all state 'cytoplasm' MNs of the newly created CellA membrane voxels are overwritten as CellB membrane and EPa is called to assign WASP and PIP2.

#### 8.5.4 Height and interlocking spines

To deposit silica over a sister rib in order to form an interlocking spine, a membrane protrusion must first be made, such that the cell has room to deposit silica. In forming a membrane protrusion over a sister rib with an actin filament, the redistribution rules must be satisfied. This means that there must be room between the sister silica and the actin agent for both membranes, and above the agent, thus maintaining membrane continuity, see Fig.8.13.

#### 8.5.5 WASP activation investigation

Using the ArtCyto, described in Chapter 4, at each time step within the CA, every membrane voxel was assessed using the EPa function to see if its WASP/PIP2 substates should be switched on or off. Also, within the Mchange rule, when the PL had been pushed-out by a growing filament, the EPa function was used to determine WASP/PIP2 activity in the newly created membrane voxels. Each time step, voxels with PIP2 switched on had a probability 'P(Plume)' of releasing a plume of profilin into one cytoplasm neighbour. EPa WASP activation conditions: WASP and PIP2 were switched on in an M voxel if:

- $\exists$  a sister membrane MN (Moore neighbourhood), i.e. only membrane voxels that existed at the interface with the sister cell could contain WASP
- $\exists$  an S voxel within a set radius (WASPradius).
- **Type-1 WASP activation:** only silica within WASPradius that was deposited in the 'forward rib growth algorithm' activates WASP and PIP2 in an M voxel, given that the sister membrane requirement is also satisfied.
- **type-2 WASP activation:** any silica within WASPradius activates WASP/PIP2, given that the sister membrane requirement is satisfied.

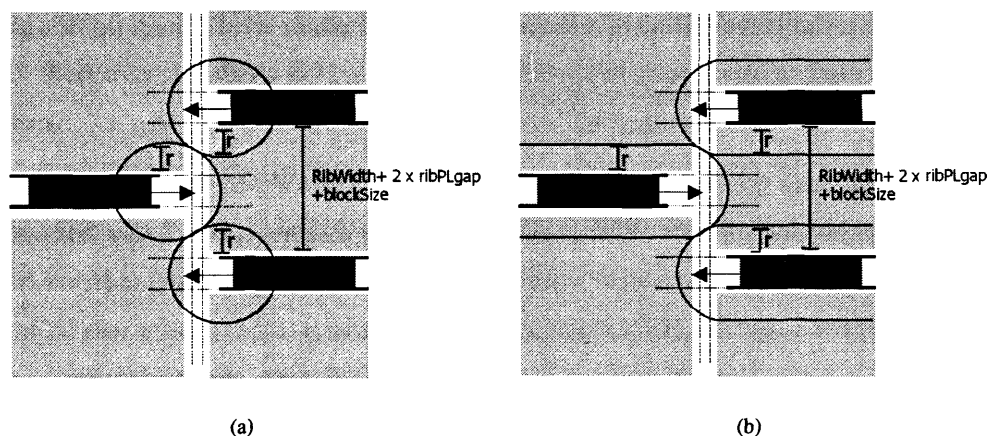


Figure 8.14: The different types of WASP activation and the importance of getting the right blockWidth. There must be room for a growing spine and the two PLs either side to pass through the space between sister ribs. (a) WASP type-1 activation. Circles of radius  $r = WASPradius$  show possible regions for WASP activation. The circle will extend forward as the rib xFront value moves forward. (b) WASP type-2 activation. Regions for possible WASP activation shown to surround all ribs up to a distance of  $r$  from the rib.

There were two options for this WASP recruitment function, as shown above. The difference between the two becomes evident when, for example, a rib from CellA has grown into the space between two CellB ribs; it will have pushed the sister's PL back into its cell. With type-2 recruitment this will trigger actin filament formation in the sister cell along the sister ribs see Fig.8.14 and Fig.8.15(d). Type-1 activation generated less opposing actin filament growth from the sister cell during spine outgrowth, only occurring during the initial stages of deposition where the radii of recruitment for the two cells meet, see Fig.8.14(a), this region was dubbed the 'battle zone' as the two sibling cells 'battle' to dominate the available space through cytoskeletal protrusions, filled in and made permanent by depositing silica. The blockWidth setting was therefore of great importance, to ensure there was room for a rib to grow through, between two sister ribs. As blockSize is increased, rib thickness increases upon entering the gap between the sister ribs, as silica deposition together with actin driven membrane protrusions was a 'greedy mechanism', filling all available space with silica.

The choice of WASP activation type for the EPa function was of paramount importance. It contributed greatly to the final shape of the spine that formed. Fig. 8.15 shows the different spine morphologies generated by the two types of WASP recruitment. Fig.8.15(d) also shows a 'false strut' a small silica outgrowth which occurred where the blocking material did not continue out into the sister cell. Blocking material was only placed within the initial boundaries of the Cellanimat. As the ArtCyto of one cell pushes the PL out into the sister cell, areas that silica can deposit in open up, beyond the blocking material boundary. Either blocking material could be placed continuously, as the membrane is pushed out, or these struts could be seen as noise, as they only form when the interactive, opposing filament growth allows one cell to dominate the other. Interestingly this domination effect, where one rib gains a majority of space over the opposing ribs can cause the dominant rib to extend faster into the sister than the others,

causing a longer spine. This is similar to the long spines seen in the separation valves of *Aulacoseira* in Fig.7.3. Both examples shown in Figs.8.15 have one dominant spine extending faster and further than the others.

It would seem that type-2 WASP activation yields the best result, however when 3D silica deposition is considered, type 2 induces opposing growth all along each rib, all through the layers, so there is no way for one rib to grow over the top of another. It is always inhibited by the sister's active cytoskeleton, as in the 2D case where it cannot grow near the sister rib (Fig.8.15(d)). So, type-1 WASP activation must be used in order to generate interlocking spines.

### 8.5.6 Clear ArtCyto

The Cellanimats only represented sections through real diatoms, focused at the site of forming spines on the valve mantle. However all edges of a Cellanimat served as real boundaries to agent movement. This means that as silica deposits less room is available for agents to occupy, whereas in real diatoms proteins would be able to move freely throughout the rest of the cell. Also, non-filamentous actin and nucleators would not stop silica depositing in real cells, as they do in this simplified model, they would probably be moved as silica deposits. To allow more realistic silica deposition an artificial clearing function was implemented at the end of the run.

Ten time steps before the end of the simulation the Clear ArtCyto function removed all ArtCyto agents from the Cellanimats, signifying that all available energy for the ArtCyto, provided by light in the EPd function, had been used up. The deactivation of WASP, and the gradual flow of all agents away from the section of the cell being modelled in a single time step. All WASP was switched off and all filamentous agents were removed, as well as non-filamentous agents. This sudden clear function was used for efficiency only, and is not meant to represent a real process, but rather to allow for a more realistic final siliceous form, where deposition has not been unrealistically inhibited by overcrowding of inactive agents in a small section.

Once all agents had been removed, silica was deposited stigmatically in all available and viable voxels that remained, as per the deposition rules. Clearly, after the removal of the ArtCyto no further membrane shape changes could occur. The ArtCyto was crucial for pushing out the membrane and creating space for 'greedy algorithm' silica to deposit in. Once the ArtCyto was removed, the silica could only fill in spaces that had been created before removal, so this function was for finalizing the valves, not for any continuation of the developmental process.

For simplicity, 3D deposition was only allowed once the ArtCyto had been cleared. After the ArtCyto was cleared and once the number of silica voxels on the current layer exceeded the threshold (SDVexpand3D) deposition could begin on the layer above, whilst still depositing on any layers below. In a larger version of the model, where more room would exist for ArtCyto agents to occupy, it is conceivable that 3D silica deposition could be executed in tandem with the cytoskeletal-driven developmental process.

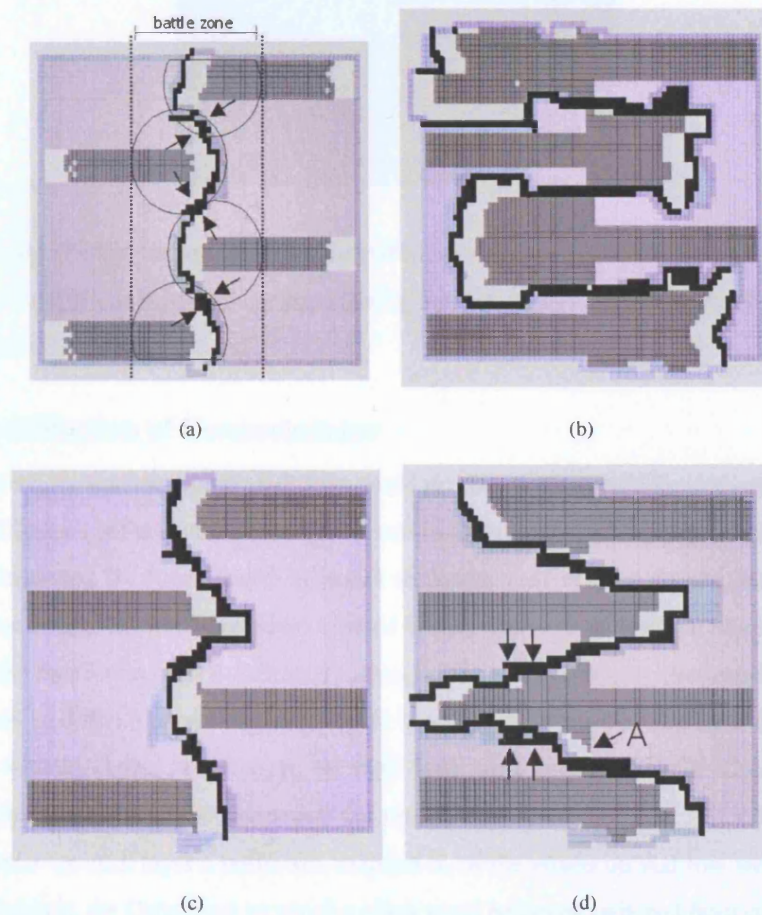


Figure 8.15: (a) type-1 WASP activation,  $t=35$  as ribs start to grow towards each other where the radii of WASP activation meet there is opposing cytoskeletal growth which maintains the straight form of the rib. This area of opposition is called the battle zone. (b)  $t= 280$  once the rib grows past the battle zone, the sister rib's radius of activation, there is no opposing force so the rib grows into all available space, forming a bulbous end. (c) Type-2 WASP activation,  $t=141$  rib growth is slower as there is always a battle between the opposing cytoskeletal growth of the sisters, initial stages look similar to type 1 recruitment. The battle zone extends to the entire breadth of the cells. (d) As WASP recruitment continues back into the cell the straight rib form persist. Arrow labeled A shows a false strut.

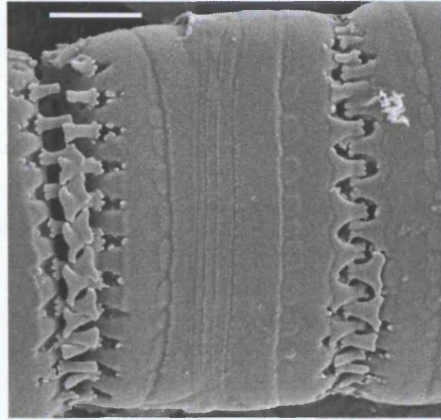


Figure 8.16: as interlocking spines are pulled apart they exhibit form resistance but will shatter and break if enough force is applied, exposing and endangering the cell. *Pseudostaurosira* SEM reproduced with permission from (Cox, 2006).

### 8.5.7 Quantification of Connectedness

To show conclusively that the Colony E-P Map could produce both separation and interlocking spines, given only a difference in the environment, quantification of these morphologies in terms of functionality was needed (following the functionality approach to fitness used in the Nature's Batik Model rather than using a subjective, observer dependent method based on how connected the morphologies appear. Functionally, the two forms behave differently when pulled apart. If highly connected — interlocking — then it would be difficult to pull the valves apart, see Fig.8.16; the separation form on the other hand is particularly suited to being pulled apart, see Fig.7.3(d). So a quantification of 'Connectedness' was created, based on how easy it would be to pull the structure apart.

For each row on each layer a point was awarded if, as the voxels on that row were considered in turn from left to right, the Cellanimat to which a silica voxel belonged switched from cellA to cellB and then back to cellA again. I.e. if cellA was pulled to the left, cellB would necessarily come with it rather than being left behind, as they are entwined. See Fig.8.17.

So, what does a given Connectedness value mean? A fully connected 2D plane would score a point for each row, as the two cells occupying it would be entwined on each row. So the full Connectedness value is equivalent to the number of rows times the number of layers. In this system there are seven layers, with the Cellanimats occupying forty-four rows initially, so the full Connectedness value would be 308 ( $7 \times 44$ ). However, no silica is deposited on the first layer (layer zero) as startHeight is set to 1. Further, on the first layer of deposition, overlapping is impossible, as deposition occurs backwards into the cell as well as forwards. The next two layers of deposition also preclude overlapping as room must be made for the two sister membranes to stretch over the rib as the ArtCyto pushes upwards and over, as described earlier in Fig. 8.13. However some connectedness is possible, as one cell pushes into the other, it could form a 2D interlocking pattern, by depositing behind previously formed sister silica ribs.

So, layer zero will always get zero Connectedness and the next three layers will always return low values, even in a well-connected system. So the top Connectedness value must be reduced to define

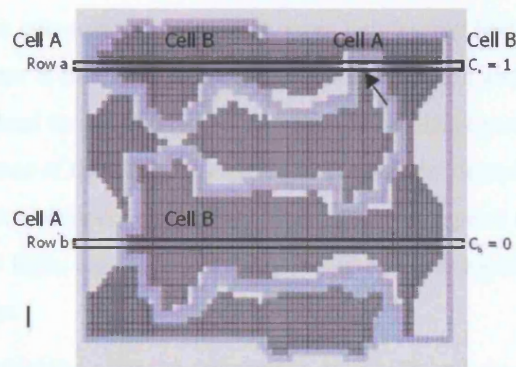


Figure 8.17: Example of the Connectedness quantification function on a slice through layer of interlocking valves. As voxels are considered in turn along a row from left to right, the current cell that the silica voxels belong to is initiated as cellA, a silica voxel is encountered belonging to CellB, close to the end of the row another cellA silica voxel is encountered before finally ending with a CellB silica voxel. This row gains a point for Connectedness. On row b, again a CellB silica voxel is encountered, but this time no further CellA silica is found, so this row returns a zero score. The Connectedness value is the sum of points awarded for all rows in all layers.

a more realistic version of a highly connected system. The suggestion is that three layers could be expected to achieve at best a quarter of the full 2D Connectedness and the other three layers achieve full 2D Connectedness. As such a well-connected system would gain an overall value of approx. 165 ( $11 \times 3 + 3 \times 44$ ). A fully unconnected system would of course return a Connectedness value of zero, this means that the two Cellanimats have grown perfect separation valves, that could pull apart with no resistance. However even with low Connectedness values the two cells might still be able to pull apart with relative ease. So a separation system is defined as one with a total Connectedness value  $< 10$  overall.

### 8.5.8 Light, time and structure

The environmental difference between the top and bottom of the water column, that this model focused on, is light. The availability of light has been equated with energy levels for the morphogenesis process. As there are no explicit energy parameters or processes in the model, the unit of time, a time step, is actually stated as a proxy for a unit of energy. To provide a system with more energy it is simply allowed more time steps to perform its task. This does not mean that the task would take longer in reality, just that it would use more energy. So for a light-deprived environment, the system would be allowed only a small number of time steps (energy) in which to grow. Indeed to avoid confusion it is best to think of time steps as 'energy steps', as they more precisely represent the time it takes to use one arbitrary unit of energy, than simply being an arbitrary measure of time.

There are two parameters that depend explicitly on time steps (light-related energy) in the model. The number of time steps given to perform the task overall (runTime) and the number of time steps that it takes to shrink a block (delay). When more time steps are allowed for the process (high runTime



setting), it tends towards a connected system. With more light/energy both parameters are given more time steps. Given that there is little experimental data on how the cell and silica interact during valve formation it is of course hard to assign appropriate values to the delay parameter. A low delay setting manifests as a low resistance of the blocking material to pressure by depositing silica: shrinking would occur faster generating cross-connections earlier. This could correspond to low-energy for the block resistance induced by low light, e.g. in Env B delay would be lower together with a low allocation of overall time for the process.

The simulation methodology offers an opportunity to modify and play out the logical morphological possibilities by setting the delay and runTime with a variety of values. If the delay setting is high, as previously discussed, this would ultimately cause cross-connection formation to be inhibited for an extended period. This was expected to allow for long protruding sister spines as seen in the separation spines of *Aulacoseira*. However, a further interesting effect of varying the delay was found. The characteristic morphology of a separation spine is that it culminates in a point, whereas interlocking spines tend to balloon out into a bulbous end. Varying the delay parameter was found to induce the two different spine tip shapes, rather than a difference in spine length.

With a low delay (fast block shrinking), the cross-connections form quickly, a sister spine will have its forward progress blocked and also, due to the curved shape of cross-connections, deposition will necessarily continue only into a point, as the curve blocks any bulbous deposition. With a high delay setting the spines continue forwards further but whilst doing this they would grow up and over sister ribs and interlock. The amount of time that it took to grow further forwards, only increased the Connectedness as it allowed the cells time to flange out over the top of sister ribs.

This model shows that altering the amount of energy available for delaying cross-connection formation (block shrinking) can affect both the spine tip shape and the length of spines. However, in the time it takes to grow long spines the connectivity also increases, as the Cellanimats have time to push the membrane up and over sister ribs increasing interconnectedness. It seems impossible, with the current model, to produce separation spines with long spines. It would be possible to generate long separation spines, i.e. have a high delay setting, if the rate of forwards rib deposition could be increased. Perhaps the reduced energy experienced in low light could result in reduced resistance from sister cells, allowing one cell to increase its forwards deposition into the other cell, whilst the energy needed to push its own membrane out over the top of ribs for interlocking remains the same, meaning that long forward spines would be observed, due to delayed cross-connections and accelerated forwards growth, but little connectedness due to a short number of time steps for the entire process. Or perhaps a change in WASP activation regime from type-1 to type-2 could be justified. It is possible to generate separation spines with long spines using type-2 WASP activation, as discussed previously, extending the 'battle zone' of the two cells' cytoskeletons would preclude overlapping membrane protrusions and thus, preclude interlocking.

See Fig.8.18 for a summary of the effects of varying the runTime and delay parameters. See the corresponding example screen shots for examples of the morphological variation, as viewed through the


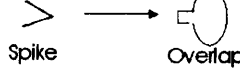
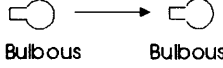
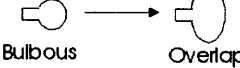
Run Time Delay	<b>LOW</b> Final t= 150	<b>High</b> Final t= 300
<b>LOW</b> Delay= 60	Connectedness= 0  Spike → Spike	Connectedness= 15  Spike → Overlap
<b>High</b> Delay= 180	Connectedness= 20  Bulbous → Bulbous	Connectedness= 162  Bulbous → Overlap

Figure 8.18: The effects on spine morphology, of varying the number of time steps allowed for the run-Time (amount of time given to complete process) and delay (time it takes to shrink a block) parameters, as viewed from the startHeight layer up through the layers in the stack (shown left to right). With low delay values cross-connections form quickly and block further spine protrusion, the curvature of cross-connections enforces a spike shape compared with an otherwise bulbous tip. Given a high runTime value all spines that have breached the ‘battle zone’ will flare out into an overlapping form. Connectedness scores are from the example runs shown in Figs.8.19 & 8.20. Env A was set with high delay and high runTime values, producing the highest Connectedness score (interlocking valves). Env B was set to have low delay and low runTime to yield the lowest Connectedness score (separation valves).

layer stack, incurred by altering these parameters in the model, Figs.8.19 & 8.20.

## 8.6 Results

The model was programmed in C++, all experiments were performed on a standard 1.8 GHz PC workstation with graphics programmed in OpenGL. To test whether the Cellanimat Colony Model could consistently produce the two alternative morphologies, given only a change in the environment, the simulations performed in examples A and D, in the previous section, were repeated one hundred times each and compared the Connectedness values obtained. It was hypothesized that this change in the environment could be enough to cause the change in morphology, between interlocking and separation spines. Env A represented the light-abundant top of the water column, so delay and runtime were both set to be **HIGH** (higher numbers of time steps (energy) allowed for each), delay=180 and runTime=300 with clear ArtCyto called at t=290. Env B represented the light-restricted bottom of the water column and thus had delay and runtime set **LOW** (less time steps (energy) available for the processes), delay=80 and runTime=150 with clear ArtCyto called at t=140. Following the example runs in section 8.5.8 the expectation was to see a higher frequency of interlocking spines in Env A and a higher frequency of separation spines in Env B, thus the Connectedness value in Env A was expected to be high (close to the value of 165 as defined in section 8.5.7) and close to zero in Env B.

The experiment was repeated one hundred times in each environment. On average Connectedness was found to be 148.26 in Env A with standard deviation 38.02 (2.d.p), and 0.68 in Env B with standard deviation 2.67 (2.d.p), see Fig.8.21. Interlocking dovetail joints were formed in Environment A and

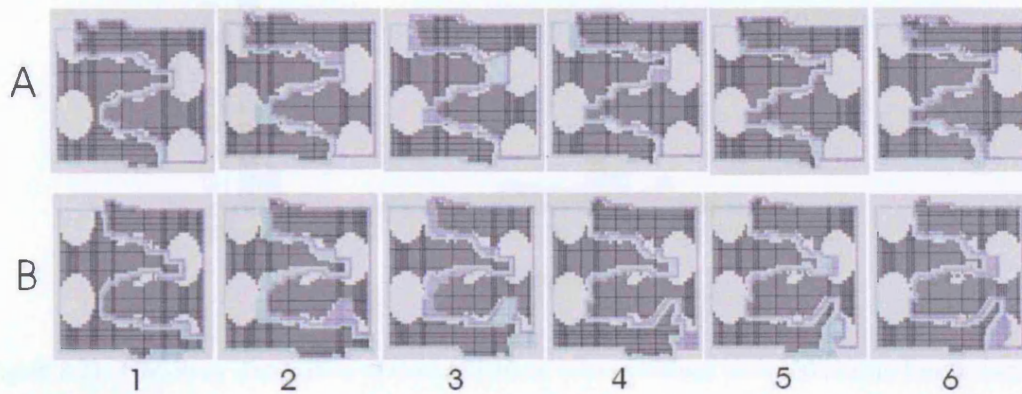


Figure 8.19: *Low delay*. Two example runs shown in 2D slices, from above, going left to right up through the layers from startHeight. Both example A and B have delay set LOW (to 60), runTime was set LOW in A (150) and HIGH in B (300), clear ArtCyto was called at  $t=140$  and  $t=290$  respectively. Spines with spike-tip morphologies are seen in both examples as detailed in Fig.8.18 with overlapping morphology seen in B.

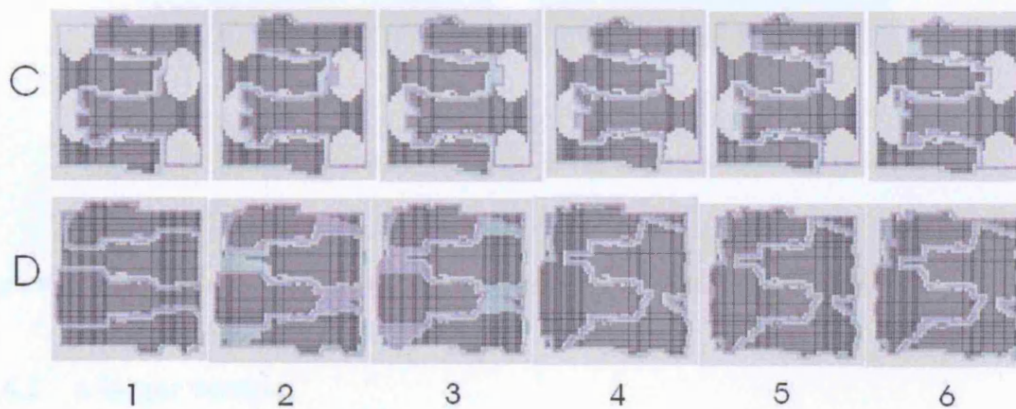


Figure 8.20: *High delay*. Two example runs shown in 2D slices, from above, going left to right up through the layers from startHeight. Both example C and D have delay set HIGH (180). runTime was set LOW in C (150) and HIGH in D (300), clear ArtCyto was called at  $t=140$  and  $t=290$  respectively. The spines deposit past the point where sister cross-connections would form, due to high delay, the tip becomes bulbous as it fills the space. In D HIGH runTime meant the spines flared out and overlapped sister ribs. Note in D, slices 2 and 3 show the membranes stretched out over sister ribs before overlapping begins in the next layer above. Also note the assimilation of membranes evident in the slice 6 of example D where the silica flaps merge.

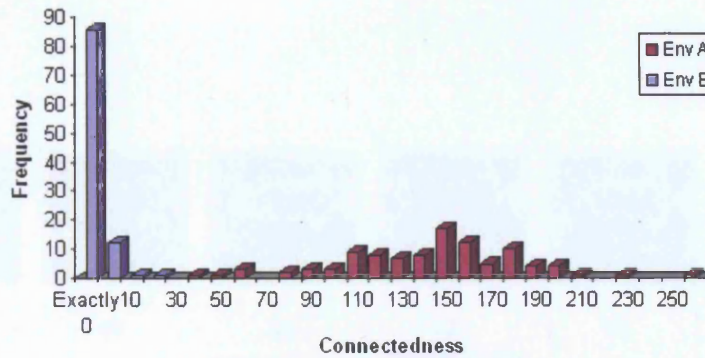


Figure 8.21: Frequency distribution of Connectedness values obtained over 100 runs in Env A and Env B showing that the system in Env B on average produced separation valves (zero Connectedness) and interlocking valves in Env A (high Connectedness values).

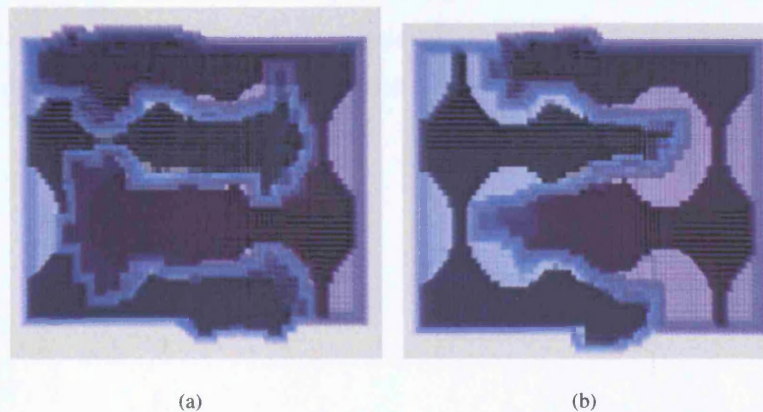


Figure 8.22: (a) interlocking dovetail joints in Env A (b) separation spines in Env B

separation spines in Environment B. See Figs.8.22(a) and 8.22(b) and Figs.8.23 and 8.24.

### 8.6.1 A larger version

A larger version of the model was run with Cellanimats containing four ribs and five blocks per row. This increased size slowed computation time, so for efficiency a lower agent ratio was used (15:8 actin to nucleators) this required higher time step allowances for both delay and runTime but kept the computation time down, as the number of agents reduced from 17,405 actin and 7455 nucleators per Cellanimat (cytoplasm volume was 49,728) to 7455 actin and 3976 nucleators per Cellanimat. With these new settings the model took around 15 minutes to run for 1000 time steps. For Env A delay was set to 300 and runTime to 1000. For Env B a delay of 180 was used and runTime was set to 300. The decreased agent volume resulted in more time steps to move the membrane. See Figs.8.25 to 8.30 and compare to the original diatom images in Fig.7.3. The examples shown in these figures obtained Connectedness values of 251 for Env A and zero for Env B.

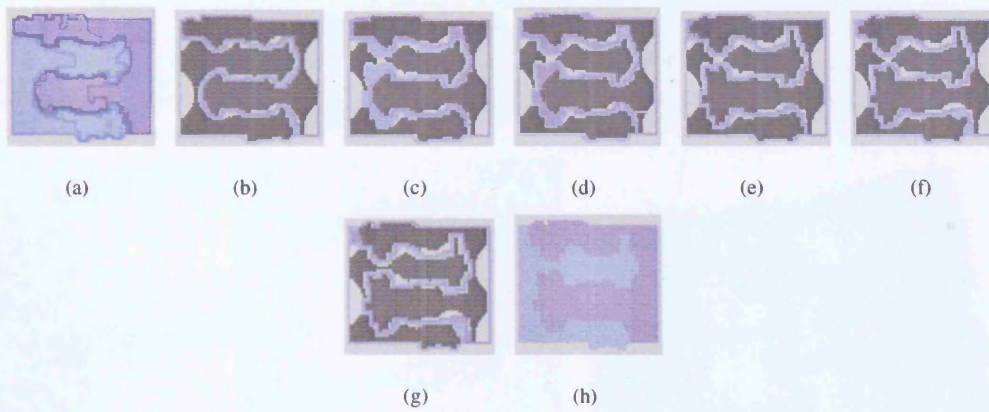


Figure 8.23: slice through view of interlocking valves shown in Fig.8.22(a). first 2 rows shown as one slice in (a) otherwise single layer slice views upwards through the layers. Cell A plasma membrane light blue, Cell B plasma membrane dark blue, silica black.

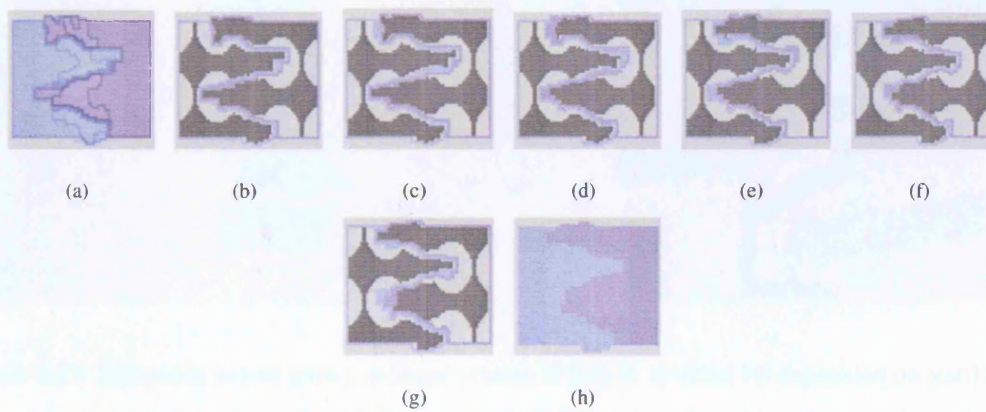


Figure 8.24: slice through view of separation valves shown in Fig.8.22(b). first 2 rows shown as one slice in (a) otherwise single layer slice views upwards through the layers. Cell A plasma membrane light blue, Cell B plasma membrane dark blue, silica black.

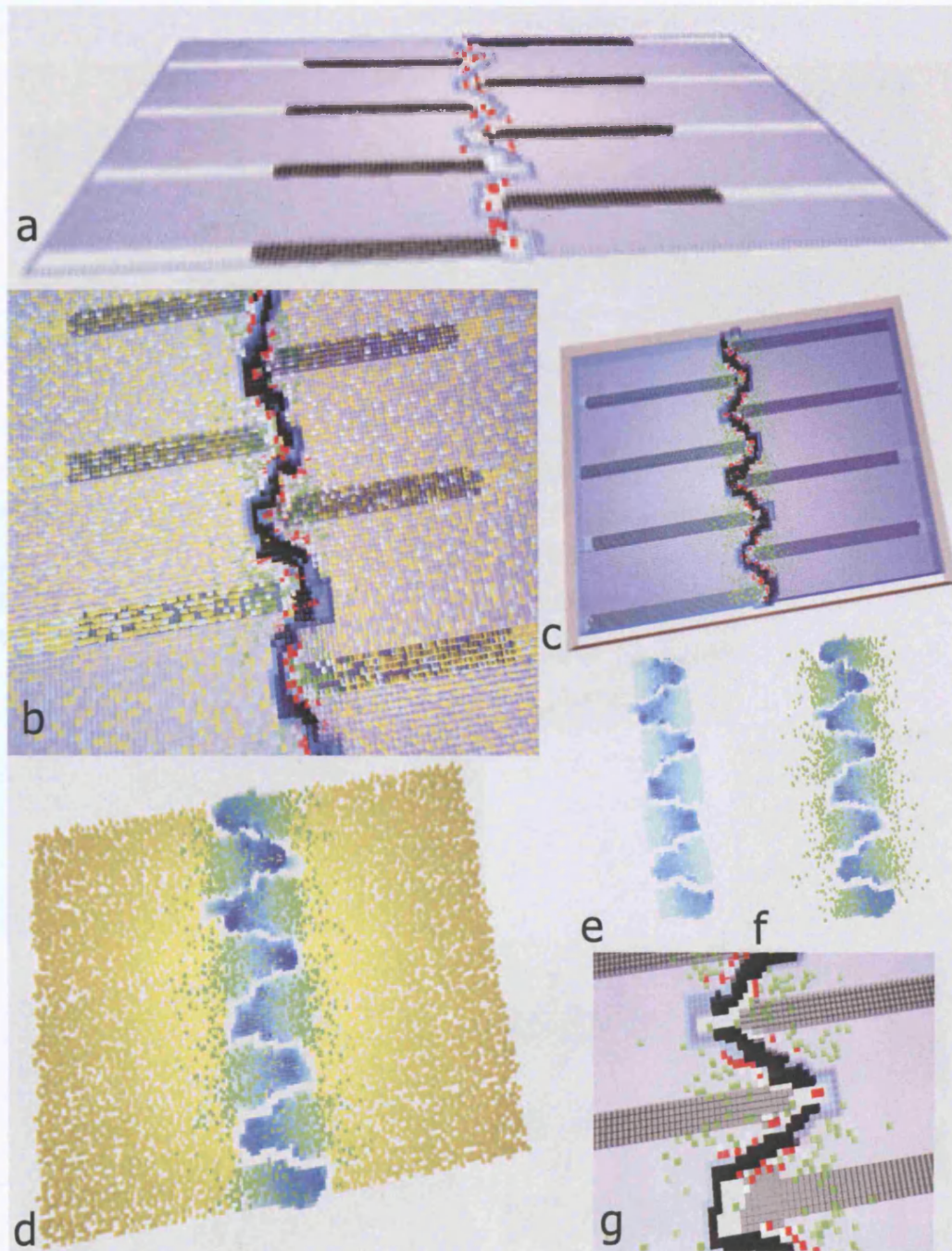


Figure 8.25: Separation valves grown in larger version in Env B. a) initial rib deposition on startHeight layer, FA agents (red) push out the membrane ahead of silica spines depositing. b) view from above of early rib deposition; battle zone shown as radius of active WASP in sister PLs (black) overlap; ArtCyto agent distribution shown (SA yellow, PA green, FA red, all N agents white). c) Initial rib deposition reaches Cellanimat edge, blocks not yet shrinking, spine deposition has reached further forwards, wider distribution of PA agents visible (green). d) Actin activation viewed from above (SA yellow, PA green, profilin gradient dark blue to light blue). e) Profilin gradient only, higher concentration at spine tip as more PIP2 are activated. f) profilin gradient and PA distribution. g) Close up view of actin filaments pushing out membrane ahead of depositing spine.

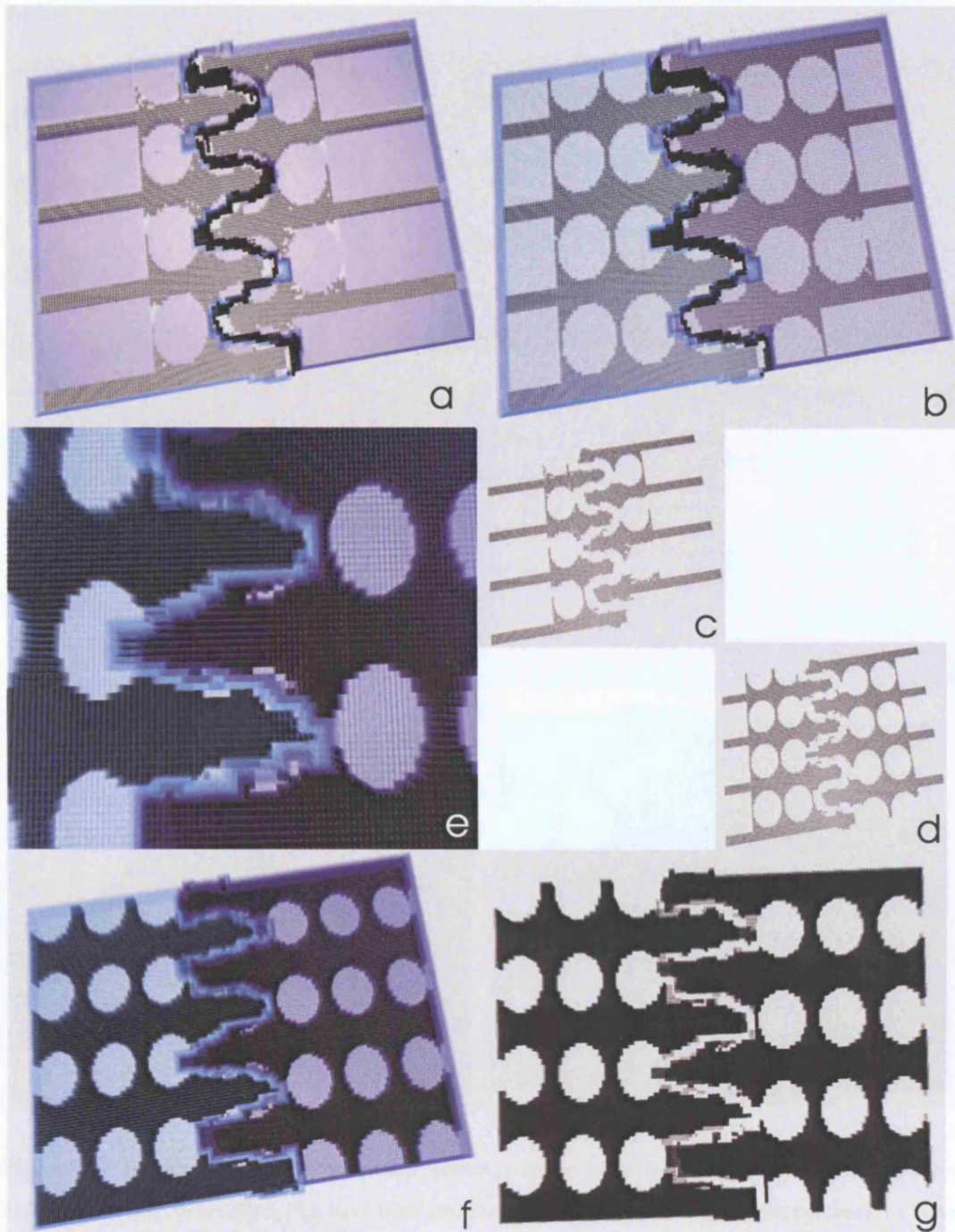


Figure 8.26: Later stages of separation valve development, grown in Env B. a) Blocks start to shrink, vimines (cross-connections) begin depositing, forming pores. b) After more time steps only the outer blocks are left to shrink, cross-connections near fully formed. c) & d) Silica-only views of forming cross-connections. e) Close up of final separation spines with point tip morphology. f) Full view from above of separation valves and PL. g) Full view of silica-only from above. Connectedness=0 of final valves at  $t=300$ .

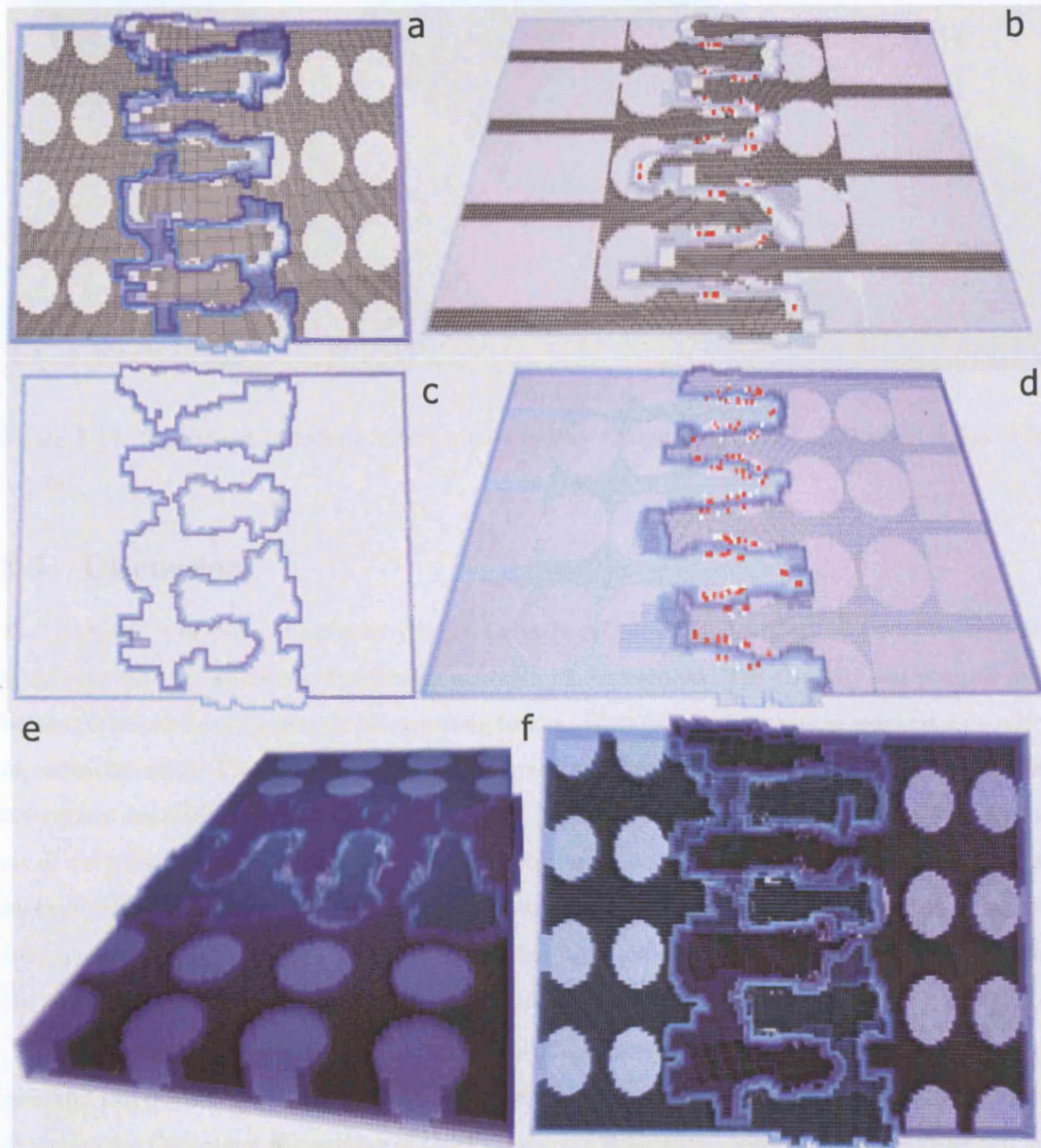


Figure 8.27: Interlocking valve development, grown in Env A with larger version. a) View from above before clear ArtCyto is called, PLs have been stretched out over sister ribs (dark blue patches). b) When blocks start to shrink, spines have grown past where the first cross-connection would have formed (due to longer delay setting), FA agents (red) pushing out membrane ahead of depositing silica. c) PL of upper layer in stack showing the space, created by the ArtCyto, to be filled by silica after clear ArtCyto is called. d) The ArtCyto can be seen either side of the sister PLs pushing against each other in the battle zone (FA red, FN white). e) Completed linking valves viewed from CellA. f) Completed valves viewed from above. Connectedness=251 at final  $t=1000$ .



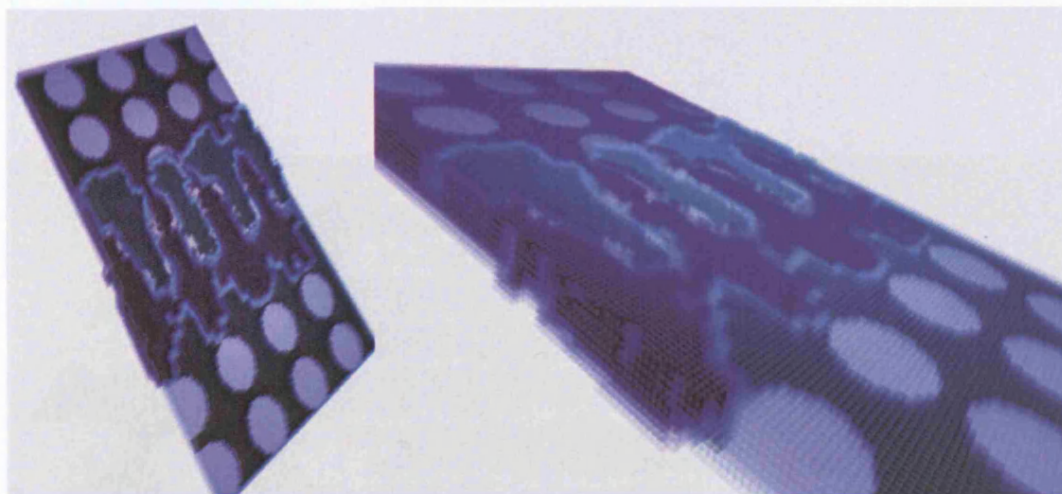


Figure 8.28: Side views of linking valves grown in Env A with larger version, Connectedness=251,  $t=1000$ .

## 8.7 Discussion

The 'complex' morphological plasticity in the Cellanimat Colony Model arises, not out of a complex model, but out of a large model comprising many simple interactions. The plasticity was possible only because it included a large number of interacting factors. There had to be a group of interactions governing silica deposition. There had to be groups of interactions governing cytoskeletal dynamics, membrane behaviours and Cellanimat-Cellanimat interactions. The global phenomena resulted from the epigenesis of the groups interactions as well as their internal interactions. This model represents a dynamical hierarchy that goes further than the original Cellanimat model. It models at the levels of proteins, cell subsystems, cells and colonies. The inclusion of silica deposition extended the model still further, without any one group of interactions, the behaviour could not have emerged.

The aim was to have a small simple illustration of the colony phenomenon, but that was sufficiently powerful and realistic to generate the behaviour. A low number of ribs (2) was used with small width (5 voxels) per Cellanimat, the number of blocks was set to three giving ample room in the sister cell for forward-spine growth. However, the larger version of the model, described in the previous section, made it easier to visualize the valves in relation to the images of real diatoms from Chapter 7. This simulation was implemented on a standard desktop workstation and ran in a number of minutes. Larger systems are entirely possible but may require more expensive computation, or more patience!

A comprehensive account of a novel model for diatom colony formation has been presented, addressing the secondary hypothesis and thesis Objective Five. The processes of building a full model in an area with little experimental data necessarily involved substantial creativity. This will of course have mixed results, some ideas within the model will inevitably be off the mark, others may be supportable. The main aim, from the point of view of diatom research, was to stimulate debate and further research to support/counter the presented mechanisms. It is important to understand this example of morphological plasticity in response to the environment as the permanency of diatom valves provides a key to

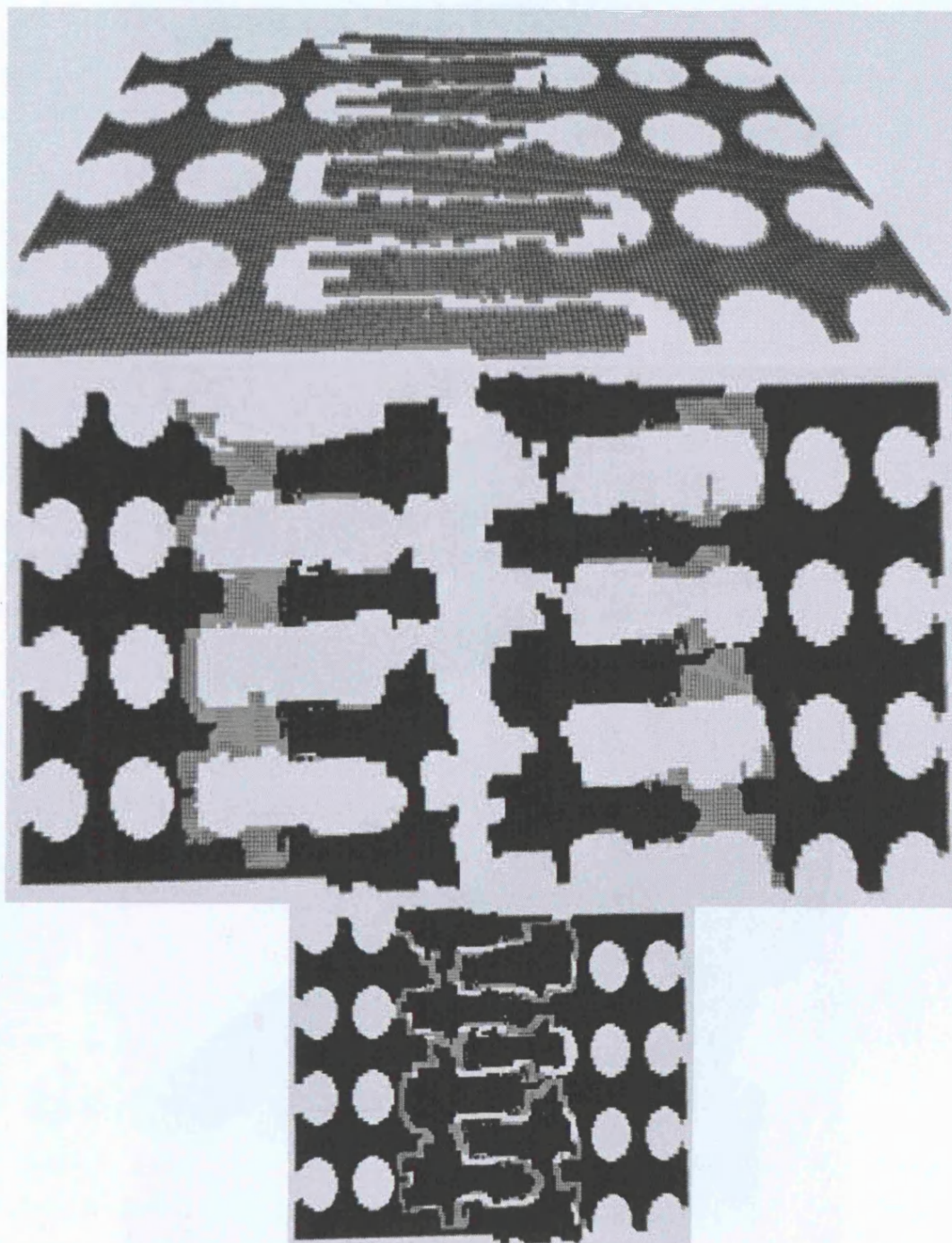


Figure 8.29: Silica only views of larger version linking valves grown in Env A, Connectedness=251,  $t=1000$ . Top) layer startHeight; middle left) CellA, middle right) CellB; bottom) view from above of final 3D valves.

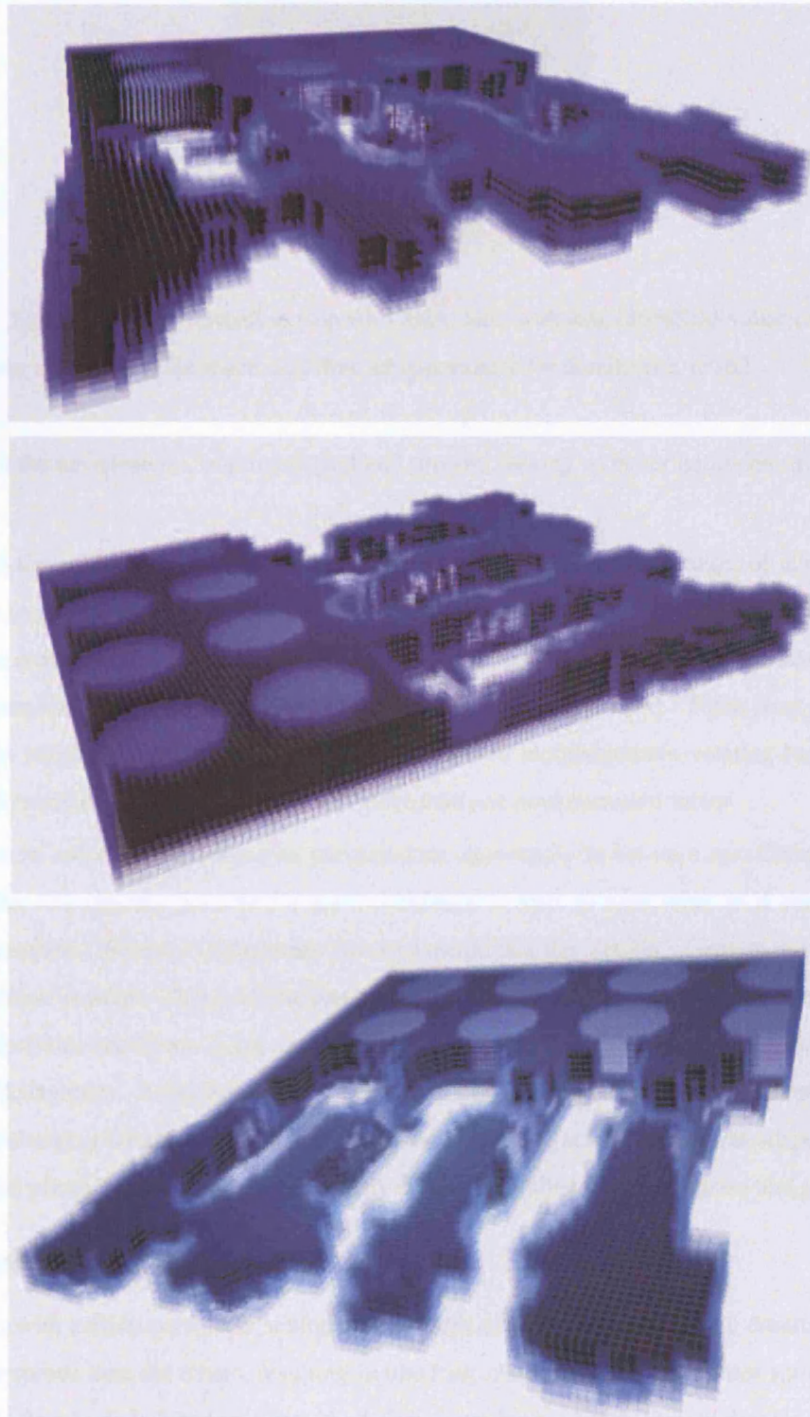


Figure 8.30: Single Cellanimat views of larger version linking valves grown in Env A, Connectedness=251,  $t=1000$ . Top and middle) CellA; bottom) CellB. Note the entire siliceous structure is contained within the plasmalemma.

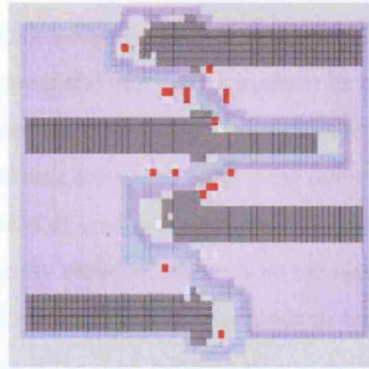


Figure 8.31: Dominant spine formation (top rib CellA, left) with low `blockSize` value ( $=\text{ribPLgap}+2$ ) causing greater competition for space, and thus an opportunity for dominance,  $t=162$ .

knowledge of the environment, of climate past and present, leaving us better equipped to predict future trends.

Through the model development a deeper understanding of how many groups of interactions may be necessary to generate such plasticity has been gained, indeed the suggestion is that the current model falls short. In order to achieve more realistic separation spines, long spines and spines such as those seen in *Skeletonema* and *Chaetoceros* additional mechanisms must be involved. There may also be many more ways in which the environment affects the progress of morphogenesis, relating back to the idea that colony formation may be an adaptation to more than one environmental factor.

The diatom colony application also presented an opportunity to set up a two-Cellanimat system and found that it is entirely possible for the Cellanimats to react to each other as if each formed the other's environment. Multiple Cellanimats however meant that the number of agents quickly rises and computation time expands. This could be resolved with a review of the algorithms involved, optimizing for speed rather than behaviour. Also, a small number of PC workstations could be linked to easily cope with many Cellanimats. It has been shown that multi-Cellanimat systems are implementable and can be useful for studying interactive growth mechanisms, social interaction and mutual-adaptation through morphological plasticity, opening up a wide array of possible follow-up experiments and projects.

### 8.7.1 Future study: Dominant Spines

Interestingly, with certain parameter settings a single rib could be seen to quickly dominate and grow at far greater speeds than the others, resulting in one long spine for every few shorter spines. This phenomenon was seemingly induced with low `blockSize` values but eradicated with higher `blockSize` values, although this was not shown conclusively in preliminary tests. The `blockSize` parameter controlled how much extra room there was between two ribs, affecting the ease with which the sister rib could pass between them. High values resulted in very little resistance between the sisters as their radii of WASP recruitment would no longer overlap. Low values cause vast overlapping of sister WASP radii, as the ribs grew past each other, resulting in an intensified 'battle zone'. Eventually, one rib would dominate and its growth would then accelerate, possibly further hindering sister rib deposition. See Fig.8.31.

If a rib accidentally generated actin filaments first it could extend relatively un-opposed by the sister ribs, allowing it to dominate the space and thus further increase its chances of actin-filament formation, accelerating growth (as a larger membrane protrusion creates a larger space near WASP to recruit further actin into filaments). This phenomenon seemed to occur more often with high values of blockSize when random movement was used instead of gradient movement of agents. This could be because agents at the growing tips were not a uniformly abundant source, with the random movement algorithm, so if one rib happened to have more agents at its tip then it could dominate the space.

It would be interesting to see if the gaps between ribs in the separation valve of *Aulacoseira* are shorter than those of the interlocking valve, as this could explain why certain spines have become dominant and extended far beyond the others, see Fig. 7.3.

### 8.7.2 Predictions and suggested experimentation

Here predictions and useful follow-up biological experiments, indicated by the simulation, are listed. This leads to the conclusion that the secondary hypothesis can be accepted.

Firstly, complete morphometrics of linking and separation valves would generate more realistic initial parameters and corroborate or refute ideas about ideal distances between ribs for generating the correct thickness and opposing growth in the battle zone. Are there any consistent differences in pore width between separation and linking spines? Study and quantification of the 'battle zone' in real diatoms would be a useful step, indeed if it could be altered in some way to see how this affects further growth, more could be revealed about the nature of the siblings' interactions. Are there any examples of badly formed valves? Morphometrics on valves such as these could give vital clues as to the necessary spacings for completion of the process.

Implementation of the plasticity experiment with real diatoms should be a high priority future experiment. Expose one culture of colony-forming diatoms to an over-abundance of light and another to constant low-illumination, simulating the positioning of the cultures at either the top (Env A) or bottom (Env B) of the water column. Is a higher frequency of separation spines seen in Env B? Indeed many experiments could be devised to further clarify the link, if any, between light/energy and structure. A parallel experiment could replace light with nutrients, or other environmental factors to explore the other possibilities.

More evidence is needed to support the 'shrinking blocks' mechanism. It is highly idealized but represents a fundamental hypothesis concerning interaction between the cell and the depositing silica, where the cell is a template and the silica deposits in a 'greedy algorithm', filling all available space. An *in vitro* system could perhaps be set up to test the validity of this theory further. Could the 'greedy algorithm' for silica deposition be tested? Perhaps by artificially removing sections of parent silica, or cross-connections during daughter valve development to see if silica deposition will continue into all available space.

Far more data are needed on exactly which cytoskeletal and transduction pathway proteins are involved in the valve forming process. These could give much needed information regarding environmental triggers and concerning the process as a whole. How is the actin cytoskeleton activated? Can silica be

causing the activation, perhaps through a WASP related pathway, or is there an entirely separate trigger, from another part of the developmental machinery?

## Chapter 9

# Summary and conclusions

Through the biological inspiration from diatom morphogenesis, yielded in Chapter 3 combined with the cytoskeleton study detailed in Chapter 4, the novel artificial system, the Cellanimat, was created. The Cellanimat was shown to be capable of adaptive behaviour, and generating a well-adapted morphology in a changing environment, through the multifunctionality experiments detailed in Chapter 5. In Chapter 6 the properties of the Cellanimat were investigated resulting in an optimized and refined version of the model. This was then implemented, together with the Nature's Batik Model developed in Chapter 3, as a test bed (The Cellanimat Colony Model) for developing new hypotheses concerning diatom colony formation. Therefore, both the primary and secondary hypotheses have been tested and shown to be true. The thesis objectives have all been achieved as detailed below.

- 1 Satisfied in Chapters 3 and 7. Diatom morphogenesis was investigated through design of novel Nature's Batik Model and a diatom colony formation literature survey, which inspired the direction of the thesis research towards the cytoskeleton and environment-related membrane shape changes.
- 2 Satisfied in Chapter 4. A novel algorithmic model based on MP was created: the Cellanimat.
- 3 Satisfied in Chapter 5. The model was shown to generate adaptive behaviour/design in a changing environment.
- 4 Satisfied in Chapter 6. The properties of the model were investigated.
- 5 Satisfied in Chapters 7 and 8. The model was used as a test bed for furthering knowledge of MP in diatom morphogenesis.

## 9.1 Summary

The goal of this thesis has been achieved, stated in Chapter 2, to investigate, at a ground level, mechanisms for morphogenesis and morphological plasticity in natural systems, and algorithmic formulations for artificial systems, through the simulation of fully embodied animats. Autonomous design principles for self-organizing adaptive systems capable of growing new structures on a 'need-to-grow' basis through a dynamic, active structural coupling between the system and environment, have been investigated and developed.

In Chapter 2 the term ‘Dynamic Morphology’ was introduced, setting out system requirements for MP. The major requirement for a DM, in order to support reconfiguration at a higher level, states that the low level components must have the capacity for interactive change and movement. A taxonomy of MP in AI systems to date was also presented. This illustrated the large gap between the capabilities of natural systems and current AI systems.

In Chapter 3 the Nature’s Batik Model was presented, which generated raphid pennate diatom valves, using a cellular automaton, exhibiting some of the functions of cell walls. At each stage of development the generated valves were consistent with observations of real diatom valve growth. The model also highlighted that morphological form can be explained as the compromise between optimizing two opposing functions: in this case as a cell wall and as a defensive structure.

Simulated models are extremely useful for investigating, visualizing and developing theories of morphogenesis. The Nature’s Batik model was however very abstracted and simple. It did not explain how the ‘organic template’ was formed or controlled. It was the intention of this work only to provide a starting point for the thesis investigation in the context of a real morphogenesis system. In order to understand how morphological plasticity of valves was being implemented focus turned to the cytoskeleton.

In Chapter 4 the Artificial Cytoskeleton was introduced as a new combined processor and effector generating lifetime adaptation of morphology in the novel animat model based on single cells: the Cellanimat. The ArtCyto was closely modelled on the eukaryotic cytoskeleton and served as a proof-of-concept that the cell’s cytoskeleton could be effectively interpreted and modelled algorithmically with agent-based simulation. The E-P Map framework, for classifying the morphogenesis process in terms of environment-system interactions, was also introduced. An example E-P Map for generating membrane protrusions, a fundamental cellular mechanism involved in many higher-level behaviours, was presented.

In Chapter 5 results were given of two experiments which illustrated the Cellanimat’s multifunctionality when using the protrusions E-P Map. In the first experiment the Cellanimat was placed in an arena with one environmental factor: a chemoattractant gradient. It was shown to perform chemotaxis through MP alone, generated by the novel mechanism. In the second experiment it was shown that if the chemoattractant gradient was changed to a solid particle the Cellanimat was able to perform phagocytosis, with no change to the system itself. This was an important result showing that environmental dependence in a growth mechanism needn’t be a drawback. It could, with the right mechanism, be exploited to generate adaptive behaviour allowing the system to perform new functions by adjusting morphology to suit the new environmental conditions. These results showed that the Cellanimat was capable of reversible MP, lifetime alterations in morphology, in relation to the environment.

The second experiment also served as validation of the Cellanimat, with the protrusions E-P Map, as a reasonable biological model. The model, originally based on the first stage of fibroblast chemotaxis could, without explicitly being programmed to, also perform phagocytosis. The biological system on which the model was based had evolved to generate both behaviours, thus a good model of this stage of chemotaxis should also generate the initial stages of phagocytosis.



The E-P Map encapsulated the ideas of Hogeweg (2002a), that morphogenesis arises out of many interacting mechanisms. The EP functions represent different mechanisms at work, so in the E-P Map overall morphological behaviours result from their interactions. Though she focused on multicellular development (Hogeweg, 2000), on the interplay of differential cell adhesion and gene regulation, in this thesis it has been illustrated that the same is true in single cell morphogenesis, considering cytoskeletal dynamics and obstacle collisions as the interacting mechanisms, where the properties of one material generate a barrier (obstacle), blocking the growth of a weaker material, thus forming a template. The E-P Map also represented the exploitation of inhomogeneity in mediums, by using the combination of EP functions to generate behaviour/morphology rather than a simple repetitive algorithm such as Reaction Diffusion Turing patterns, which tend to assume unrealistic medium uniformity (Hogeweg, 2002a).

In Chapter 6 results of seven studies were given, into the dynamics and optimization of the Cellanimat as an artificial system. Improvements in function definitions and parameter settings resulted in significant improvements in performance. The system was found to be reasonably robust to the stochastic nature of functions when high numbers of receptors and agents were used. Through investigations into the Critical Saturation Point a link was uncovered between over-saturation of proteins and improved performance. Recycling was found to be mostly redundant as a mechanism as no constraints on energy expenditure were imposed. However, as in real cells, if protein production cost the Cellanimat, then recycling would be expected to play a major role.

The Cellanimat as a developmental model was shown to reduce scalability problems. Results from evolutionary experiments with the Cellanimat, described in Chapter 6 showed that even though the size of the genotype was small, it could be used in conjunction with the E-P Map to generate complex, adaptive forms and behaviours. Evolution of fit genotypes optimizing speed and performance were found after only ten generations, showing the system is evolvable.

Relating back to the advantages of developmental encodings for system morphology design in section 2.3.4. From the results in Chapter 6 it can be stated that the model exhibits all advantageous properties of an indirect encoding: robustness, scalability, evolvability, adaptability and complexity in form. It more importantly overcame the major limitation of environment dependence by incorporating environmental information into the growth process.

The thesis was brought together in the final chapters, where the Nature's Batik Model was combined with the optimized Cellanimat model and E-P Map framework to investigate a real, and as yet unexplained, example of irreversible morphological plasticity in diatoms. First, a detailed literature review was presented in Chapter 7 illustrating some of the complexities involved when attempting to unravel how and why MP occurs in nature.

The Cellanimat Colony Model was presented in Chapter 8. It showed the importance of timing in the developmental process, how changes in the timing regime can lead to a bifurcation in morphology. The role of energy levels, affected by environmental changes, in regulating timing during diatom morphogenesis was highlighted. It was shown that a single system, combined with changes in energy levels due to light regime changes in the environment, could generate both separation and interlocking spine

morphologies. The model serves as an example of system perception of environmental factors without the use of specific sensor channels. The environment does not need to only 'input' through designated sensors when the processor is fully embodied, as with the ArtCyto. Physics and energy laws affect all matter universally, they do not need to go through sensor 'gateways' to get in and have an effect.

### 9.1.1 Specific contributions

The major contribution of this thesis was to the understanding of adaptive behaviour and design of adaptive systems. The role of MP in life, adaptation and design has been emphasized and new algorithms, frameworks and definitions have been presented to stimulate and facilitate further exploration and development of MP for next-generation AI systems. Following the cheap design principle, novel mechanisms were developed, based on morphological plasticity in nature, allowing an adaptive system to cope in a changing environment through plasticity in design, both generating well adapted-form and adaptive behaviour without a centralised controller.

Below is a list of specific contributions made by this thesis:

- Introduced Dynamic Morphology definition stating requirements for an MP capable animat
- Constructed a Taxonomy of MP in AI
- Created novel model 'Nature's Batik' for simulating diatom valve morphogenesis
- Created novel framework for generating well-adapted and adaptive morphologies: the E-P Map
- Created novel mechanism for generating MP: the Artificial Cytoskeleton
- Created novel model the Cellanimat powered by the Artificial Cytoskeleton
- Showed with the Cellanimat an artificial system can have adaptive morphology over a lifetime
- Showed with the Cellanimat an artificial system can demonstrate adaptive behaviour without a brain
- Detailed investigation of Cellanimat parameters, functions and optimization
- Detailed investigation of Cellanimat dynamics
- Created novel multi-Cellanimat model for investigating diatom colony formation
- investigation of diatom colony morphogenesis mechanisms
- showed that diatom colony formation dynamics could be generated by a single morphogenesis mechanism
- made predictions for biological experiments from the simulated MP model of diatom colony formation

## 9.2 Conclusions

This thesis has shown that through environmental interaction in the developmental/growth processes morphologies can themselves 1) produce interesting adaptive behaviour and 2) continually change to remain well-adapted to environmental changes. Morphological plasticity can provide a solution to the problem of static, environment-dependent morphologies and offers an alternative route to adaptive behaviour, providing ‘no-brainer’ adaptive behaviour.

The Cellanimat is a cheap design model. Environment-system interactions are exploited to generate adaptive behaviour and morphology. One of the interesting and important aspects of cheap design, discussed in Chapter 2, is that sensorimotor coordination enhances the perceptual capabilities of the situated system (Iida, 2005). There was evidence of sensorimotor coordination in the Cellanimat enhancing ‘perception’ when exposure to the chemoattractant was increased by trapping pockets of it between growing protrusions, which caused a positive feedback loop stimulating further growth and further exposure.

The Cellanimat is an adaptive system that satisfies Di Paolo’s (Di Paolo, 2006) extended definition of agency: *natural agency*. In natural agency he impresses the requirement that the agents must *actively* (in the same sense used in the E-P Map) affect their environments, rather than only being affected upon. He draws the distinction between structural coupling of organism and environment (which can be observed due to the physical constraints of the world rather than through any activity in the organism) and the *regulation* of structural coupling which is something only done by activity in the organism. He concluded that only regulating systems can be said to be performing *behaviour*. Indeed in the quote below he uses the example of unicellular phagocytosis as an example of active regulation of the environment.

“Parametrical regulation such as active transport through the selective opening and closing of ion channels is widespread in uni-cellular organisms and is one of the most common examples of control of the conditions of physical exchange between organism and environment. More sophisticated control involves the whole cell, as in the displacement towards nutrient-rich regions of the medium, or the construction of protective biofilms, or the projection of pseudopodia to engulf another cell in phagocytosis.” (Di Paolo, 2006)

Di Paolo’s addition to the original Varela, F. J. (1979) definition of structural coupling allows an important distinction to be made between the ‘living system’, capable of active regulation, and the non-living environment, which is not. The Cellanimat on both protein and whole cell levels exhibits active regulation of the coupling. The component parts can alter their local environment through re-organization of sub-component parts. For example, at the component level, agent binding activity can alter membrane shape (rule A2 in the Cellanimat); at the whole Cellanimat level, membrane protrusions extend and redistribute the local chemoattractant gradient (EP<sub>3</sub> in the protrusions E-P Map). This regulation exchange has been seen to benefit the system in the three example experiments, in chemotaxis it reached the source, in phagocytosis it engulfed the particle and in the colony model it was able to control colony length (form separation valves) as light levels dropped, decreasing the chance of dropping out of the photic zone.

Di Paolo’s natural agency is therefore an important definition, given the original aim to develop an

adaptive system based on morphological computation rather than an abstracted controller. In conclusion, the system, through active, regulated structural coupling does indeed exhibit 'life-like' qualities of behaviour and agency, and as such warrants further study in terms of its adaptivity and control capabilities.

## 9.3 Future work

Work on the Cellanimat is continuing in three key areas, related to the three stages of research development identified in Chapter 1: (i) further work with biologists to improve the fidelity of the Cellanimat model and/or explore its capabilities as a biological modelling tool in other cell biology domains; (ii) further exploration of the Cellanimat properties and dynamics for the investigation of improved developmental algorithms and adaptive systems (iii) applicability in other domains, such as autonomous software agents and portfolio optimization.

### 9.3.1 Biological modelling

The Cellanimat and E-P Map framework were used in this thesis to explore a real case of morphological plasticity in diatoms. This work was however, only a starting point. The predictions and future studies outlined at the end of Chapter 8 are all prospective experiments for further work. Once more biological data has been gathered, based on these predictions, improvement and model updating can begin. Through a cycle of model predictions - biological data - model corrections it is hoped that understanding the actual mechanisms involved in diatom colony formation may improve.

The modelling approach of the Cellanimat, using a hybrid of heterogenous swarm agents and cellular automata, combined with the E-P Map framework is applicable to many protein or cell based systems, not just the cytoskeleton. This thesis work has inspired several MSc thesis projects related to cancer drug delivery, modelling the extracellular matrix rather than the cytoskeleton, e.g. (Semenova, 2005). It is also to be applied in a new context to angiogenesis (blood vessel formation) plasticity to different tissue environments in an upcoming project at Cancer Research UK. For a full discussion of the merits of the Cellanimat modelling framework for biological and medical research see (Clack, 2006).

### 9.3.2 Cellanimat properties as a developmental/adaptive system

The components of the Cellanimat necessary for MP were considered as a simple starting point. There are many directions that research could take from here, e.g. addition of cytoskeletal mechanisms such as organelle transport, further investigation of evolvability, or relating back to the idea of an implicit embryogeny, see Chapter 2, new E-P Maps could be evolved, keeping just the basic rules of interaction between Cellanimat macromolecules. Here just a handful of possible directions will be outlined.

In the Cellanimat a set amount of each protein was initialized, in order for focus to lie solely on the cytoskeletal dynamics. In a more involved model, however the inclusion of a genetic regulatory network (GRN) is proposed, allowing the levels of proteins synthesized to vary in relation to current needs. It would also be interesting to involve energy constraints, to investigate efficiency of protein production and recycling mechanisms further.

The interesting self-organizing dynamics of lipid membranes have been explored within Artificial Chemistry research (Hutton, 2002). With the Cellanimat however, the focus was on investigating situ-

ated cytoskeletal dynamics and so a less biologically-loyal model of lipid dynamics was used, though interesting properties were still observed, for example the assimilation of same-cell membranes in the colony model. It would be interesting to merge Artificial Chemistry membrane models with the ArtCyto to investigate further realism in morphology changes, through the combination of two self-organising processes. Such a combination could be relevant to self-replication modelling, central to Artificial Chemistry research, as the microtubule cytoskeleton coordinates cell division with the formation of the mitotic spindle in real cells (Alberts, B. et al., 1994).

In the protrusions E-P Map receptors had no movement across membrane surfaces directly, though distribution did change as the membrane shape and size changed during growth. Receptor clustering however, is an interesting biological phenomenon (Alberts, B. et al., 1994) of strategic and economic importance - if needed receptors can be 'delivered' to a desirable site improving the strength and speed of a reaction without the cost of large scale synthesis. To investigate the effects of such clustering on adaptive performance, the receptors could, in a future version, be upgraded and modelled as agents, with rules of interaction and movement.

Multi-Cellanimat systems were investigated in the Cellanimat Colony model but it would be interesting to explore this further, with more than two Cellanimats, possibly modelling a multicellular system with cell signalling pathways for communication.

It would be useful to compare the Cellanimat, as a fully embodied cognitive agent, to an animat using a more traditional abstract neural controller. One possible task could be 'ball catching', similar to phagocytosis but the particle is free moving around the arena. Fig.9.1 shows screen shots of a preliminary ball catching experiment. The Cellanimat could perform chemotaxis to actively find the particle rather than waiting for a surface collision. With a randomly moving ball this could be a hard task for a neural network to predict where to move to next and catch it in time.

### 9.3.3 Applications in other domains

There are possible software applications that are currently being explored, such as financial portfolio optimization. The Cellanimat was instantiated in 2D in an environment containing shares with changing prices in a recent MSc project (Zhang, 2005). Receptors activated when share prices changed favourably and protrusions into the environment represented the buying of shares. Indeed any problem space that could be reformulated spatially is a potential application of the Cellanimat, such as infotaxis - movement towards desired information in a spatially arranged network.

One of the main applications considered by morpho-functional machines and collective robotics involves traversing difficult terrains to obtain objects, or people or assume functional shapes like bridges. It was important to instantiate the Cellanimat in simulation, as robotic models currently lack the plasticity in materials to produce such complex forms. At this early stage of MP investigation it seemed logical to use the most flexible method for study. However, a robotic implementation of the Cellanimat has been considered, which could be an interesting direction to take. Utilizing collective robotics for the cytoskeletal agents, and a flexible rubber/spring based membrane fence containing them, the Cellanimats ability to cope in changing, real environments could be tested.

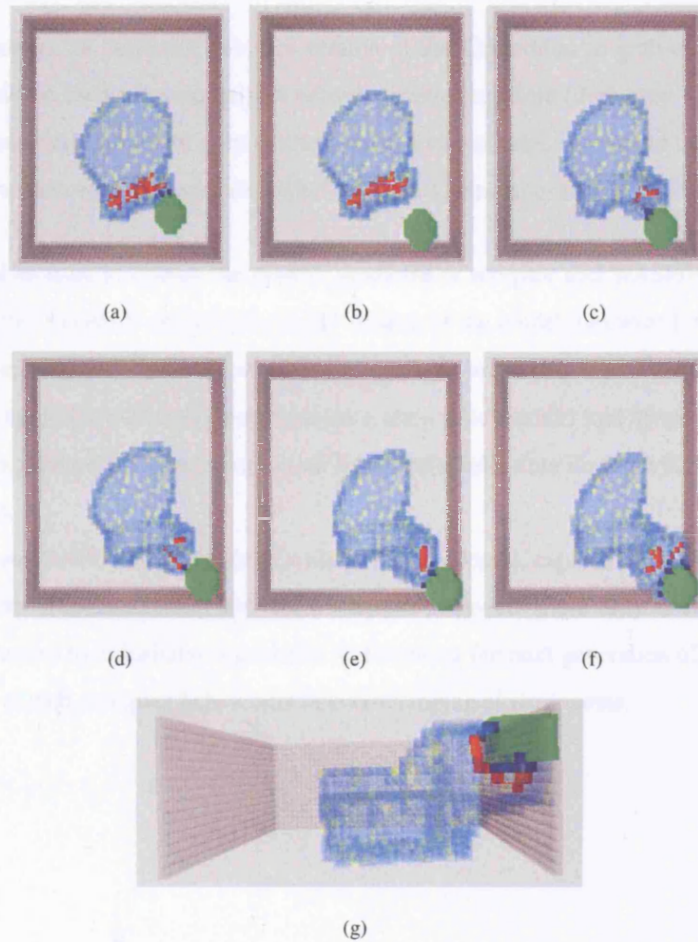


Figure 9.1: Screen shots of one preliminary run in the ball catching experiment. The Cellanimat protrudes an 'arm' trapping the particle in the corner of the environment.

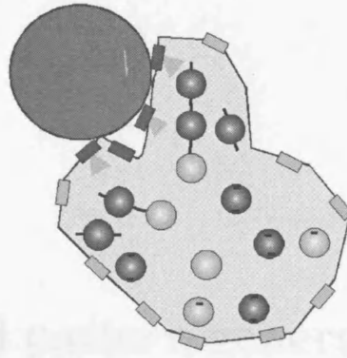


Figure 9.2: Schematic of collective robotics version of the Cellanimat to grab an object. Lights and light sensors could be used to communicate between active receptors (dark grey boxes) and the actin-bots/nucleator-bots (dark grey/light grey circles). actin and nucleator-bots could have connecting arms allowing for connection and disconnection with filaments. Connecting arms could fold in when inactive.

Lights could be used to convey the profilin gradients or receptor and WASP/PIP2 activations, see Fig 9.2. Initially this system is envisaged as a 2D version of the model, however it is conceivable that a 3D model could be built where the bots are more like modules in a modular robot, able to move over each other. Actin-bots could have two opposing connector arms which would fold inwards when inactive. To find a neighbouring filament to join to they could have a spin behaviour during which they try to connect to any neighbours.

There are many fruitful directions that Dynamic Morphologies, capable of morphological plasticity, could lead, in terms of understanding intelligent adaptive behaviour more fully, encompassing all living creatures from humans to unicellular organisms, and creating the next generation of artificial intelligent systems, capable of rich, complex behaviours in ever-changing environments.

## Appendix A

# Basic shape and pattern generative algorithms

There are a variety of methods/algorithms to choose from if creating a shape or pattern, or a whole morphology, artificially. Here we will give a brief introduction to the major ones, used in most AI morphological models for their simplicity and ability to generate higher-level complexity from low-level interactions and simple rules. There are many mathematical methods relating to shapes and surfaces. These are however, often descriptive rather than generative, they globally define a process rather than allowing it to self-organize and generate itself from lower-level components. The idea of self-organization and interaction between components is more intuitive, and relevant when considering biological generation of forms, as such its use can improve dialog between the disciplines.

## A.1 Cellular Automata

A Cellular Automaton (CA) is a grid-based, discrete computational system in which every grid cell can be one of a set of states, and a finite set of local rules determines how the state of cells change. The state of every cell in the grid is iteratively updated every time step. A cell's state is changed in response to the states of its local neighbourhood (which comprises the cells surrounding it within a given radius) according to the specific rules of the CA. The Moore Neighbourhood (MN), which takes its name from its pioneer Edward F. Moore, is defined, in the 2D case, as the eight grid cells sharing a side or vertex, see Fig. A.1.

Cellular automata are useful for studying a variety of phenomena (Wuenche, A. and Lesser, M. J., 1992; Burks, 1970) and have been used in particular to model pattern formation as it occurs in many domains because of their general property of local interactions to produce global phenomenon, meaning that they provide a good generic model of other models of pattern formation, for example the Turing system, described in section A.3, (Bonabeau, E. et al., 1992). Computer simulations of CA's can be used to generate aesthetic patterns as well as for modelling biology (Sims, 1991; Bentley, 2002).

## A.2 L-systems

In 1968 Aristid Lindenmayer introduced L-systems in (Lindenmayer, 1968). They exhibited the curious phenomenon of "data base amplification" (Prusinkiewicz, P. et al., 1995): they have the ability to generate complex structures from small data sets. The concept behind L-systems looks at biological methods of growth within a discrete mathematical framework. There are many discrete entities that occur natu-



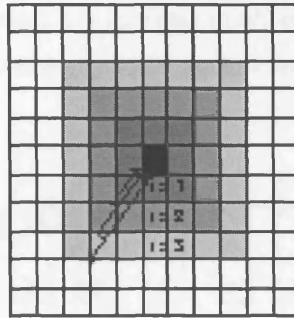


Figure A.1: A CA grid cell shown in black and its neighbours of radius 1, 2 and 3.

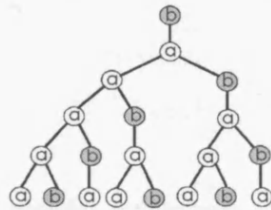


Figure A.2: First few iterations of the example L-system given in text.

rally in the biological world, genes and cells for example. In development these different units interact to bring about the processes of growth and differentiation (Herman, G. T. and Rozenberg, G., 1975).

An L-system has three components, an alphabet, an axiom and a set of re-writing rules, also called the next state functions. The best way to describe the processes involved in an L-system is through an example. This particular example is of a PDOL-system, a propagating, deterministic 0-context L-system.

- Alphabet:  $a, b$
- Axiom:  $a$
- Rules:  $b$  goes to  $a$  &  $a$  goes to  $ab$

The method is to take the axiom, apply the rules to each element of it then write the result below, then take every element of this new row and apply the rules, writing the result below this one, this then continues *ad infinitum*. See Fig. A.2. Due to the branching structure produced they have been used effectively to simulate plant growth (Prusinkiewicz, P. et al., 1995).

### A.3 Reaction Diffusion

The Turing system of reaction-diffusion of chemicals (Turing, 1952) models the development of pattern without positional information (Wolpert, L. and Stein, W. D., 1984). The reaction diffusion mechanism is one of inhibition. The existing structures diffuse 'inhibitor' chemicals which suppress the formation of similar cells within a certain radius, determined by the threshold of 'reaction'. That is, a cell will react by developing into a cell such as the existing ones only when the amount of inhibitor detected is below a certain threshold. See fig. A.3 for an illustration of how reaction diffusion works. In experiments

performed with reaction diffusion systems it is very easy to add one more element, another cell type or a diffusing activator and the level of complexity of the patterns can increase by an order of magnitude.

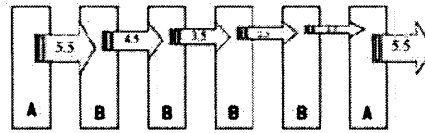


Figure A.3: Reaction Diffusion. When the threshold is set to 1.5, all cells receiving less inhibitor are not inhibited from becoming cell type A.

## A.4 Agent Swarms

There are many species that construct complex architectures. Social insects can be seen to generate hugely intricate patterns and structures when nest building. The possible organizational mechanism put forward by Grassé (1959) to explain how this can occur is *stigmergy*. The basic idea is that the coordination of individuals' tasks depends not on any communication between them but on the nest structure itself (Bonabeau, E. et al., 1992). The idea is that a termite picks up a soil pellet, impregnates it with a *cement pheromone* which then diffuses away. The termites are attracted by this pheromone, meaning that they tend to drop their soil pellets in the same area. The process of self organization is distributed, meaning that there is no centralized controller ordering the insects or agents to behave in a certain way, only the structure/environment combined with some rules of reaction.

*Swarm intelligence* is a Nouvelle AI idea where a group of agents may be able to perform tasks, without the use of explicit representations, of their environment or fellow agents, i.e the swarm is a self organizing system. Craig Reynold's Boids (Reynolds, 1987) are the classic example of this, where the interaction of the agents together with their simple, 'innate' rules produce flocking behaviour. The entire process is based on a succession of *sensorimotor loops*, where the agents adapt their current trajectory based only on the information they receive about the environment, which includes their fellow boids. *Stigmergic* swarm intelligence occurs when the innate rules require that the agents produce and react to pheromones (Bonabeau, E. et al., 2000; Bentley, 2002).

## Appendix B

# Glossary

This glossary of biological terms is divided into two sections: first, general cell biology terms used within Chapters 4 and 5; secondly, diatom related terms used in Chapters 3, 7 and 8.

### B.1 Cell Biology terms

**Actin** Structural protein of the cytoskeleton polymerizes to form microfilaments.

**Arp2/3** Molecular complex residing within cell cytoplasm which nucleates (starts) actin filaments.

**Binding site** The reactive parts of a macromolecule that directly participate in its specific combination with another molecule.

**Cisternae** Membrane bounded sacks located in the endoplasmic reticulum, as well as other areas.

**Centrosome** The microtubule organising centre, from which the microtubules grow, located around the nucleus. .

**Cofilin** Accessory protein of the cytoskeleton which severs actin filaments.

**Cytokinesis** during cell division, after division of the nucleus the cytoplasm, organelles and cellular components are, in the usual case, redistributed equally to each daughter cell.

**Eukaryote** Organism whose cells have chromosomes separated from the cytoplasm by a two membrane nuclear envelope.

**Fibroblast** Resident cell of connective tissue, secretes fibronectin amongst other things.

**Filopodia** Plural of filopodium, a thin protrusion from a cell, usually supported by actin microfilaments.

**Flagellum** Long thin projection from a cell used in movement.

**Lamellapodia** sheet like membrane protrusions comprised of actin microfilament networks.

**Lipid** Any of a heterogeneous group of fatlike substances characterised by being water insoluble and being extractable by nonpolar (or fat) solvents such as alcohol.

**Macromolecule** term relating to large molecules including, proteins, nucleic acids and carbohydrates and lipids.

**Macrophage** Relatively long lived phagocytic cell of mammalian tissues.

**Microspike** A thin protrusion from a cell, usually supported by bundled actin microfilaments, also called filopodia.

**Microtubule** Polymer of tubulin monomers arranged in a cylindrical tube. .

**Microfilament** Single-strand polymer of actin monomers .

**Meiosis** Special form of cell division in which each daughter cell receives half the amount of DNA. It is the cell division by which eggs and sperm are produced.

**Mitosis** Process by which a cell separates its duplicated genome into two identical halves, generally followed immediately by cytokinesis resulting in two identical daughter cells with a roughly equal distribution of organelles and other cellular components.

**Monomer** A single molecule that is the subunit of a polymer.

**Organelle** A structurally discrete component of a cell.

**PIP2** Phosphatidylinositol 4,5-bisphosphate, found in biomembranes and a precursor to certain cellular signals.

**Plasmalemma** Archaic name for the plasma membrane of a cell.

**Polymer** A macromolecule made of repeating (monomer) units.

**Profilin** Accessory cytoskeletal protein that binds to actin, activating it allowing it to bind onto filaments.

**Prokaryote** Organisms, namely bacteria and cyanobacteria, characterised by the possession of a simple naked DNA chromosome, occasionally two such chromosome, without a nuclear membrane and possessing a very small range of organelles, generally only a plasma membrane and ribosomes.

**Protein** Any of a group of complex organic compounds which contain carbon, hydrogen, oxygen, nitrogen and usually sulphur, the characteristic element being nitrogen and which are widely distributed in plants and animals.

**Receptor** Molecular structure within a cell or on the surface characterised by selective binding of a specific substance and a specific physiologic effect.

**Ribosome** An organelle composed of RNA and ribosomal proteins (known as a Ribonucleoprotein). It translates mRNA into a polypeptide chain (e.g., a protein). It can be thought of as a factory that builds a protein from a set of genetic instructions. Ribosomes can float freely in the cytoplasm (the internal fluid of the cell) or bind to the endoplasmic reticulum, or to the nuclear envelope.

**Vesicle** Membrane bound sack, possibly containing other cellular material.

**WASP** Wiskott-Aldrich Syndrome Protein: a 502-amino acid protein in the transduction pathway dependent upon Cdc42 and PIP2 for activation. Once activated it can bind to the Arp2/3 complex and serve as a nucleation point for actin organization.

## B.2 Diatom related terms

**Apices** Plural of apex, meaning to be at the apex or tip.

**Apical** Longitudinal plane of symmetry.

**Autotroph** Organism that produces organic compounds from carbon dioxide as a carbon source, using either light or reactions of inorganic chemical compounds, as a source of energy.

**Auxospore** Larger cell created by sexual reproduction. Has a primary organic wall, composed mainly of polysaccharides, silica bands are then laid down. The auxospore wall is far less limiting than the usual valves and girdle structure, so when it divides the valves that form have a modified morphology (auxosporulation is the formation of the auxospore).

**Chromophyte** (or chromista) Eukaryotic supergroup, which may be treated as a separate kingdom or included among the Protista. They include all algae whose chloroplasts contain chlorophylls a and c (including diatoms), as well as various colorless forms that are closely related to them.

**Chlorophyceae** class of green algae in the plantae kingdom, distinguishable by their flagellum and clear green colour.

**Cingulum** All elements of the girdle region.

**Cleavage furrow** A groove formed from the cell membrane in a dividing cell. As cytokinesis continues the furrow deepens. .

**Diatom** (Gr. dia 'through'; tomos 'cutting', i.e. 'cut in half') Major group of eukaryotic algae, and are one of the most common types of phytoplankton. Belonging to the kingdom Protista the heterokontophyta division (subgroup of chromophyta) and the Bacillariophyceae class. Most diatoms are unicellular, although some form chains or simple colonies. A characteristic feature of diatom

cells is that they are encased within a unique cell wall made of silica. .

**Dinophyta** large group of flagellate protists. About half are photosynthetic making up the largest group of eukaryotic algae aside from diatoms.

**Entrain** vertically move a particle or organism up through the water column via water currents.

**Epicingulum** Larger (and thus older) elements of the girdle region.

**Epitheca** The epivalve and associated epicingulum.

**Epivalve** Larger (and thus older) of the frustules two valves.

**Extrametabolites** substances given off by organisms which, as they accumulate in the environment, affect the life processes of other organisms.

**Frustule** Silica structure surrounding the cell comprised of two valves and their associated cingulum elements.

**Genus** Taxonomic grouping in the classification of living organisms (plural genera) comprised of species. .

**Grazers** Animal that eats low-lying vegetation.

**Hypocingulum** Smaller (and thus younger) elements comprising the girdle region.

**Hypotheca** The hypovalve and associated hypocingulum.

**Hypovalve** Smaller ( and thus newer) of two valves of a frustule.

**Interlocking valve** valve of a colonial diatom that permanently connects the cell to its sister.

**Mantle** Side part of the valve.

**Mucilage** Thick gluey substance, often produced by plants. Mucilage is another term for exopolysaccharides.

**Paleoecological** Branch of ecology that deals with the interaction between ancient organisms and their environment.

**Pelagic zone** part of the open sea or ocean comprising the water column.

**Phagotrophic** Organisms that feed by ingesting particulate organic carbon or intact cells, feed by phagocytosis.

**Photic zone** (also euphotic zone) Depth of water exposed to sufficient sunlight for photosynthesis to occur.

**Phototaxis** Organism movement in response to the stimulus light, advantageous for phototrophic organisms: they can orient themselves most efficiently to receive light for photosynthesis.

**Phytoplankton** The autotrophic component of the plankton that drifts in the water column.

**Process (morphological term)** An outgrowth or protruding morphological part.

**Protist** Heterogeneous group of living things, comprising those eukaryotes that are neither animals, plants, nor fungi. They are usually treated as the kingdom Protista or Protoctista.

**Protoplast** The actual organic diatom cell within the siliceous frustule, consisting of a cytoplasmic layer that lines the interior of the frustule and surrounds a large central vacuole, within the cytoplasmic layer there is a diploid nucleus and two to several pigment-bearing plastids (the site of photosynthesis).

**Radiolarian** Amoeboid protozoa that produce intricate mineral skeletons, typically with a central capsule dividing the cell into inner and outer portions. They are found as plankton throughout the ocean, and their shells are important fossils.

**Raphe** A seam or continuous ridge. Used to describe the long vertical rib of silica on the valve (Raphe sternum) which can have contain one or two hollow slits (raphe slit).

**Resting spore** Metabolically inactive spore formed in times of low light, nutrients or other stresses. They hav thicker silica walls so sink to the bottom of the sea, if they can return to favourable conditions normal cell function may resume.

**Ruderals** Tolerate frequent turbulence or transportation through light gradient

**SDV** Silica deposition vesicle. also called the silicalemma. The membrane sack within which silica is deposited.

**Separation valve** specialized valve developed by some colonial diatoms allowing cells to drift apart, splitting the colony.

**Seta** Stiff hair, projection or bristle.

**Species** The basic unit of biodiversity. In scientific classification, a species is assigned a two-part name in Latin. The genus is listed first (and capitalized), followed by a specific epithet.

**Sponge spicules** Skeletal structures that appear in some types of sponges. They are made of either calcium carbonate or silica.

**Strutted process** Morphological term. Tube penetrating the silica framework of a valve and supported internally by two or more buttresses (also known as fulcra)

**Taxon** (plural taxa) A grouping of organisms (named or unnamed). Once named, a taxon will usually have a rank and can be placed at a particular level in a hierarchy, broadly following this scheme of ranks in hierarchical order: kingdom, phylum, class, order, family, genus, species.

**Transapical** Latitudinal plane of symmetry.

**Turgor pressure** normal fullness or tension produced by the fluid content of blood vessels, capillaries, and plant or animal cells



**Uniseriate** Single row of pores.

**Valve** A structural component of the diatom frustule, two valves fit together like the two halves of a petri dish forming (along with the girdle bands) the frustule .

**Vegetative cell** See resting spore.

**Vimines** Cross-connections of silica that grow between virga to form the pores.

**Virgae** Ribs of silica that grow out perpendicular to the raphe sternum .

**Water column** Vertical section of the sea or lake; the water mass between the surface and the bottom.

# Bibliography

- Aderem, A. How to eat something bigger than your head. *Cell*, 114(1):5–8, 2002.
- Alberts, B., Bray, D., Lewis, J., Raff, M., Roberts, K., and Watson, J. D. *Molecular Biology of The Cell*. Garland Publishing, 3rd edition, 1994.
- Almeida e Costa, F. and Rocha, L. M. Embodied and situated cognition. *Artificial Life*, 11(1):5–11, 2005.
- Azuma, T., Takeda, K., Doi, T., Muto, K., Akutsu, M., and Sawada, M. and Adachi, S. The influence of temperature on sex determination in sockeye salmon *Oncorhynchus nerka*. *Aquaculture*, 234(1-4): 461–473, 2004.
- Barbieri, M. *The Organic Codes: The Birth of Semantic Biology*. Cambridge University Press, 2001.
- Beer, R. Dynamical approaches to cognitive science. *Trends in Cognitive Science*, 4(3):91–99, 2000.
- Behera, N. and Nanjundiah, V. Phenotypic plasticity can potentiate rapid evolutionary change. *Journal of Theoretical Biology*, 226:177–184, 2004.
- Bentley, K. Exploring aesthetic pattern formation. In Soddu, C, editor, *Proc. of 5th Ann. Int. Conf. on Generative Art, Milan*, pages 20.1–20.12, 2002.
- Bentley, K. and Clack, C. The Artificial Cytoskeleton for lifetime adaptation in morphology. In Bedau et al, M., editor, *Workshop Proc. of the 9th Int. Conf. on the Simulation and Synthesis of Living Systems (Alife9)*, pages 13–16, 2004.
- Bentley, K. and Clack, C. Morphological plasticity: environmentally driven morphogenesis. In Capcarrere, M. S., Freitas, A. A., Bentley, P. J., Johnson, C. G. and Timmis, J., editor, *Advances in Artificial Life: 8th European Conference, ECAL 2005*, pages 118–127. Springer Verlag, 2005.
- Bentley, K., Cox, E. J., and Bentley, P. J. Nature's batik: a computer evolution model of diatom valve morphogenesis. *Journal of Nanoscience and Nanotechnology*, 5(1):25–34, 2005.
- Bentley, P. J. *Evolutionary Design by Computers*. Morgan Kaufmann, 1999a.
- Bentley, P. J. From coffee tables to hospitals: generic evolutionary design. In Bentley, P. J., editor, *Evolutionary Design by Computers*, pages 405–423. Morgan Kauffman, 1999b.

- Bentley, P. J. and Corne, D. W. Introduction to creative evolutionary systems. In Bentley, P. J and Corne, D. W., editors, *Creative Evolutionary Systems*, pages 1–76. Morgan Kaufman, 2002.
- Bentley, P. J. and Kumar, S. Three ways to grow designs: a comparison of embryogenies for an evolutionary design problem. In et al., Banzhaf, W., editor, *Proceedings of the Genetic and Evolutionary Computation Conference (GECCO'99)*, pages 35–43, 1999.
- Blank, G. S. and Sullivan, C. W. Diatom mineralization of silicic acid. VII. Influence of microtubule drugs on symmetry and pattern formation in valves of *Navicula saprophila* during morphogenesis. *Journal of Phycology*, 19:294–301, 1983.
- Bonabeau, E., Guerin, S., Snyers, D., Kuntz, P., and Theraulaz, G. Three dimensional architectures grown by simple stigmergic agents. *Biosystems*, 56:13–32, 1992.
- Bonabeau, E., Dorigo, M., and Theraulaz, G. Inspiration for optimisation from social insect behaviour. *Nature*, 406:39–42, 2000.
- Bongard, J. Repeated structure and dissociation of genotypic and phenotypic complexity in artificial ontogeny. In Spector, L. and Goodman, E. D., editor, *GECCO-2001*, pages 829–836. Morgan Kaufmann, 2001.
- Bongard, J. Evolving complete agents using artificial ontogeny. In Pfeifer, R. and Hara, F., editors, *Morpho-functional Machines: The New Species (Designing Embodied Intelligence)*, pages 237–258. Springer-Verlag, 2003.
- Braitenberg, V. *Vehicles: Experiments in Synthetic Psychology*. MIT Press, 1984.
- Bray, D. *Cell Movements: From Molecules to Motility*. Garland Science, 2nd edition, 2001.
- Brett, C. and Waldron, K. *Physiology and Biochemistry of Plant Cell Walls*. Chapman and Hall, 1996.
- Brooks, R. A. Intelligence without reason. In *Proc. IJCAI-91*, pages 569–595, 1991a.
- Brooks, R. A. Challenges for complete creature architectures. In Meyer, J-A., Wilson, and Stewart W., editors, *From animals to animats: Proceedings of the First International Conference on Simulation of Adaptive Behavior*, pages 434–443, 1991b.
- Brooks, R. A. Intelligence without representation. *Artificial Intelligence*, 47:139–159, 1991c.
- Burks, A. (ed.). *Essays on Cellular Automata*. University of Illinois Press, 1970.
- Canter, H. M. Fungal and protozoan parasites and their importance in the ecology of the phytoplankton. *Annu. Rep., Freshwater Biol. Assoc.*, 47:43–50, 1979.
- Canter, H. M. and Jaworski, G. H. M. Some observations on the alga *Fragilaria crotonensis* Kitton and its parasitism by two chytridaceous fungi. *Annu. Bot.*, 49:429–446, 1982.

- Canter, H. M. and Jaworski, G. H. M. A further study on parasitism of the diatom *Fragilaria crotonensis* Kitton by chytridaceous fungi in culture. *Annu. Bot.*, 52:549–463, 1983.
- Capcarrere, M. S., Freitas, A. A., Bentley, P. J., Johnson, C. G. and Timmis, J., editor. *Proceedings of the 8th European Conference on Artificial Life (ECAL05)*, Lecture Notes in Computer Science, 2005. Springer-Verlag.
- Castellano, F., Chavrier, P., and Caron, E. Actin dynamics during phagocytosis. *Seminars in Immunology*, 13:347–355, 2001.
- Chapman, C. D., Saitou, K., and Jakiela, M. J. Genetic algorithms as an approach to configuration and topology design. In *Proc. Design Automation Conf. DE-Vol*, pages 485–498. A.S.M.E, 1993.
- Chiappino, M. L. and Volcani, B. E. Studies on the biochemistry and fine structure of silica shell formation in diatoms. VII. Sequential cell wall development in the pennate *Navicula pelliculosa*. *Protoplasma*, 93:191–204, 1977.
- Chirikjian, G. S. Kinematics of a metamorphic robotic system. In *Proc. of IEEE Int. Conf. on Robotics and Automation*, pages 449–455, 1994.
- Clack, C. D. Bioscience computing and the role of computational simulation in biology and medicine. In Verhaegh, W., Aarts, E. and Korst, J., editors, *Intelligent Algorithms*, pages 3–19. Springer, 2006.
- Coates, P. and Carranza, P. M. Swarm modelling: the use of Swarm Intelligence to generate architectural form. In Soddu, C, editor, *Proceedings of the 3rd International Conference on Generative Art, Milan*, 2000.
- Cohn, S. A., Nash, J., and Pickett-Heaps, J. D. The effect of drugs on diatom valve morphogenesis. *Protoplasma*, 149:130–143, 1989.
- Cox, E. J. Morphological variation in widely distributed taxa: taxonomic and ecological implications. In *Proceedings of the 13th International Diatom Symposium*, pages 335–345, 1994.
- Cox, E. J. Assessing and designation diatom taxa at or below the species level: a consideration of current status and some suggested guidelines for the future. *Nova Hedwigia*, 65:13–26, 1997.
- Cox, E. J. Variation in patterns of valve morphogenesis between representatives of six biraphid diatom genera (bacillariophyceae). *J. Phycol.*, 35:1297–1312, 1999.
- Cox, E. J. Raphe loss and spine formation in *Diademesmis gallica* (bacillariophyta) - an intriguing example of phenotypic plasticity in a diatom. *Nova Hedwigia*, 130:163–176, 2006.
- Cox, E. J. The evolution of morphogenetic complexity in single celled plants. In Cronk, Q. C. B., Bateman, R. M. and Hawkind, J. A., editor, *Developmental Genetics and Plant Evolution*, pages 459–492. Taylor and Francis, 2002.

- Cox, E. J. and Ross, R. The striae of pennate diatoms. In *Proceedings of the 6th Symposium on Recent and Fossil Diatoms*, pages 267–278, 1980.
- Crawford, R. M. Filament formation in the diatom genera *Melosira*. *Nova Hedwigia*, 64:121–133, 1979.
- Davey, M. C. The relationship between size, density and sinking velocity through the life cycle of *Melosira granulata* (Bacillariophyta). *Diatom Research*, 1(1):1–18, 1986.
- Davey, M. C. and Crawford, R. M. Filament formation in the diatom *Melosira granulata*. *Journal of Phycology*, 22:144–150, 1986.
- Davey, M. C. and Walsby, A. E. The form resistance of sinking algal chains. *British Phycological Journal*, 20:243–248, 1985.
- Dellaert, F. and Beer, R. A developmental model for the evolution of complete autonomous agents. In et al, P.Maes, editor, *From Animals to Animats Proc. 4th Int. Conf. SAB '96*, pages 393–401, 1996.
- Dellaert, F. and Beer, R. Toward an evolvable model of development for autonomous agent synthesis. In *in Proc. Artificial Life IV*, pages 246–257. MIT Press, 1994.
- Di Paolo, E. Autopoiesis, adaptivity, teleology, agency. *Phenomenology and the Cognitive Sciences*, 2006. Forthcoming.
- Edgar, L. A. Fine structure of *Caloneis amphibaena* (Bacillariophyceae). *Journal of Phycology*, 16:62, 1980.
- Edgar, S. M. *Phylogeny of Aulacoseira (Bacillariophyta)*. PhD thesis, University of Texas, 2003.
- Edgar, L. A. and Pickett-Heaps, J. D. Valve morphogenesis in the pennate diatom *Navicula cuspidata*. *Journal of Phycology*, 20:47–61, 1984.
- Eggenberger, P. Evolving morphologies of simulated 3d organisms based on differential gene expression. In Husbands, P. and Harvey, I., editors, (*Proceedings of the 4th European Conf. on Artificial Life (ECAL97)*), pages 205–213. Cambridge: MIT Press, 1997.
- Eggenberger-Hotz, P. Comparing direct and developmental encoding schemes in artificial evolution: a case study in evolving lens shapes. In *Proc. IEEE congress on Evolutionary Computation CEC*, pages 752–757. IEEE Press, 2004.
- Emmeche, C. Life as an abstract phenomenon: is artificial life possible? In Varela, Francisco J. and Bourgine, Paul, editors, *Toward a Practice of Autonomous Systems. Proceedings of the First European Conference on Artificial Life*, pages 446–474. MIT Press, 1992.
- Endo, I., Yamasaki, F., Maeno, T., and Kitano, H. A method for co-evolving morphology and walking pattern of biped humanoid robot. In *Proc. IEEE Intl. Conf. on Robotics and Automation*, pages 2775–2780, 2002.

- Fernando, C. and Sojakka, S. Pattern recognition in a bucket. In Banzhaf, W., Christaller, T., Dittrich, P., Kim, J.T., and Ziegler, J., editors, *Proc. 7th Euro. Conf. on Artificial Life (ECAL 2003)*, pages 588–597. Springer Verlag, 2003.
- Floreano, D. and Urzelai, J. Evolution of adaptive-synapse controllers. In Floreano et al, D., editor, *Advances in Artificial Life. Proceedings of the 5th European Conference on Artificial Life*, 1999.
- Floridi, L. *Philosophy and Computing: An Introduction*. Routledge, 1999.
- Fodor, J. A. *The Language of Thought*. Harvard University Press, 1975.
- Fryxell, G. A. Chain forming diatoms: three species of Chaetoceraceae. *Journal of Phycology*, 14(1): 62–71, 1978.
- Fryxell, G. A. and Miller, W. I. . Chain forming diatoms: Three araphid species. *Bacillaria*, 1:113–136, 1978.
- Funes, P. *Evolution of Complexity in Real-World Domains*. PhD thesis, Brandeis University, 2001.
- Funes, P. and Pollack, J. B. Evolutionary body building: adaptive physical designs for robots. *Artificial Life*, 4(4):337–357, 1998.
- Glazier, J. A. and Graner, F. Simulation of the differential adhesion driven rearrangement of biological cells. *Physical Review E*, 47(3):2128–2154, 1993.
- Goodwin, B. C., Kauffman, S., and Murray, J. D. Is morphogenesis an intrinsically robust process? *J. Theor. Biol.*, 163:135–144, 1993.
- Gordon, R. and Parkinson, J. Potential roles for diatomists in nanotechnology. *Journal of Nanoscience and Nanotechnology*, 5:35–40, 2005.
- Gordon, R., Björkland, N. K., Robinson, G. G. C., and Kling, H. J. Sheared drops and pennate diatoms. *Nova Hedwigia*, 112:289–299, 1996.
- Grassé, P.-P. *La Reconstruction du nid et les coordinations inter-individuelles chez Bellicositermes natalensis et Cubitermes sp. La théorie de la stigmergie*. Elsevier Science, 1959.
- Groß, R., Bonani M., Mondada F., and Dorigo M. Autonomous self-assembly in a swarmbot. In Murase, K., Sekiyama, K., Kubota, N., Naniwa, T., and Sitte, J., editors, *Proceedings of the 3rd Intl. Symposium on Autonomous Minirobots for Research and Entertainment*, pages 314–322. Springer-Verlag, 2006.
- Guillot, A. and Meyer, J-A. The animat contribution to cognitive systems research. *Journal of Cognitive Systems Research*, 2(2):157–165, 2001.
- Hara, F. and Pfeifer, R. On the relation among morphology, material and control in morpho-functional machines. In Meyer, J-A., Berthoz, A., Floreano, D., Roitblat, H. L. and Wilson, S. W., editor, *From*

- Animals to Animats 6: Proceedings of the Sixth Intl. Conf. on Simulation of Adaptive Behaviour SAB00*, pages 33–40. MIT Press, 2000.
- Harvey, I., Husbands, P., Cliff, D., Thompson, A., and Jakobi, N. Evolutionary robotics at sussex. In Jamshidi, M., Pin, F., and Dauchez, P., editors, *In Robotics and Manufacturing: Recent Trends in Research and Applications Proceedings of ISRAM96, International Symposium on Robotics and Manufacturing, Montpellier, France*, volume 6, pages 293–298, 1996.
- Herman, G. T. and Rozenberg, G. *Developmental systems and languages*. North-Holland publishing company oxford, 1975.
- Hogeweg, P. Shapes in the shadow: Evolutionary dynamics of morphogenesis. *Artificial Life*, 6: 85–101, 2000.
- Hogeweg, P. Computing an organism: on the interface between informatic and dynamic process. *BioSystems*, 64:97–109, 2002a.
- Hogeweg, P. Multilevel processes in evolution and development: computational models and biological insights. In Lässig, M. and Valleriani, A., editors, *Statistical Physics*, pages 217–239. Springer Verlag, 2002b.
- Holland, J. *On Growth Form and Computers*, chapter Foreword. Academic Press, 2003.
- Holland, J. A. *Adaptation in Natural and Artificial Systems*. MIT Press, Cambridge MA, 1975.
- Holt, M. R. and Koffer, A. Cell motility: Proline-rich proteins promote protrusions. *TRENDS in Cell Biology*, 11(1):38–46, 2001.
- Hornby, G. and Pollack, J. Evolving l-systems to generate virtual creatures. *Computers & Graphics*, 25 (6):1041–1048, 2001a.
- Hornby, G. and Pollack, J. The advantages of generative grammatical encodings for physical design. In *Congr. on Evolutionary Computation*, pages 868–875, 2001b.
- Hornby, G. S. and Pollack, J. B. Body-brain co-evolution using l-systems as a generative encoding. In *Genetic and Evolutionary Computation Conference*, pages 600–607, 2001.
- Hutton, T. J. Evolvable self-replicating molecules in an artificial chemistry. *Artificial Life*, 8(4): 341–356, 2002.
- Iida, F. Cheap design approach to adaptive behaviour: Walking and sensing through body dynamics. In *In Workshop Proc. International Symposium on Adaptive Motion of Animals and Machines*, 2005.
- Kawai, N. and Hara, F. Formation of morphology and morpho-function in a linear cluster robotic system. In Pfeifer, R. et al, editor, *From Animals to Animats, Proc. 5th Int. Conf. SAB'98*, pages 459–464, 1998.

- Kröger, N. and Sumper, M. Diatom cell wall proteins and the cell biology of silica biomineralization. *Protist*, 149:213–219, 1998.
- Kröger, N., Deutzmann, R., Bergsdorf, C. and Sumper, M. Species-specific polyamines from diatoms control silica morphology. *Proc. Nat. Acad. Sci. U. S.*, 97:14133–14138, 2000.
- Kumar, S. *Investigating Computational Models of Development for the Construction of Shape and Form*. PhD thesis, Department of Computer Science, University College London. UCL, 2004.
- Lee, D. T. Medial axis transformation of a planar shape. *IEEE Trans. Pattern Anal. Mach. Intell. PAMI.*, 4:363–369, 1982.
- Lenaerts, T., Groß, D., and Watson, R. On the modelling of dynamical hierarchies: Introduction to the workshop wdh 2002. In Bilotta, E., Groß, D., Smith, T., Lenaerts, T., Bullock, S., Lund, H. H., Bird, J., Watson, R., Pantano, P., Pagliarini, L., Abbass, H., Standish, R., and Bedau, M., editors, *Proceedings of Artificial Life VIII Workshops*, pages 37–44, 2002.
- Lestrel, P. E. *Morphometrics for the Life Sciences*. World Scientific, 2000.
- Li, C. W. and Volcani, B. E. Morphogenesis of the labiate process in centric diatoms. *Protoplasma*, 124:147–156, 1985.
- Lindenmayer, A. Mathematical models for cellular interaction in development, parts i and ii. *Theoretical Biology*, 18:280–315, 1968.
- Lipson, H. and Pollack, J. Automatic design and manufacture of robotic lifeforms. *Nature*, 406: 974–978, 2000.
- Lungarella, M., Metta, G., Pfeifer, R., and Sandini, G. Developmental robotics: a survey. *Connection Science*, 0(0):1–40, 2004.
- Lürling, M. and Van Donk, E. Grazer induced colony formation in *Scenedesmus acutus* (Chlorophyceae) ecomorph expression at different temperatures. *Journal of Phycology*, 35(6): 1120–1126, 1999.
- MacDonald, J. D. On the structure of the diatomaceous frustule, and its genetic cycle. *Ann. Mag. Nat. Hist., Ser. 4*, 3:1, 1869.
- Mann, D. G. The species concept in diatoms. *Phycologia*, 38:437–495, 1999.
- Mann, D. G. and Droop, S. J. M. *Biogeography of Freshwater Algae*, volume 118 of *Developments in Hydrobiology*, chapter Biodiversity, biogeography and conservation of diatoms, pages 19–32. Kluwer academic publishers, 1996.
- Marée, A. F. M. and Hogeweg, P. How amoeboids self-organize into a fruiting body: Multicellular coordination in *Dictyostelium discoideum*. *Developmental Biology*, 98(7):3879–3883, 2001.



- Maturana, H. and Varela, F. J. *Autopoiesis and Cognition: The Realization of the Living*, volume 42 of *Boston Studies in the Philosophy of Science*. D. Reidel, 1980.
- May, R. C. and Machesky, L. M. Phagocytosis and the actin cytoskeleton. *Journal of Cell Science*, 114 (6):1061–1077, 2001.
- Mech, R. and Prusinkiewicz, P. Visual models of plants interacting with their environment. In *Proc. 23rd Ann. Conf. on Computer Graphics (SIGGRAPH)*, pages 397–410, 1996.
- Medlin, L. K. Morphological and genetic variation within the diatom *Skeletonema costatum* (bacillariophyta) evidence for a new species, *Skeletonema pseudocostatum*. *Journal of Phycology*, 27:514–524, 1991.
- Meyers, L. A. and Bull, J. J. Fighting change with change: adaptive variation in an uncertain world. *TRENDS in Ecology and Evolution*, 17(12):551–557, 2002.
- Miki, H. and Takenawa, T. Regulation of actin dynamics by WASP family proteins. *Journal of Biochemistry*, 134:309–313, 2003.
- Miller, J. F. Evolving developmental programs for adaptation, morphogenesis, and self-repair. In Banzhaf, W., Christaller, T., Dittrich, P., Kim, J. T., and Ziegler, J., editors, *Proc. Seventh European Conference on Artificial Life*, pages 256–265. Springer, 2003.
- Mondada, F., Franzi, E., and Ienne, P. Mobile robot miniaturisation: a tool for investigation in control algorithms. In *Proceedings of the 3rd International Symposium on Experimental Robotics*, pages 501–513. Springer-Verlag, 1993.
- Murata, S., Tomita, K., Yoshida, E., Kurokawa, H., and Kokaj, S. Self-reconfigurable robot module design and simulation. In *Proc. Int. Conf. Intelligent Autonomous System 6 (IAS6)*, pages 911–917, 2000.
- Niedergang, F. and Chavrier, P. Signalling and membrane dynamics during phagocytosis: many roads lead to the phagosome. *Current Opinion in Cell Biology*, 16:422–428, 2004.
- Nolfi, S., Floreano, D., Miglino, O., and Mondada, F. How to evolve autonomous robots: different approaches in evolutionary robotics. In *Artificial Life IV*, pages 190–197. MIT Press/Bradford Books, 1994.
- Ogarty, T. C., editor. *Evolutionary Computing: Selected Papers of the 1994 AISB Workshop*, volume 865 of *Lecture Notes in Computer Science*, 1994. Springer-Verlag.
- O’Grady, R., Größ, R., Mondada, F., Bonani, M., and Dorigo, M. Self-assembly on demand in a group of physical autonomous mobile robots navigating rough terrain. In Capcarrere, M. S., Freitas, A. A., Bentley, P. J., Johnson, C. G. and Timmis, J., editor, *Advances in Artificial Life: Proc. of the 8th European Conf. on Artificial Life (ECAL05)*, pages 272–281. Springer Verlag, 2005.

- Ozturkeri, C. and Capcarrere, M. S. Self-repair ability of a toroidal and non-toroidal cellular developmental model. In *Advances in Artificial Life: 8th European Conference, ECAL 2005*, pages 138–148. Springer Verlag, 2005.
- Paasche, E., Johansson, S., and Evensen, D. L. An Effect of Osmotic Pressure on Valve Morphology of the diatom *Skeletonema subsalsum* (A. Cleve) Bethge. *Phycologia*, 14(4):205–211, 1975.
- Parkinson, J., Brechet, Y., and Gordon, R. Centric diatom morphogenesis: a model based on a DLA algorithm investigating the potential role of microtubules. *Biochim Biophys Acta*, 1452:89–102, 1999.
- Paul, C. Morphology and computation. In et al, Schaal, editor, *Proceedings of the International Conference on the Simulation of Adaptive Behaviour*, pages 33–38, 2004.
- Paulin, J. K. The development of stigmergic homeostasis in termites. Master's thesis, University of Sussex, 2004.
- Penrose, L. Self-reproducing machines. *Scientific American*, 200:105–113, 1959.
- Pfeifer, R. On the role of morphology and materials in adaptive behavior. In Meyer, J.-A., Berthoz, A., Floreano, D., Roitblat, H., and Wilson, S. W., editors, *From Animals to Animats 6. Proc. of the 6th Int. Conf. on Simulation of Adaptive Behaviour*, pages 23–32. Cambridge, Mass.: MIT Press, 2000.
- Pfeifer, R. New robotics: Design principles for intelligent systems. *Artificial Life: Special Issue on New Robotics, Evolution and Embodied Cognition*, 11:99–120, 2004.
- Pfeifer, R. Building “fungus eaters”: design principles of autonomous agents. In Maes, P., Mataric, M. J., Meyer, J.-A., Pollack, J., and Wilson, S. W., editors, *From Animals to Animats 4: Proc. Intl. Conf. on Simulation of Adaptive Behaviour*. MIT Press, 1996.
- Pfeifer, R. Morpho-functional Machines: basics and research issues. In *Morpho-functional Machines: The New Species*, pages 1–21. Springer-Verlag, 2003.
- Pfeifer, R. and Iida, F. Morphological computation: connecting body, brain and environment. *Japanese Scientific Monthly*, 58(2):48–54, 2005.
- Pfeifer, R. and Scheier, C. *Understanding Intelligence*. MIT Press, 1999.
- Pickett-Heaps, J. D. Cell division and morphogenesis of the centric diatom *Chaetoceros decipiens* (Bacillariophyceae) II. electron microscopy and a new paradigm for tip growth. *Journal of Phycology*, 34(6):995–1004, 1998.
- Pickett-Heaps, J. D., Tippet, D. H., and Andreozzi, J. A. Cell division in the pennate diatom *Pinnularia*. IV. Valve morphogenesis. *Biol. Cell*, 35:295–304, 1979.
- Pickett-Heaps, J. D., Cohn, S., Schmid, A.-M. M., and Tippet, D. H. Valve morphogenesis in *Suirella*. *Journal of Phycology*, 24:35–49, 1988.

- Pickett-Heaps, J., Schmid, A.-M. M., and Edgar, L. A. The cell biology of diatom valve formation. *Prog. Phycol. Res.*, 7:1, 1990.
- Piersma, T. and Drent, J. Phenotypic flexibility and the evolution of organismal design. *TRENDS in Ecology and Evolution*, 18(5):228–233, 2003.
- Porter, K. G. The plant-animal interface in freshwater ecosystems. *Am. Sci.*, 65(2):159–170, 1977.
- Prusinkiewicz, P., Hammel, M., and Mech, R. The artificial life of plants. artificial life for graphics, animation and virtual reality. In *SIGGRAPH '95 Course notes*, volume 7, pages 1.1 –1.38. ACM Press, 1995.
- Quick, T., Dautenhahn, K., Nehaniv, C., and Roberts, G. On bots and bacteria: ontology independent embodiment. In *Proc. of ECAL99*, pages 339–343, 1999.
- Reynolds, C. S. *The Ecology of Freshwater Phytoplankton*. Cambridge University Press, 1984.
- Reynolds, C. S. *Vegetation processes in the pelagic: a model for ecosystem theory*, volume 9 of *Excellence in Ecology*. Inter-Research, 1994.
- Reynolds, C. S. Functional morphology of freshwater phytoplankton. In Sandgren, C. D., editor, *Growth and Reproductive Strategies of Freshwater Phytoplankton*, pages 388–433. Cambridge University Press, 1988.
- Reynolds, C. W. Flocks, herds, and schools: A distributed behavioral model. *Computer Graphics*, 21(4):25–34, 1987. (SIGGRAPH '87 Conference Proceedings).
- Rieffel, J. and Pollack, J. Automated assembly as situated development: using artificial ontogenies to evolve buildable 3-d objects. In *Proceedings of the 2005 conference on Genetic and evolutionary computation (GECCO)*, pages 99–106. ACM Press, 2005.
- Rizzotti, M. *Early evolution : from the appearance of the first cell to the first modern organisms*. Birkhäuser, 2000.
- Roggen, D. and Federici. Multi-cellular development: is there scalability and robustness to gain? In *Proceedings of PPSN VIII 2004 The 8th International Conference on Parallel Problem Solving from Nature*, pages 391–400, 2004.
- Round, F. E. Some observations on colonies and ultrastructure of the frustule of *Coenobiodiscus muriformis* and its transfer to *Planktoniella*. *Journal of Phycology*, 8:222–231, 1972.
- Round, F.E. and Crawford, R. M. and Mann, D. G. *The Diatoms: Biology and Morphology of the Genera*. Cambridge University Press, 1990.
- Sarno, D. and Kooistra, W. H. C. F. Diversity in the genus *Skeletonema* (bacillariophyceae). ii. an assessment of the taxonomy of *S. Costatum*-like species with the description of four new species. *Journal of Phycology*, 41(1):151–176, 2005.

- Savill, N. J. and Hogeweg, P. Modelling morphogenesis: from single cells to crawling slugs. *Journal of Theoretical Biology*, 184(3):229–235, 1997.
- Schmid, A-M. M. Valve morphogenesis in diatoms: A pattern related filamentous system in pennates and the effect of APM, colchicine and osmotic pressure. *Nova Hedwigia*, 33:811–847, 1980.
- Schmid, A-M. M. Influence of environmental factors on the development of the valve in diatoms. *Protoplasma*, 99:99–115, 1979.
- Schmid, A-M. M. Wall morphogenesis in *Coscinodiscus wailesii* Gran et Angst. II. Cytoplasmic events of valve morphogenesis. In Ricard, M., editor, *Proceedings of the 8th Diatom Symposium, Paris 1984*, pages 293–314, 1986.
- Schmid, A-M. M. Tricornate spines in *Thalassiosira eccentrica* as a result of valve modelling. In *7th Diatom Symposium*, pages 71–89, 1982.
- Schultz, M. E. Salinity-related polymorphism in the brackish-water diatom *Cyclotella cryptica*. *Can. J. Bot.*, 49:1285–1289, 1971.
- Semenova, A. Simulation of cancer tumour therapy using agent-based programming and a cellular automaton. Msci thesis, University College London, 2005.
- Sims, K. Artificial evolution for computer graphics. In *Computer Graphics (Siggraph '91 proceedings)*, pages 319–328, 1991.
- Sims, K. Evolving virtual creatures. In *Computer Graphics (SIGGRAPH 94)*, pages 15–22, 1994a.
- Sims, K. Evolving 3d morphology and behaviour by competition. In Maes, Brooks &, editor, *Proc. Artificial Life IV*, pages 28–39. MIT Press, 1994b.
- Singer, S. J. and Nicolson, G. L. The fluid mosaic model of the structure of cell membranes. *Science*, 175:720–31, 1972.
- Sipper, M., Sanchez, E., Mange, D., Tomassini, M., Pérez-Urbe, A., and Stauffer, A. A phylogenetic, ontogenetic, and epigenetic view of bio-inspired hardware systems. *IEEE Transactions on Evolutionary Computation*, 1(1):83–97, 1997.
- Smayda, T. J. The suspension and sinking of phytoplankton in the sea. *Oceanography and Marine Biology Annual Review*, 8:353–414, 1970.
- Smith, G. and Sternberg, M. J. E. Prediction of protein-protein interactions by docking methods. *Current Opinion in Structural Biology*, 12:28–35, 2002.
- Sommer, U. Growth and survival strategies of planktonic diatoms. In Sandgre, C. D., editor, *Growth and Reproduction Strategies of Freshwater Phytoplankton*, pages 227–260. Cambridge University Press, 1988.

- Strawson, G. Realistic materialist monism. In S.R. Hameroff, A.W. Kaszniak and D.J. Chalmers, editors, *Toward a Science of Consciousness III*. MIT Press, 2000.
- Suzuki, K. and Ikegami, T. Self-repairing and mobility of a simple cell model. In Pollack, J. et al, editor, *Proc. 9th Int. Conf. on Synthesis and Simulation of Living Systems (ALife9)*, pages 421–426, 2004.
- Svitkina, M. and Borisy, G. G. Arp2/3 complex and adf/cofilin in dendritic organization and treadmilling of actin filament array in lamellipodia. *J. Cell Biol*, 145(5):1009–1026, 1999.
- Syvertsen, E. E. *Thalassiosira rotula* and *t. gravida*: Ecology and morphology. In Simonsen, R. and Cramer, J., editors, *Proceeding of the 4th Symposium on Recent and Fossil Marine Diatoms*, pages 99–112. Nova Hedwigia, 1977.
- Taylor, T. and Massey, C. Recent developments in the evolution of morphologies and controllers for physically simulated creatures. *Artificial Life*, 7(1):77–87, 2001.
- Todd, P., Wilson, W. S., Somayaji, A. B., and Yanco, H. A. The blind breeding the blind, adaptive behaviour without looking. In Cliff, D., Husbands, P., Meyer, J-A, and Wilson, S., editors, *From Animals to Animats 3: Proc. 3rd Int. Conf. on Simulation of Adaptive Behaviour*, pages 228–237, 1994.
- Trianni V., Nolfi S., and Dorigo M. Cooperative hole avoidance in a swarm-bot. *Robotics and Autonomous Systems*, 54(2):97–103, 2006.
- Trobajo, R., Cox, E. J., and Quintana, X. D. The Effects of Some Environment Variables on the Morphology of *Nitzschia frustulum* (Bacillariophyta) in Relation to its use as a Bioindicator. *Nova Hedwigia*, 79(3-4):433–445, 2002.
- Turing, A. M. The chemical basis of morphogenesis. *Phil. Trans. Roy. Soc. of London, Series B:Biological Sciences*, 237:37–72, 1952.
- Van Gelder, T. The dynamical hypothesis in cognitive science. *Behavioural and Brain Sciences*, 21: 1–14, 1998.
- Varela, F. J. *Principles of Biological Autonomy*. Elsevier, 1979.
- Varela, F. J., Thompson, E. T., and Rosch, E. *The Embodied Mind: Cognitive Science and Human Experience*. MIT Press, 1993.
- Vaughan, E., Di Paolo, E., and Harvey, I. The evolution of control and adaptation in a 3d powered passive dynamic walker. In Bedau, M. et. al., editor, *Proc. 9th Intl. Conf. on the Simulation and Synthesis of Living Systems, ALIFE'9*. MIT Press, 2004.
- Widnell, C. C. and Pfenninger, K. H., editors. *Essential Cell Biology*. Williams and Wilkins, 1990.

- Wilson, S. W. The Animat path to AI. In Meyer et al, J. A., editor, *Proc. 1st Intl. Conf. On Simulation of Adaptive Behaviour (SAB90)*, pages 15–22. MIT Press, 1990.
- Wolpert, L. and Stein, W. D. Positional information and pattern formation. In Malacinski, G. M. and Bryant, S. V., editors, *Pattern Formation*, pages 3–22. Macmillan Publishing Company, New York, 1984.
- Wuenche, A. and Lesser, M. J. *The Global Dynamics of Cellular Automata; An Atlas of Basin of Attraction Fields of One-Dimensional Cellular Automata*. Addison-Wesley, 1992.
- Yakushin, A. *Ecology and morphology of selected diatom species in the genus Aulacoseira*. PhD thesis, University of Ulster, 1997.
- Yim, M. Rhombic dodecahedron shape for self-assembling robots. Technical Report P9710777, Xerox Palo Alto Research Centre, 1997.
- Zhang, B. Cytoskeleton simulation applied in equity portfolio management. Master's thesis, University College London, 2005.
- Zingone, A., Percopo, I., Sims, P. A., and Sarno, D. Diversity in the genus *Skeletonema* (Bacillariophyceae). I. A re-examination of the type of material of *S.costatum* with the description of *S.grevillei* sp. nov. *Journal of Phycology*, 41(1):140–150, 2005.
- Zirbel, M. J., Veron, F., and Latz, M. I. The reversible effect of fluid flow on the morphology of *Ceratocorys horrida* (peridinales dinophyta). *Journal of Phycology*, 36:46–58, 2000.